Marine productivity and terrigenous matter supply: The variability of the Subtropical Convergence around Tasmania during the last 500 ka

Doctoral Thesis

Submitted in partial fulfilment of the requirements for the doctoral degree
at the Faculty of Mathematics and Natural Sciences of the
Christian-Albrechts-University
Kiel, Germany

by

Natasja Brughmans

Kiel 2003

Promoter/Referent/in: Prof. Dr. W.-C. Dullo

Copromoter/Korreferent/in: Prof. Dr. W. Kuhnt

Day of the disputation/Tag der mündlichen Prüfung:

Approved for print/Zum Druck genehmigt:

The Dean/Der Dekan

Dank u wel!

Sincere, I would like to thank some people who supported me during my time in Kiel and especially during the realisation of this PhD-thesis.

Thank you Prof. Dr. W.-C. Dullo for purposing this theme and the possibility of realizing the presented thesis. Thank you Prof. Dr. W. Kuhnt for being copromoter. I would like to thank Dr. Dirk Nürnberg for the supervision: The discussions we had, gave me new insights and other ideas. Dr. Joachim Schönfeld was more than just the neighbour of the office. Any time I could pass by and he was prepared to give clear explanations. Carolyn Wegner, Anja Wolf, Arne Sturm, Jeroen Groeneveld and Nikolaus Gusonne and plenty of other collegues were always there if a small talk or an intense discussion was needed. They are just great! For the insights in the laboratory work several technicians were prepared to show me the different handing steps, to introduce me to the instruments and to discuss the problems with me, especially thank you Bettina Domeyer, Bastian Fessler, Regina Suerberg, Kristin Nass and Anke Bleyer. For the preparations of the large amount of samples several students assisted me. I was really lucky that Gema Martinez-Mendez, Sophie Hansen and Torben Gehrts accompanied me during almost the whole time period of the PhD. It was just great to work together with them. This project was made possible by the financial support of the DFG (German Research Group).

A lot of friends in Kiel were always there to support and encourage me. I would like to thank all the people from the association of the Planetarium, especially Torsten, Judith, Tim, Julia and Kenan for the great moments together, the encouragements and patience. The girls from the soccer team TSV Russee/VfB Kiel need to be mentioned in here. It was great to kick a ball together, especially thanks to Mareike. A big hug is given to my best friend Carsten. Thank you for being so uncomplicated, especially thank you for always being there during the last weeks of finishing this work.

Special thanks deserve my supporters from Belgium. Thank you Johan and Gert for always being reachable. My sister Saskia deserves a big hug for the relaxing words on the telephone. Most grateful I am to my parents. They gave me the chance to come to Kiel and encouraged me to go on.

To all of them thanks a lot and ‘een dikke knuffel’!

Natasja Kiel, May 2003

CONTENTS

ABSTRACT

This study focussed on temporal and spatial changes in export productivity and terrigenous flux, in response to the varying oceanographic frontal system, in the Tasmanian Seaway since 500 ka. Four sites, drilled during ODP-Leg 189, were studied: Site 1168 (western Tasmanian margin), Sites 1170 and 1171 (Tasman Rise), and Site 1172 (East Tasman Plateau).

Downcore variations in geochemical proxy data allowed to reconstruct the position of the oceanographic frontal system in the Southern Ocean since 500 ka. The paleoproductivity was assessed from the accumulation rates of carbonate, organic carbon, excess barium and chlorins. For the first time chlorin was used in the Southern Ocean to reconstruct paleoproductivity. Siliciclastic material, by means of the aluminium, iron and titanium concentrations, was used as proxy for the supply of terrigenous matter. Their ratios provided evidence for the origin of the terrigenous material as being wind-blown dust.

In general, the interglacial periods were characterised by less productivity and a lower terrigenous supply. The Subtropical Convergence was located south of 49°S during the interglacial isotopic stages 1 - 7. During marine isotopic stages 9 - 13, increased export productivity suggests a increased influence of Subantarctic Surface Water at the southern Site 1171. This indicates a position of the Subtropical Convergence and the zone of the westerlies more to the north.

During the glacials the frontal system was shifted to the north. The Subtropical Convergence reached as far north as between 42°S and 39°S east of Tasmania and between 44°S and 40°30'S west of Tasmania during the glacials. Reduced productivity during marine isotopic stages 8, 10 and 12 at the southern Site 1171 suggests that the Subantarctic Front was located to the north of Site 1171. The high glacial productivity in the nutrient-rich Subantarctic Surface Water was mainly caused by an increased supply of iron, delivered by strengthened westerly winds. These results indicate that the "Iron Hypothesis" is applicable for the studied area.

It can be concluded that strong glacial/interglacial changes have determined the variations in the oceanographic frontal system in the Tasmanian Seaway. In general, the frontal system in the study area shifted to the south since 500 ka.

KURZFASSUNG

Im Mittelpunkt dieser Studie stand die Rekonstruktion von räumlichen und zeitlichen Variationen des ozeanographischen Frontensystems im tasmanischen Seeweg während der letzten 500.000 Jahre. Insgesamt wurden vier ODP-Bohrungen von Leg 189 untersucht: Kern 1168 (westlicher Tasmanien-Graben), Kern 1170 und 1171 (Tasmanischer Rücken) sowie Kern 1172 (östliches Tasmanien-Plateau).

Variationen in der Sedimentzusammensetzung spiegeln Verlagerungen des ozeanographischen Frontensystems wider und wurden anhand von geochemischen Proxies untersucht. Akkumulationsraten von Carbonat, organischem Kohlenstoff, biogenem Barium und Chlorinen dienten der Abschätzung der Exportproduktivität. Erstmalig wurden die Akkumulationsraten von Chlorinen zur Rekonstruktion der Paläoproduktivität im Südpolarmeer einbezogen. Die Anteile siliziklastischen Materials, insbesondere Aluminium-, Eisen- und Titan-Konzentrationen, wurden für die Bestimmung des Terrigeneintrags herangezogen. Die Elementverhältnisse geben Auskunft über den Transport des terrigenen Materials, das hauptsächlich durch die Westwinde eingetragen wurde.

Die Interglaziale sind im allgemeinen durch geringere Produktivität und Terrigenzufuhr gekennzeichnet. Während der interglazialen Isotopenstadien 1 bis 7 lag die maximale Ausdehnung der Subtropischen-Konvergenz-Zone südlich von etwa 49°S. In den Isotopenstadien 9 bis 13 spiegelt eine gesteigerte Produktivität den verstärkten Einfluss Subantarktischen Oberflächenwassers an der südlichen Station 1171 wider, was auf eine nördlichere Position der Subtropischen-Konvergenz-Zone und des Westwindgürtels hindeutet.

Während der Glaziale war das gesamte Frontensystem, Subtropische-Konvergenz-Zone und Subantarktische Front, deutlich nach Norden verschoben. Östlich von Tasmanien lag die Subtropische-Konvergenz-Zone zwischen 42°S und 39°S, westlich von Tasmanien zwischen 44°S und 40°30'S. Während der frühen glazialen Isotopenstadien 8, 10 und 12 lag die Subantarktische Front nördlich der Kernstation 1171, worauf reduzierte Produktivitätswerte schließen lassen. Generell war die glaziale Bioproduktivität im nährstoffreichen Subantarktischen Oberflächenwasser um ein Vielfaches erhöht und wurde hauptsächlich durch die verstärkte Eisenzufuhr (Windeintrag) gesteuert, womit die gängigen Modelle der „Eisendüngung" auch für das Untersuchungsgebiet gelten.

Zusammenfassend lässt sich sagen, dass das ozeanographische Frontensystem im Tasmanischen Seeweg während der letzten 500.000 Jahre starken Schwankungen im Glazial-Interglazial-Wechsel unterworfen war, überprägt von einer langfristigen Südwärtsverlagerung.

SAMENVATTING

Het doel van deze studie was de reconstructie van de positie van oceanografische fronten in het gebied rondom Tasmanië gedurende de laatste 500.000 jaar. Dit gebeurde op basis van veranderingen die zich door de tijd heen in de terrigene aanvoer en de marine productiviteit voordeden. Vier sedimentkernen van ODP-Leg 189 werden onderzocht: Kern 1168 (westelijke Tasman Margin), Kernen 1170 en 1171 (Tasman Rise), en Kern 1172 (oostelijk Tasman Plateau).

Veranderingen in de samenstelling van de sedimenten werden onderzocht met behulp van verschillende proxies, die variaties in het oceanografisch frontensysteem weergeven. Bij het bepalen ven de exportproducitvteit werd gebruik gemaakt van de accumulatie van carbonaat, organische koolstof, biogeen barium en chlorine. Nooit eerder werd chlorine als productiviteitsproxy in de zuidelijke Oceaan toegepast. De terrigene toevoer werd bepaald aan hand van de hoeveelheid siliciclastisch materiaal, gemeten door middel van de concentraties van aluminium, ijzer en titaan. De onderlinge verhoudingen tussen deze elementen geven aanwijzigen over het transportmechanisme van het terrigene materiaal, met name windtoevoer.

De interglacialen worden over het algemeen gekenmerkt door een beperktere productiviteit en terrigene toevoer. Tijdens de interglaciale isotopenstadia 1 - 7 bevond de Subtropische Convergentie zich ten zuiden van 49°S. De toegenomen productiviteit tijdens isotopenstadia 9 - 13 weerspiegelt een versterkte invloed van subantarctisch oppervlaktewater over de zuidelijke locatie van kern 1171. Dit duidt op een meer noordelijke positie van de Subtropische Convergentie en de zone van westelijke winden.

Tijdens de glacialen was het volledige frontensysteem duidelijk meer naar het noorden verschoven. Ten oosten van Tasmanië bevond de Subtropische Convergentie zich tussen 42°S en 39°S, ten westen van Tasmanië tussen 44°S en 40°30'S. De lagere productiviteit tijdens de glaciale isotopenstadia 8, 10 en 12 doet vermoeden dat het Subantarctisch Front ten noorden van de locatie van kern 1171 lag. De hoge glaciale productiviteit in het nutriëntrijke subantarctische oppervlaktewater werd voornamelijk veroorzaakt door extra toevoer van ijzer, aangevoerd door sterkere westelijke winden. Deze waarnemingen bevestigen dat de "ijzerhypothese" voor het onderzochte gebied van toepassing is.

Samenvattend kan gesteld worden dat sterke glaciale/interglaciale veranderingen het oceanografische frontensysteem in het gebied rondom Tasmanië bepaald hebben. Gedurende de laatste 500.000 jaar heeft een algemene verschuiving van het frontensysteem naar het zuiden plaats gevonden.

1. INTRODUCTION

The Southern Ocean connects the water masses of the major ocean basins: Atlantic, Pacific and Indian oceans. Therefore, it is one of the key areas influencing global climate dynamics. In the Southern Ocean, the Antarctic Circumpolar Current (ACC) is the main current. It surrounds the Antarctic continent without any barrier, and climatically isolates Antarctica. The ACC is driven by strong westerly winds, which also promote the development of the surface ocean frontal systems bounding the ACC. Three main fronts are defined: the Subtropical Convergence (STC) to the north of the current ring, the Subantarctic Front (SAF) within it and the Antarctic Polar Front (APF) to the south (Withworth, 1988). These frontal systems are highly dynamic today. On geological timescales, they were displaced to the north during glacial and to the south during interglacial periods (e.g. Howard & Prell, 1992; Francois et al., 1993; Connell & Sikes, 1997; Frank et al., 2000). The late Pleistocene frontal dynamics are well constrained in the Atlantic sector of the Southern Ocean (e.g. Peterson & Whithworth, 1989; Brathauer & Abelmann, 1999; Frank et al., 2000). The paleo-dynamics of the system was addressed only by a few studies in the Indian and Pacific sectors of the Southern Ocean (Fig. 1). They mainly focus on the response of pelagic microfossil assemblages (Morley, 1989; Nees, 1997; Kawagata, 2001). Other papers considered the last glacial cycles, back to marine isotopic stage 6 (MIS 6) (Bareille et al., 1994; Howard & Prell, 1994; Ikehara et al., 2000).

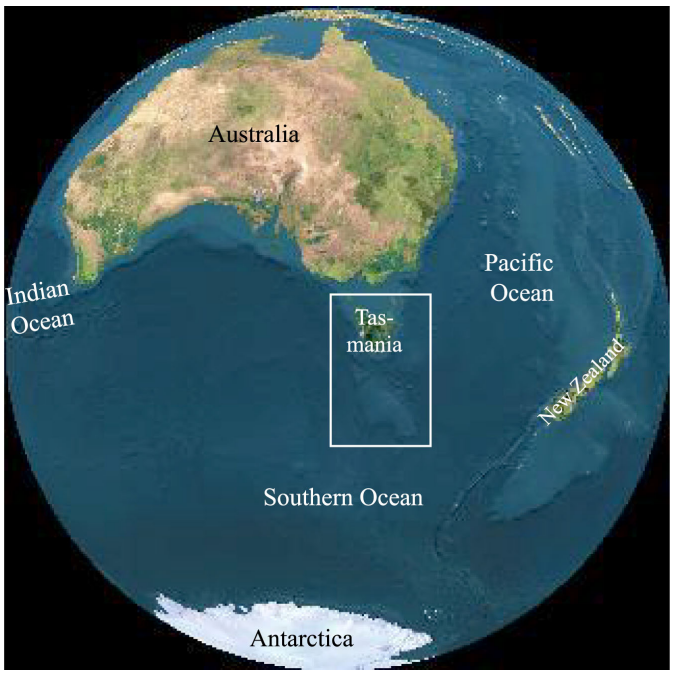

Fig. 1 View of the Australian sector of the Southern Ocean from outer space (Height: 2500 km). The white rectangle indicates the study area.

The area around Tasmania is one of the few places in the Southern Ocean where well-preserved, continuous and carbonate-rich Cenozoic sediment successions are present at latitudes of 40-50°S (Exon et al., 2001). They were explored during the Ocean Drilling Program Leg 189 in March-May 2000 (Exon et al., 2001). Four of the ODP-Leg 189

sites were studied. Those sites were drilled in water depths from 2100 m to 2800 m off Tasmania (Fig. 2): Site 1168 lies on the western Tasmania margin, Sites 1170 and 1171 on the Tasman Rise and Site 1172 on the East Tasman Plateau. This study focus on the dynamics of surface water productivity, variations in terrigenous supply, oscillations in subtropical and polar fronts, and changing strength of surface currents in the Tasman region as the result of climatic changes over the last 500 000 years.

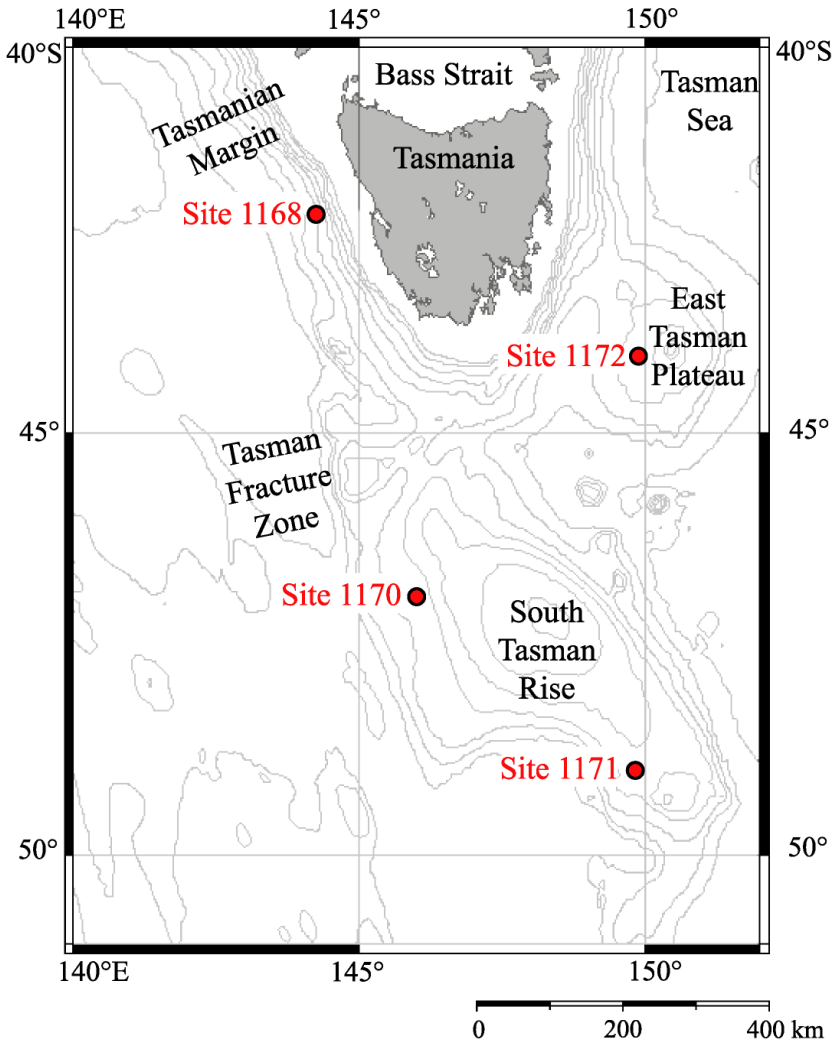

Fig. 2 Detailed map of the locations of the four studied sites. All sites were drilled during ODP Leg-189. Site 1168 is situated west of Tasmania, on the western Tasman Margin, sites 1170 and 1171 lies to the south, on the Tasman Rise and site 1172 lies on the East Tasman Plateau. Map created by GMT (http://www.aquarius.geomar. de/cgi-bin/map-cgi.pl).

1.1 Previous work in the study area

Estimates of paleo-productivity and terrigenous supply are presented in this study. In pelagic sediments, the surface ocean productivity is often reflected in the carbonate content. Systematically lower carbonate content concentrations during the glacials were reported from sediment cores to the south of Tasmania (e.g. Martinez, 1994; Connell & Sikes, 1997). The total organic carbon (TOC) measured to the south of Tasmania shows a maximum during the Last Glacial Maximum (LGM) (Ikehara et al., 2000). Since the carbonate content can be influenced by dissolution or dilution, we used additionally proxies to constrain productivity changes, in particular organic carbon, chlorin-pigment and excess barium. A new proxy for the paleo-productivity is pigment concentrations (Harris et al., 1996). They correlate with the total organic carbon concentrations (e.g. Bishop, 1988; Emerson & Hedges, 1988). Excess barium is suggested as a paleo-productivity proxy in the Atlantic Sector of the Southern Ocean by Gingele & Dahmke (1994) and by Nürnberg et al. (1997). Nürnberg et al. (1997) also demonstrated that sediment-geochemical studies are valuable in defining paleo-positions of oceanographic fronts.

The Southern Ocean marine productivity is of particular importance for the global ocean because it comprises up to a third of the entire world's ocean productivity (Berger & Herguera, 1992). However, the Southern Ocean is not as productive as expected from the abundance of nutrients (Landing & Bruland, 1987). The lack of iron, as stated in the iron hypothesis by Martin (1990), could be the reason for this discrepancy. In order to constrain this deficit and possible relationships, the terrigenous supply was quantified, by means of aluminium, iron and titanium concentrations and the percentage of siliciclastic material. Several studies reported a higher terrigenous flux in the Southern Ocean during glacial periods (Petit et al., 1990; Hesse, 1994; Lean & McCave, 1998; Latimer & Filippelli, 2001). For this terrigenous matter different sources are discussed. Latimer & Filippelli (2001) suggest that the iron flux has a hemipelagic origin. Hesse (1997) instead, discussed an eolian origin. In order to address this problem, we attempted to define the origin of the terrigenous matter for the Australian sector of the Southern Ocean. Observations from continental Australia suggest arid climatic conditions during glacials with intensification in frequency and velocity of winds that may cause this increase in terrigenous supply (e.g. Thiede, 1979; McTainsh & Lynch, 1996; Okada & Wells, 1997).

The switch in wind pattern during the glacial periods effectively influenced the position of the frontal system. The studied cores are located around the present position of the STC. Marine productivity showed a maximum during glacial times in the Atlantic sector (e.g. Nürnberg et al., 1997; Latimer & Filippelli, 2001), the Indian sector (e.g. Prell et al., 1979; Morley, 1989) and the Pacific sector (e.g. Fenner et al., 1992; Kawagata, 1999) of the Southern Ocean. Late Pleistocene fluctuations of the position of the STC around Tasmania are roughly outlined by Passlow et al. (1997). Therefore, the reconstruction of glacial/interglacial variations of the STC since the last 500 ka is the main aim of the presented study.

1.2 Research objectives

As described above, the primary aim of the thesis was to provide insights in the changing oceanographic frontal system in the Australian sector of the Southern Ocean during the last 500 ka. A multi-proxy approach was conducted to reconstruct the first geochemical history in that particular area. Other major questions addressed during this thesis are following topics:

- Assess marine productivity through time from various proxy data.
- Identify glacial/interglacial paleo-indicator patterns.
- Define sources, transport paths and forcing of the terrigenous supply.
- Reveal the interplay between marine productivity and terrigenous flux; what is the role of iron fertilization due to dust supply?
- Study of the glacial/interglacial variations in oceanographic front systems (e.g. Subtropical Convergence), and in the surface currents around Tasmania (e.g. East Australian Current).

2. GEOLOGIC AND OCEANOGRAPHIC SETTINGS

2.1 Regional geological settings

The continental slope west of Tasmania ranges from a depth between 200 m and 4000 m with an average slope of 4°. The slope is underlain by continental basement. Oligocene to recent pelagic carbonates cover Upper-Cretaceous and Palaeogene shallow marine sandstone, siltstone and mudstone. They are widely distributed in the deep waters west of Tasmania. Between Australia and Tasmania, the Bass Strait forms a shallow shelf channel. This strait connects the Great Australian Bight and the Tasman Sea (Fig. 2). At present, nearly no sedimentation takes place on the continental shelf around Tasmania (e.g. Moore et al., 1992; Kawahata, 2002).

The Tasmanian offshore region is build up of continental crust from three different regional areas: the East Tasman Plateau (Exon et al., 1997), the Tasmanian margin (Moore et al., 1992) and the South Tasman Rise (Hinz et al., 1985) (Fig. 2). The East Tasman Plateau (ETP) forms a flat circular platform at 2600 m below sea level. It is surrounded by oceanic crust and underlained by continental basement rocks. The top of the plateau is formed by a seamount, rising till 1800 m. It has developed as the result of hot spot volcanism. The plateau is covered by Oligocene to Holocene pelagic carbonates and Cretaceous to Eocene siliciclastic sediments (Nees, 1997). To the east and south, the margin of the ETP is steep and well outlined by a narrow channel (Royer & Rollet, 1997). The ETP is separated from southeast Tasmania, by the 3200 m deep East Tasman saddle.

The South Tasman Rise (STR) is a large submarine plateau of continental origin. Though situated south of Tasmania, it is in fact part of the Australian continent. The STR is oriented northwest-southeast and rises to 1000 m below sea level. It is surrounded on three sides by Late Cretaceous and Palaeogene oceanic crust (Exon et al., 1997; Royer & Rollet, 1997). The WNW-trending South Tasman Saddle, that separates the STR from Tasmania, is more than 3000 m deep and filled with sedimentary and volcanic deposits. The flanks of the STR are characterised by dominantly pelagic deposits that are reworked as slumps, mass-flow and gravity-flow deposits (Whitmore & Belton, 1997). The Tasman escarpment, the northernmost part of the Tasman Fracture Zone that extends south to Antarctica, dominates the western side of the STR. This scarp is up to 2000 m high (Connell & Sikes, 1997). It separates the area south of

the South Tasman Rise from the rough uncovered crust to the west. The fracture zone is related to Late-Cretaceous to Early-Cenozoic extensional tectonism (Exon et al., 1997). To the west of the Tasman Fracture Zone, the oceanic crust is characterised by numerous horst and graben features, which are east-west oriented.

2.2 Oceanographic settings

2.2.1 General overview

Several global current systems meet at the study area, all at a specific water depth. The water masses are characterised by their oxygen concentration, temperature, salinity and density (e.g. Peterson & Whithworth, 1989). Table 1 provides an overview of present water masses, their abbreviations, and distinguishing marks. The different surface water masses, separated by oceanographic fronts are depicted in Figure 3. In contrary, Figure 4 shows the deeper water masses, discussed later in this chapter.

Tab. 1 Characteristics of major water masses and fronts of the Southwest Pacific Ocean. PSU = Practical Salinity Unit; SuSuI = summer surface isotherm (Tchernia, 1980; Passlow et al., 1997; Cooke et al., 2002).

	Water Mass/Front		Abbr.	Depth [m]	Temp [°C]	σ-Density	Salinity [psu]	Oxygen [ml/l]
Surface water masses	Subtropical Surface Water		STSW	0-400	> 15	-	-	-
	Subtropical Convergence (Front)		STC	Separates STSW from SASW at 15° SuSuI				
	Subantarctic Surface Water		SASW	surface	8-15	-	-	-
	Subantarctic Front		SAF	Separates SASW from CSW at 8° SuSuI				
	Circumpolar Surface Water		CSW	surface	5-8	-	-	-
	Antarctic Polar Front		APF	Separates CSW from Antarctic Water, icebergs present				
Deep water masses	Subantarctic Mode Water		SAMW	400-600	6.0-10.0	26.8-27.2	34.0-34.2	
	Antarctic Intermediate Water		AAIW	600-1450	3.2-7.0	27.2-27.4	34.3-34.4	3.2-4.7
	Circumpolar Deep Water	Upper	CPDWu	1450-2900	1.6-1.8	36.5-37.0	34.6-34.7	3.0-3.4
		Lower	CDPWi	2900-seafloor	0.6-1.6	37.0-46.0	34.7-34.8	3.6-4.7
	North Atlantic Deep Water		NADW	-	0.6-0.9	-	<34.7	-
	Antarctic Bottom Water		AABW	-	-0.9	-	34.6-34.7	-

The Antarctic Circumpolar Current (ACC) is the main global current, connecting all major oceans and influences different depth intervals in the southern hemisphere (Withworth, 1988). It is the most powerful current, driven by the strong westerly winds between 45° and 55°S (Gordon, 1988). There are no landmasses to slow down, break up or deviate this great continuum stretch of seawater. Due to minor density variations with

depth, the ACC is almost barotropic. Therefore pressure changes are able to reach the ocean floor and the influence of the current is noticeable also at striking depths. This means that the overall mass transport of the ACC contains also a vertical component (Rintoul, 1998).

2.2.2 Frontal System

The surface water masses are separated by frontal systems, with distinct oceanographic characteristics, forming in response to wind stress (e.g. Klinck & Smith, 1993; Hesse & McTainsh, 1999). As the wind pattern changes during glacial/interglacial periods, the surface water masses exhibit variations. During the glacial times, the fronts are situated more to the north than during interglacials (e.g. Ikehara et al., 2000; Klinck &Smith, 1993; Lean & McCave, 1998). The fluctuations in the frontal system are studied here, therefore the present situation is described into detail. Actually all fronts in the Australian sector of the Southern Ocean lies more in the South as in the Indian Ocean (Tchernia, 1980; Orsi et al., 1995). From north to south, three fronts can be

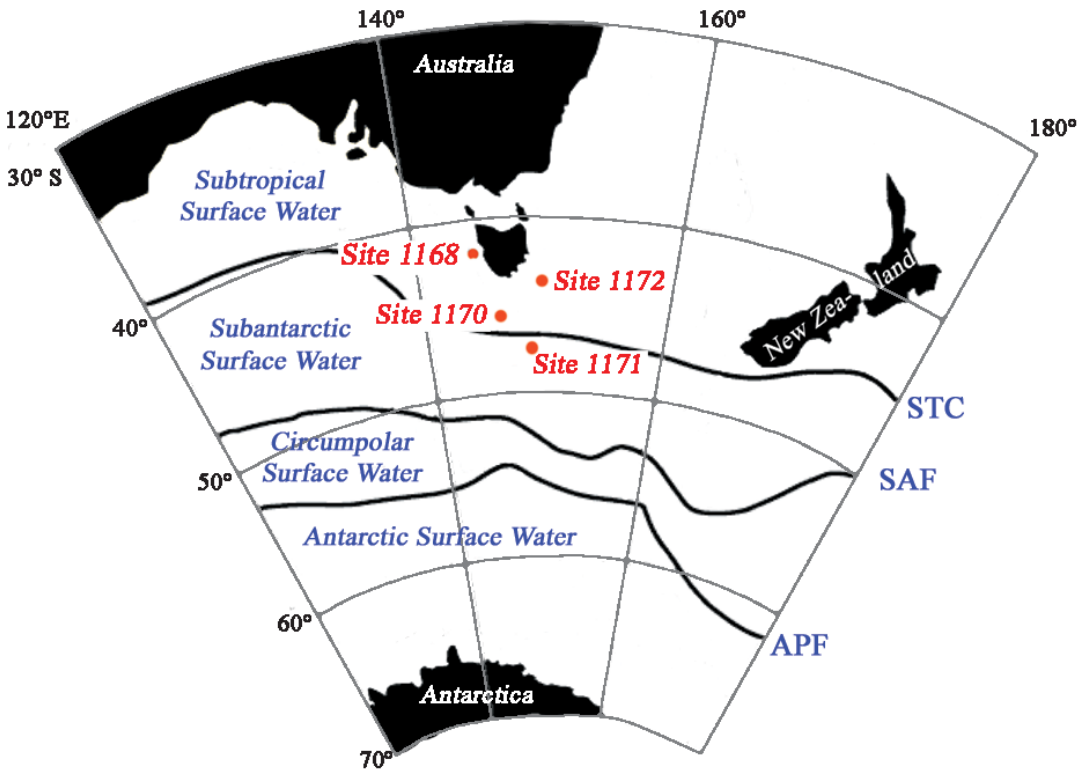

Fig. 3 Overview of the surface water masses and fronts in the Southern Ocean between Tasmania and Antarctica. Modified after Rintoul (1998). The four studied sites are indicated. STC = Subtropical Convergence; SAF = Subantarctic Front; APF = Antarctic Polar Front.

differentiated (Fig. 3). The northernmost is the Subtropical Convergence (STC, or Subtropical Front). It is the boundary between warm, saline, subtropical surface waters, driven by the southeast trade wind and cold, less-saline subantarctic surface waters driven by westerly winds (Rea & Bloomstine, 1986; Passlow, 1997). The STC is the northern boundary of the ACC, where Subantarctic waters prevails. In the Australian sector of the Southern Ocean, the STC separate the Subantarctic Current and the Tasman Current (Martinez, 1994). Between 43-47°S, the STC is displaced to the south when compared to the Indian Ocean (Tchernia, 1980; Creswell, 1987; Orsi et al., 1995). The STC is centred on 46°S and lies just south of the saddle between Tasmania and the southern Tasman Rise (Rintoul & Bullister, 1999). The STC shifts seasonally: in summer it follows the 15°C surface isotherm, in winter the 10°C surface isotherm (Garner, 1959). Remarkable is the close spacing of the isohalines within the STC (Villanoy & Tomczak, 1991). At the STC, a high seasonal phytoplankton production takes place, causing an enhanced biogene sediment flux to the seafloor (Francois et al., 1993).

The Subantarctic Front (SAF) marks the transition between subantarctic and antarctic water masses. It shows as well a seasonal variability. In the study area, the SAF is situated at 50-51°S, around 200 km south of the southern Tasman Rise (Rintoul & Bullister, 1999) (Fig. 3).

The southernmost frontal system in the study area is the Antarctic Polar Front (APF, Antarctic Convergence) at 54°S and therefore 200 km to the south of the SAF (Rintoul& Bullister, 1999). It is delineated by a strong surface temperature gradient. This causes the sudden death of many planktic species. Therefore, there is a high flux of nutrients to the ocean. The APF and STC are particularly key components of the sensitive, climatically relevant Southern Ocean (Howard & Prell, 1992).

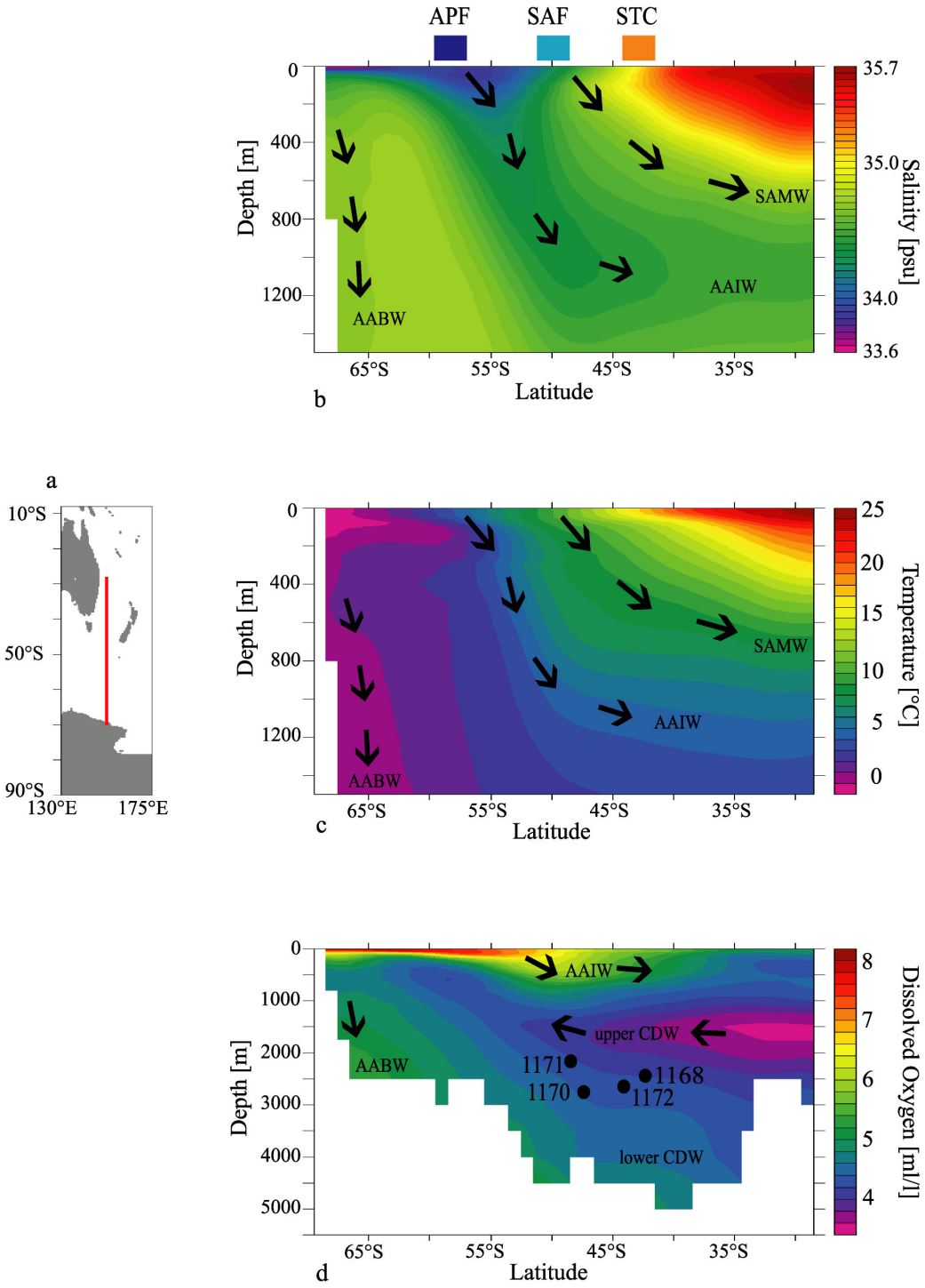

Fig. 4 Modern distribution pattern across a north-south transect to the east of Australia and Tasmania (a), modified after Levitus (1982): the salinity (austral summer) (b); water temperature (annual mean) (c); and dissolved oxygen (annual data) (d).
The plots clearly show the formation of Antarctic Intermediate Water (AAIW) and Subantarctic Mode Water (SAMW). Front structure of surface water is also visible. Water masses, currents, and Leg 189 sites are indicated.
APF = Antarctic Polar Front; SAF = Subantarctic Front; STC = Subtropical Convergence
CDW = Circumpolar Deep Water; AABW = Antarctic Bottom Water.
Note: Depth scale in lowermost image (d) is different.

2.2.3 Water Masses

Surface Water Masses

Different surface water masses characterise the study area (Fig. 3). From north to south they show following marks. The nutrient-rich Subtropical Surface Water (STSW), situated between the STC and SAF. South of the STC, the cooler nutrient-poor Subantarctic Surface Water (SASW) is driven eastward across the South Tasman Rise. This is caused by the prevailing westerly winds as the northern part of the ACC. The SASW extend to great depths, sweeping the seabed even at 2000 m in certain places (Orsi et al., 1995). The well-ventilated and cool water of the Circumpolar Surface Water (CSW) is situated between the SAF and APF. The Antarctic Surface Water (AASW) is influenced by ice melting in the summer. Therefore the water mass prevails characteristics of low temperature and low salinity. The influence of the AASW can be traced within the upper 150 m of the water column.

Intermediate Water Masses

Two main intermediate water masses are differentiated in the study area, both are formed under the influence of the STC. The Subantarctic Mode Water (SAMW) is present at a depth from 400-600 m and is situated north of the SAF (Morris et al., 2001) (Fig. 4). The SAMW is an almost isothermal (8-10°C), 200 m thick and well oxygenated subsurface layer. It originates in the southeast Pacific Ocean between 43-48°S (Kawagata, 1999).

The most extensive and important water mass at intermediate depths in the world ocean is the Antarctic Intermediate Water (AAIW). It is formed along the APF and deepens away from the front down to 1500 m water depth (Tomczak & Godfrey, 1994). The AAIW has an oxygen saturation level of up to 95%, where the high-oxygen level originates south of the APF. In the study area, it is beneath the Australian Subantarctic Water.

Deep Water Masses

The Circumpolar Deep Water (CDW) lies beneath the AAIW and flows northward into the Pacific (Fig. 4). It is composed out of water from the Weddell Sea (45%), the Pacific and Indian Ocean intermediate water masses (30%) and deep water from the NADW

(25%) (Rutberg et al., 2000). Within the CDW, three distinct units are defined: the upper CDW (CDWu), the lower i CDW (CDWi) and the lower ii CDW (CDWii).

The North Atlantic Deep Water (NADW) is formed in the North Atlantic Ocean, from where it flows down south through the Atlantic Ocean and rises in between 40° and 50°S to become part of the ACC (Peterson & Whithworth, 1989). It is a young and high-oxygenated current. Remnants of the NADW are overlying the AABW (Rutberg et al., 2000).

Bottom Water Masses

The Antarctic Bottom Water (AABW) is formed by the vertical convection along the Antarctica continental shelf, caused by the freezing of sea ice (Tomczak & Godfrey, 1994). It is mainly formed in the Weddell and Ross Sea. The cool and dense water sinks to the bottom and mixes with water of the ACC and the NADW (Kolla et al., 1976). After reaching the seafloor, the AABW flows northward and can be traced into all ocean basins, even in the northern hemisphere. In the study area, the AABW spreads deeper than 4000 m and shows a lower salinity, lower temperature and higher oxygen content, in comparison with the CPDW (Orsi et al., 1995; Harris et al., 1999). The studied sites are with a maximum depth of 2700 m above this bottom water masses.

2.2.4 Surface currents

The described water masses are present in the whole Southern Ocean. Apart from those water masses there are several local current systems in the study area (Fig. 5). The East Australian Current (EAC) dominates the present surface circulation in the western Tasman Sea. The EAC originates in the Coral Sea and runs southward along the east coast of Australia. It transports high temperature (20-26°C) and low salinity (35.4 -35.6) waters from the equatorial region in a narrow band, southwards into the Tasman Sea, sometimes as far as 42°S (Macaulay, 2000). The EAC is still present in a depth of at least 200 m. Beneath the EAC, there is a compensating northward current. The meandering EAC becomes unstable near Tasmania, and forms anti-cyclonic eddies. They usually mix the water column down to a depth of 400 m and may even affect the thermal structure down to 1300 m.

The Leeuwin Current originates at the western Australian coast. It transports warm, low saline, and nutrient-depleted tropical waters from northwest Australia southward to

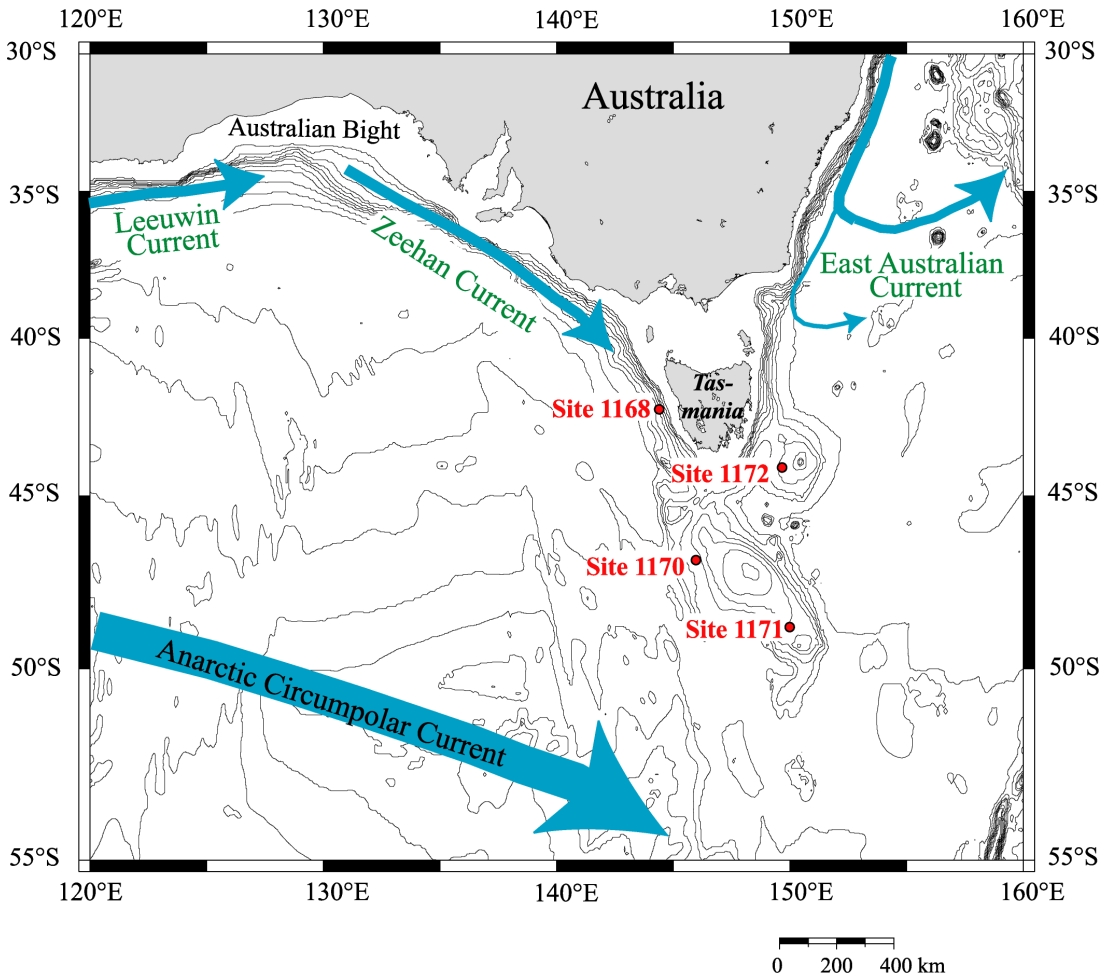

Fig. 5 This map is showing the surface currents around Tasmania. The Antarctic Circumpolar Current is also indicated. The four studied sites are shown in red.

Cape Leeuwin and then turns eastwards into the Great Australian Bight. In the North, the Leeuwin Current is broad with a width of more than 200 km, but its depth is limited to only 50 m. Further south, it deepens and becomes a relatively narrow current with a whereas its width diminishes to less than 100 km. The Leeuwin Current is mainly driven by the prevailing westerly winds in winter (Godfrey et al., 1986).

Within the Australian Bight, the seasonally changing wind-induced current along the shelf edge is composed of the Leeuwin Current in the western part. The Zeehan Current is the remnant of the Leeuwin Current, running down the Tasmanian west coast. It is about 40 km wide and 50 m deep. During winter the Zeehan Current even rounds southern Tasmania, moving up the east coast and merging with the remnants of the EAC (Baines et al., 1983; Thompson & Veronis, 1983; Cresswell, 2000). Together they

are flowing into the Tasman Sea. In the summer period, the EAC and Zeehan Current converge off southern Tasmania before fading into the Southern Ocean.

The Flinders current is a current beneath the Leeuwin and South Australian currents. It is flowing northwest and is the northern part of a large anticyclonic deep ocean gyre. This cold and nutrient-rich water can move onto the shelf when the Leeuwin Current weakens during summer (James et al., 2001).

3. MATERIAL AND METHODS

3.1 Material

Late-Quaternary sediments from four ODP-sites from Leg 189 in the Australian sector of the Southern Ocean were considered in this study. The campaign took place in spring 2000 (Exon et al., 2001). Leg 189-Site 1168 is situated on the western Tasmania margin, Sites 1170 and 1171 on the Tasman Rise and Site 1172, on the East Tasman Plateau (Fig. 2; Tab. 2). The two northernmost sites (1168 and 1172) drilled during Leg 189 are located in temperate (cool subtropical) waters north of the present-day position of the Subtropical Convergence (Fig. 2). The southern sites (1170 and 1171) investigated in this study are located in subantarctic waters between the Subtropical Front and the Subantarctic Front (Exon et al., 2001). The area drilled during Leg 189 therefore lies, at present, north of and straddling the Subtropical Front and south to the region near the Subantarctic Front. The Polar Front lies farther to the south of our southernmost site. All cores are situated at present above the carbonate-compensation depth (Thunell, 1976; Tomczak & Godfrey, 1994; Exon et al., 2001).

Though up to four holes were drilled at each site, only samples from the A-Hole were analysed. By using different series from shipboard and shore-based taken samples, a final resolution of 5 cm sample spacing was achieved over the uppermost 10 to 13 m of the cores (Tab. 2). For the main interpretation, only samples from the last 500 000 years (500 ka) were considered.

Tab. 2 Location of the investigated cores, maximum sample depth and the number of investigated samples.

Site	Latitude [°S]	Longitude [°E]	Water depth [mbsl]	Maximum sampling depth [mbsf]	Number of samples
1168A	42°36.581'	144°24.762'	2463	10.25	199
1170A	47°09.044'	146°02.988'	2704	12.60	250
1171A	48°29.966'	149°06.690'	2148	10.05	198
1172A	43°57.585'	149°55.969'	2622	10.73	211

Aboard of “RV Joides Resolution”, several measurements were directly performed. In this study, following shipboard data with a sampling of 2 cm are used: the lightness (L*) from spectrophotometer measurements, and the GRAPE density from multi-sensor core logging (Exon et al., 2001). The lightness is known to coincide with the amount of carbonate in the cores. A comparison between both parameters was performed. Each

150 cm, i.e. once per core section, the dry bulk density was measured and used here for accumulation rate calculations. The sediments consist mainly of nannofossil oozes with a high foraminifer content.

3.2 Methods

To reconstruct the glacial/interglacial changes in the Tasman Sea, different environmental proxies describing the paleoproductivity and terrigenous supply were used. For assessing paleoproductivity, the amount and accumulation rates of organic carbon, carbonate, chlorin, and Ba_{exc} were determined. Ti, Al, Fe and the calculation of the amount of siliciclastic material defined the terrigenous flux. This data were accomplished by shipboard logging data as mentioned above (Section 3.1).

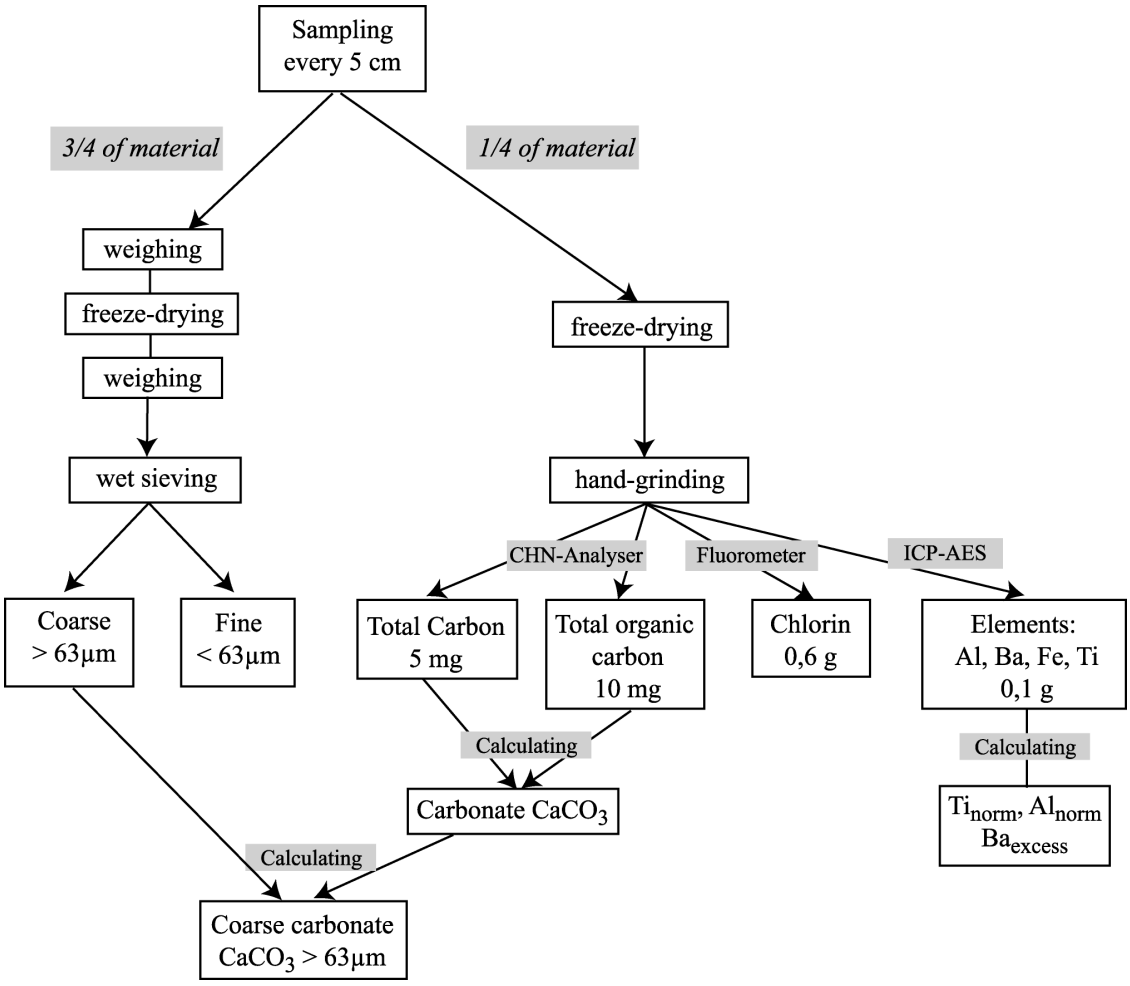

Fig. 6. Flow chart showing the different steps proceeded during the handling and analysis of the samples for this study. For the hand-grounded material on the right side, the amount of sediment, necessary for each analysis is indicated

The different steps performed during this study are shown in the flow-scheme (Fig. 6). First, the samples were divided into two parts:

- One fourth of the material was freeze-dried and grinded in an agate motar for the chemical analysis. The concentration of organic carbon (TOC), total carbon (TC), pigments, and the elements Al, Fe, Ti and Ba were measured.
- The other part (3/4) was also freeze-dried. Then it was weighed and washed through a sieve with a 63-µm mesh. The residues were dried, weighed again and the proportion of the coarse and fine (<63 m) material was assessed.

3.2.1 Carbonate and organic carbon

In this study, the determination of $CaCO_3$ was done with the separation of the inorganic and organic carbon. First, the total amount of carbon (TC) was measured. Therefore, 5 to 6 mg of freeze-dried, ground material was weighed into a tin vial. Second, for the determination of the organic carbon (TOC), 10 mg was weighed into a silver capsule. By adding a 10% HCl-solution to this capsule, the inorganic component reacted with the acid. The addition of HCl was repeated until visually no more CO_2 was observed. The sample was dried by 70°C. The determination of the carbon was done with a CARLO ERBA NA 1500 CN analyser at GEOMAR. The vials were combusted at 1000°C in a stream of oxygen. Helium was used as a carrier gas and the oxygen was removed. The reduced gases were separated by gas chromatography and registered with a thermal conductivity detector.

The carbonate content was calculated using the following formula, :

$$CaCO_3 = 8.333 \cdot (TC - TOC)$$

Results are given in weight percent of the whole rock.

To reduce the errors due to the sample in-homogeneities and balance display variations, all samples were measured twice to produce an average value. Each run on the CN analyser consisted of 19 samples (double measurements), three blank positions, one internal standard sample, four measurements of Acetanilide (as the National Bureau of Standards certified standard reference) and four positions of soil standard, which are taken of the same source throughout all measurements. Linear regression of carbon versus area counts was computed (least-squares method) for the soil standard and Acetanilide to evaluate the variations of each run. The internal standard sample for TC

(n=77) gave a concentration of 11.29±0.023 % and for TOC (n=25) 0.228±0.014 %. The reproducibility of TC is 0.204 % and therefore around 2 %. For TOC it lies with a one-sigma value of 0.035 % by 15 %.

The sand content of deep-sea carbonates is a sensitive indicator of changes in carbonate dissolution (Bickert, 1992; Broecker & Clark, 1999). The sand content (foraminifer shells) decreases as dissolution progresses (Haug & Tiedemann, 1998). The foraminifer proportion of the carbonate fraction is calculated by using the following formula:

$$\%\, coarse\ carbonate = \frac{\%\, coarse material}{\%\, carbonate} \cdot 100$$

The percentage of siliciclastic material was calculated using the following formula:

$$\%\, siliciclastic\ material = 100 - (\%\, carbonate + \%\, TOC + \%\, opal)$$

Opal has been analysed on about 50 samples from all four cores (according to the method of (Müller & Schneider, 1993). Unfortunately, the amount of opal in the sample was below the detection limit of the method (2% opal). Hence, the amount of is neglected in the formula above.

3.2.2 Chlorin

Chlorins largely reflect marine productivity, since terrestrially derived chlorophyll degradation products rapidly deteriorate and commonly do not contribute to the chlorin concentrations measured in the pelagic realm (pers. com. C. Schubert, EAWAG, Limnological Research Centre, Switzerland, January 2001). Chlorins do include a whole suite of degradation products of phytoplanktonic chlorophyll (Harris & Maxwell, 1995). They are strongly criticized due to problems in preservation and remineralisation in the upper water column and after deposition. The main decomposition of chlorins in the sediment takes place in the upper centimetre and therefore soon after deposition (Schönfeld, 2001). However, from comparison with accepted proxies of paleoproductivity (e.g. Opal, TOC), it appears that chlorin concentrations in deep-sea sediments reliably reflect variations in primary productivity, although we do not know if the response is linear (Harris et al., 1996; Kowalewska et al., 1999). This primary productivity is mainly controlled by the availability of nutrients in the surface water. The chlorins in extracts of the sediments are entirely transformation products of

chlorophyll a and consist mainly of phytins and phorbides, which have similar characteristics in u.v./vis absorption spectra (Harris et al., 1996).

The determination of chlorins is done on two probes of each 0.6 g grinded sample material (double measurements). The chlorins are extracted with acetone in three steps under sonication and subsequent centrifugation. The samples are cooled with ice after each extraction. The analysis is always done under low light conditions to prevent decomposition of the chlorins. Sediment extracts are measured with a TD-700 fluorometer (GAT) immediately after the third extraction. Chlorophyll-a (sigma), which is acidified with 2 ml of hydrochloric acid, is used as a standard. Every twelfth measurement, an internal standard sample was measured to check the extractions and the drift of the fluorometer. For Site 1168, the internal standard (n = 26) gives a mean chlorin concentration of 113.63±4.49 ng/g. The internal standard sample of Site 1172 (n = 26) gave a concentration of 403.55±7.59 ng/g. Hence, the reproducibility of the method is roughly 10 %.

3.2.3 Major Elements and Barium

The concentration of Al, Ti and Fe in pelagic sediments is considered as a proxy for continental input (Bareille et al., 1994; Duce & Tindale, 1991). Aluminium is bound in aluminosilicate minerals, which are mostly detrital, although some Al can be derived from oceanic volcanic rocks, hydrothermal exhalations and authigenic growth. Titanium is much less abundant than Al and restricted to certain minerals like ilmenite, rutile, titano-magnetite and augite. In many open-ocean environments Ti is dominantly hosted in aluminosilicate phases, added through eolian processes, and generally immobile after deposition (Murray et al., 1993; Murray & Leinen, 1996). Titanium can also be bounded to volcanic material. Iron in pelagic and semi-pelagic sediments is mainly bound to clays, and therefore to detritic components too, and present in authigenic minerals (Wedepohl, 1971).

Barium in sediments is mostly present as barite, which is formed, when particulate organic matter is descending to the bottom through the water column (Dehairs et al., 1980). Barite contributes up to 90 % of the total Ba concentration into the pelagic sediment, while clastic material provides an important source of Ba closer to the continent (Gingele & Dahmke, 1994). Dymond et al. (1992) estimate that around 70 % of the produced biogenic Ba in the water column, is lost to the bottom deposits by

dissolution. The amount of terrigenous Ba remains comparably constant. Biogenic barium (Ba_{exc}) allows estimations of export- and primary productivity (Francois et al., 1995). Despite the unsolved problem of how barite particles were actually formed in the water column, Ba_{exc} bears a high potential to reconstruct changes in ocean surface productivity through time (e.g. Lea & Boyle, 1989; Dickens & Owen, 1994; Nürnberg et al., 1997; Schroeder et al., 1997; Frank et al., 2000).

For the determination of the major and minor elements of the bulk sediment, the sediment samples were dissolved by acid digestion. One hundred gram sample material was weighed directly into Savillex Teflon cups. The digestion was performed by applying together 2 ml HF-suprapur (40%), 2 ml HNO_3-suprapur (65%) and 3 ml $HClO_4$-analytic (60%) at 185°C for 8 hours. Subsequently, the acid was evaporated to almost dryness, and the residues were dissolved by 1 ml HNO_3 (65%), evaporated and then dissolved again with 1 ml HNO_3 and 5 ml deionised water. The cups were closed and heated at 140 °C for another 4 hours. Finally, the Teflon cups were filled up to 25 ml with deionised (Milli-Q) water and this solution was stored in pre-cleaned polyethylene bottles.

Measurements were carried out on an ISA JOBIN YVON ICP-AES. Four reference levels calibrate the instrument. From the acid digestion, the solution was diluted 1:10 with deionised yttrium-water. The yttrium (1:1000) in the water is used by the spectrometer as internal standard. It compensates irregular transport of the solution and voltage changes in the electric system. The used specific wavelengths of each measured element were for Al 308.215 nm, Ba 455.403 nm, Fe 238.204 nm and Ti 334.941 nm.

Tab. 3 The results of the standard samples with their standard error of mean (SDM) and standard deviations (SD) (p = 0.01). The reproducibility is within the official range (Manheim, 1976; Govindaraju, 1984).

		This study			Official	
		Mean	**SDM**	**SD**	**Mean**	**SD**
KH-2 n = 58	Al_2O_3 (%)	2.28	0.045	0.34	2.35	0.3
	FeO (%)	0.30	0.008	0.06	0.3	0.05
MAG-1 n = 23	TiO_2 (%)	0.78	0.006	0.03	0.75	0.07
	Ba (µg/g)	478	7.59	36.44	480	41
	FeO (%)	6.10	0.04	0.19	6.12	0.6

To control the accuracy of the acid digestion, on every series of 30 cups, one sample was doubled, a blank and two samples of international reference material (KH-2 and

MAG-1) were added. Table 3 gives an overview of the measured and defined concentrations for those two standards (Manheim et al., 1976; Govindaraju, 1984).

The reproducibility for the measurements at the ICP-AES is given by repeated measurements of an internal standard. After every tenth measurement, this standard was set in as a sample. For Al, the mean concentration of this internal standard (n = 79) was 20.30±0.18 mg/l, for Ba 19.4±0.13 mg/l, for Fe 40.81±0.42 mg/l and for Ti 1.98±0.02 mg/l. Therefore, all elements are roughly about ± 1 %. The doubled samples, prepared during the acid digestion, give further indications on the reproducibility. There is a good correlation for all measured elements as indicated by the correlation coefficient r (r > 0.98; n = 72; p = 0.01) (Fig. 7).

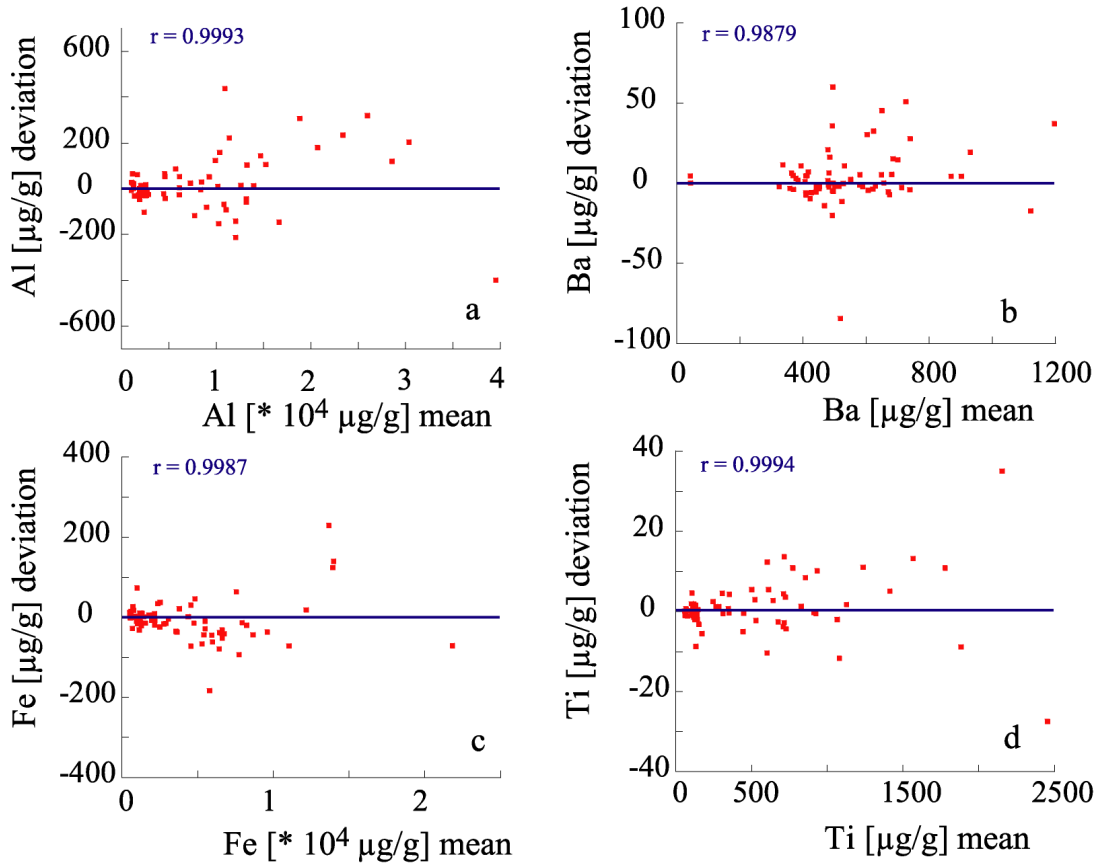

Fig. 7 The reproducibility of the ICP-AES analysis is proven by the duplicate measurements of 71 samples. The mean concentration of the two measurements is plotted against the standard deviation for the elements aluminium (a), barium (b), iron (c) and titanium (d). The correlation coefficients r, as well as the lines of zero deviation are shown for all four elements (n = 72; p = 0.01).

Al, Ti, Fe and Ba were analysed at the same time. Al, Ti and Fe give are indicators for the amount of terrigenous material. To assess the percentage of terrigenous material, the Al and Ti concentration were normalised for the average crust, Al: 83.99 µg/g and Ti:

5.31 µg/g (Taylor & Mc Lennan, 1985). The Al/Ti and Fe/Al ratios can be used to differentiate between different sources of terrigenous material (e.g. Taylor & Mc Lennan, 1985; Latimer & Filippelli, 2001).

In order to apply the Ba signal as a proxy for paleoproductivity the total barium was (Ba_{tot}) corrected for the non-biogenic portion inferred by terrigenous material (Dehairs et al., 1980; Schmitz, 1987; Dickens, 2001). Two different ways of correcting for the non-biogenic portion were applied.

In the first one, the Ba_{tot} content was normalised by Ti or Al, which are assumed to represent the terrigenous portion. Following calculation is applied:

$$Ba_{exc} = Ba_{tot} - Ti_{tot} \cdot \left(\frac{Ba}{Ti} \right)_{upper\ crust}$$

$$Ba_{exc} = Ba_{tot} - Al_{tot} \cdot \left(\frac{Ba}{Al} \right)_{upper\ crust}$$

Where Ba_{exc} is the biogenic barium, Ba_{tot} is the measured Ba, Ti_{tot} (Al_{tot}) is the measured Ti (Al) content of the sample and $(Ba/Ti)_{upper\ crust}$ or $(Ba/Al)_{upper\ crust}$ represents the ratios of average upper crust. Local values for this ratios were missing. Therefore the values mentioned by Wedepohl (1971) and McLennan (1995) were used. The Ba/Ti-ratio for the upper crust amounts 0.126 and the Ba/Al-ratio 0.0065. By calculation the Ba_{exc}, the Ba deposited from a terrigenous source is also defined by the second part in the formula.

The second way was to estimate the amount of 'background' barium (Ba_{bg}) in contrast to the barium provided by discrete barium particles. The normative barite content in the sediment is estimated by adding up the four main sediment constituents to a Ba_{bg}. The fixed barium values used for the calculations are 30 ppm for carbonate (Lea & Boyle, 1989), 120 ppm for biogenic silica, 60 ppm for particulate organic matter (Riley & Roth, 1971; Martin & Knauer, 1973), and 400 ppm for terrigenous matter. TOC measurements were used as a proxy for organic matter. The calculation of the portion of siliciclastic material represented the amount of terrigenous matter. Whereby Gingele & Dahmke (1994) proved that in carbonaceous cores, the detrital correction has little effect on Ba_{net} values.

$$Ba_{bg} = (30\ ppm \cdot \%\, CaCO_3 \div 100) + (120\ ppm \cdot \%\, opal \div 100) + (60\ ppm \cdot \%\, TOC \div 100) + (400\ ppm \cdot \%\, siliciclastic \div 100)$$

After subtracting the Ba_{bg} from the Ba_{tot} content, the resulting 'net' barium concentration (Ba_{net}) was attributed to biogenic barite.

$$Ba_{net} = Ba_{tot} - Ba_{bg}$$

3.2.4 Age model

To reconstruct temporal variations, a stratigraphic framework is necessary. Concentrations of a single sedimentary component can be diluted or enhanced by the sedimentation rates. For this reason, ages should replace depths and sedimentation rates should be taken into account. Later changes provide information on variations in the accumulation rate of each proxy. A discussion of the different approaches to construct the stratigraphy, is presented by Nürnberg et al (submitted).

The age model for Sites 1168 and 1170 is based on benthic oxygen isotope curves of the foraminifers (> 250 µm) *Cibicidoides wuellestorfi* and *Cibicidoides mundulus*. Accomplishing measurements on *Uvigerina peregrina* (Site 1168 only), and *Uvigerina pygmea* (Site 1170 only) were also taken into consideration. For selected depth intervals of Site 1168, stable isotope analyses were performed on planktonic species (*Globigerina bulloides*) from the 125-250 µm sediment fraction. The oxygen and carbon stable isotope analyses for Site 1172 were conducted on mixed benthic foraminifers of the genus *Cibicidoides*. The isotopic analysis of the sites were performed at different laboratories: Site 1168 at the Leibniz-Laboratory at the University of Kiel (Finnigan MAT 251 mass spectrometer), Site 1170 at GEOMAR (Finnigan MAT 252 mass spectrometer) and Site 1172 at the Lamont-Doherty Earth Observatory in New York (Optima mass spectrometer). The reproducibility for the measurements at both Kiel institutes was ± 0.08 ‰ for $\delta^{18}O$ and ± 0.04 ‰ for $\delta^{13}C$. Reproducibility at the Lamont-Doherty Earth Observatory laboratory is better than 0.08 ‰ and 0.06 ‰ for respectively $\delta^{18}O$ and $\delta^{13}C$.

For Sites 1168 and 1170, the oxygen isotope curves were graphically correlated with the stacked standard records from Imbrie et al. (1984), Martinson et al. (1987) and Shackleton et al. (1990). The nomenclature proposed by Prell et al. (1986) and

Tiedemann et al. (1994) was used to define the marine oxygen isotope events (MIS) at the sites. The age model of Site 1172 was established by correlating the measurements to the reference record of Shackleton et al. (1990).

For Site 1171, oxygen isotope measurements are not available. Therefore, the high-resolution lightness curve of that site was graphically correlated with the lightness data from Sites 1170 and 1172. By doing so, tie points were transferred from the two existing age models to that for Site 1171. They do not necessary match the standard oxygen isotope events.

3.2.5 Sedimentation and accumulation rates

Based on the age models described above, the sedimentation rates (SR in cm/kyr) for all sites were calculated using the following formula:

$$SR = \frac{depthB - depthA}{ageB - ageA}$$

In order to calculate mass-based accumulation rates (AR in g/cm^2 kyr) that are unaffected by depositional dilution, dry bulk densities (DBD; g/cm^3) are necessary (van Andel et al., 1975). In this study, the DBD's were calculated from the shipboard GRAPE density records, where GRAPE stands for the measurements done at the Gamma Ray Attenuation Porosity Evaluator on board of JOIDES Resolution. Those GRAPE density records show a clearly defined relationship to single DBD-measurements (Fig. 8). The product of DBD and SR yields bulk accumulation rate (AR; g/cm^2 kyr). In turn, individual elemental accumulation rates are calculated from:

$$AR_{element} = \frac{AR \cdot weight\%_{element}}{100}$$

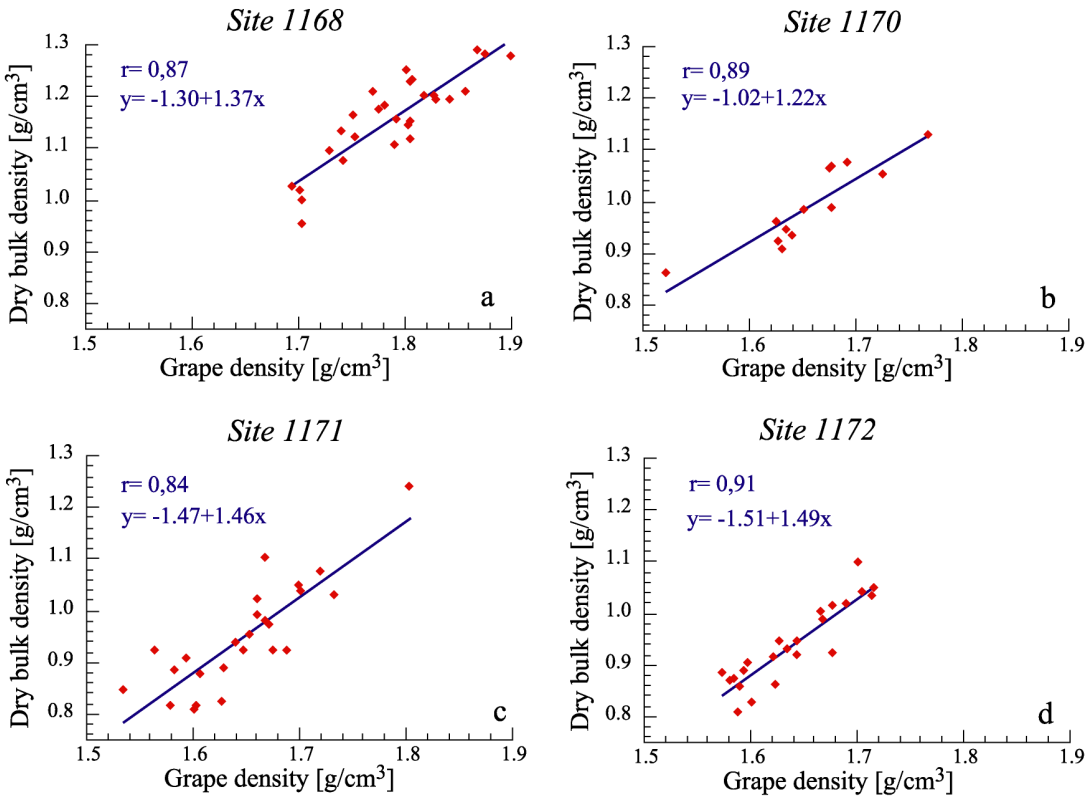

Fig. 8 The shipboard data dry bulk density versus grape density (Exon et al. 2001) for sites 1168 (a), 1170 (b), 1171 (c) and 1172 (d). The correlation factor r is indicated for the four sites. In order to calculate bulk accumulation rates for all analysed samples, the dry bulk densities assessed from the grape density data were used. Therefore, the formula of the line of best fit - indicated in blue - is applied (n = 25; p = 0.01).

Several empirical equations for estimating paleoproductivity (PaP) were obtained by directly comparing primary productivity production in surface waters with organic carbon accumulation rates in the underlying sediments. (Müller and Suess, 1979; Dymond et al. 1992; Sarnthein et al., 1992). The Sarnthein et al. (1992) approach appears to be best applicable to predominantly biogenic sediments in the pelagic environment (Bickert et al., 1992). Therefore, this equation was applied:

$$PaP = 61.39 \cdot (TOC \cdot DBD \cdot SR/10)^{0.25} \cdot SR_{cf}^{-0.049} \cdot z^{015}$$

with PaP in gC/m^{2}a and z in m for the water depth. SR_{cf} represents the calculated TOC-free sedimentation rate in cm/kyr:

$$SR_{cf} = SR \cdot (1 - TOC)/100$$

4. RESULTS

An overview of the results of investigated proxies is given here to demonstrate existing correlations and differences. The northern Sites 1168 and 1172 show similar values and downcore variations and the southern Sites 1170 and 1171, both located on the Tasman Rise, show likewise values and downcore variations as well. Therefore, the description follows mainly this order of the sites studied. Figure 9 gives an overview of the presented and discussed cores in the study area. The number of analysed samples (n) is different at each Site: n_{1168} = 199; n_{1170} = 250; n_{1171} = 198; n_{1172} = 211 (Tab. 2). Geochemical and sedimentological parameters are on every sample analysed. Only the chlorin-concentrations were determined on a smaller subset of samples and n is mentioned separately.

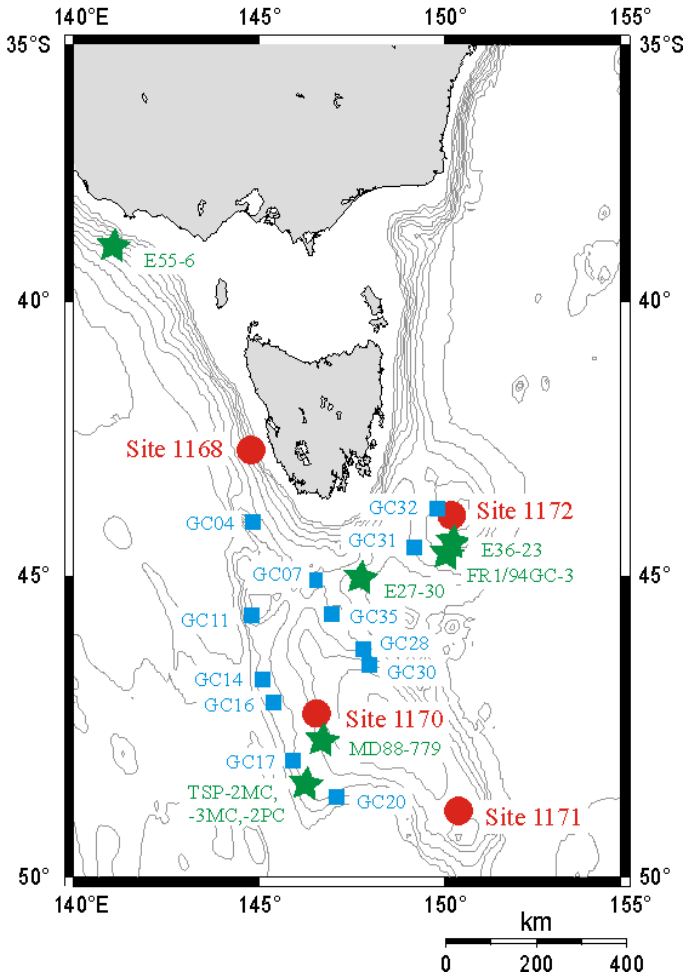

Fig. 9 Overview of the discussed cores in the study area: the studied sites 1168, 1170, 1171, and 1172 (red circles); the cores studied by Connell & Sikes (1997) (blue squares) and indicated with green asteriks are cores studied by: Hesse (1994, E26-4); Martinez (1994, E36-23); Passlow (1997, E27-30; E55-6); Nees et al. (1999, FR1/94GC-3; MD88-779) and Ikehara et al. (2000, TSP-2MC, -3MC, -2PC).

4.1 Carbonate, organic carbon, and coarse material

4.1.1 Carbonate and organic carbon

The analysed sediments exhibit high carbonate concentrations at all sites (Fig. 10; Tab. 4). This carbonate mainly constitutes of foraminifers and calcareous nannoplankton (Exon et al., 2001). The overall range is between 57.84 % (minimum of Site 1168) and 97.31 % (maximum of Site 1171).

Tab. 4 Overview of the mean, maximum and minimum carbonate and total organic carbon (TOC) in weight-percentages for the studied sites. For Sites 1170 and 1171 no analyses (n.a.) of TOC were performed due to concentrations below the detection limt.

Site	$CaCO_3$ [wt %]			TOC [wt %]		
	Mean	Min	Max	Mean	Min	Max
1168	78.28	57.84	89.9	0.28	0.09	0.55
1170	90.88	81.68	96.53	n.a.		
1171	94.75	89.02	97.31	n.a.		
1172	83.33	71.77	90.86	0.23	0.09	0.44

The carbonate content is calculated from the measured total amount of carbon (TC) and the amount of organic carbon (TOC). The TOC measurements at the southern Sites 1170 and 1171 did not to produce reliable results. Hence, the carbonate concentrations for these sites are only based on the TC-values. Disregarding the TOC at the southern sites, a maximal error of 4 % overestimation the carbonate concentration is inferred. This is deduced from the maximal TOC value measured in this study (0.55 % at Site 1168), hence the highest measured value in a regional context.

The northern Sites 1168 and 1172 show a lower carbonate content with the same variations around the mean carbonate concentration for each site (Fig. 10). The lowest concentration is at Site 1168 (78 %), then Site 1172 (83 %), followed by Site 1170 (91 %), whereas the highest mean carbonate concentration occurs at the southernmost Site 1171 (94 %). The magnitude of the glacial/interglacial variations is influenced by the dilution of terrigenous material. During the glacial, the percentage of carbonate decreases, while the amount of detrital components, meaning the terrestrial input, increased in all cores studied (Section 4.4). The same observation is made by Connell & Sikes (1997), studying cores south of Tasmania.

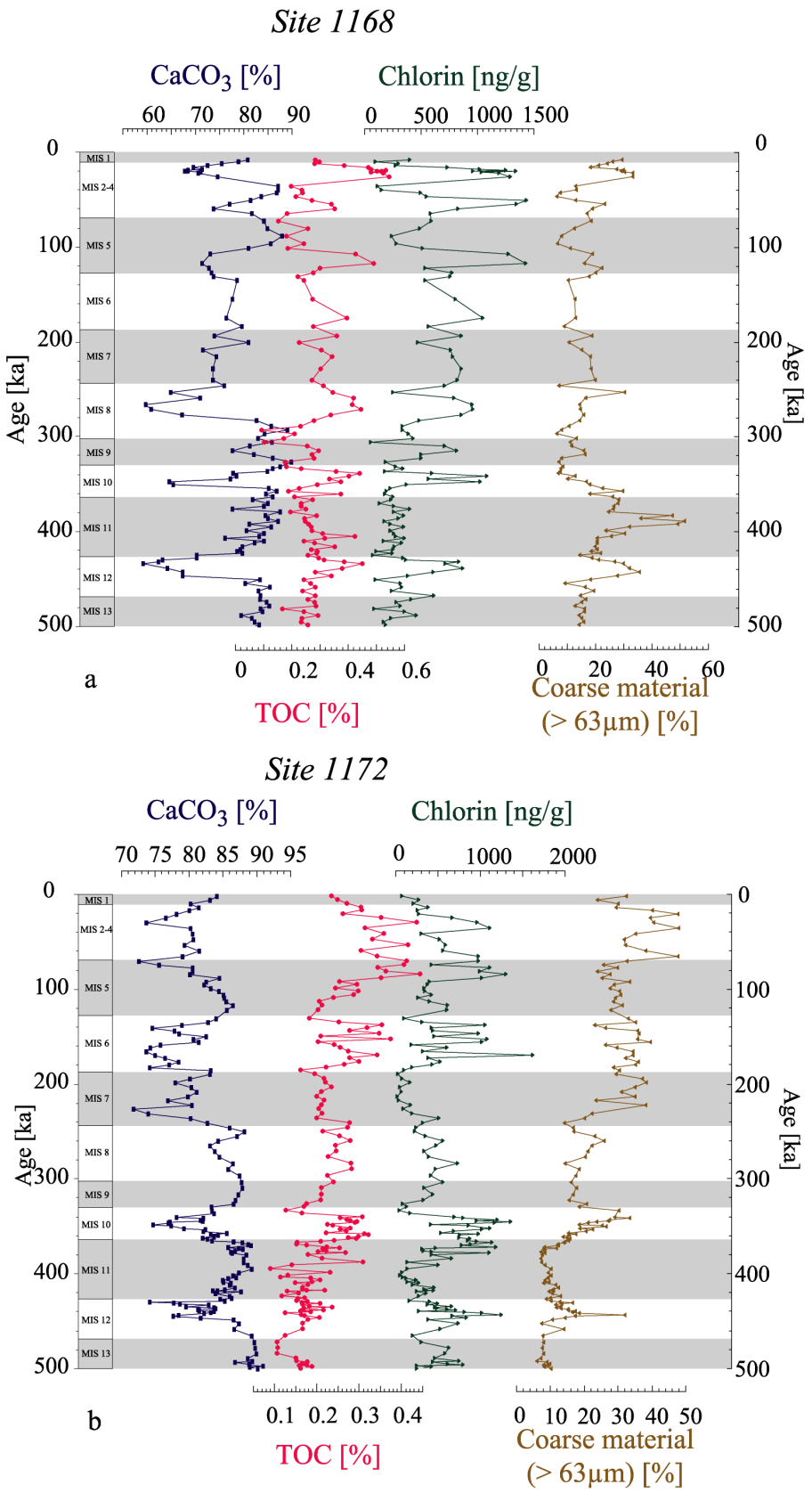

Fig. 10 Downcore records of the concentrations of several proxies for the studied sites: 1168 (a), 1172 (b), 1170 (c) and 1171 (d). The shown records are the concentrations of $CaCO_3$ (blue squares), TOC (pink dots) and chlorin (green triangles). The amount of sand-sized material, particles larger than 63 µm, is added as well (brown triangles). The sites are presented in couples of the northern sites (1168 and 1172) and the southern sites (1170 and 1171). The marine isotope stages (MIS) are indicated, interglacials are shaded. See next page for Sites 1170 (c) and 1171 (d).

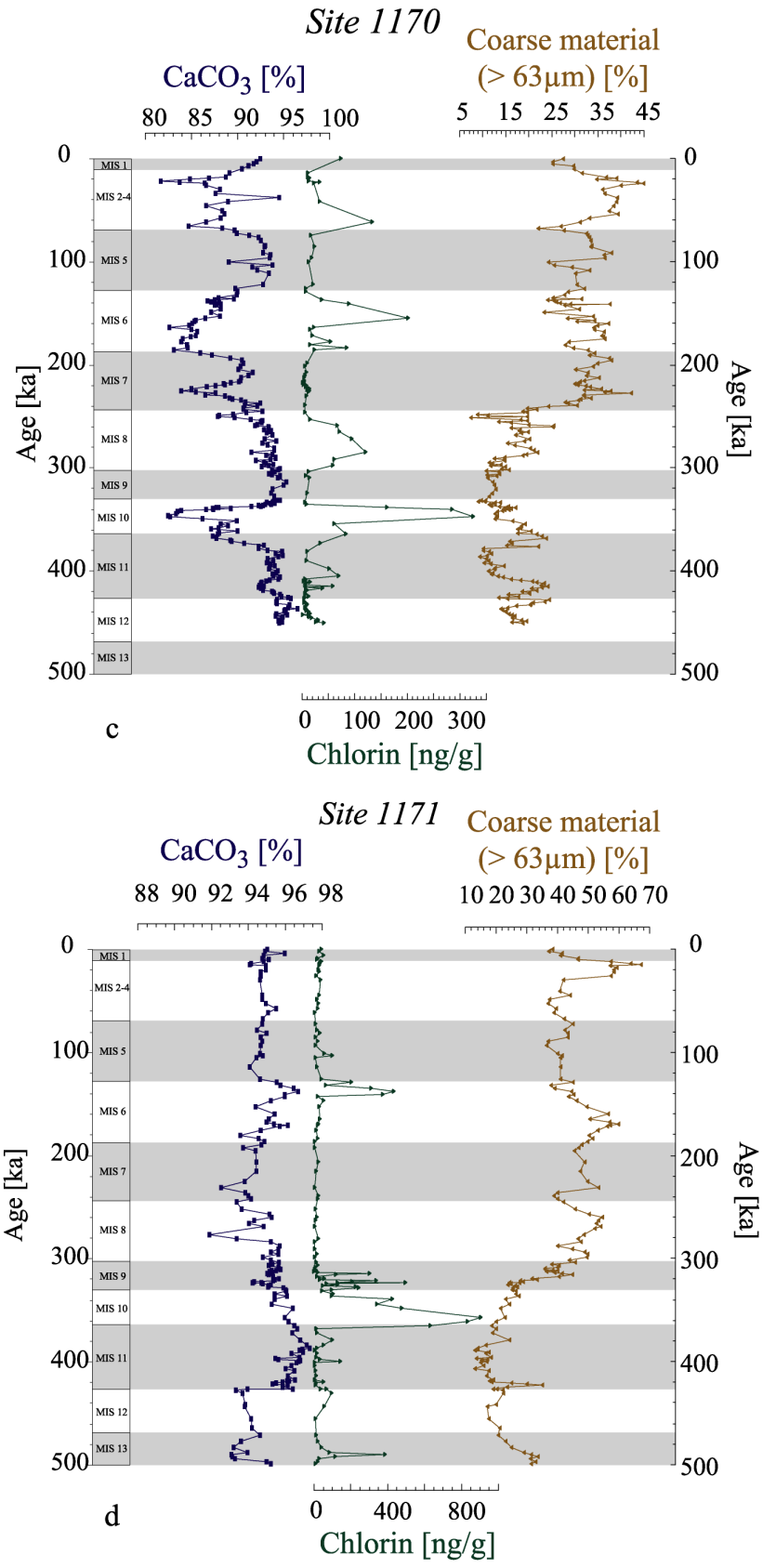

Fig 10 continued: site 1170 (c) and site 1171 (d).

A correlation between lightness (L*), given in Table 5, and carbonate concentrations is present for Sites 1170 (r = 0.81) and 1172 (r = 0.76). The correlation coefficient for the two other Sites (1168 and 1171) is 0.55 (Fig. 11) (p = 0.01). According to Nagao & Nakashima (1992), the L*-values of the spectro-photometrical analysis is expected to correlate with the carbonate content of pelagic sediments having a TOC-content of less than 0.6 %, with a correlation coefficient of 0.82. Measured TOC-concentrations in the study area show a maximum of 0.55 %, so within the proposed range. Anyhow, the correlation in this study is lower as expected. A problem of the measurements of the lightness is a direct comparison between the different instruments (Nagao & Nakashima, 1992).

Tab. 5 Mean, maximum and minimum of coarse fraction (>63µm) and coarse carbonate, and the shipboard measured lightness (L) for the studied sites.*

Site	Coarse fraction > 63 µm [%]			Coarse $CaCO_3$ [%]			Lightness (L*)		
	Mean	Min	Max	Mean	Min	Max	Mean	Min	Max
1168	18.17	6.22	51.54	23.64	7.38	60.51	61.18	48.47	70.31
1170	22.48	7.41	44.79	24.98	8.26	5.82	73.7	59.96	82.88
1171	37.55	13.07	67.25	39.42	13.51	71.49	77.33	51.15	87.1
1172	19.76	6.06	47.84	24.13	6.78	61.04	64.54	40.65	73.95

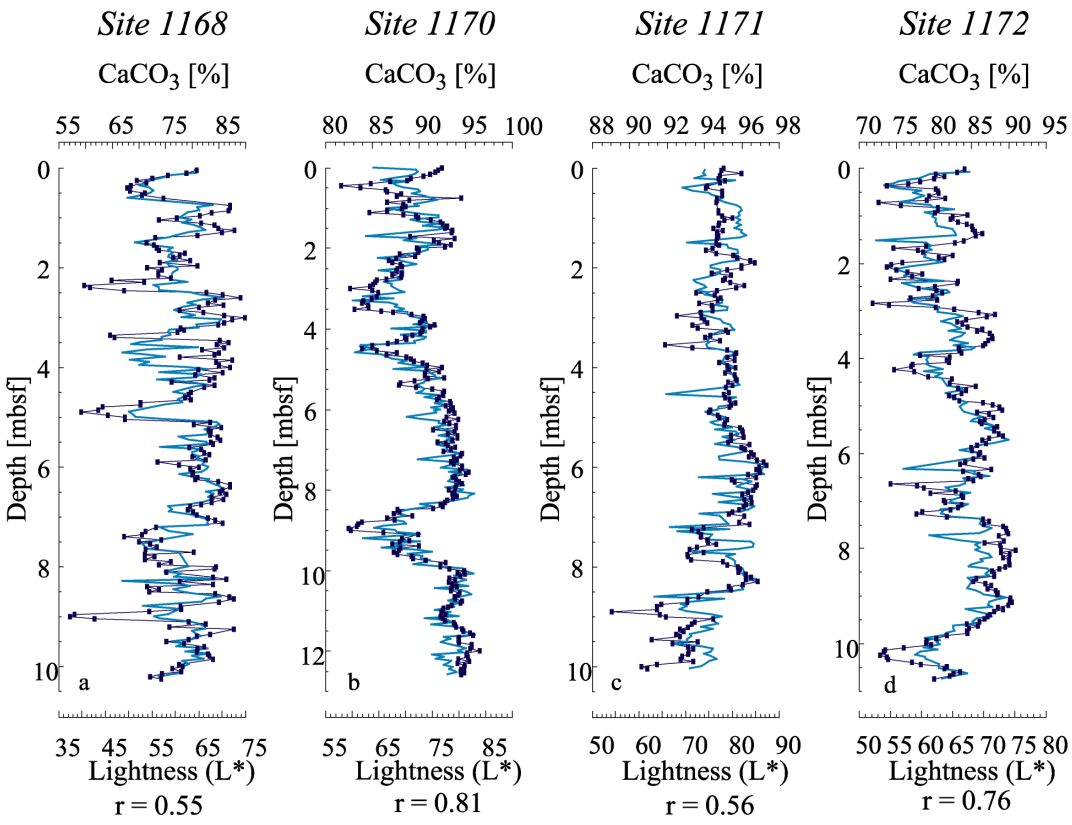

Fig. 11 The percentage of carbonate (% $CaCO_3$, dark blue squares) and lightness (L, light blue) plotted versus depth for the four studied sites: 1168 (a), 1170 (b), 1171 (c) and 1172 (d). The correlation coefficient r is indicated (p = 0.01).*

High carbonate concentrations are found in several other cores in the Australian Sector of the Southern Ocean (e.g. Martinez, 1994; Connell & Sikes, 1997). A carbonate content of 60 to 85 % during MIS 4-2, and a maximum of up to 90 % during MIS 1 and 5 are described for several cores on the South Tasman Rise (Hesse, 1997; Nees et al., 1999). Equivalent carbonate concentrations occur in the cores studied by Connell & Sikes (1997) to the south of Tasmania (Fig. 9), their range is between 60 and 85 % during the glacials and are typically around 90 % during the interglacials. This is in agreement with the values observed in this study. In the cores from the deep between the South Tasman Rise and Tasmania (2900 to 3500 m), the mean glacial amount of carbonate is 80 % and the glacial/interglacial variations are between 10 and 30 % of that mean carbonate concentration. Similar observations are made for the studied Sites 1168, 1170 and 1172. Instead, the cores on the South Tasman Rise, retrieved from water depths shallower than 2700 m only show a variation of less than 5 % of the mean carbonate concentration and shallower cores show a higher mean carbonate concentration than the deeper ones. This observation is in accordance with the described carbonate measurements of Site 1171, situated at a water depth of 2148 m. At that site, the carbonate percentage is the highest among the studied cores through the entire time-interval (mean of 94.75 %) and the variations are small (within 5 % of mean) (Fig. 10, Tab. 4).

Martinez (1994) observed a general increase in the carbonate preservation over the past 500 kyr in the Tasman Sea. Also in other areas of the Southern Ocean, a long-term trend of increase in carbonate preservation over the past 500 ka is reported from deeper cores in the Atlantic Sector of the Southern Ocean by Howard & Prell (1994), and for the Pacific Ocean by Schroeder et al. (1997). These observations cannot be confirmed by the new data. In contrast, at Sites 1170 and 1172, there is an overall decrease in the carbonate concentration until the end of MIS 2. During MIS 1, a sudden increase in the carbonate concentration is found. Connell & Sikes (1997) states that older interglacial periods generally have slightly higher carbonate concentrations than during the Holocene. This trend is revealed at Sites 1168, 1170, 1172. At Site 1171, it is hard to see a general trend for this proxy due to the less changing carbonate concentrations.

Close to Site 1168, Passlow et al. (1997) studied core E55-6 (38°51.2’S, 141°03.8’E, 2346 m, Fig. 9) on benthic faunal and dissolution changes. They mentioned a dissolution event during MIS 4. In the carbonate percentage of MIS 4 at Site 1168, a

decrease of 85 % carbonate to 73 % carbonate was observed. This could be caused by a probably local dissolution event, but this cannot be further constrained by the studied proxies. An impressive increase in the TOC content (0.18 % to 0.36 %) at that site is present during MIS 4. Looking at the accumulation of carbonate and TOC, the SR overprints the pattern at MIS 4 and no change is present (Section 4.5). Moreover, in the Australia sector of the Southern Ocean, the present lysocline is situated at a depth of 3400 m (Takahashi et al., 1980). Therefore the studied sites are situated above the present-day lysocline, resulting in a good carbonate preservation.

At Site 1168, the TOC concentrations increase during almost all glacial stages: during MIS 10, 8, 4-2, and at the end of MIS 12 as well as at the beginning of the interglacial MIS 5 (Fig. 10). During the glacial MIS 6, the TOC-concentration stayed at the same level as during MIS 7 (0.3 %) The carbonate content shows always a minimum during those glacial phases. For Site 1172, the TOC values do not show these large variations during the MIS mentioned above for Site 1168. The TOC concentrations rather can be divided into two parts: a sudden decrease of 0.3 % to 0.12 % takes place at 345 ka. Before and after 345 ka, a linear increase can be observed. The carbonate concentrations at Site 1172 show minima during MIS 12, 10, 7, 6, at the end of MIS 5, and during MIS 2-4. Minima during the same MIS are revealed at Site 1170, except for MIS 12, where data are missing. At Site 1171, the carbonate content is between 97.31 % and 89.02 %, and for the last 500 ka the minimum is even as high as 91.89 %. Therefore, no pronounced changes are visible. Ikehara et al. (2000) mentioned a TOC decrease at cores from the South Tasman Rise from the Last Glacial Maximum (LGM) to the onset of the deglaciation. This is supported by the measured TOC-concentrations at Sites 1168 and 1172.

4.1.2 Coarse fraction

The temporal and spatial variability in the proportion of the sand-sized material exhibits a similar pattern as the carbonate concentrations (Fig. 10). Inspection of the coarse fraction under the dissecting microscope revealed that planktonic foraminifers dominate the component spectrum. The northern Sites 1168 and 1172 exhibit a smaller portion of coarse material (mean of 18.17 % and 19.76 % respectively) than the southernmost Site 1171 (37.55 %). In the middle of the range, Site 1170 shows a mean of 22.48 % material coarser than 63 µm. This site has the smallest range (7.41-44.79 %) of all sites.

The amount of coarse carbonate is calculated from the carbonate percentage and the amount of coarse material within the sample (Section 3.2.1). Three Sites (1168, 1170 and 1172) show almost the same mean coarse carbonate content of 24 % (Tab. 5). Only at Site 1171, there is a much larger content of almost 40 %.

None of the sites show a consistent trend of increased or decreased portions of material larger then 63 µm linked to glacial/interglacial variations, except for the transition from MIS 11/10 (except Site 1170) and MIS 2/1 (Fig. 10). The records of Sites 1170, 1171 and 1172 show an up-core increase during the studied time interval of 500 ka. At Site 1168, the portion of sand-sized material does not show this increasing trend (Fig. 10).

With more than 50 % of coarse material, Site 1168 displays a prominent maximum during MIS 11. This maximum is composed of reworked coarse biogenic carbonate of shallow water shells and corals, inferred from visual inspection of the sample residues, especially in the fraction coarser than 250 µm. Only during MIS 11 and only at Site 1168, this material was observed.

At Site 1168, an increase form 18 to 34 % of coarse carbonate takes place from 500 to 350 ka, followed by a sudden decrease to 8 % at MIS 11/10 (Fig. 10). During MIS 9, a constant portion of coarse material of 20 % is present, decreasing to only 8 % during MIS 8, which is followed by an increase to 22 % (MIS 8/7). The portion of coarse carbonate remains between 22 and 13 % until the transition from MIS 2/1 where an increase of up to 45 % can be observed, directly followed by a decrease to 18 %. During MIS 1, the portion of coarse carbonate successively increased again to about 30 %.

In general, Site 1172 reveals a linear increase with time in the portion of coarse carbonate (Fig. 10). At 500 ka, just 9 % of the carbonate exists of coarse material. Then, at the transition MIS 11/10, a spectacular increase to 33 % is present. At the beginning of MIS 9, a plateau of 17 % is reached and last till the beginning of MIS 7. The sudden change at MIS 10/9 coincides with a decrease in TOC. After an increase to 45 % in the middle of MIS 7, a slow decrease to 30 %, reached at the end of MIS 5, is observed. A high portion of coarse material of 60 % is present during MIS 4-2, followed by a decrease to 30 %.

Site 1170 shows only small variability with a range of 10 to 20 % from 450 till 245 ka (Fig. 10). At the beginning of MIS 7, a distinct increase to 35 % can be seen. This

portion of coarse carbonate (30-40 %) stays until 20 ka (MIS 2/1), where it first increases to 50 % and then decreases to 30 %. At Site 1171, a decrease from 35 % to 13 % takes place from 500 to 390 ka. A linear increase to 25 % (390 ka - 325 ka), followed by an increase between 325 and 317 ka to 46 % (during MIS 9) can be detected. Then two plateaus with more or less a constant coarse carbonate percentage are present: 55 % between 317 and 150 ka and 45 % between 150 and 30 ka. From 30 to 12 ka, the portion of coarse material rises to a maximum value of 60 %, directly followed by a linear decrease to 40 % during MIS 1.

In core E27-30 (45°04.0' S, 147°13.7'E, 3552 m), located at the deep between Tasmania and the South Tasman Rise, downcore variations in the portion of coarse sand, do not appear to have a clear consistent trend of increasing or decreasing values linked to glacial or interglacial periods (Connell & Sikes, 1997). As these observations are made on the Tasman Rise, that paper suggests that different currents are dominant on various parts of the Tasman Rise (Connell & Sikes, 1997).

4.2 Chlorin

This study presents the first downcore records of chlorin for the Southern Ocean. The measurements of chlorin at the pelagic Sites 1170 and 1171 were difficult because the proper calibration for most of their samples was below the detection limit of the fluorometer. Therefore, just for half of the samples the amount of chlorin was determined at the southern Sites 1170 and 1171 (Tab. 6).

Tab. 6 Mean, maximum and minimum concentrations of chlorin [ng/g]. Due to the low concentrations, close to the detection limit of the fluorometer, not all samples could be measured. The number of analysed samples is given.

Site	Chlorin [ng/g]			Number of analysed samples (n)
	Mean	Min	Max	
1168	416.7	35.7	1432.6	195
1170	31.5	1.2	324.9	104
1171	56.1	1.9	635.6	126
1172	497.5	15.3	1619.2	205

The chlorin-concentrations range from 1.2 to 324.9 ng/g for Site 1170. At Site 1171 the maximum even almost doubled to 635.6 ng/g. The concentrations of chlorin at the northern Sites 1168 and 1172 are clearly higher (mean of 416.7 and 497.5 ng/g respectively). These northern sites show a similar range in chlorin concentration: 35.7 to 1432.6 ng/g for Site 1168 compared to 15.3 to 1619.2 ng/g for Site 1172 (Fig 10).

Even at Sites 1170 and 1171, where the measurements were close to the detection limit, distinct maxima in the chlorin concentration are present during MIS 10, 8, 6, 4 (Site 1170) and MIS 10 and 6 (Site 1171) (Fig. 10). At Sites 1168 and 1172 substantially higher chlorin values are present during all glacials since MIS 13. The increase during MIS 8 at Site 1172 is not pronounced. At Site 1168 the chlorin concentration increased also at the beginning of MIS 5.

In the present study, there is an evident similarity between the chlorin concentrations and the changes in TOC-concentration, by the visual comparison of the minima and maxima. The correlation coefficient is 0.72 for Site 1168 and 0.64 for Site 1172 (p=0.01) (Fig. 12). By comparing TOC and chlorin, the differentiation into terrigenous and marine organic matter becomes possible (Kowalewska et al. 1999). The similar downcore variations of TOC and chlorin concentrations at Sites 1168 and 1172 support the contention of enhanced marine productivity at these positions during glacials. Variations in the oxygen content in the bottom water may influence the TOC preservation and hence the chlorin record as well (Harris et al., 1996).

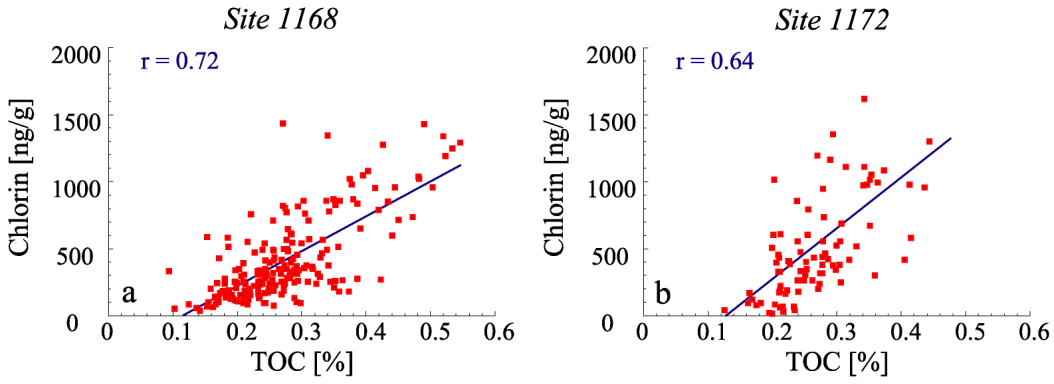

Fig. 12 Relationship between organic carbon (TOC) and chlorin for the sites 1168 (a) and 1172 (b). The blue line represents the linear regression, with the correlation coefficient r.

4.3 Barium

The total Ba concentration is used to calculate the amount of biogene Ba and of terrigene Ba (Tab. 7, Fig. 13). Two different approaches for the calculation of biogene Ba were performed: via the concentration of Al and Ti (Ba_{exc} and Ba_{terr}), and via the calculation of the amount of 'background' Ba (Ba_{net} and Ba_{bg}) (Section 3.2.3). The Ba_{tot} concentrations do not differ very much at the four sites, but looking to the Ba_{exc}/Ba_{net} or Ba_{terr}/Ba_{bg}, spatial and temporal changes are revealed.

Tab. 7 Mean, maximum and minimum concentrations of Ba and the calculated Banet- and Baexc-concentrations via Ti and Al in µg/g.

Site	Ba [µg/g]			Ba_{net} [µg/g]			Ba_{exc} via Ti [µg/g]			Ba_{exc} via Al [µg/g]		
	Mean	Min	Max	Mean	Min	Max	Mean	Min	Max	Mean	Min	Max
1168	485	144	853	370	61	721	360	98	557	383	101	619
1170	641	353	1159	571	292	1056	606	345	1061	609	345	1050
1171	508	264	934	451	217	877	493	258	897	495	259	905
1172	515	342	777	418	265	654	435	305	608	450	308	640

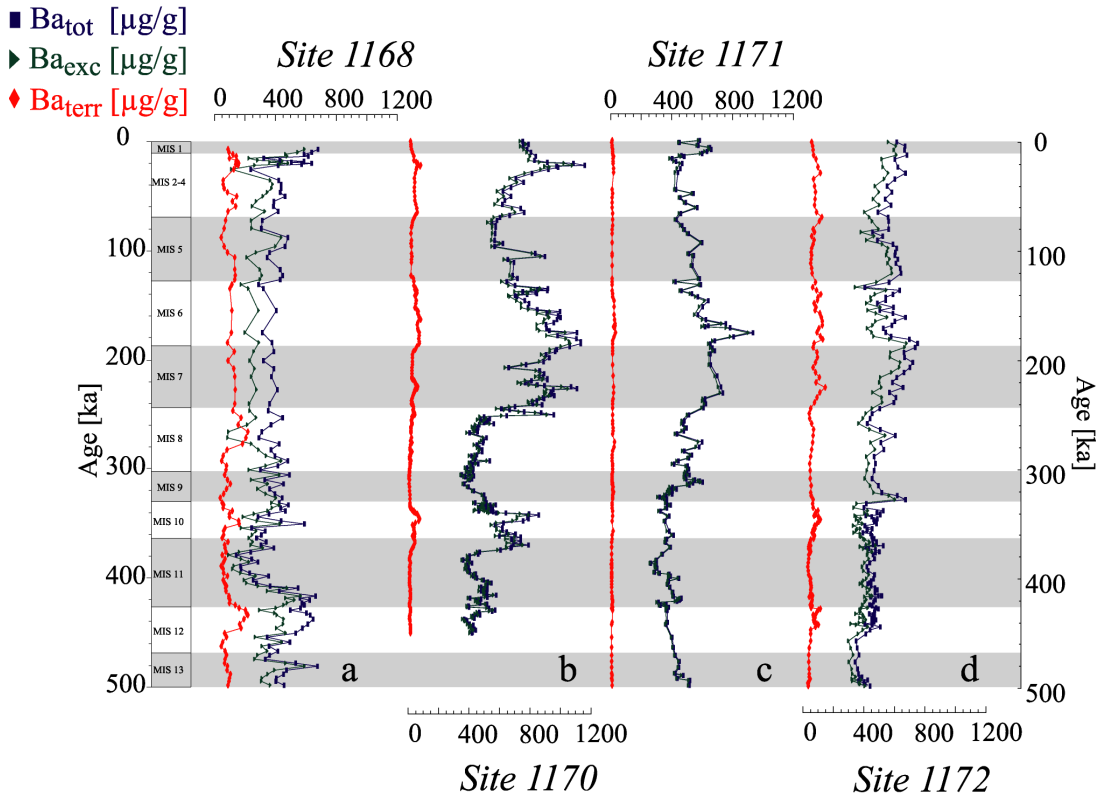

Fig. 13 Downcore records of the total concentration of barium (blue squares) and the calculated excess (green triangles) and terrigenous (red diamonds) barium for the four studied sites: 1168 (a), 1170 (b), 1171 (c), 1172 (d). The interglacial stages are shaded.

Although the concentrations of Ba_{exc} are low, they show a remarkable difference from northern to southern sites. The closer the site is to Tasmania, the less Ba_{exc} is present (Tab. 7): 360 µg/g (Site 1168) < 435 µg/g (1172) < 493 µg/g (1171) < 606 µg/g (1170). The range is between 98 µg/g (minimum of Site 1168) and 1061 (maximum for Site 1170). This implies that the amount of Ba_{terr} is lowest at the southern, pelagic sites.

As can be seen in Table 7, the calculations of Ba_{exc} via Ti or Al differ from each other by less than 3 %, consist with Nürnberg et al. (1997). In the formula for the Ba_{net} calculation, the amount of opal is neglected, as the amount of opal was below the detection limit of the applied method. The calculations of the Ba_{exc} and Ba_{net} values

gave also the same amount of non-terrigenous Ba. Therefore, the downcore pattern runs similar (Fig. 14). This is quite an important result because the Ba_{terr} and Ba_{bg} concentrations were determined with independent factors: the concentration of Ti and the Ba/Ti-ratio, and the carbonate and TOC content respectively. It indicates that the used average crust values for Ba/Ti (0.126) and Ba/Al (0.0065) are reasonable for this study. In the following, only the Ba_{exc} calculated by Ti is considered.

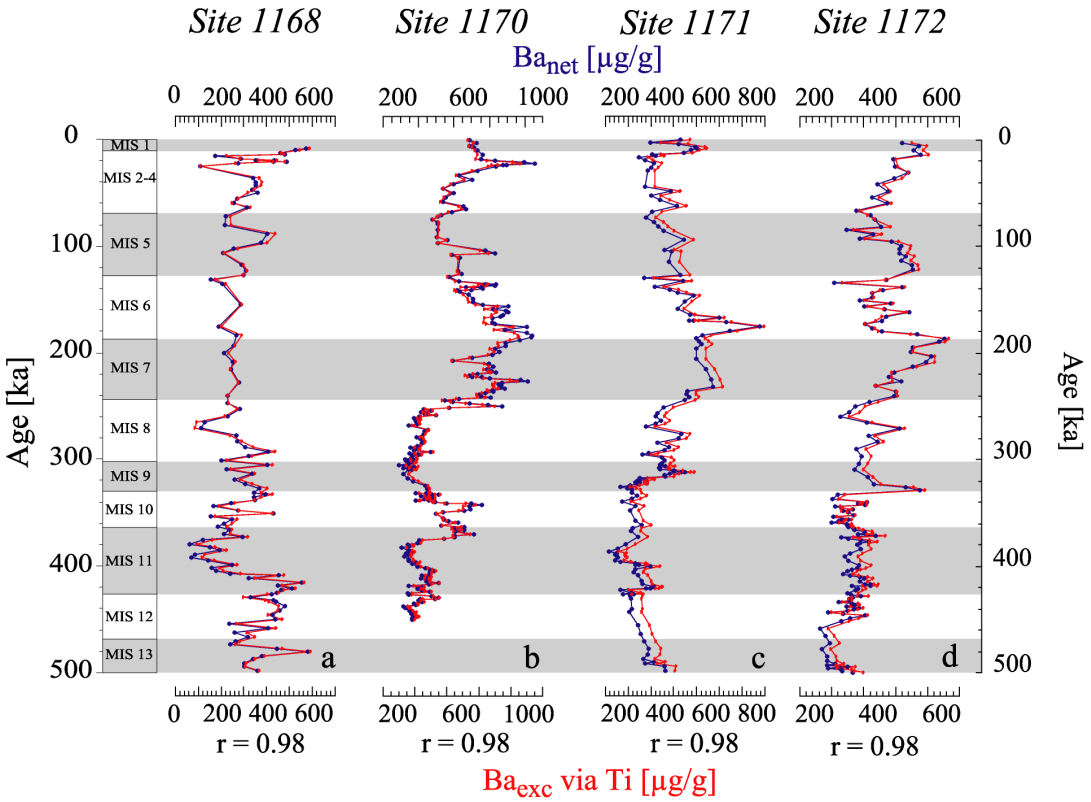

Fig. 14 Downcore record of the concentration of biogene barium for the four studied sites: 1168 (a), 1170 (b), 1171 (c), 1172 (d). The Ba_{net} (blue cirlces) is calculated via the percentage of carbonate, TOC and siliciclastic material. Whereas Ba_{exc} (red triangles) is computed by substracting Ba_{terr} (calculated via the amount terrigenous Ti) from Ba_{tot}. The interglacial stages are shaded.

A typical glacial/interglacial pattern of the Ba_{exc}-concentrations is not seen. The downcore records of the Ba_{exc}-concentration do not match with any of the other paleoproductivity proxies (Fig. 10,13). The changes in Ba_{exc} coincide with the changes in the amount of coarse carbonate for the pelagic Sites 1170 and 1171. The correlation coefficient between both proxies amounts to 0.73 and 0.70 respectively ($p = 0.01$). At Sites 1168 and 1172, the correlation coefficient is 0.21 and 0.45 respectively ($p = 0.01$). The high correlation between Ba_{exc} and TOC, mentioned by Gingele & Dahmke (1994) in sediment cores and by Wefer (1989) for sediment traps, cannot be seen in this study ($r = 0.25$; $p = 0.01$).

4.4 Terrigenous elements: Al, Fe, Ti

The amount of terrigenous material is low at all studied sites. The terrigenous (or siliciclastic) portion is mainly restricted to the silt and clay fractions, lithogenic particles larger than 63 µm were not found in the residues. The northern Sites 1168 and 1172 show the highest Al, Fe and Ti-concentrations (988 and 628 µg/g Ti respectively) (Tab. 8; Fig. 15). In contrast, the southern Sites 1170 (278 µg/g Ti) and 1171 (117 µg/g Ti) show low concentrations.

Tab. 8 Mean, maximum and minimum concentrations of the elements Al, Fe and Ti [µg/g], as well as the percentage of siliciclastic material, for the studied sites.

Site	Al [µg/g]			Fe [µg/g]			Ti [µg/g]			Siliciclastic material [%]		
	Mean	Min	Max	Mean	Min	Max	Mean	Min	Max	Mean	Min	Max
1168	15762	6566	36065	8500	3389	17403	988	365	2353	2158	10.1	42.92
1170	4891	1267	1356	2630	661	8099	278	62	773	9.12	3.47	18.32
1171	2005	743	4399	1101	325	2558	117	45	292	5.25	2.69	10.98
1172	10024	5145	21117	5510	2479	11707	628	294	1342	16.65	9.04	28.23

Aluminium, Ti and Fe show a good correlation between each other for all Sites: r (Al versus Ti) ≥ 0.97; r (Al versus Fe) ≥ 0.88; r (Ti versus Fe) ≥ 0.89 (Fig. 16) ($p = 0.01$). Since these three elements show good correlations, it may be concluded that they originated from the same source and were transported to the sediment by the same mechanism of transport (Latimer & Filippelli, 2001; Robert et al., 2001; Nürnberg et al., submitted). Due to the good correlation of Ti with the other elements of terrigenous origin and due to the immobility of Ti after deposition (Murray et al., 1993; Murray & Leinen, 1996), the Ti values are discussed preferably.

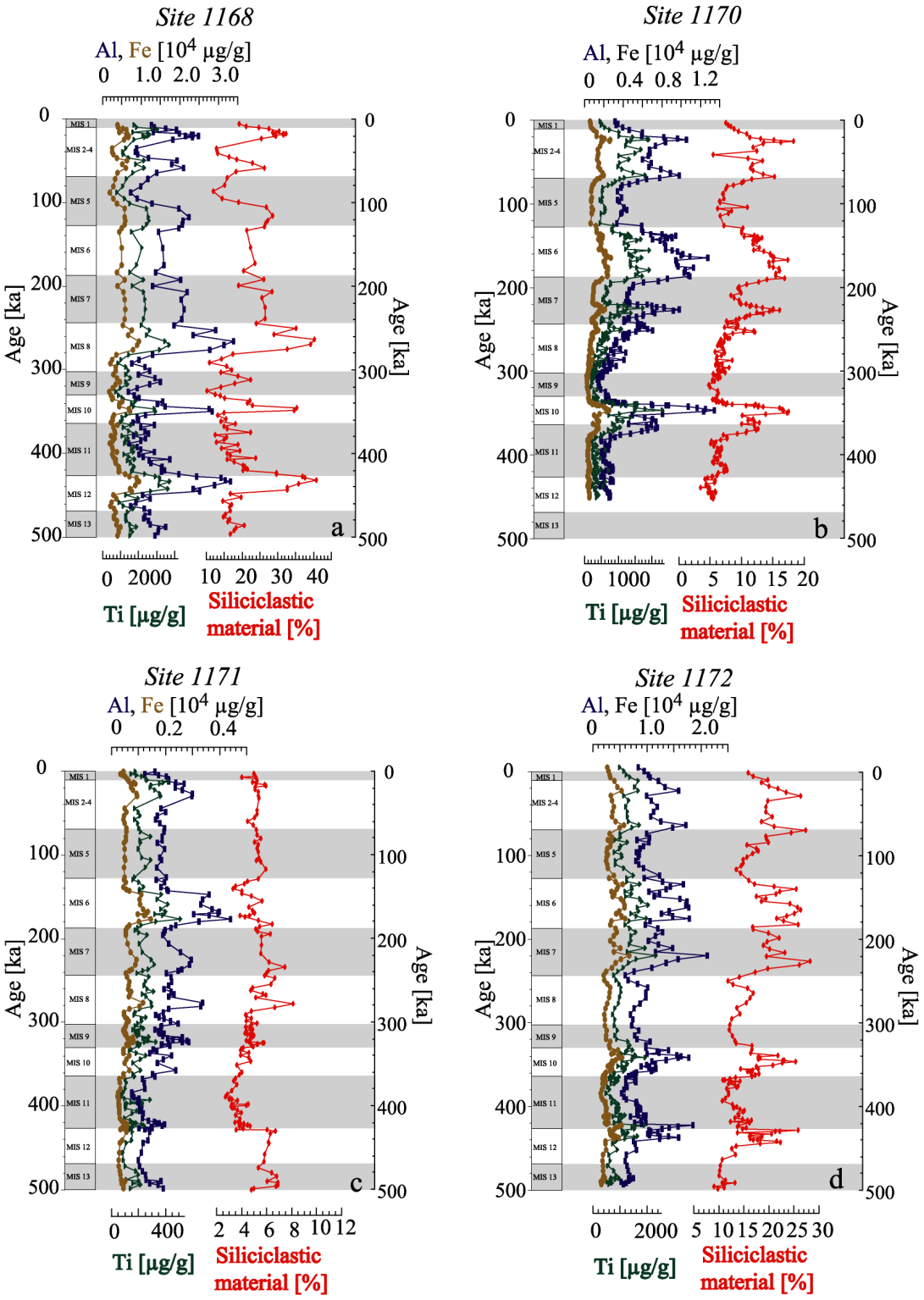

Fig. 15 The downcore records of the terrigenous elements Al (blue squares), Ti (brown dots) and Fe (green triangles) and of the amount siliciclastic material (red diamonds) are shown for the four studied sites: 1168 (a), 1170 (b), 1171 (c) and 1172 (d). Interglacial stages are shaded.

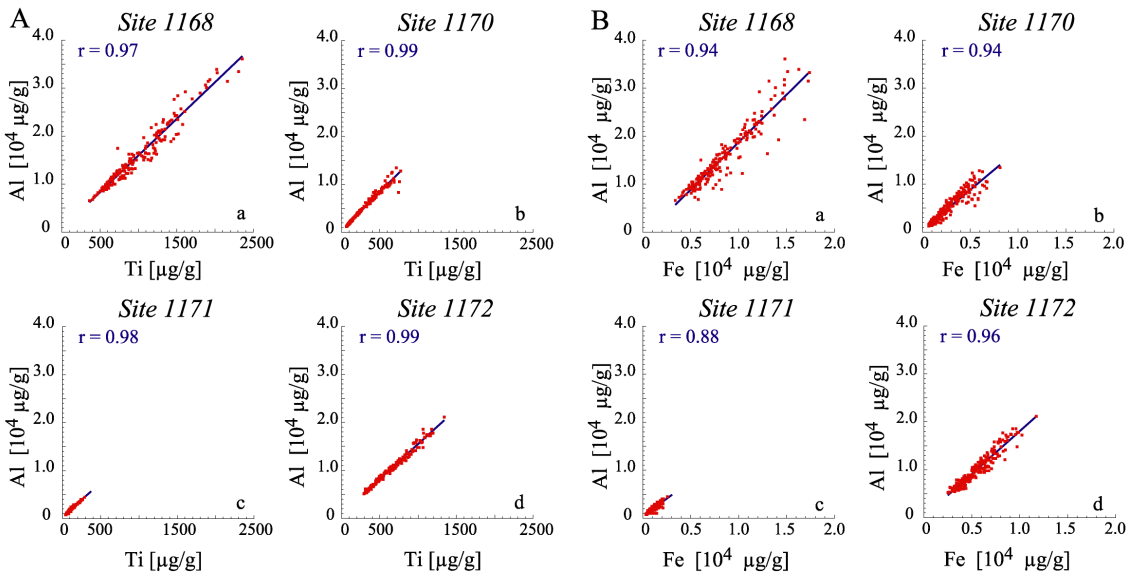

Fig. 16 Relationship between the terrigenous elements Al-Ti (A) and Al-Fe (B) for the four studied sites: 1168 (a), 1170 (b), 1171 (c) and 1172 (d). The blue lines show the line of best fit. In addition, the corresponding correlation factor r is given (p = 0.01).

Although the absolute amount of deposited Ti is small, the downcore variations of the Ti-concentrations run similar with the TOC and chlorin concentrations. Therefore, higher Ti-concentrations are observed during most glacials. Even for Site 1172, where the correspondence is not that obvious, the Ti-content increased during MIS 12, 10, 6, 2-4 and during the interglacial MIS 7. At Site 1168, an increase in the Ti-concentration is present during MIS 12, 10, 8, 4-2 and at the beginning of MIS 5. Sites 1170 and 1171 exhibit higher Ti-concentrations during MIS 10, 6, 2-4 and during interglacial MIS 7. At Site 1171 there is also an increase in the Ti-concentration during MIS 9 and 8.

The Al/Ti and Fe/Al ratios (Tab. 9) are used to differentiate between different sources of terrigenous material (e.g. Taylor & Mc Lennan, 1985; Latimer & Filippelli, 2001). In the study area, the Al/Ti ratio (mol/mol) stayed almost constant over the studied time interval but is slightly different from site to site: lower at the northern sites (Site 1168: 28.56; Site 1172: 27.31) than for the southern sites (Site 1170: 31.93; Site 1171: 31.00) (Fig. 17). The Fe/Al ratio is 0.27±0.02 (mol/mol) for the four sites and shows no systematic downcore variation (Fig. 17).

Tab. 9 Mean, maximum and minimum values for the Al/Ti and Fe/Al ratios [mol/mol], for the studied sites.

Site	Al/Ti [mol/mol]			Fe/Al [mol/mol]		
	Mean	Min	Max	Mean	Min	Max
1168	28.56	22.79	33.45	0.27	0.19	0.44
1170	31.93	19.86	36.09	0.26	0.18	0.49
1171	31.00	39.09	21.01	0.27	0.16	0.49
1172	27.31	24.79	34.57	0.29	0.21	0.34

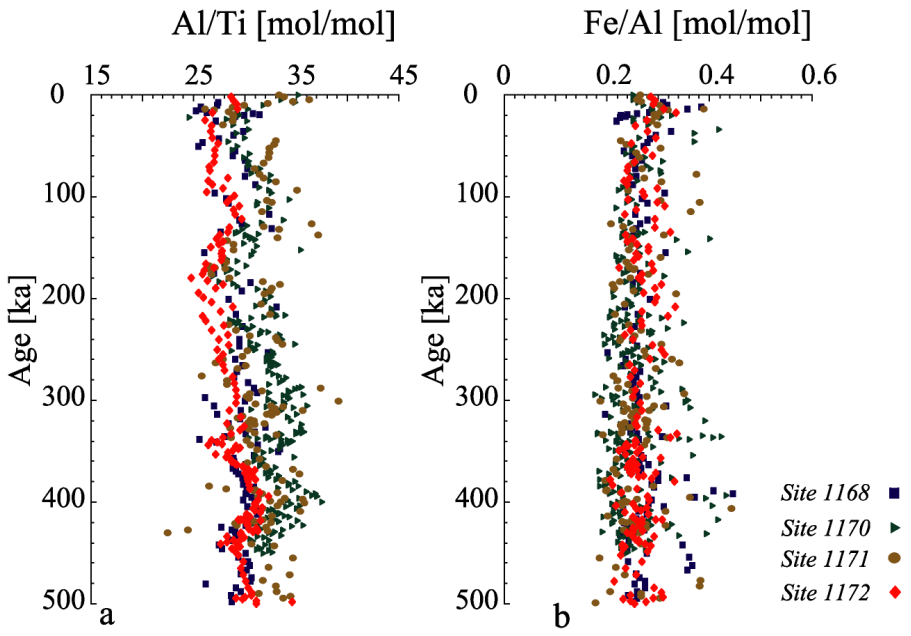

Fig. 17 Downcore record of the Al/Ti (a) and the Fe/Al (b) ratios for the studied sites: 1168 (blue square), 1170 (green triangle), 1171 (brown dot) and 1172 (red diamond).

By comparing the trends of Al to the Ti/Al-ratio, scavenging of Al can be detected (Murray & Leinen, 1996) (Fig. 18). Visually, the downcore records of Al and Ti/Al run similar for all four sites, although the correlation coefficients are not good ($r = 0.38 – 0.58$; $p = 0.01$). Therefore, scavenging was not important at the sites during the studied time interval.

Normalisation of Ti and Al-values produced the same downcore trends (Fig. 19). The values differ from each other by less than 0.5 %. This indicates that the normalisation with the used values for the average crust is reliable in the area. By comparing the normalised Ti-values with the calculated percentage of siliciclastic material, a good correlation for the three Sites 1168, 1170 and 1172 can be seen ($r > 0.94$; $p = 0.01$).

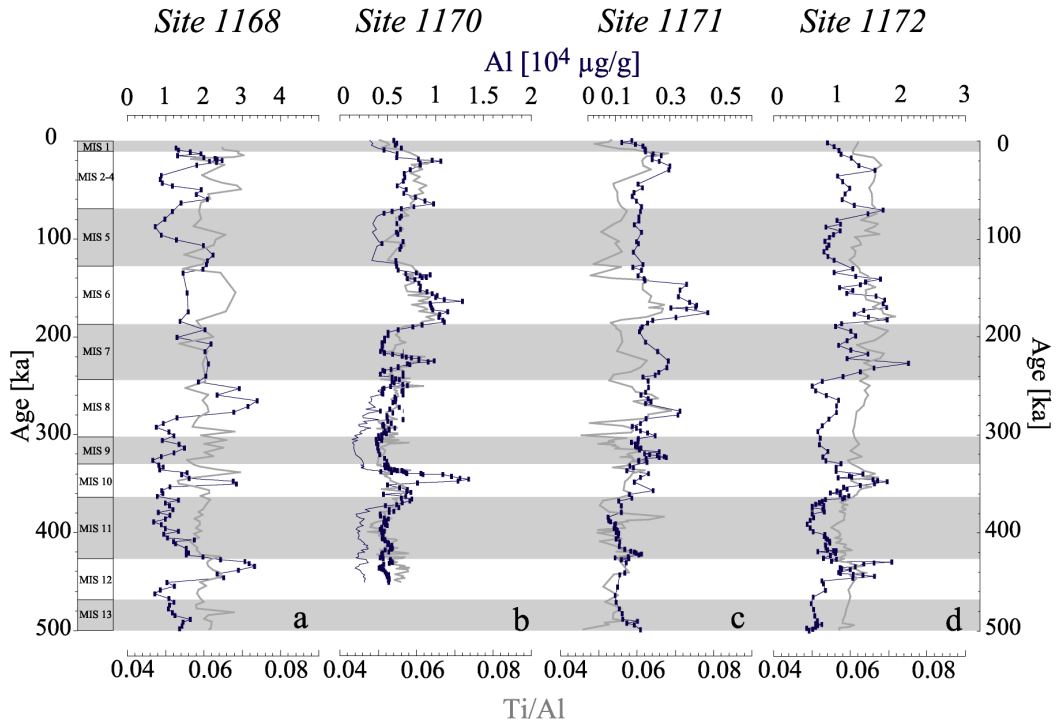

Fig. 18 Downcore records of the Al-concentrations (blue squares) and the Ti/Al-ratios (grey line) for the studies sites: 1168 (a), 1170 (b), 1171 (c) and 1172 (d). As both records run similar, scavenging of Al can be excluded (Murray & Leinen, 1996). Remark: the lower scale is the same for all sites, whereas the upper scale is different. Interglacial stages are shaded.

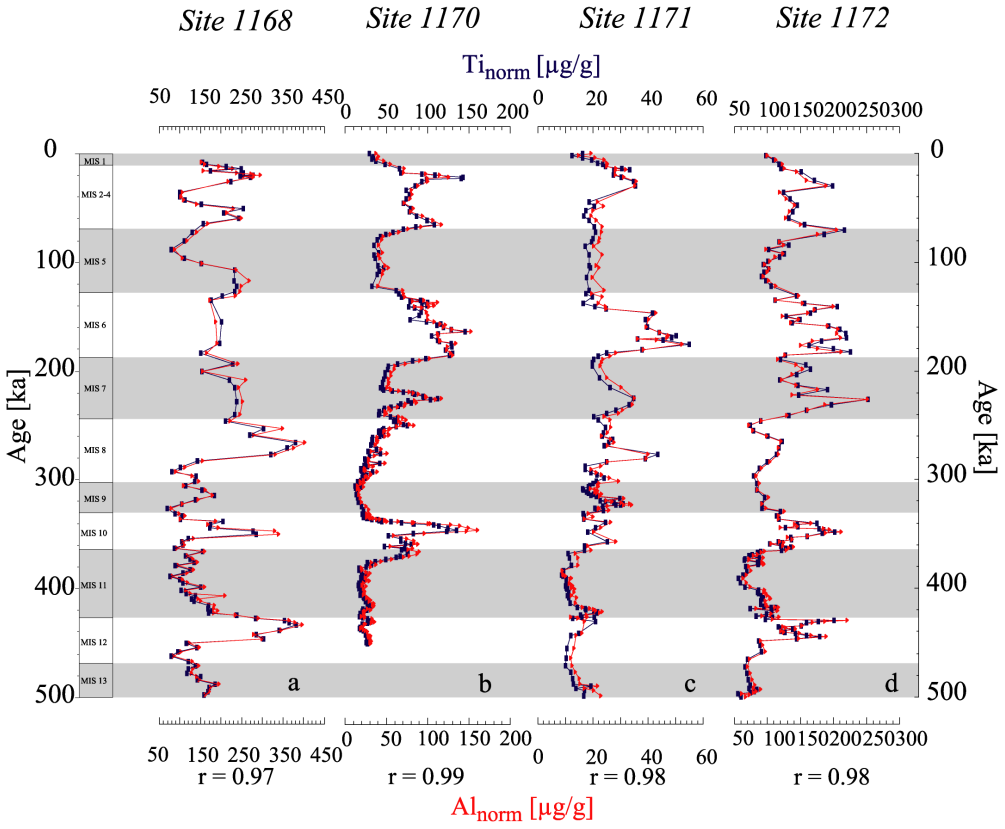

Fig. 19 Downcore records of normalised Ti (blue squares) and normailised Al (red triangles) concentrations for the four studied sites: 1168 (a), 1170 (b), 1171 (c) and 1172 (d). The curves show a similar pattern for both proxies as indicators for terrigenous supply. The correlation factor r is indicated (p = 0.01). Interglacial periods are shaded.

4.5 Sedimentation and Accumulation rates

4.5.1 Overview

The sedimentation rates (SR) range between 1.36 cm/kyr (minimum of Site 1168) and 3.67 cm/kyr (maximum of Site 1170) (Tab. 10, Fig. 20). There are several maxima, for instance 10.00 cm/kyr from 333 to 339 ka at Site 1170. They could be effected by insufficient sample resolution in combination with the densely spaced age control points, as discussed in Nürnberg et al. (submitted). Variations in SR are generally not considered as internal scatter and the age model has been produced as precise as possible. Long-term environmental changes in the study area are, however, not considered to have happened as sudden overturns within a few hundred years. To avoid the over-interpretation of the sudden changes in SR, a simple 7-point moving average SR-record was used to calculate the accumulation rates (AR) (Fig. 20).

Tab. 10 Mean, maximum and minimum sedimentation rate (cm/kyr), as well as the mean, maximum and minimum dry bulk density (g/cm^3).

Site	Sedimentation rate [cm/kyr]			Dry bulk density [g/cm^3]		
	Mean	Min	Max	Mean	Min	Max
1168	1.35	0.5	4.71	1.09	0.73	1.34
1170	3.67	1.24	10	0.97	0.67	1.15
1171	2.36	0.71	6.65	0.95	0.74	1.11
1172	2.84	0.77	9.22	0.87	0.51	0.99

Site 1170 shows the highest variability in the SR. The are higher than 2 cm/kyr during MIS 10 and 6 and at the transitions MIS 12/11, 9/8, 8/7 and 2/1. At Site 1171, there are large increases in the SR during the interglacials MIS 11 (SR > 2 cm/kyr) and 9 (SR > 4 cm/kyr) and at the transition MIS 2/1 (SR > 2 cm/kyr). The SR at Site 1172 increases to 3.4 cm/kyr during the glacials MIS 12 and 10. Also during MIS 11 and 6, the SR stays high (> 1.4 cm/kyr) at Site 1172. Site 1168 shows a less pronounced temporal variability in SR compared to the other three studied sites. Only during MIS 11 till MIS 10 and at the transition MIS 2/1 the SR was clearly increased (>2 cm/kyr). Winnowing could have influenced the low SR at Site 1168. However the correlation between the Ti/Al and the Ti disagrees with that assumption (Murray & Leinen, 1996) (Fig. 18).

Nees et al. (1999) denote a SR of 1 to 2 cm/kyr for core MD88-779 (47°50.69'S, 146°32.75'E, 2260 m), situated directly to the south of Site 1170. This is markedly lower than the SR from this study. Core E26-4 (45°04.7'S, 160°04.2'E), situated to the

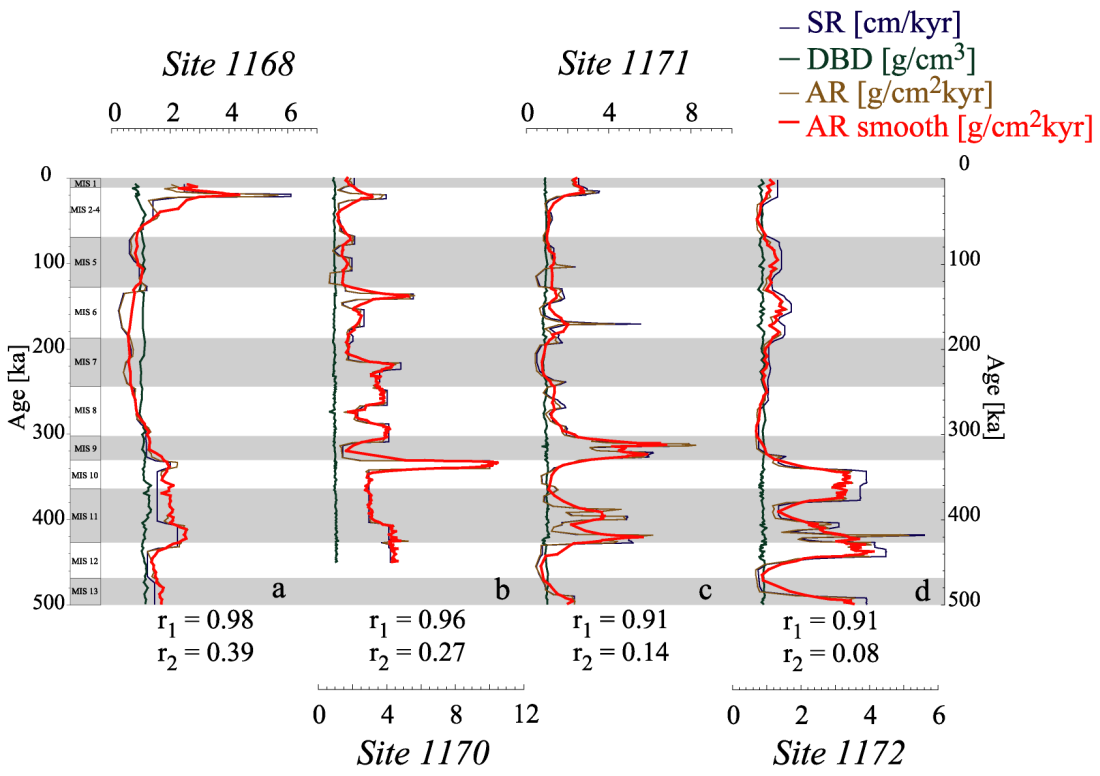

Fig. 20 The downcore sedimentation rate (SR, blue), dry bulk density (DBD, green), bulk accumulation rate (AR, brown) and 7-points moving average AR (AR smooth, red) records of the four studied sites: 1168(a), 1170 (b), 1171 (c) and 1172 (d). The relation between the SR and AR is indicated by the correlation factor r_1 ($p = 0.01$). The correlation coefficient between the AR and DBD, indicated by r_2, does not show a correlation ($p = 0.01$). Therefore, the accumulation rates of the individual proxies are most influenced by the SR. Interglacial stages are shaded.

east of the study area and at a waterdepth of 478 m clearly above the studied cores, exhibits a SR of about 1.2 cm/kyr (Hesse, 1994). In this shallower core, slightly higher values occured between marine isotopic stages (MIS) 11 and 7. Connell & Sikes (1997) studied cores on the South Tasman Rise with a SR between 2 and 5 cm/kyr, which fit with the data from the presented study. Therefore, the SR in the entire Tasman Sea seems to be characterised by those values.

The calculation of the dry bulk densities (DBD), necessary for the assessment of the AR (Section 3.2.5), has an internal error of 8 % (Fig. 8). The range of the DBD for the studied sites is within typical values for deep-sea sediments: between 0.51 g/cm^3 (minimum of Site 1172) and 1.34 g/cm^3 (maximum of Site 1168). The highest DBD are displayed at the western Site 1168 (mean of 1.09 g/cm^3), whereas the eastern Site 1172 shows the lowest values (mean of 0.87 g/cm^3). The DBD of the southern Sites 1170 and 1171 is largely similar (mean of 0.97 g/cm^3 and 0.95 g/cm^3 respectively). Connell &

Sikes (1997) studied cores on the South Tasman Rise. They found a DBD between 0.6 and 1.2 g/cm^3. The DBD of the studied cores is within the same range.

Due to the low range in DBD of the sediments, the calculated AR mimics the SR curve (Dickens & Owen, 1994; Schroeder et al., 1997). This is indicated by the correlation coefficients between the SR - bulk AR and SR – DBD (Fig. 20). The correlation coefficient of the former two parameters is larger than 0.89, whereas r (SR – DBD) lies between 0.08 and 0.39.

4.5.2. Accumulation rates of the individual proxies

The variability in AR for the different proxies is displayed in Figure 21. As pointed out before, the remarkable changes are coupled with the variations in SR and in the concentration of the individual proxy. Although considerable variations in the absolute concentrations and dynamics of the different proxies are observed, the calculation of accumulation rates gives a similar pattern for all proxies.

At Site 1168, the accumulation of the productivity proxies – represented by carbonate, TOC, chlorin and Ba_{exc} - and of the terrigenous matter – represented by Ti - was high during the glacials MIS 10, 8, 4-2 and at the transitions MIS 12/11 and 6/5. For the same proxies, the other near-land Site 1172 also reveals a higher accumulation during glacials MIS 12, 10 and 6. Site 1170, to the South, exhibits an increase in the accumulation of the described proxies during glacials MIS 10, 8, 6 and 2 and also during interglacial MIS 7. At the southernmost Site 1171, there is mainly an increase in the AR of the productivity proxies and the terrigenous matter during the older interglacials MIS 13, 11 and 9. An increase of the mentioned proxies is also observed at the transition MIS 2/1 at Site 1171.

A minimum in the carbonate concentration is observed during most glacials at the studied sites, however, the carbonate accumulation rates are markedly elevated during these glacials (compare Fig. 10 to Fig. 21). This observation coincides with the study of Hesse (1997) from the west of Tasmania and the Tasman Rise. The similarity between the bulk accumulation rate and the carbonate accumulation rate reflects the fact that carbonate is the primary sediment component, due to high concentrations (Schroeder et al. 1997)

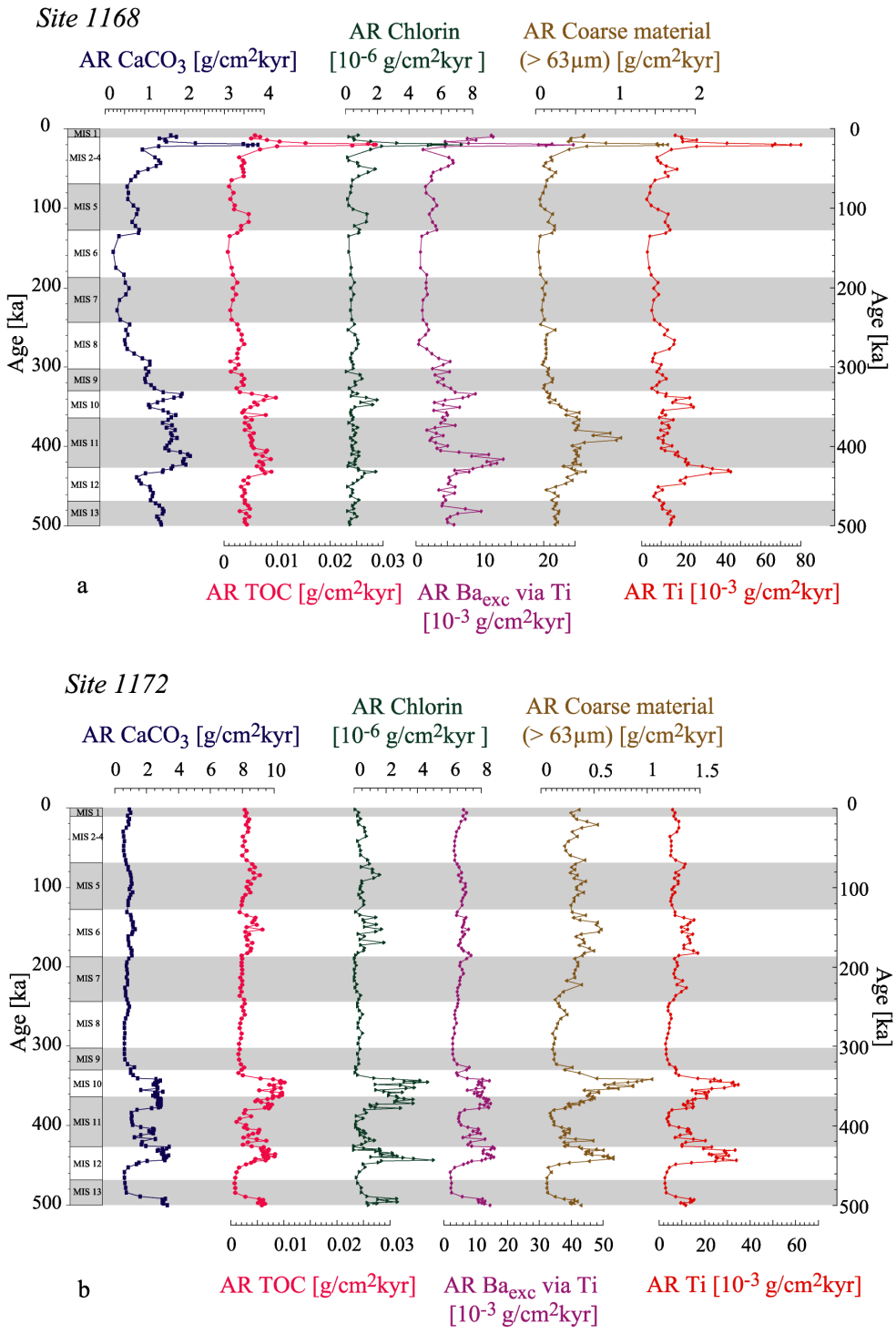

Fig. 21 Downcore record of the accumulation rates of different proxies for the studied sites: 1168 (a), 1172 (b), 1170 (c),1171(d). Due to the larger similarities between the northern sites 1168 and 1172, and the two southern sites 1170 and 1171, the graphs are shown by these couples. See next page for later two sites.
The shown records are the accumulation rates of carbonate ($CaCO_3$, blue squares), organic carbon (TOC, pink dots), chlorin (green triangles), excess barium (violet dots), coarse material (brown triangles) and titanium (red diamonds). The marine isotopic stages (MIS) are indicated. Interglacial periods are shaded.

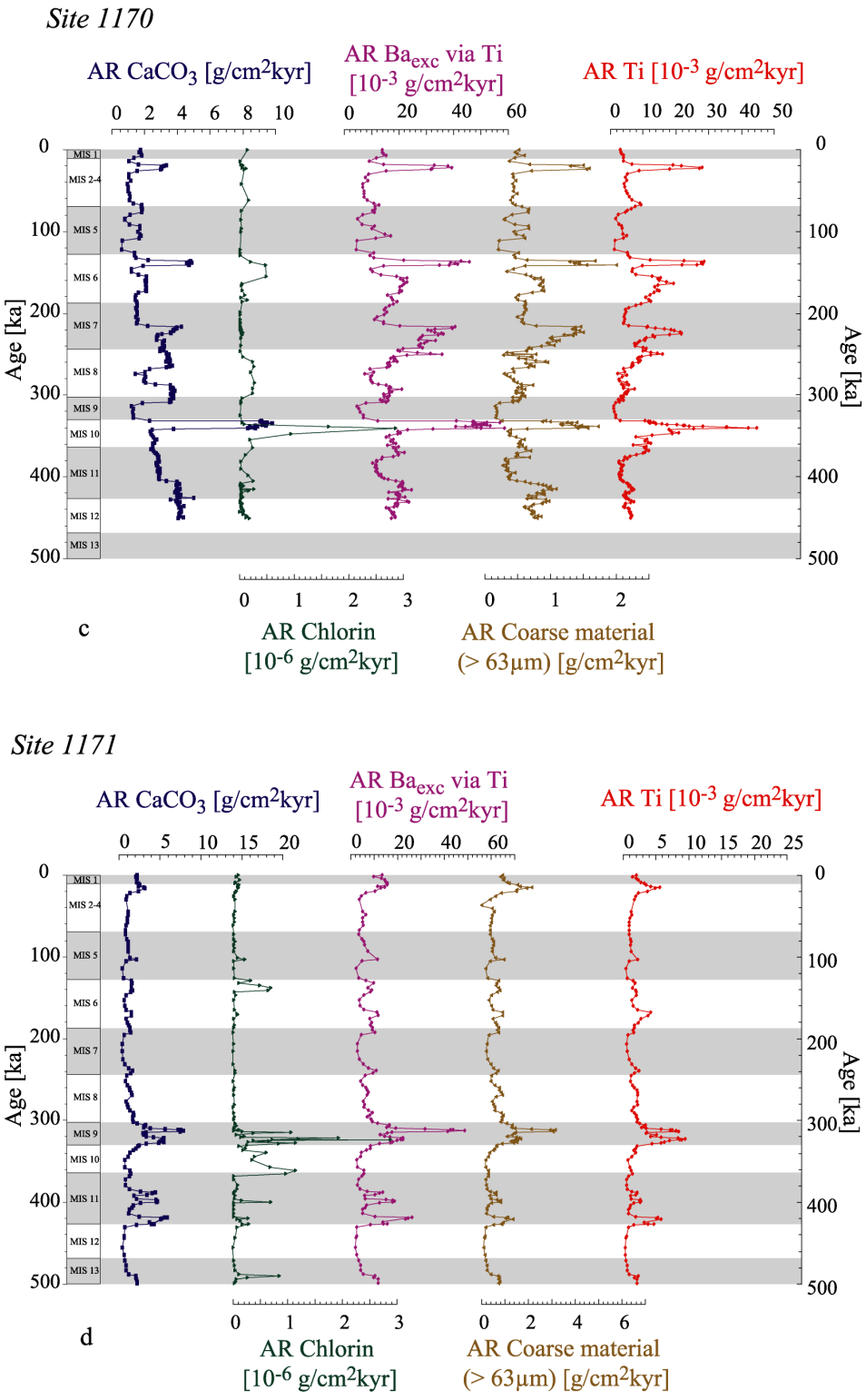

Fig 21 continued: site 1170 (c) and site 1171 (d).

The correlation coefficient of the AR of TOC and chlorin is even higher than for the pure concentrations (Site 1168 r = 0.91, Site 1172 r = 0.92; p = 0.01) (Fig. 22 and 12). Therefore, the variations in the chlorin concentrations and the accumulation of chlorins are interpreted as changes in the export productivity. The calculation of the paleoproductivity (PaP) based on the AR of TOC. Therefore they are only performed for Sites 1168 and 1172 (Section 3.2.5). The PaP varies between 70 and 170 gC/m^{2}a. The PaP-signal runs similar with the changes in the AR of the different proxies: the highest PaP (170 gC/m^{2}a) at Site 1168 was calculated at during MIS 2, whereas at Site 1172, higher PaP (140 gC/m^{2}a) was revealed during MIS 12 and 10.

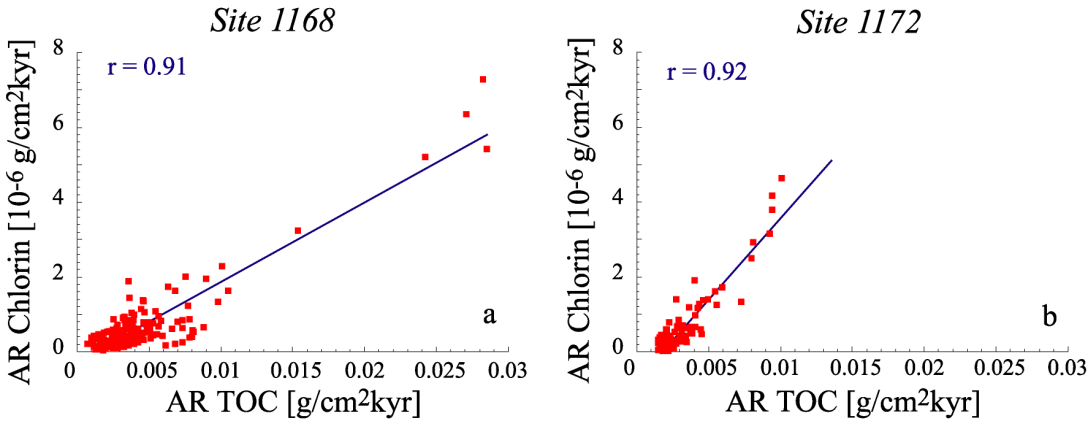

Fig. 22 Relationship between the accumulation rate of organic carbon (TOC) and the accumulation rate of chlorin for the sites 1168 (a) and 1172 (b). The blue line represents thee regression line, with the correlation coefficient r. See also Figure 11, where the absolute concentrations are compared. Due to the fact that both proxies do correlate in this study, also chlorin can be used as an indicator for paleoproductivity.

During times of high sedimentation, the portion of coarse carbonate is clearly increased (Fig. 21). Several reasons for this phenomenon can be assumed: either the planktonic foraminiferal productivity is higher, or there is likewise a higher production of other planktonic organisms, for instance coccolitophores (Howard & Prell, 1994; Broecker & Clark, 1999; Ruehlemann et al., 1999). At the studied sites, similar glacial/interglacial variations in the accumulation of the coarse carbonate have been observed (Fig. 21). The accumulation of the coarse carbonate reflects presumably the abundance of foraminifers. At Site 1168, the accumulation of coarse carbonate is high during MIS 12, 10 and 4-2 and due to the large amount of redeposited coarse carbonate (52 %) during MIS 11. For Site 1172, the higher accumulation of coarse carbonate is present during MIS 12, 10 and 6. At Site 1170, higher accumulation rates of coarse carbonate during MIS 12, 10, 8, 7, 6 and 4-2 are observed, meaning mainly during glacial periods. A

higher accumulation of coarse carbonate at Site 1171 took place during MIS 13, 11, 9, 6 and 4-2, i.e. in early interglacials and later glacials.

The range of the AR of Ba_{exc} for the studied sites is between 0.0005 g/cm^2 kyr (minimum of Site 1168) and 0.022 g/cm^2 kyr (maximum of Site 1170) (Fig. 21). This coincides with the AR of Ba_{exc} mentioned for core PS2082-1 (43°13'S, 11°44'E, 4610 m) situated in the Subantarctic Zone (Nürnberg at al., 1997). In this core, the AR of Ba_{exc} ranges between 0.0006 and 0.007 g/cm^2 kyr and glacial/interglacial variations are mentioned. Such variations can also be observed at the studied sites (Fig. 21).

The AR of Ti is around 0.04 g/cm^2 kyr during glacials and as low as 0.002 g/cm^2 kyr during interglacials. Latimer and Filippelli (2001) studied the terrigenous flux to core E45-29 (44°53'S, 106°31'E, 3863 m) situated to the east of the study area. They reported an AR of Ti between 0.01 g/cm^2 kyr and 0.0005 g/cm^2 kyr, therefore with a larger range than seen in the studied cores. The increase in the flux of Ti for the four studied sites took place mainly at the same time intervals than the increases of the other proxies. This indicates a link between the terrigenous flux and the export productivity.

5. DISCUSSION

5.1 Source and fluxes of terrigenous matter

5.1.1 Al/Ti and Fe/Al ratios to identify the source of terrigenous material

The Al/Ti and Fe/Al ratios can be used to identify the source type of detrital material, since different rock types have different ratios (e.g. Taylor & Mc Lennan, 1985; Latimer & Filippelli, 2001). Regarding the Fe/Al ratio, windblown dust exhibits an average of 0.28 (Pye, 1987); continental crust 0.84, i.e. fluvial input, and hydrothermal sources 1.61 (Taylor & McLennan, 1985). The Fe/Al ratio is 0.27±0.02 for all four sites and does not show any downcore variations (Fig. 17). Hence the terrigenous matter could be mainly derived from windblown dust. The Al/Ti ratio is slightly different at the four sites but the changes within one site are small (Fig. 17). The Al/Ti ratios exhibit values in a range from 21 to 36 (±1.3). According to Pye (1987), the Al/Ti ratio of windblown material is 21. Again, this points to dust as terrigenous source. For comparison, the Al/Ti ratio of average continental crust is 15.6, average upper crust is 26.8, granites are even 40 but basalt or oceanic crust are lower than 10 (Taylor & McLennan, 1985). Both ratios (Al/Ti and Fe/Al) therefore suggest that continental dust could be the main source for terrigenous matter in the studied cores, and the terrigenous source did not change over the last 500 kyr (Latimer & Filippelli, 2001).

Far from the shore, the terrigenous component of deep-sea sediments in general consists of eolian dust (Rea & Bloomstine, 1986). The South Tasman Rise is situated 330 km offshore and it is separated from the Australian continental margin by a 3200 m deep trough. Such topography largely prevents terrigenous supply via turbidity currents (Stein & Robert, 1985). The terrigenous sediment supply to Sites 1170 and 1171 thus must be attributed mainly to eolian dust. Only Site 1168 could be influenced directly by turbidity currents due to its position on the steep continental margin. But the correlation between the Ba_{exc} and the ratio of Ba/Ti ($r = 0.72$) reveals that turbidite deposition is unlikely (Murray & Leinen, 1996). Site 1172 is situated on the East Tasman Plateau, around 800 m higher than the depression separating the plateau from the continent. Therefore, a direct input from continental material can be doubted. As the Al/Ti and Ti downcore records show a similar pattern for all sites, sediment focussing, as transport mechanism of terrigenous matter, is excluded (Murray & Leinen, 1996) (Fig. 18).

Latimer & Filippelli (2001) stated that hemipelagic matter should be a source of terrigenous material in core E45-29 (44°53'S, 106°31'E, 3863 m), to the west of the study area. The overall driving force behind the increased terrigenous input during glacials may have been the sea level: a lowered sea level at the onset of glacial intervals caused an enhanced continental shelf denudation, suspension discharge and increased turbidite deposition (Schönfeld & Kudras, 1993). Consequently the hemipelagic input to the seafloor increased. Direct river inflow from the Australian continent over the Tasman Plateau is, on the other hand, less likely (Ikehara et al., 2000). This indicates that the input of material by rivers is not causing the permanent flux of terrigenous input presented in the samples of the studied sites.

5.1.2 Fluxes of terrigenous matter

To further constrain the potential source for the terrigenous material, the accumulation of siliciclastic material and of Ti were compared to the dust record of the Vostok ice core (Petit et al., 1999). Stacking the accumulation rates of the siliciclastic material and the Ti for the four studied sites, results in a clear glacial/interglacial variability (Fig. 23). Enhanced accumulation of Ti and siliciclastic material is present during transitions or glacials MIS 12/11, 10, 7/8, 6, 4-2. The stacked records match to the dust record of the Vostok ice core, revealing that eolian dust contributes to the glacially enhanced supply in the study area.

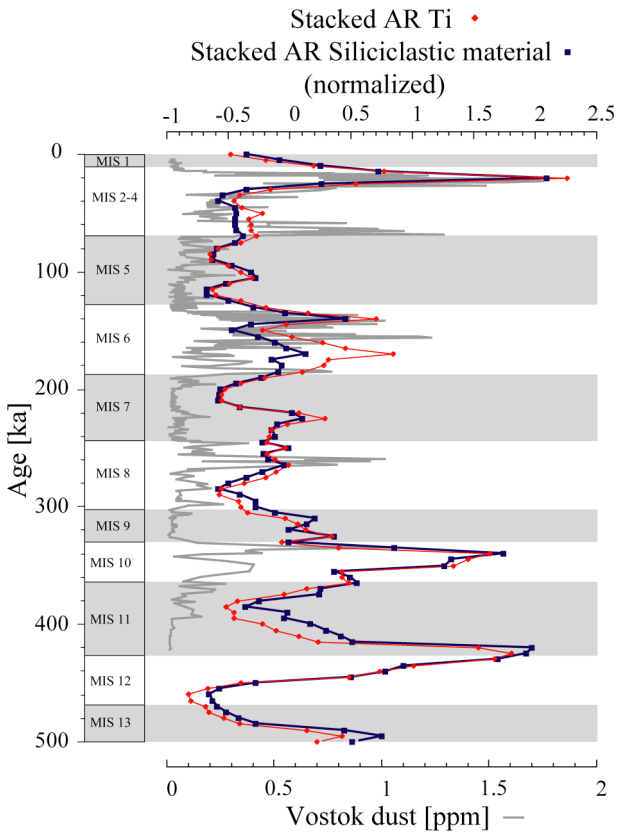

Fig. 23 Stacked records of the accumulation rates of Ti (red diamonds) and siliciclastic material (blue squares) normalized to unit variance for the studied sites 1168, 1170, 1171 and 1172. For comparison, the Vostok dust record is shown (Petit et al., 1999). Interglacial stages are shaded.

The iron accumulation rates for Sites 1168, 1170 and 1172 are 5-10 mg/cm^{2}kyr during interglacial periods, and increased to 40 mg/cm^{2}kyr during glacial times.

Such iron accumulation rates are comparable to glacial/interglacial variations described in South Atlantic and Southern Indian Ocean sites from similar latitudes (Kumar et al., 1995; Latimer & Fillipelli, 2001). Site 1171 has an exceptional status due to the very low concentrations of terrigenous matter. Iron accumulation rates at that position are 2.5 mg/cm^{2}kyr during interglacials and up to 6 mg/cm^{2}kyr during glacials. These concentrations compare to values reported by Murray et al. (1993) for the equatorial Pacific on comparable time scales. According to Ikehara et al. (2000), the eolian flux in the Tasman Sea increased during the glacials by a factor of 1.5 to 3 compared to the interglacials. The studied glacial/interglacial variations are within the same range. Duce & Tindale (1991) estimate the present eolian iron flux to about 0.1-1 mg/cm^{2}kyr in the study area, which is much lower than the interglacial iron accumulation within the studied sites (minimum of 2.5 mg/cm^{2}kyr). The iron flux mismatch between the sediment record and the measured modern iron fluxes was already mentioned in former studies (Murray et al. 1993; Kumar et al., 1995). Murray et al. (1993) discussed the possibility that eolian iron fluxes are generally underestimated, because dust storms were presumably not adequately considered.

An increase in glacial dust deposition is mentioned by several authors (e.g. Petit et al., 1981; Petit et al., 1990; Rea, 1994; Mahowald et al., 1999). Numerous modelling studies show similar observations (e.g. Lautenschlager & Herterich, 1990; Klinck & Smith, 1993; Mahowald et al., 1999; Latimer & Filippelli, 2001). Hesse (1997) found glacial peaks in the dust flux in the Tasman Sea. In the Indian Ocean, 3 to 5 times more dust entered the sediment during the glacial comparing to the interglacial periods (Rea, 1994). According to Latimer & Filippelli (2001) the accumulation of iron in the southern Indian Ocean was ten times higher during glacial times and exceeded the estimated regional eolian flux by 50 times. The estimated fallout of dust at Antarctica, seen in ice-cores, is also much higher during glacial periods than during interglacials (1000 to 2000 ng/g in glacials, 50 ng/g in interglacials) (Petit et al., 1999).

Although the entire southern hemisphere shows a very low dust input of a few mg/cm^2 kyr (Rea & Bloomstine, 1986; Duce & Tindale, 1991), Australia is known as the largest contemporary dust source area in the southern hemisphere (Rea, 1994). The Cenozoic dust record of the southern hemisphere, described by Stein & Robert (1985), suggests an increase in aridity in the Australian source regions since 3 Ma. Australia has a dry-land climate with main south to southeasterly winds. In southeast Australia, the

westerly winds are known to carry dust eastward across the Tasman Sea and even as far as the New Zealand Alps (Collyer et al., 1984; Hesse, 1997; Stein & Robert, 1985). The eolian origin of the sediments is also indicated by the quartz content in deep-sea sediments from the Tasman Sea, which shows a distinct decrease from the Australian continent toward the east (Thiede, 1979).

The increase in eolian supply during the glacials is in agreement with observations from Australia that suggest arid climatic conditions with an intensification in frequency and velocity of winds from the continental interior (Thiede, 1979; McTainsh & Lynch, 1996). The model of Mahowald et al. (1999) predicts an expanded Australian source area of dust during the Last Glacial Maximum (LGM, around 18 kyr before present). Material of the continent Australia contributed dust to the south-western Pacific Ocean in general during the LGM with around three times more material than at present (Hesse, 1994). Galloway (1965) stated that during the LGM the late Quaternary desert environment in Australia was widespread. The zone of westerly winds shifted northward during the LGM (Thiede, 1979), and an increase of wind strength of about 70 % for southern hemisphere westerly winds is suggested (Lautenschlager & Herterich, 1990). On the basis of aerosol content determinations in the Vostok ice core, Petit et al. (1981) suggested a wind strengthening of 50-80% for the subantarctic glacial ocean. Kutzbach & Guetter (1986) presented a west-wind drift movement of about 5°N during austral summer at LGM. Therefore, the enhanced flux of eolian material might have been not only due to the extensive arid continent Australia but are inferred by the glacially intensified westerly winds. However, Hesse & McTainsh (1999) demonstrated by the particle size distribution of eolian dust over the Tasman Sea, that mid-latitude westerly winds in the southern Australian region were similar during the Holocene and LGM. If so, the temporal variations in dust supply are linked to the varying expansion of source areas (Hesse & McTainsh, 1999).

5.2 Iron Hypothesis

If a higher productivity event takes place while there is an enhanced input of terrigenous material, the hypothesis of particulate iron influencing the primary productivity is proposed. This ‘Iron Hypothesis’ was the first time named by Martin (1990). It states that iron is a limiting factor for marine phytoplankton growth in vast areas of the oceans. The primary productivity in the Southern Ocean today is in the order of 7.4 x 10^{13} g/a (Martin, 1990).

Martin et al. (1994) performed a test whereby they enriched the equatorial Pacific Ocean with iron. This caused a doubling of plant biomass, a threefold increase in chlorophyll and a fourfold increase in plant production. In the high-nitrate low-chlorophyll (HNLC) ocean areas, a limited phytoplankton growth and biomass is characteristic. Sedwick et al. (1997) inferred from micronutrient water sample studies southwest of Tasmania, that today's primary productivity within the Australian subantarctic region is limited by iron and silicate availability. Kumar et al. (1995) found biologically iron associated with glacially increased dust fluxes. Therefore they stated that relieved iron limitation induced an enhanced surface primary productivity. The phytoplankton growth is limited by the iron bioavailability as assured by Ikehara et al. (2000).

In a further step, Broecker & Henderson (1998) proposed to invoke the oceanic nitrogen cycle in the control of glacial/interglacial changes in CO_2 in order to explain the time lag between global atmospheric CO_2 rise and the dust flux decrease in the Southern Ocean. Since iron fertilization fosters nitrogen fixation (Falkowski, 1997), the increased supply of fixed nitrogen to the ocean via enhanced dust flux might have caused increased surface ocean productivity during glacial times, which would allow a greater CO_2 draw down in surface waters. Therefore, the changes in iron availability in the past Southern Ocean, causing an increased primary production and the export of TOC, could have had an effect on the atmospheric CO_2-pressure in the glacial/interglacial times (Fig. 24).

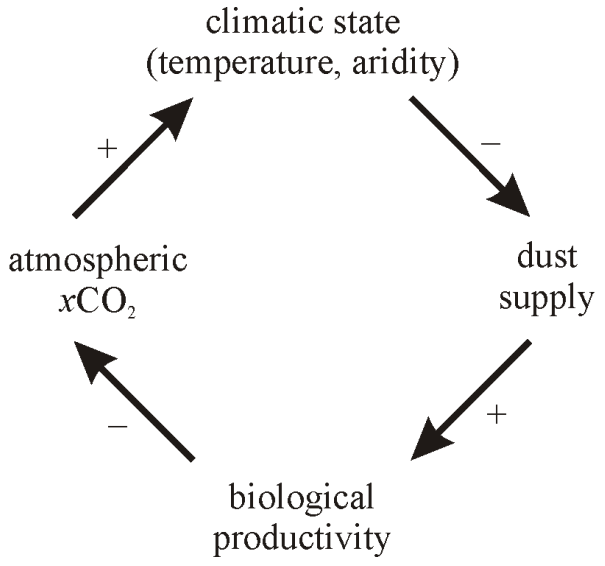

Fig. 24 Schematic overview of the 'iron hypothesis' and the simplified feedback mechanisms in the climate system, as indicated in this study. Dust, the strength of the biological pump, CO_2 and the state of the climate (influencing the temperature and aridity of the source area of dust) are involved. Modified after Martin et al (1994) and Ridgwell & Watson (2002).

Although Fe is the fourth most abundant element in the Earth's crust (Taylor & McLennan, 1985), the amount present in the ocean is low (smaller then 1 nmol/kg) (e.g. Landing & Bruland, 1987; Martin & Gordon, 1988;

Martin et al., 1990; Mortlock et al., 1991). Iron depth profiles through the water column are depleted at the surface and enriched in deeper parts (Martin, 1990). Fulfilling the phytoplankton's offshore demand for iron seems to be a problem. It appears that adequate Fe amounts are supplied to the oligotrophic gyres via long-range transport and fallout of Fe-rich atmospheric dust, originally derived from terrigeneous and arid regions (Duce & Tindale, 1991; Martin & Gordon, 1988). The wind speeds during the LGM were 1.3 to 1.6 times higher than today and the tropical areas were 5 times larger (Petit et al., 1981; Sarnthein et al., 1988). Accordingly, the Fe-enriched atmospheric dust load was 10 to 20 times larger during glacial times. Due to the drier environment in Australia, more dust was present for transport (Collyer et al., 1984; Goudie, 1983; Hesse, 1994; Hesse & McTainsh, 1999).

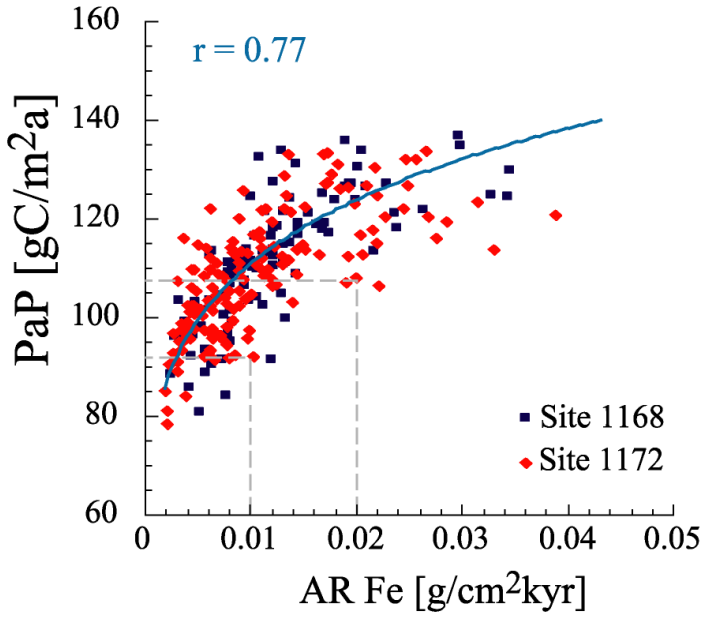

Fig. 25 Accumulation rate of Fe versus the estimated paleoproductivity (PaP) for sites 1168 (blue squares) and 1172 (red diamonds). Paleoproductivity was calculated from TOC using the equation of Sarnthein et al. (1992). The correlation coefficient r is indicated.

The calculation of the paleoproductivity (PaP) by means of TOC gives an extra parameter to asses validity of the iron hypothesis for the study area. From Figure 25, it can be seen that an increase in the accumulation of terrigenous matter (by means of the AR Fe) causes an increase of the amount of export productivity. The correlation coefficient of 0.77 between the PaP and AR Fe indicates a relation between both factors (Fig. 25). The terrigenous supply is most likely important for the primary productivity in the study area.

However, if the export productivity was only influenced by the eolian iron supply, an equally enhanced glacial productivity in the whole study area is expected. Distinct differences between the eastern and western sites (1172 and 1168 respectively) are

observed. This will be influenced by the position of the wind plume, orientated to the east of Australia, by the position of the westerly winds, and by the temporal and spatial variations in the surface hydrography. The East Australian Current can be strong enough to flow all over the East Tasman Plateau and push the STC more to the south. This would bring a nutrient poor water mass over the East Tasman Plateau and over Site 1172. On the western site of Tasmania (1168), also a strengthening of the Zeehan Current, or local upwelling influences the depositionary environment.

5.3 The variability of the Southern Ocean frontal system since 500 ka

In the following, changes in the oceanographic frontal system in the study area over the last 500 kyr will be discussed. Today, the Subtropical Convergence (STC) is situated in between the cores studied. This provides an excellent opportunity to constrain changes in the position of the STC and related processes. The changes in the paleo-latitude of the STC through the Quaternary, south and southeast of Australia are documented in several studies (e.g. Belkin & Gorson, 1996; Connell & Sikes, 1997; Dickens & Owen, 1994; Fenner et al., 1992; Francois et al., 1993; Howard & Prell, 1992; Kawagata, 2001; Passlow et al., 1997; Peterson & Whithworth, 1989). Former studies are situated in deeper waters with carbonate dissolution (e.g. Howard & Prell, 1992), cover just the last two glacial periods (e.g. Connell & Sikes, 1997) or are based on faunal changes (e.g. Kawagata, 2001). In the this study, the time period is extended to six glacials, the studied sites are situated above the present-day lysocline and geochemical proxy data were the basis to define the position of the water masses and surface fronts.

The STC displays enhanced primary production. Factors that may influence productivity changes are variations in oceanic circulation, changes in upwelling intensity or variations in nutrient supply due to eolian and/or fluvial input. With certain exceptions, export productivity was enhanced during the glacial stages at all studied sites. This could be related to the changing position of the frontal system in the Southern Ocean (Francois et al., 1993; Passlow et al., 1997). The export productivity was defined on hand of the variations in the accumulation of carbonate, TOC, chlorin and Ba_{exc}. If the STC was present to the north of a certain site, an enhancement or maximum in the accumulation of those export productivity proxies should occur (Fig. 26). During that time, nutrient-rich Subantarctic Surface Water (SASW) prevailed over that site. The increase in export productivity is additionally driven by the higher flux of terrigenous matter, i.e. iron fertilisation. The flux of terrigenous matter was

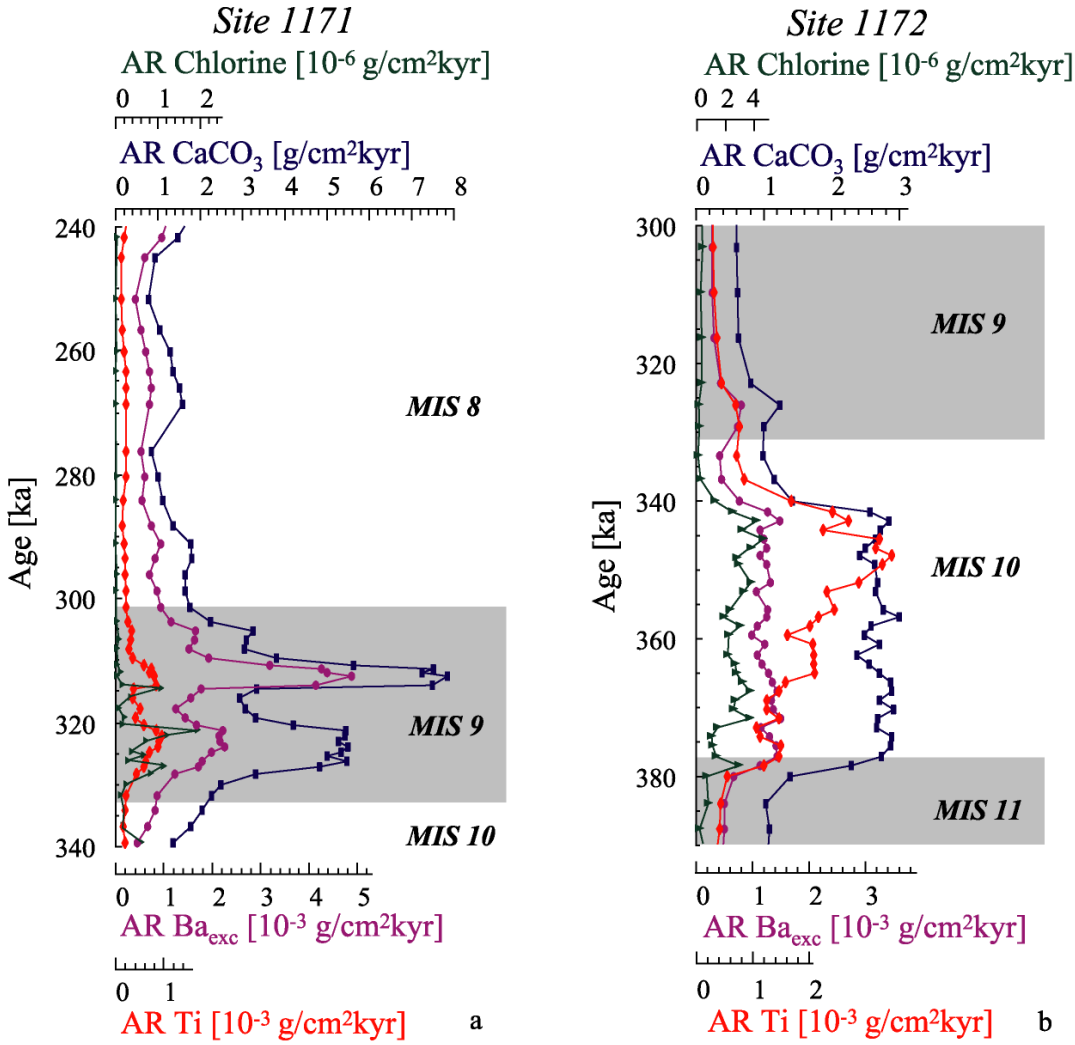

Fig 26 Downcore record for site 1171 (a) of the time-interval between 240 ka and 340 ka and site 1172 (b) of the time-interval between 300 ka and 900 ka. The accumulation rates of carbonate (blue squares), chlorin (green triangles), Ba_{exc} (pink dots) and Ti (red diamonds) are shown. The fact that the accumulation of those proxies exhibits a maximum at site 1171 during interglacial MIS 9 (a) and at site 1172 during glacial MIS 10 (b), the position of the STC should be north of the sites during that particular time. The interglacials are shaded.

defined by the accumulation of Ti (and Al, Fe). The increased flux of terrigenous matter most likely points to the changing strength and direction of the zone of westerly winds.

The variations in the accumulation of coarse carbonate were taken in consideration as well. However, their changeability runs similar with the variations in the accumulation of the export productivity proxies and will be not considered in detail. Changes in the strength of the East Australian Current (EAC) and the Zeehan Current may have had an impact on the regional productivity pattern.

The paleoceanographic situation in the study area since the last 500 ka is discussed from recent to older periods. First the interglacial (uneven MIS-numbers) and thereafter the glacial (even MIS-numbers) will be discussed.

5.3.1 Interglacial periods

Mainly during all interglacial periods in the study area, the SASW withdrew from the area around Tasmania. A low productivity and less terrigenous matter supply to the northern sites during interglacial times indicated that the STC retreated to the south and was situated around the Tasman Rise (Fig. 21). A similar pattern of the surface water masses and the oceanographic fronts is present during all the interglacials since 500 ka (Fig. 27-a,c,e,g,i,k). The export productivity and the terrigenous matter fluxes are low at Sites 1168, 1170 and 1172, except during MIS 5 at Site 1168, MIS 7 at Site 1170 and MIS 13 at Site 1172. The minima in the accumulation of the proxies point to the presence of the Subtropical Surface Water (STSW) over those sites. Also at Site 1171, the STSW is situated over the site during the later interglacials MIS 1, 5 and 7 (Fig. 25-a,c,e), due to the low export productivity and terrigenous supply. But during the older interglacial periods MIS 9, 11 and 13, an increase in the accumulation rates (Fig. 21), points to the position of the STC over that site (Fig. 27-g,i,k). Therefore the maximal extend of the STC during interglacial times since 500 ka can be defined as 48°S.

Exceptional are the circumstances at certain sites during three interglacial times: MIS 5, 7 and 13 (Fig. 27-c,e,k). The increase in the accumulation of the export productivity and terrigenous matter during MIS 5 at Site 1168 is probably more a local phenomenon, rather than an indication of the STC position (Fig. 27c). This is also indicated by Passlow et al. (1997). That study mentioned a poleward excursion of the STC with respect to core E27-30 (45°04.0'S, 147°13.7'E, 3552 m) situated more to the south of Site 1168, during MIS 5. A possible explanation is upwelling along the margin of Tasmania as proposed by James et al. (2001).

Fig. 27 a-k (next two pages) Overview of the presented descriptive model of the variability of the position of the Subtropical Convergence (STC), the Subantarctic Front (SAF) and the Subantarctic Surface Water (SASW) in between both frontal zones, since 500 ka. The four studied sites are presented. The changes in the accumulation of the export productivity (green snails) and terrigenous matter (orange wheels) proxies are used as the basis for the changes in the Southern Ocean palaeoceanography. The marine oxygen isotope events (MIS) were defined using the nomenclature proposed by Prell et al. (1986) and Tiedemann et al. (1994).

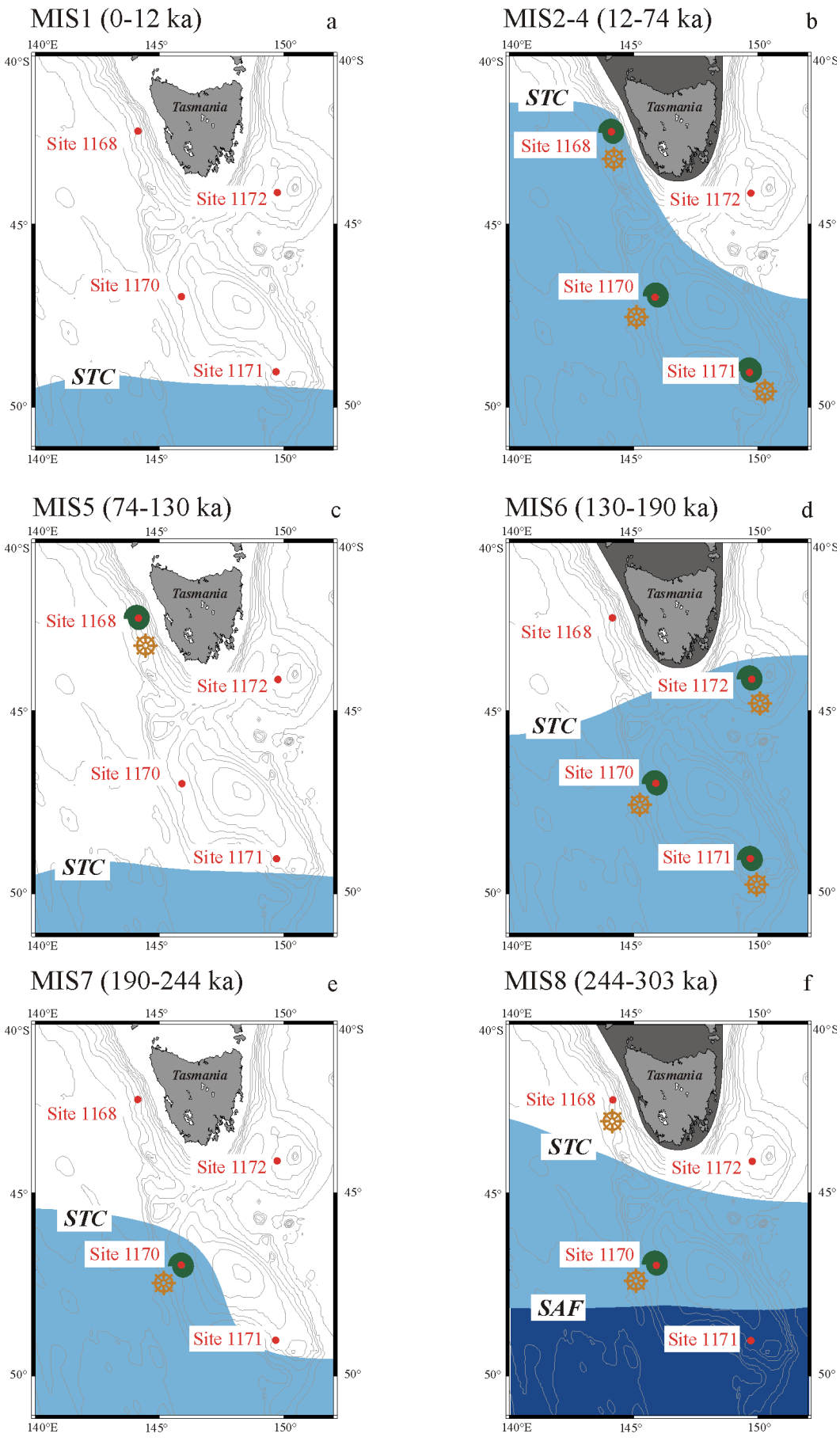
MIS1 (0-12 ka)
a
MIS2-4 (12-74 ka)
b
MIS5 (74-130 ka)
c
MIS6 (130-190 ka)
d
MIS7 (190-244 ka)
e
MIS8 (244-303 ka)
f
Tasmania
Site 1168
Site 1172
Site 1170
Site 1171
STC
SAF
140°E
145°
150°
40°S
45°
50°

Fig. 27 a-f

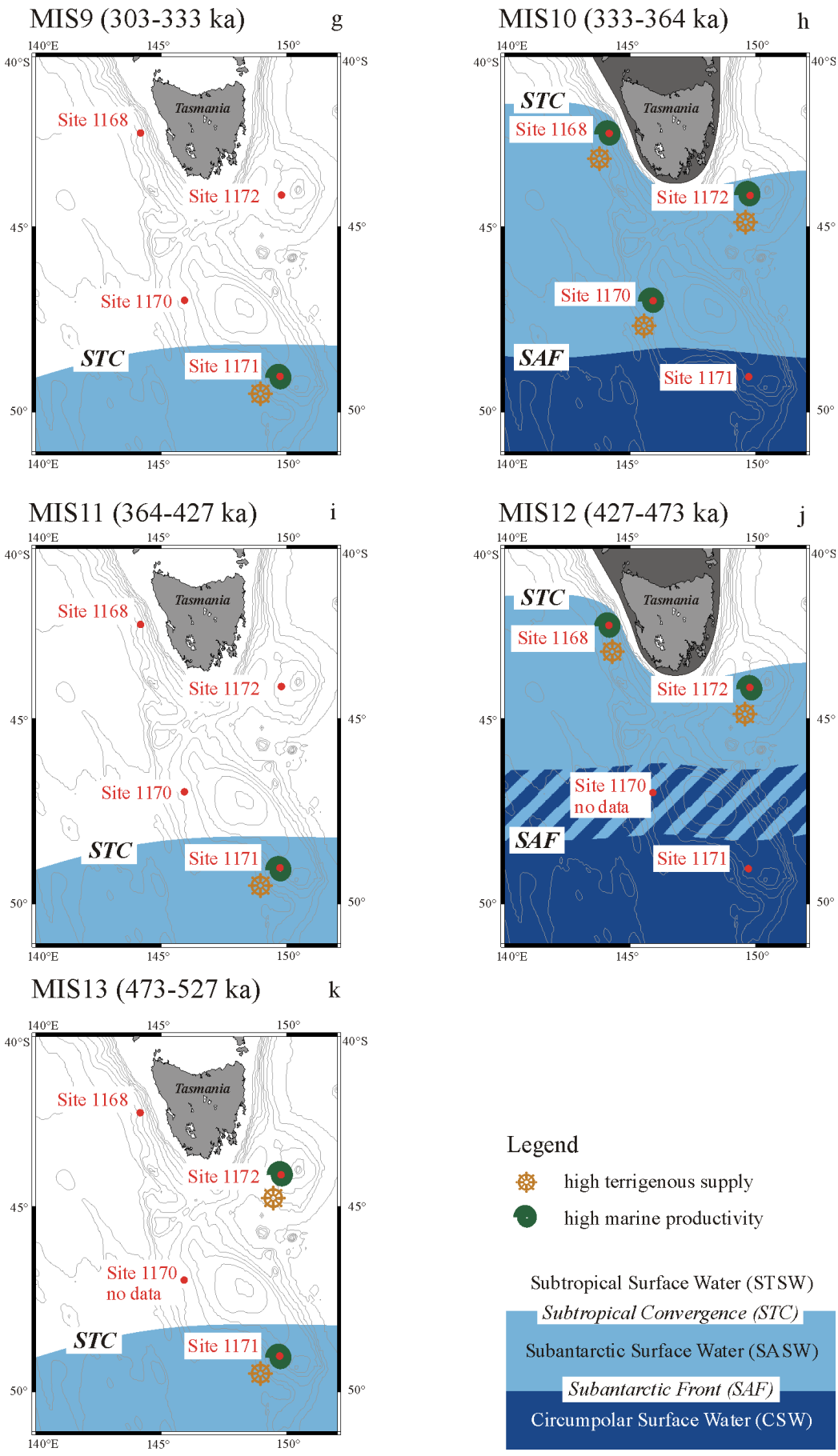

Fig. 27 g-k (continued)

During MIS 7, the position of the STC changed (Fig. 27e). At Site 1170, a higher productivity and terrigenous flux was present. This is in opposite to Site 1171, where no indications for an increase in accumulation of productivity or terrigenous matter are observed (Fig. 21). Both sites are situated within 150 km of each other on the Tasman Rise. After these results, the STC most probably oscillates between both sites. The difference in the accumulation of the terrigenous matter between Sites 1170 and 1171 is presumably caused by the pattern of the westerly wind zone. It probably reached over Site 1170 but did not influence the southern Site 1171. As data are missing for MIS 13 at Site 1170, it is hard to detect the northern extent of the STC during that interglacial period (Fig. 27k). Sites 1171 and 1172 exhibit a higher export productivity and terrigenous flux. The STC reached over the position of Site 1171, but it is uncertain if it reached as far north as Site 1172. The increase in the accumulation of Ti indicates that the input of continental material increased at Site 1171 and 1172. This induced a higher marine and export productivity, notable in the export productivity pattern (Fig. 21).

5.3.2 Glacial periods

The variability of the frontal system in the study area during the glacial periods is larger (Fig. 27-b,d,f,h,j). During glacial MIS 2-4, the accumulation of the export productivity proxies and the terrigenous matter proxies is high at Sites 1168, 1170 and 1171 (Fig. 21). Therefore, it is concluded that the STC was present to the north of these three sites (Fig. 27b). At the west of Tasmania, the STC reached at least 42°30'S, being its maximal northern extent. To the east of Tasmania, at Site 1172, no increase in productivity and terrigenous flux is observed. After these results, the East Australian Current is probably strengthened during that time and influenced the surface water over the East Tasman Plateau. Therefore the STC was pushed away, more to the south. During the next glacial MIS 6 (Fig. 27d), the situation is the other way around: a larger flux of terrigenous matter and export productivity proxies to the east of Tasmania (Site 1172), but not to the west (Site 1168) (Fig. 21). The zone of the westerly winds most likely did not reach latter site. The STC therefore reached at least 44°S to the east of Tasmania. This observation coincides with studies of cores close to the position of Site 1172: core E36-23 (43°53.02'S, 150°03.02'E, 2521 m) (Martinez, 1994) and core FR1/94-GC-3 (44°15.38'S, 149°59.47'S, 2667 m) (Nees et al., 1999). The two southern sites studied (1170 and 1171) also show an increased productivity and terrigenous matter flux during MIS 6 (Fig. 21). Therefore, in whole study area, except for the west

of Tasmania, the SASW is present. During glacial MIS 8, the extension of the SASW is limited to the central part of the study area (Fig. 27f). Only at Site 1170, an increased flux in the studied proxies is present. Therefore the STC did not reach 44°S to the east nor 42°30'S to the west of Tasmania. These results agree with the study of Martinez (1994), who assessed short-time excursions of the STC into the southern Tasman Sea during the glacials MIS 6, 10 and 12, and not during MIS 8. In the southern part of the study area, the Subantarctic Front (SAF) is present between Sites 1170 and 1171, around 48°S. The SAF was situated at the same position during MIS 10. But to the north, the SASW extended and almost covered the whole study area as the two northern sites (1168 and 1172) exhibit an increase in the accumulation of the productivity and terrigenous matter proxies. The same northern extent was present during MIS 12. Since data at Site 1170 are missing for that time interval, the position of the SAF cannot be more precise than to the north of Site 1171.

A maximal extend of the STC and northern position of the SAF in the study area could be determined. The study of Martinez (1994) proved, that the STC never reached to 39°S to the east of Tasmania and the study of Passlow et al. (1997) indicated that ODP Site 593 (40°30.47'S, 167°40.47'E, 1068 m) was also never reached by the STC. Therefore and with the data of this study, the maximal northern paleo-latitude of the STC during glacial times is between 39°S and 42°30'S to the west of Tasmania and between 40°30'S and 44°S to the east of Tasmania. During those glacials, the maximal northern extend of the SAF was between 47°S and 48°30'S.

6. CONCLUSIONS

A multi-proxy study of ODP-Leg 189 sites from the Tasmanian Seaway (Southern Ocean) is presented herein. The studied sites were: Site 1168 to the west, Site 1172 to the east, and Sites 1170 and 1171 to the south of Tasmania. The downcore records over the last 500 kyrs provided insights in paleoproductivity, terrigenous supply and varying position of the oceanographic frontal system around Tasmania during glacial/interglacial changes.

Carbonate, total organic carbon, biogene barium and chlorin were analysed and their accumulation rates were calculated to reconstruct paleoproductivity. Chlorin concentrations were assessed for the first time in the Southern Ocean. The chlorin and total organic carbon concentrations and accumulation rates displayed synchronous downcore variations, indicating that chlorin reflects export productivity for the study area. The high carbonate concentrations at all sites indicate a generally high calcareous nannoplankton and foraminifer production since at least 500 ka. The carbonate concentration at the southern Sites 1170 and 1171 reaches 98 %. An increased terrigenous input at the northern Sites 1168 and 1172 dilutes the carbonate content to about 80 %.

Terrigenous matter was assessed by the analysis of the aluminium, titanium and iron concentrations and by the calculation of the amount of siliciclastic material. The simultaneous variations in these proxies during the last 500 kyrs point to the same sources and pathways for terrigenous material. The ratios Fe/Al and Al/Ti indicate wind as the main transport mechanism. The records of the accumulation rates of the terrigenous matter match the dust record of the Vostok ice core, whereby all records show an enhanced terrigenous input during the glacials. This increased accumulation of terrigenous material is probably caused by an intensification of the atmospheric circulation during the colder periods. The enhanced input of terrigenous matter caused an increase in export productivity in the studied area by iron fertilisation. This link between the terrigenous supply and the paleoproductivity indicated that the “Iron Hypothesis” (Martin, 1990) is plausible for the Tasmanian Seaway.

The reconstruction of the northern and southern boundary of the Subantarctic Surface Water (SASW) allowed describing the paleo-position of the Subtropical Convergence (STC) and the Subantarctic Front (SAF). The glacial/interglacial variations of the

studied proxies in combination with published data allowed establishing a scenario of the changing position of the oceanographic frontal system around Tasmania for the last 500 kyrs.

The interglacials were, in general, characterised by low productivity and small terrigenous supply. During MIS 1, 5, and 7 the STC was located

south of 49°S. During MIS 9, 11 and 13 increased export productivity at the southernmost Site 1171 suggests an enhanced influence of the SASW, and the STC located to the north of that site. The other sites were not affected by the SASW during MIS 9, 11 and 13. During most glacials an increased paleoproductivity and terrigenous flux were observed in the whole study area. This indicates that the frontal system and the zone of westerly winds were shifted to the north. The STC was located between 39°S and 42°S west of Tasmania and between 40°30'S and 44°S east of Tasmania. The SAF was only present in the study area during MIS 8, 10 and 12, when it crossed the southernmost Site 1171 as indicated by reduced paleoproductivity. On the long-term scale, the frontal system in the study area slightly shifted to the south since 500 ka.

All previous approaches only were able to consider the last full glacial-interglacial cycle. The present study revealed the regularity of the frontal fluctuations throughout the late Pleistocene. This study showed that variations in geochemical proxies could be used to reconstruct the temporal and spatial variability of surface water masses. The described variations in the paleo-position of the frontal system in the region around Tasmania provide new insights in the surface water dynamics of the Southern Ocean circulation system.

7. REFERENCES

Baines, P., Edwards, R. & Fandry, C., 1983. Observations of a new baroclinic current along the western continental slope of Bass Strait. Australian Journal of Marine Freshwater Research, 34: 155-157.

Bareille, G., Grousset, F., Labracherie, M., Labeyrie, L. & Petit, J.-R., 1994. Origin of detrial fluxes in the Southeast Indian Ocean during the last climatic cycles. Paleoceanography, 9(6): 799-819.

Belkin, I.M. & Gorson, A.L., 1996. Southern Ocean fronts from the Greenwich meridian to Tasmania. Journal of Geophysical Research, 101(C2): 3675-3696.

Berger, W. & Herguera, J., 1992. Reading the sedimentary record of the ocean's productivity. In: Falkowski, P.W., A. (Editor), Primary productivity and biochemical cycles in the sea. Plenum Press, New York, pp. 455-486.

Bickert, T., 1992. Rekonstruktion der spätquartären Bodenwasserzirkulation im östlichen Südatlantik über stabile Isotope benthischer Foraminiferen., 27. Berichte, Fachbereich Geowissenschaften, Universität Bremen, Bremen, 205 pp.

Bishop, J., 1988. The barite-opal-organic carbon association in oceanic particulate matter. Nature, 332: 341-343.

Brathauer, U. & Abelmann, A., 1999. Late Quaternary variations in sea surface temperatures and their relationship to orbital forcing recorded in the Southern Ocean (Atlantic Sector). Paleoceanography, 14(2): 135-148.

Broecker, W. & Henderson, G., 1998. The sequence of events surrounding Termination II and their implications for the cause of glacial-interglacial CO_2-changes. Paleoceanography, 13(4): 352-364.

Broecker, W. & Clark, E., 1999. $CaCO_3$ size distribution: A paleocarbonate iron proxy? Paleoceanography, 14(5): 596-604.

Collyer, F., B, B., Churchman, G., Clarkson, T. & Steiner, J., 1984. Trans-Tasman dust transport event. Weather and Climate, 4: 42-46.

Connell, R. & Sikes, E., 1997. Controls on Late Quaternary sedimentation of the South Tasman Rise. Australian Journal of Earth Sciences, 44: 667-675.

Cooke, P., Nelson, C., Crundwell, M. & Spiegler, D., 2002. Bolboforma as monitors of Cenozoic paleoceanographic changes in the Southern Ocean. Paleogeography, Paleoclimatology, Paleoecology, 188: 73-100.

Creswell, G., 1987. The East Australian Current. CSIRO Marine Laboratory Information Sheet, Number 3.

Cresswell, G., 2000. The Zeehan Current. CSIRO Marine Laboratory Information Sheet, Number 20.

Dehairs, F., Chesselet, R. & Jedwab, J., 1980. Discrete suspended particles of barite and the barium cycle in the open ocean. Earth and Planetary Science Letters, 49: 528-550.

Dickens, G., 2001. Sulfate profiles and barium fronts in sediment on the Blake Ridge: Present and past methane fluxes through a large gas hydrate reservoir. Geochimica et cosmochimica Acta, 4: 529-543.

Dickens, G. & Owen, R., 1994. Late Miocene-early Pliocene manganese reduction in the central Indian Ocean: Expansion of the intermediate water oxygen minimum zone. Paleoceanography, 9: 169-181.

Duce, R. & Tindale, N., 1991. Chemistry and biology of iron and other trace metals. Limnological Oceanography, 36(8): 1715-1726.

Dymond, J., Suess, E. & Lyle, M., 1992. Barium in deep-sea sediment: a geochemical proxy for paleoproductivity. Paleoceanography, 7(2): 163-181.

Emerson, S. & Hedges, J., 1988. Processes controlling the organic carbon content of open ocean sediments. Paleoceanography, 3(5): 621-634.

Exon, N., Moore, M. & Hill, P., 1997. Geological framework of the South Tasman Ridge, south of Tasmania, and its sedimentary basins. Australian Journal of Earth Sciences, 44: 561-577.

Exon, N., Kennett, J., Malone, P. & Leg 189-Shipboard Scientific Party, 2001. The Tasmanian Gateway: Cenozoic Climate and Oceanographic Development Sites 1168-1172. Proceedings of the Ocean Drilling Program, Initial Reports, 189.

Falkowski, P., 1997. Evolution of the nitrogen cycle and its influence on the biological pump in the ocean. Nature, 387: 272-275.

Fenner, J., Carter, L. & Stewart, R., 1992. Late Quaternary paleoclimate and paleoceanographic change over northern Chatham Rise, New Zealand. Marine Geology, 7(1): 79-117.

Francois, R., Bacon, M., Altabet, M. & Labeyrie, L., 1993. Glacial/interglacial changes in sediment rain rate in the SW Indian sector of subantarctic waters as recorded by ^{230}Th, ^{231}Pa, U, and ∂^{15}N. Paleoceanography, 8(5): 611-629.

Francois, R., Honjo, S., Manganini, S. & Ravizza, G., 1995. Biogenic barium fluxes to the deep-sea: Implications for paleoproductivity reconstruction. Global Biochemical Cycles, 9(2): 289-303.

Frank, M., Gersonde, R., Ruettgers-Van der Loeff, M., Bohrmann, G., Nuernberg, C., Kubik, P., Suter, M. & Mangini, A., 2000. Similar glacial and interglacial export bioproductivity in the Atlantic sector of the Southern Ocean: Multi-proxy evidence and implications for global atmospheric CO_2. Paleoceanography, 15(6): 624-658.

Galloway, 1965. Late Quaternary climates in Australia. Journal of Geology, 73: 603-618.

Garner, D., 1959. The subtropical convergence in New Zealand waters. Australian Journal of Marine and Freshwater Research, 2: 315-337.

Gingele, F. & Dahmke, A., 1994. Discrete barite particles and barium as tracers of paleoproducitivity in south Atlantic sediments. Paleoceanography, 9(1): 151-168.

Godfrey, J., Vaudry, D. & Hahn, S., 1986. Observations of the shelf-edge current South of Australia, winter 1982. Journal of Physical Oceanography, 16: 668-679.

Gordon, A., 1988. The Southern Ocean and global climate. Oceanus, 31: 39-46.

Goudie, A., 1983. Dust storms in space and time. Progress in Physical Geography, 7: 502-530.

Govindaraju, C., 1984. Compilation of working values and sample description for 170 international reference samples of many silicate rocks and minerals. Geostandards Newsletter. Centre de Recherches Pétrographiques et Géochimiques, Cedex.

Harris, P.G. & Maxwell, J.R., 1995. A novel method for he rapid determination of chlorin concentrations at high stratigraphic resolution in marine sediments. Organic Geochemistry, 23(9): 853-856.

Harris, P., Zhao, M., Rosell-Melé, A., Tiedemann, R., Sarnthein, M. & Maxwell, J., 1996. Chlorin accumulation rate as a proxy for Quaternary marine primary production. Nature, 383: 63-65.

Harris, P., Howard, W., O'Brien, P., Sedwick, P. & Sikes, E., 1999. Quaternary Antarctic ice-sheet fluctuation and Southern Ocean paleoceanography: natural variability studies at the Antarctic CRC. Journal of Australian Geology and Geophysics, 17(5/6): 105-119.

Haug, G. & Tiedemann, R., 1998. Effects of the formation of the Isthmus of Panama on Atlantic Ocean thermohaline circulation. Nature, 393: 673-676.

Hesse, P., 1994. The record of continental dust from Australia in Tasman Sea sediments. Quaternary Science Reviews, 13: 257-272.

Hesse, P., 1997. Mineral magnetic 'tracing' of aeolian dust in southwest Pacific sediments. Paleogeography, Paleoclimatology, Paleoecology, 131: 327-353.

Hesse, P. & McTainsh, G., 1999. Last Glacial Maximum to early Holocene wind strength in the mid-latitudes of the Southern Hemisphere from aeolian dust in the Tasman Sea. Quaternary Research, 52: 343-349.

Hinz, K. & SONNE-36 Scientific Party, 1985. Geophysical, geological, and geochemical studies off west Tasmania and on the South Tasman Rise. Bundesanstalt für Gewissenschaften und Rohstoffen. Cruise Report, SO-36B.

Howard, W. & Prell, L., 1992. Late Quaternary surface circulation of the Southern Indian Ocean and its relationsship to orbital variations. Paleoceanography, 7(1): 97-117.

Howard, W. & Prell, L., 1994. Late Quaternary $CaCO_3$ production and preservation in the southern Ocean: implications for oceanic and atmospheric carbon cycling. Paleoceanography, 9(3): 453-482.

Ikehara, M., Kawamura, K., Ohkouchi, N., Murayama, M., Nakamura, T. & Taira, A., 2000. Variations of terrestrial input and marine productivity in the Southern Ocean (48°S) during the last two glaciations. Paleoceanography, 15(2): 170-180.

Imbrie, J., Hays, J., Martinson, D., McIntyre, A., Morley, J., Pias, N., Prell, W. & Shackleton, N., 1984. The orbital theory of Pleistocene climate: support from a revised chronology of the marine delta 18O record. In: Berger, A., Imbrie, J., Hays, J., Kukla, G., Saltzman, B. (Editor), Milankovitch and Climate. D. Reidel Publishing, Dordrecht, pp. 269-305.

James, N., Bone, Y., Collins, L. & Kyser, T., 2001. Surficial sediments of the great Australian Bight: facies dynamics and oceanography on a vast cool-water carbonate shelf. Journal of Sedimentary Geology, 71(4): 549-567.

Kawagata, S., 1999. Late Quaternary benthic foaminifera from three Tasman Sea cores, southwest Pacific Ocean. Science Reports, 20: 1-46.

Kawagata, S., 2001. Tasman Front shifts and associated paleoceanographic changes during the last 250000 years: Foraminiferal evidence from the Lord Howe Rise. Marine micropaleontology, 41: 167-191.

Kawahata, H., 2002. Shifts in oceanic and atmospheric boundaries in the Tasman Sea (southwest Pacific) during the Late Pleistocene: evidence from organic carbon and lithognic fluxes. Paleogeography, Paleoclimatology, Paleoecology, 184: 225-249.

Kawahata, H. & Ohta, H., 2000. Sinking and suspended particles in the southwest Pacific. Marine Freswater Research, 51: 113-126.

Klinck, J. & Smith, D., 1993. Effect of wind changes during the last glacial maximum on the circulation in the Southern Ocean. Paleoceanography, 8(4): 427-433.

Kolla, V., Sullivan, L., Streeter, S. & Lamgseth, M., 1976. Spreading of Antarctic bottom water and its effects on the floor of the Indian Ocean inferred from bottom-water potential temperatre, turbidity, and sea-floor photography. Marine Geology, 21: 171-189.

Kowalewska, G., Winterhalter, B., Talbot, H., Maxwell, J. & Konat, J., 1999. Chlorins in sediments of the Gotland Deep (Baltic Sea). Oceanologia, 41(1): 81-97.

Kumar, N., Anderson, R., Mortlock, R., Froehlich, P., Kubik, P., Dittrich-Hannen, B. & Suter, M., 1995. Increased biological productivity and export production in the glacial Southern Ocean. Nature, 378: 675-680.

Kutzbach, J. & Guetter, P., 1986. The influence of changing orbital parameters and surface boundary conditions for the past 18000 years. Journal of atmospheric sciences, 43: 1726-1759.

Landing, W. & Bruland, K., 1987. The contrasting biogeochemistry of iron and manganese in the Pacific Ocean. Geochemica et Cosmochemica Acta, 51: 29-43.

Latimer, J. & Philippelli, G., 2001. Terrigenous input and paleoproductivity in the Southern Ocean. Paleoceanography, 16(6): 627-643.

Lautenschlager, M. & Herterich, K., 1990. Atmospheric response to ice age conditions: Climatology near the Earth's surface. Journal of Geophysical Research, 95: 22547-2255.

Lea, D. & Boyle, E., 1989. Barium content of benthic foraminifera controlled by bottom-water composition. Nature, 339: 751-753.

Lean, C. & McCave, I., 1998. Glacial to interglacial mineral magnetic and paleoceanographic changes at Chatham Rise, SW Pacific Ocean. Earth and Planetary Science Letters, 163: 247-260.

Levitus, S., 1982. Climatologically Atlas of the World Ocean. National Oceanic and Atmospheric Administration, Rockville, Md., 133 pp.

Macaulay, C., 2000. The East Australian Current. Extra Volume of CSIRO-Reports.

Mahowald, N., Kohfeld, K., Hansson, M., Balkanski, Y., Harrison, S., Prentce, I., Schulz, M. & Rodhe, H., 1999. Dust sources and deposition during the last glacial maximum and current climate: A comparison of model results with paleodata from ice cores and marine sediments. Journal of Geophysical Research, 15: 15895-15916.

Manheim, F., Hathaway, J., Flanagan, F. & Fletcher, J., 1976. Marine mud, MAG-1, from the Gulf of Maine. In: Flanagan, F. (Editor), Description and analysis of eight new USGS rock standards. United Stated Government Printing Office, Washington, pp. 25-28.

Martin, J., 1990. Glacial-interglacial CO_2 change: the iron hypothesis. Paleoceanography, 5(1): 1-13.Martin, J. & Knauer, G., 1973. The chemical composition of plankton. Geochemica et Cosmochemica Acta, 37: 1639-1653.

Martin, J. & Gordon, R., 1988. Northeast Pacific iron distribution in relation to phytoplankton productivity. Deep-Sea Research, 35: 177-196.

Martin, J., Gordon, R. & Fitzwater, S., 1990. Iron in Antarctic waters. Nature, 345(Letters to nature): 156-158.

Martin, J. et al., 1994. Testing the iron hypothesis in ecosystems of the equatorial Pacific Ocean. Nature, 371: 123-129.

Martinez, J., 1994. Late Pleistocene palaeoceanography of the Tasman Sea: Implications for the dynamics of the warm pool in the western Pacific. Paleogeography, Paleoclimatology, Paleoecology, 112: 19-62.

Martinson, D., Pisias, N., Hays, J., Imbrie, J., Moore, T. & Shackleton, N., 1987. Age dating and the orbital theory of ice ages: Development of a high-resolution 0 to 300000-Year chronostratigraphy. Quaternary Research, 27: 1-29.

McLennan, S., 1995. Sediments and soils: chemistry and abundances. In: T, A. (Editor), Rock physics and phase relations: A handbook of physical constants. AGU Reference Shelf. American Geophysical Union, Washington.

McTainsh, G. & Lynch, A., 1996. Quantitative estimates of the effect of climate change on dust storm activity in Australia during the Last Glacial Maximum. Geomorphology, 17: 263-271.

Moore, A., Willcox, J., Exon, N. & O'Brien, G., 1992. Continental shelf basins on the west Tasmania margin. APEA Journal, 32: 231-250.

Morley, J., 1989. Variations in high-latitude oceanographic fronts in the Southern Indian Ocean: an estimation based on faunal changes. Paleoceanography, 4(5): 547-554.

Morris, M., Stanton, B. & Neil, H., 2001. Subantarctic oceanography around New Zealand: preliminary results from an ongoing survey. New Zealand Journal of Marine and Freshwater Research, 35: 499-519.

Mortlock, R., Charles, C., Froehlich, P., Zibello, M., Saltzman, J., Hays, J. & Burckle, L., 1991. Evidence for lower productivity in the Antarctic Ocean during the last glaciation. Nature, 351: 220-223.

Müller, P. & Suess, E., 1979. Productivity, sedimentary rate, and sedimentary organic matter in the oceans. I. Organic carbon preservation. Deep Sea Research, 26a: 1347-1362.

Müller, P. & Schneider, R., 1993. An automated leaching method for the determination of opal in sediments and particulate matter. Deep-Sea Research I, 40(3): 425-444.

Murray, R. & Leinen, M., 1996. Scavenged excess aluminum and its relationship to bulk titanium in biogenic sediment form the central equatorial Pacific Ocean. Geochimica et Cosmochimica Acta, 60(20): 3896-3878.

Murray, R., Leinen, M. & Isern, A., 1993. Biogenic flux of Al to sediment in the central equatorial Pacific Ocean: Evidence for increased productivity during glacial periods. Paleoceanography, 8(5): 651-670.

Nagao, S. & Nakashima, S., 1992. The factors controlling vertical colour variations of North Atlantic Madeira abyssal plain sediments. Marine Geology, 109: 83-94.

Nees, S., 1997. Late Quaternary palaeoceanography of the Tasman Sea: the benthic foraminiferal view. Palaeogeography, Palaeoclimatology, Palaeoecology, 131: 365-389.

Nees, S., Armand, L., De Decker, P., Labracherie, M. & Passlow, V., 1999. A diatom and benthic foraminiferal record from the South Tasman Rise (southeastern Indian Ocean): implications for palaeoceanographic changes for the last 200,000 years. Marine Micropaleontology, 38: 69-89.

Nürnberg, C., Bohrman, G., Schlueter, M. & Frank, M., 1997. Barium accumulation in the Atlantic sector of the Southern Ocean: Results from 190000-year records. Paleoceanography, 12(4): 594-603.

Nürnberg, D., Brughmans, N., Schönfeld, J., Ninnemann, U. & Dullo, C., submitted. Marine productivity, terrigenous flux and sea surface temperatures around Tasmania - Implications for glacial/interglacial changes in the Subtropical Convergence Zone (ODP Leg 189).

Okada, H. & Wells, P., 1997. Late Quaternary nannofossil indicators of climate change in two deep-sea cores associated with the Leeuwin Current off Western Australia. Paleogeography, Paleoclimatology, Paleoecology, 131: 413-432.

Orsi, A., Whitworth III, T. & Nowlin Jr., W., 1995. On the meridional extent and fronts of the Antarctic Circumpolar Current. Deep-Sea Research I, 42(5): 641-673.

Passlow, P., 1997. Quaternary ostracods as paleoceanographic indicators: a case study off southern Australia. Paleogeography, Paleoclimatology, Paleoecology, 131: 315-325.

Passlow, V., Pinxian, W. & Chivas, A., 1997. Late Quaternary paleoceanography near Tasmania, southern Australia. Paleogeography, Paleoclimatology, Paleoecology, 131: 433-463.

Peterson, R. & Whithworth III, T., 1989. The subantarctic and polar fronts in relation to deep water masses through the southwestern Atlantic. Journal of Geophysical Research, 94 (C8): 10817-10838.

Petit, J.-R., Briat, M. & Royer, A., 1981. Ice age aerosol content from East Antarctic ice core samples and past wind strength. Nature, 293: 391-394.

Petit, J., Mounier, L., Jouzel, J., Korotkevich, Y., Kotlyakov, V. & Lorius, C., 1990. Paleoclimatological and chronological implications of the Vostok core dust record. Nature, 343: 56-58.

Petit, J. et al., 1999. Climate and atmospheric history of the past 420000 years from the Vostok ice core, Antarctica. Nature, 399: 429-436.

Prell, W., Hutson, W. & Williams, D., 1979. The subtropical convergence an Late Quaternary circulation in the Southern Indian Ocean. Marine Micropaleontology, 4: 225-234.

Prell, W., Imbrie, J., Martinson, D., Morley, J., Pisias, N., Shackleton, N. & Streeter, H., 1986. Graphic correlation of oxygen isotope stratigraphy application to the Late Quaternary. Paleoceanography, 1: 137-162.

Pye, K., 1987. Aeolian dust and dust deposits. Academic Press, London, 334 pp.

Rea, D., 1990. Aspects of atmospheric circulation: the Late Pleistocene (0-950000 yr) record of eolian deposition in the Pacific Ocean. Paleogeography, Paleoclimatology, Paleoecology, 78: 217-227.

Rea, D., 1994. The paleoclimatic record provided by eolian deposition in the deep sea: the geologic history of wind. Reviews of Geophysics, 32(2): 159-195.

Rea, D. & Bloomstine, M., 1986. Neogene history of the south Pacific tradewinds: evidence for hemispherical asymmetry of atmospheric circulation. Paleogeography, Paleoclimatology, Paleoecology, 55: 55-64.

Ridgwell, A. & Watson, A., 2002. Feedback between aeolian dust, climate and atmospheric CO2 in glacial time. Paleoceanography, 17(4): 11-22.

Riley, J. & Roth, I., 1971. The distribution of trace elements in some species of phytoplankton growth in culture. Journal of the Marine Biological Association of the U.K., 51: 63-72.

Rintoul, S., 1998. Southern Ocean Currents and Climate. CSIRO Research Paper.

Rintoul, S. & Bullister, J., 1999. A late winter hydrographic section from Tasmania to Antarctica. Deep-Sea Research Part I., 46: 1417-1454.

Robert, C. and scientific Party ODP-Leg 189, 2001. L'ouverture océanique au sud de la Tasmanie durant le Paléogène et ses conséquences paléocéanographiques: résultats préliminaires de la minéralogie des argiles. Sciences de la Terre et des Planètes, 332: 323-329.

Royer, J.-Y. & Rollet, N., 1997. Plate-tectonic setting of the Tasman region. Australian Journal of Earth Sciences, 44: 543-560.

Ruehlemann, C., Mueller, P. & Schneider, R., 1999. Organic carbon and carbonate as paleoproductivity proxies: examples from high and low productivity areas of the tropical Atlantic. In: Fischer, G., Wefer, G. (Editor), Use of proxies in paleoceanography, examples from South Atlantic. Springer, Berlin, pp. 315-344.

Rutberg, R., Hemming, S. & Goldstein, S., 2000. Reduced North Atlantic Deep Water flux to the glacial Southern Ocean inferred from neodymium isotope ratios. Nature, 405: 935-938.

Sarnthein, M., Winn, K., Duplessy, J.-C. & Fontugne, M., 1988. Global variations of surface ocean productivity in low- and mid-latitudes: influence on CO_2 reservoirs of the deep ocean and atmosphere during the last 21000 years. Paleoceanography, 3: 361-399.

Sarnthein, M., Pflaumann, U., Ross, R., Tiedemann, R. &Winn, K., 1992. Transfer functions to reconstruct ocean paleoproductivity: A comparison. In: Summerhayes, C., Prell, W. & Emeis, K.-C. (Editors), Upwelling systems. Evolution since the early Miocene. Geological Society Special Publication, pp. 411-427.

Schmitz, B., 1987. Barium, equatorial high productivity, and the northward wandering of the Indian continent. Paleoceanography, 2(1): 63-77.

Schönfeld, J.K., H., 1993. Hemipelagic sediment accumulation rates in the South China Sea related to Late Quaternary sea-level changes. Quaternary Research, 40: 368-379.

Schönfeld, J., 2001. Benthic foraminifera and pore-water oxygen profiles: a re-assessment of species boundary conditions at the western Iberian margin. Journal of Foraminiferal Research, 31(2): 86-107.

Schroeder, J., Murray, R., Leinen, M., Pflaum, R. & Janecek, T., 1997. Barium in equatorial Pacific carbonate sediment: Terrigenous, oxide, and biogenic associations. Paleoceanography, 12(1): 125-146.

Sedwick, P., Edwards, P., Mackey, D., Griffith, F. & Parslow, J., 1997. Iron and manganese in surface waters of the Australian Subantarctic region. Deep Sea Research, 44: 1239-1253.

Shackleton, N., Berger, A. & Peltier, W., 1990. An alternative astronomical calibration of the lower Pleistocene timescale based on ODP Site 677. Earth Sciences, 81: 251-261.

Stein, R. & Robert, C., 1985. Siliciclastic sediments at Sites 588, 590, and 591: Neogene and Paleogene evolution in the southwest Pacific and Australian climate. Initial Reports DSDP, 90: 1437-1455.

Takahashi, T., Broecker, W., Bainbridge, A. &Weiss, R., 1980. Carbonate chemistry of the Atlantic, Pacific and Indian Oceans: the results of the GEOSECS expeditions, 1972-1978., Technical Reports 1. Lamont Doherty Earth Observations, Palisades.

Taylor, S. & Mc Lennan, S., 1985. The Continental Crust: Its Composition and Evolution. Blackwell, Oxford, 312 pp.

Tchernia, P., 1980. Descriptive regional oceanography, Oxford.

Thiede, J., 1979. Wind regimes over the late Quaternary southwest Pacific Ocean. Geology, 7: 259-262.

Thompson, R. & Veronis, G., 1983. Poleward boundary current off Western Australia. Australian Journal of Marine Freshwater Research, 34: 173-185.

Thunell, R., 1976. Optimum indices of calcium carbonate dissolution in deep-sea sediments. Geology, 4: 525-528.

Tiedemann, R., Sarnthein, M. & Shackleton, N., 1994. Astronomic timescales for the Pliocene Atlantic delta 18O and dust flux records of Ocean Drilling Program site 659. Paleoceanography, 9: 619-638.

Tomczak, M. & Godfrey, J., 1994. Regional Oceanography: An Introduction. Pergamon Press, Elsevier Science Ltd., Oxford, 422 pp.

van Andel, T., Heath, G. & Moore, T., 1975. Cenozoic History and Paleoceanography of the Central Equatorial Pacific. Geological Society of America, Memoir 143: 1-134.

Villanoy, C. & Tomczak, M., 1991. Influence of Bass Strait Water on the Tasman Sea thermocline. Australian Journal of Marine and Freshwater Research, 42: 451-464.

Wedepohl, K., 1971. Environmental influence on the chemical composition of shales and clays. In: Ahrens, L., Press, K., Runcorn, S., Urey, H. (Editor), Physics and chemistry of the Earth. Pergamon Press, Oxford, pp. 307-333.

Wefer, G., 1989. Particle flux in the ocean: effects of episodic production. In: Berger, W. (Editor), Productivity of the ocean: Present and Past. John Wiley, New York, pp. 139-153.

Whitmore, G. & Belton, D., 1997. Sedimentology of the South Tasman Rise, south of Tasmania, from 'groundtruthed' acoustic facies mapping. Australian Journal of Earth Sciences, 44: 677-688.

Withworth III, T., 1988. The antarctic circumpolar current. Oceanis, 31(2): 53-58.

APPENDIX

A: Concentrations of analysed proxies

A 1	–	A 5:	Site 1168A
A 6	–	A12:	Site 1170A
A13	–	A17:	Site 1171A
A18	–	A23:	Site 1172A

B: Accumulation rates of analysed proxies

B 1	–	B 5:	Site 1168A
B 6	–	B12:	Site 1170A
B13	–	B17:	Site 1171A
B18	–	B23:	Site 1172A

Site 1168A - Concentrations of the analysed proxies

Site	Hole	Core	Type	Section	Top [cm]	Bottom [cm]	Volume [cc]	Sample depth [mbsf]	Age [ka]	Lightness (L*)	Carbonate [%]	TOC [%]	Siliciclastics [%]	Coarse fraction [% > 63µm]	Chlorin [ng/g]	Aluminium [µg/g]	total Barium [µg/g]	Iron [µg/g]	Titanium [µg/g]
1168	A	1	H	1	5	7	15	0.05	7.81	64.04	80.86	0.284	19.14	29.35	399.2	12696.51	678.36	8122.62	822.47
1168	A	1	H	1	10	13	15	0.10	9.82	64.36	78.90	0.299	21.10	25.89	93.4	13393.27	639.58	8810.38	870.97
1168	A	1	H	1	15	18	15	0.15	11.83	59.15	75.38	0.281	24.62	24.02	299.1	16362.31	587.71	13023.66	1128.03
1168	A	1	H	1	20	23	15	0.20	13.83	56.71	72.50	0.387	27.50	20.96	276.7	19191.38	617.68	14192.50	1320.78
1168	A	1	H	1	25	28	15	0.25	15.84	54.52	69.62	0.472	30.38	18.14	734.6	13133.06	323.83	7822.37	923.84
1168	A	1	H	1	30	33	15	0.30	17.85	53.87	71.41	0.482	28.59	27.36	1020.2	19948.53	428.63	11649.39	1346.96
1168	A	1	H	1	35	38	15	0.35	18.67	52.23	68.46	0.534	31.54	29.85	1248.8	22925.62	586.36	12259.39	1321.16
1168	A	1	H	1	40	43	15	0.40	19.49	54.26	67.77	0.504	32.23	29.07	956.0	23442.84	506.55	11658.72	1324.30
1168	A	1	H	1	45	48	15	0.45	20.30	55.20	68.38	0.520	31.62	29.16	1338.7	24761.05	639.87	11653.79	1468.32
1168	A	1	H	1	50	53	15	0.50	21.12	54.47	71.12	0.481	28.88	30.36	1035.0	21379.09	570.10	10457.82	1306.92
1168	A	1	H	1	55	58	15	0.55	21.94	53.25	70.55	0.524	29.45	33.12	1193.4	23303.28	418.75	10884.68	1435.72
1168	A	1	H	1	60	63	15	0.60	25.47	49.65	74.53	0.547	25.47	33.20	1292.8	18187.78	238.26	8220.87	1188.39
1168	A	1	H	1	75	78	15	0.75	36.08	67.84	87.12	0.198	12.88	12.87	112.4	8860.24	423.23	5974.37	526.45
1168	A	1	H	1	80	83	15	0.80	39.61	64.54	87.07	0.235	12.93	13.06	148.9	8550.48	437.19	5226.81	525.81
1168	A	1	H	1	85	88	15	0.85	43.14	65.03	86.78	0.239	13.22	7.50	493.4	9162.11	438.77	5391.03	591.75
1168	A	1	H	1	90	93	15	0.90	46.68	62.45	83.59	0.216	16.41	6.24	548.8	11808.95	432.44	6836.18	809.69
1168	A	1	H	1	95	98	15	0.95	50.21	61.44	81.46	0.271	18.54	12.79	1432.6	19272.80	463.86	10831.06	1341.45
1168	A	1	H	1	100	103	15	1.00	54.84	60.68	77.08	0.341	22.92	23.12	1343.0	17938.68	391.96	8638.48	1094.54
1168	A	1	H	1	105	108	15	1.05	59.46	63.23	73.73	0.353	26.27	18.93	826.2	20917.34	387.67	10804.22	1288.00
1168	A	1	H	1	110	113	15	1.10	64.09	61.38	81.69	0.185	18.31	17.02	581.5	14065.78	418.89	7802.47	832.62
1168	A	1	H	1	115	118	15	1.15	72.16	63.79	84.13	0.154	15.87	18.37	589.6	11762.77	314.71	6229.73	690.73
1168	A	1	H	1	120	123	15	1.20	80.24	65.46	84.85	0.257	15.15	12.38	488.0	9851.80	307.80	5236.92	582.90
1168	A	1	H	1	125	128	15	1.25	88.31	66.22	87.99	0.181	12.01	7.90	239.7	7244.16	483.66	3771.67	414.39
1168	A	1	H	1	130	133	15	1.30	96.38	62.86	85.57	0.244	14.43	6.46	278.4	8900.53	464.38	5748.69	583.17
1168	A	1	H	1	135	138	15	1.35	101.62	60.08	80.94	0.187	19.06	10.90	513.9	12853.89	361.08	7136.35	809.73
1168	A	1	H	1	140	143	15	1.40	106.85	58.50	73.12	0.426	26.88	18.86	1274.3	19813.02	345.78	11478.29	1237.36
1168	A	1	H	2	0	3	15	1.50	117.32	51.16	71.43	0.490	28.57	15.88	1430.7	22414.27	431.05	11896.62	1229.52
1168	A	1	H	2	5	8	15	1.55	122.56	53.76	72.76	0.300	27.24	22.14	538.0	20894.71	447.78	12103.12	1257.49
1168	A	1	H	2	10	13	15	1.60	126.74	59.25	73.32	0.277	26.68	19.94	775.2	20656.13	433.28	11364.65	1234.29
1168	A	1	H	2	15	18	15	1.65	130.92	58.27	73.71	0.222	26.29	17.62	757.4	19708.11	289.63	10505.24	1072.73
1168	A	1	H	2	20	23	15	1.70	135.10	59.26	78.66	0.242	21.34	10.33	538.7	14539.61	321.82	7612.78	933.11
1168	A	1	H	2	25	28	15	1.75	155.08	58.55	77.65	0.274	22.35	12.72	806.4	15627.10	405.61	10156.90	1064.97
1168	A	1	H	2	30	33	15	1.80	175.05	58.29	76.40	0.396	23.60	12.80	1046.9	15874.89	313.73	8729.67	1042.57
1168	A	1	H	2	35	38	15	1.85	184.06	60.21	79.55	0.276	20.45	8.92	566.9	13770.44	378.53	7159.15	799.55
1168	A	1	H	2	40	43	15	1.90	193.07	57.89	73.92	0.359	26.08	18.61	857.4	20253.52	389.22	10715.81	1209.75
1168	A	1	H	2	45	48	15	1.95	200.56	58.58	81.04	0.227	18.96	10.60	468.9	13009.59	319.56	7647.17	811.64
1168	A	1	H	2	50	53	15	2.00	208.05	60.21	71.56	0.305	28.44	14.96	762.9	21828.26	391.06	10633.94	1169.19
1168	A	1	H	2	55	58	15	2.05	215.54	60.41	74.36	0.342	25.64	18.08	780.8	20296.34	373.77	10911.27	1235.67
1168	A	1	H	2	60	63	15	2.10	227.87	59.23	73.64	0.303	26.36	18.29	857.5	21164.54	412.23	11116.04	1261.14

Site	Hole	Core	Type	Section	Top [cm]	Bottom [cm]	Volume [cc]	Sample depth [mbsf]	Age [ka]	Lightness (L*)	Carbonate [%]	TOC [%]	Siliciclastics [%]	Coarse fraction [% > 63µm]	Chlorin [ng/g]	Aluminium [µg/g]	total Barium [µg/g]	Iron [µg/g]	Titanium [µg/g]
1168	A	1	H	2	65	68	15	2.15	240.19	59.19	73.58	0.271	26.42	19.76	822.9	20557.83	363.27	10666.44	1237.91
1168	A	1	H	2	70	73	15	2.20	246.56	59.04	76.03	0.311	23.97	6.84	709.4	18581.40	353.59	9963.20	1118.90
1168	A	1	H	2	75	78	15	2.25	252.93	59.12	64.86	0.345	35.14	30.15	252.5	29233.38	446.77	12184.74	1609.39
1168	A	1	H	2	80	83	15	2.30	259.30	62.43	71.01	0.419	28.99	16.56	791.1	23386.95	371.45	11475.45	1428.09
1168	A	1	H	2	85	88	15	2.35	265.67	55.19	59.76	0.414	40.24	14.28	950.9	33865.38	310.19	16264.47	2018.86
1168	A	1	H	2	90	93	15	2.40	271.39	56.28	60.85	0.445	39.15	14.51	956.3	31498.52	293.18	17305.62	1912.52
1168	A	1	H	2	95	98	15	2.45	277.11	56.45	67.28	0.338	32.72	15.63	859.9	27768.10	424.41	14752.81	1699.30
1168	A	1	H	2	100	103	15	2.50	282.82	63.14	82.64	0.279	17.36	14.38	481.6	12965.58	372.36	6778.61	758.51
1168	A	1	H	2	105	108	15	2.55	288.54	64.78	85.75	0.232	14.25	10.58	331.6	9347.94	396.78	4819.17	536.82
1168	A	1	H	2	110	113	15	2.60	292.83	70.31	89.06	0.094	10.94	7.82	334.8	7554.01	483.23	4039.95	429.72
1168	A	1	H	2	115	118	15	2.65	297.12	65.70	84.32	0.209	15.68	6.22	389.3	10913.22	415.36	5947.74	741.45
1168	A	1	H	2	120	123	15	2.70	301.42	62.52	82.89	0.172	17.11	13.17	428.7	12199.38	302.52	6571.88	722.11
1168	A	1	H	2	125	128	15	2.75	305.71	64.19	85.87	0.102	14.13	11.06	54.2	9192.61	491.77	6022.69	605.23
1168	A	1	H	2	130	133	15	2.80	310.00	61.49	81.24	0.256	18.76	11.49	710.1	13519.52	330.27	7218.52	810.30
1168	A	1	H	2	135	138	15	2.85	314.20	59.54	77.59	0.295	22.41	15.84	816.8	14977.17	454.13	6080.65	974.62
1168	A	1	H	2	140	143	15	2.90	318.40	60.88	82.11	0.273	17.89	16.15	498.7	12120.70	361.92	6419.62	729.07
1168	A	1	H	2	145	148	15	2.95	322.60	64.09	85.94	0.278	14.06	7.78	497.7	8914.57	395.67	4560.99	555.97
1168	A	1	H	3	0	3	15	3.00	326.80	61.25	89.90	0.178	10.10	6.90	187.1	6566.65	443.13	3389.81	364.68
1168	A	1	H	3	5	8	15	3.05	331.00	69.69	87.50	0.181	12.50	8.28	274.8	8180.82	426.31	4156.83	469.40
1168	A	1	H	3	10	13	15	3.10	333.50	69.08	86.02	0.235	13.98	7.67	338.7	9452.86	484.44	5049.87	557.15
1168	A	1	H	3	15	18	15	3.15	336.00	64.35	84.90	0.358	15.10	7.49	178.4	8514.44	435.28	5427.21	538.80
1168	A	1	H	3	20	23	15	3.20	338.50	64.93	77.79	0.441	22.21	6.75	597.4	15615.20	465.40	8458.45	1082.58
1168	A	1	H	3	25	28	15	3.25	341.00	58.59	78.51	0.404	21.49	12.75	1080.8	14127.80	358.81	7564.85	921.37
1168	A	1	H	3	30	33	15	3.30	344.20	58.36	77.16	0.333	22.84	9.91	563.9	16196.42	287.17	8029.11	918.31
1168	A	1	H	3	35	38	15	3.35	347.40	58.85	64.66	0.375	35.34	16.73	1022.4	27674.47	438.99	13406.43	1468.33
1168	A	1	H	3	40	43	15	3.40	350.60	56.85	65.38	0.292	34.62	17.81	370.9	28433.48	591.05	13798.67	1515.60
1168	A	1	H	3	45	48	15	3.45	353.80	56.96	85.08	0.226	14.92	22.52	224.7	11146.41	245.04	6171.24	639.93
1168	A	1	H	3	50	53	15	3.50	357.00	52.44	86.75	0.188	13.25	29.65	189.1	9017.65	332.48	5081.56	553.40
1168	A	1	H	3	55	58	15	3.55	360.20	50.37	84.57	0.373	15.43	17.76	179.4	9298.69	308.11	5069.32	570.00
1168	A	1	H	3	60	63	15	3.60	363.40	64.70	85.92	0.210	14.08	26.05	251.9	7822.08	275.29	4558.49	461.66
1168	A	1	H	3	65	68	15	3.65	366.60	53.85	81.83	0.273	18.17	28.04	230.7	13417.39	339.01	7399.01	825.79
1168	A	1	H	3	70	73	15	3.70	369.80	48.57	84.98	0.233	15.02	27.77	130.6	9927.98	304.02	5375.07	605.03
1168	A	1	H	3	75	78	15	3.75	373.00	53.71	84.23	0.233	15.77	26.48	254.2	10953.40	389.61	6808.98	661.51
1168	A	1	H	3	80	83	15	3.80	376.20	57.72	77.66	0.250	22.34	26.23	397.7	11900.21	238.30	8752.13	710.02
1168	A	1	H	3	85	88	15	3.85	379.40	50.14	87.52	0.196	12.48	24.54	256.4	8079.35	144.01	5031.59	472.58
1168	A	1	H	3	90	93	15	3.90	382.60	54.19	84.39	0.288	15.61	47.23	345.8	11095.44	244.81	6616.60	660.41
1168	A	1	H	3	95	98	15	3.95	385.80	52.13	84.99	0.246	15.01	36.05	300.8	9867.61	285.85	5966.19	567.21
1168	A	1	H	3	100	103	15	4.00	389.00	62.08	87.09	0.248	12.91	51.54	173.1	6834.97	171.36	5777.52	401.86
1168	A	1	H	3	105	108	15	4.05	392.20	66.81	81.16	0.259	18.84	49.11	225.5	8918.42	174.34	8246.37	525.69
1168	A	1	H	3	110	113	15	4.10	395.40	56.47	85.67	0.269	14.33	31.83	347.7	9890.60	233.19	7615.29	572.62

Site	Hole	Core	Type	Section	Top [cm]	Bottom [cm]	Volume [cc]	Sample depth [mbsf]	Age [ka]	Lightness (L*)	Carbonate [%]	TOC [%]	Siliciclastics [%]	Coarse fraction [% > 63µm]	Chlorin [ng/g]	Aluminium [µg/g]	total Barium [µg/g]	Iron [µg/g]	Titanium [µg/g]
1168	A	1	H	3	115	118	15	4.15	398.60	65.35	80.58	0.273	19.42	23.56	229.4	13403.77	357.04	7992.05	796.00
1168	A	1	H	3	120	123	15	4.20	401.80	64.22	84.18	0.309	15.82	30.36	256.0	9481.75	253.28	5523.07	544.10
1168	A	1	H	3	125	128	15	4.25	405.00	56.00	83.24	0.423	16.76	25.39	272.1	10426.94	276.81	6727.73	611.22
1168	A	1	H	3	130	133	15	4.30	407.23	61.77	76.13	0.317	23.87	20.41	351.6	17490.70	366.06	8371.89	732.59
1168	A	1	H	3	135	138	15	4.35	409.46	66.73	84.19	0.243	15.81	20.55	169.1	12068.95	549.17	6530.03	679.96
1168	A	1	H	3	140	143	15	4.40	411.69	63.78	82.22	0.282	17.78	20.42	327.9	12557.54	424.13	7242.43	714.09
1168	A	1	H	4	0	3	15	4.50	416.15	59.40	79.76	0.353	20.24	19.81	260.5	15384.25	663.14	8212.59	896.55
1168	A	1	H	4	5	8	15	4.55	418.39	62.02	79.27	0.269	20.73	20.43	252.6	15321.97	563.27	8054.51	889.63
1168	A	1	H	4	10	13	15	4.60	420.62	61.54	78.58	0.292	21.42	18.30	102.6	16011.77	626.04	7754.08	940.71
1168	A	1	H	4	15	18	15	4.65	422.85	60.38	79.76	0.289	20.24	21.77	247.0	15296.82	573.64	7595.64	901.56
1168	A	1	H	4	20	23	15	4.70	425.08	61.40	70.36	0.257	29.64	14.25	74.4	19676.76	590.65	10877.68	1259.76
1168	A	1	H	4	25	28	15	4.75	427.31	57.69	70.28	0.296	29.72	18.65	339.4	24302.20	565.83	13730.67	1502.23
1168	A	1	H	4	30	33	15	4.80	429.54		63.15	0.316	36.85	20.96	363.0	30664.78	499.09	14753.48	1872.74
1168	A	1	H	4	35	38	15	4.85	431.77		62.35	0.387	37.65	26.60	836.6	31784.73	601.96	14804.65	1932.48
1168	A	1	H	4	40	43	15	4.90	434.00	49.94	59.20	0.450	40.80	29.83	716.9	33226.11	628.13	17403.56	2026.56
1168	A	1	H	4	45	48	15	4.95	438.11	50.90	64.23	0.380	35.77	31.91	867.1	29018.88	647.99	14599.47	1805.95
1168	A	1	H	4	50	53	15	5.00	442.22	51.37	67.43	0.285	32.57	35.59	610.3	23467.66	613.26	16898.40	1516.65
1168	A	1	H	4	55	58	15	5.05	446.33	57.15	67.42	0.342	32.58	27.66	378.6	25124.90	579.55	12457.87	1605.99
1168	A	1	H	4	60	63	15	5.10	450.44	68.68	83.28	0.244	16.72	18.03	95.1	10366.89	533.54	5966.77	611.40
1168	A	1	H	4	65	68	15	5.15	454.56	69.23	80.33	0.268	19.67	8.98	313.1	12321.98	346.36	9181.03	745.42
1168	A	1	H	4	70	73	15	5.20	458.67	67.98	85.48	0.283	14.52	16.17	326.0	8589.77	494.81	4280.79	502.30
1168	A	1	H	4	75	78	15	5.25	462.78	66.17	83.00	0.239	17.00	19.30	236.8	7184.27	357.75	5452.18	417.75
1168	A	1	H	4	80	83	15	5.30	466.89	67.01	83.42	0.284	16.58	14.51	613.6	10829.43	416.61	8015.05	637.70
1168	A	1	H	4	85	88	15	5.35	471.00	66.51	83.28	0.257	16.72	16.50	412.4	12189.67	361.68	6482.85	730.16
1168	A	1	H	4	90	93	15	5.40	474.42	60.64	84.67	0.282	15.33	14.90	283.1	10982.71	332.16	5977.60	635.34
1168	A	1	H	4	95	98	15	5.45	477.83	62.79	85.23	0.287	14.77	12.65	314.3	10702.24	534.88	6082.06	621.42
1168	A	1	H	4	100	103	15	5.50	481.25	66.38	83.43	0.167	16.57	15.95	86.7	11828.91	677.20	6238.85	801.16
1168	A	1	H	4	105	108	15	5.55	484.67	66.85	83.96	0.244	16.04	16.07	349.7	12378.28	474.35	7041.11	754.79
1168	A	1	H	4	110	113	15	5.60	488.08	56.65	79.43	0.293	20.57	14.05	456.8	16402.35	454.32	8783.61	983.18
1168	A	1	H	4	115	118	15	5.65	491.50	65.60	81.63	0.236	18.37	14.95	230.5	14575.36	407.65	7291.97	903.61
1168	A	1	H	4	120	123	15	5.70	494.92	63.43	82.28	0.233	17.72	15.76	165.2	14329.78	402.33	7660.82	885.84
1168	A	1	H	4	125	128	15	5.75	498.33	63.62	83.19	0.257	16.81	14.00	187.7	13583.82	456.66	7087.15	838.61
1168	A	1	H	4	130	133	15	5.80	501.75	65.06	80.06	0.272	19.94	15.21	183.2	13865.62	461.07	7620.88	833.82
1168	A	1	H	4	135	138	15	5.85	505.17	64.25	82.44	0.200	17.56	15.18	245.1	13890.28	512.27	7070.07	841.69
1168	A	1	H	4	140	143	15	5.90	508.58	66.15	73.52	0.461	26.48	20.32		16192.14	433.97	9141.35	873.15
1168	A	1	H	4	145	148	15	5.95	512.00	65.61	77.53	0.391	22.47	17.65	651.7	15249.97	433.55	8670.62	896.56
1168	A	1	H	5	0	3	15	6.00	517.95	66.97	81.24	0.285	18.76	23.66	544.6	13755.32	438.09	7204.40	808.77
1168	A	1	H	5	5	8	15	6.05	523.90	66.54	79.55	0.293	20.45	18.28	314.8	12768.05	417.92	7033.14	725.82
1168	A	1	H	5	10	13	15	6.10	529.84	65.49	80.08	0.255	19.92	18.72	494.5	14755.12	432.93	8006.18	883.68
1168	A	1	H	5	15	18	15	6.15	535.79	60.76	80.01	0.242	19.99	18.04	317.1	16060.76	407.63	7744.55	1024.16

Site	Hole	Core	Type	Section	Top [cm]	Bottom [cm]	Volume [cc]	Sample depth [mbsf]	Age [ka]	Lightness (L*)	Carbonate [%]	TOC [%]	Siliciclastics [%]	Coarse fraction [% > 63µm]	Chlorin [ng/g]	Aluminium [µg/g]	total Barium [µg/g]	Iron [µg/g]	Titanium [µg/g]
1168	A	1	H	5	20	23	15	6.20	541.74	63.78	80.98	0.274	19.02	14.17	242.7	14882.13	449.88	8001.75	916.71
1168	A	1	H	5	25	28	15	6.25	547.68	67.06	80.62	0.213	19.38	14.66	231.7	11904.72	525.51	7279.36	714.53
1168	A	1	H	5	30	33	15	6.30	553.63	66.62	84.90	0.220	15.10	18.06	200.4	10908.57	445.72	5794.81	633.49
1168	A	1	H	5	35	38	15	6.35	559.58	68.37	87.15	0.159	12.85	14.61	199.0	9036.37	457.47	4769.18	531.16
1168	A	1	H	5	40	43	15	6.40	565.53	69.41	87.10	0.173	12.90	14.13	169.6	9137.57	508.16	5138.93	520.87
1168	A	1	H	5	45	48	15	6.45	571.47	69.70	85.71	0.169	14.29	16.02	243.1	10176.81	512.28	5158.22	589.18
1168	A	1	H	5	50	53	15	6.50	577.42	66.42	85.10	0.193	14.90	13.92	127.5	10209.08	483.27	5607.48	600.60
1168	A	1	H	5	55	58	15	6.55	583.37	67.97	86.45	0.198	13.55	13.76	341.6	11590.22	435.58	5859.70	676.63
1168	A	1	H	5	60	63	15	6.60	589.32	66.87	83.69	0.241	16.31	13.81	333.1	11258.95	398.00	6109.94	655.90
1168	A	1	H	5	65	68	15	6.65	595.26	68.01	85.80	0.231	14.20	11.26	306.9	10448.72	433.27	5128.89	595.39
1168	A	1	H	5	70	73	15	6.70	601.21	65.73	83.61	0.245	16.39	10.25	310.3	11492.58	526.24	5863.58	648.93
1168	A	1	H	5	75	78	15	6.75	607.16	62.94	81.63	0.249	18.37	15.92	202.5	13865.48	495.45	7477.31	790.67
1168	A	1	H	5	80	83	15	6.80	613.11	58.33	79.62	0.304	20.38	15.36	354.7	14523.48	403.86	7494.55	921.90
1168	A	1	H	5	85	88	15	6.85	619.05	59.21	79.21	0.323	20.79	12.29	240.1	15011.50	560.44	7377.18	1069.73
1168	A	1	H	5	90	93	15	6.90	625.00	58.56	80.21	0.307	19.79	17.77	378.2	13235.05	570.79	7582.06	960.63
1168	A	1	H	5	95	98	15	6.95	629.41	63.04	80.84	0.277	19.16	15.63	278.5	12227.47	634.32	6585.55	842.35
1168	A	1	H	CC	0	3	15	7.02	635.58		82.89	0.192	17.11	17.75	155.4	10016.91	579.50	5747.45	697.48
1168	A	1	H	CC	5	8	15	7.07	639.99	66.92	84.28	0.210	15.72	23.41	137.7	9073.76	504.03	7316.84	614.61
1168	A	1	H	CC	10	13	15	7.12	644.40	66.82	85.74	0.196	14.26	22.33	117.7	9762.77	567.81	5190.96	652.64
1168	A	1	H	CC	15	18	15	7.17	648.81	66.89				16.90					
1168	A	1	H	CC	20	23	15	7.22	653.22	56.42	73.23	0.328	26.77	17.00	289.2	19035.58	692.17	9583.53	1300.11
1168	A	2	H	1	0	3	15	7.30	660.27	58.56	71.24	0.205	28.76	17.40	152.2	23123.47	711.04	12129.29	1408.29
1168	A	2	H	1	5	8	15	7.35	664.68	63.62	70.56	0.238	29.44	13.79	306.0				
1168	A	2	H	1	10	13	15	7.40	669.09		67.23	0.350	32.77	13.86	870.0	25635.76	572.37	13431.37	1553.31
1168	A	2	H	1	15	18	15	7.45	673.50	57.08	74.16	0.339	25.84	18.80	494.5	20587.82	551.31	11324.48	1284.00
1168	A	2	H	1	20	23	15	7.50	677.91		70.06	0.286	29.94	17.53	424.2	22428.91	596.83	11869.24	1383.76
1168	A	2	H	1	25	28	15	7.55	682.32	52.76	72.10	0.232	27.90	17.21	204.4	22404.83	646.00	11684.48	1374.38
1168	A	2	H	1	30	33	15	7.60	686.73		73.38	0.264	26.62	19.32	348.6	20810.48	582.74	11206.64	1279.68
1168	A	2	H	1	35	38	15	7.65	691.14	53.78	71.25	0.258	28.75	18.74	434.6	16608.29	450.99	8358.66	1006.13
1168	A	2	H	1	40	43	15	7.70	695.55	60.55	80.34	0.212	19.66	17.71	183.3	12680.15	498.33	6488.56	770.45
1168	A	2	H	1	45	48	15	7.75	699.96		71.06	0.312	28.94	19.41	571.2	22716.49	548.50	12468.13	1385.71
1168	A	2	H	1	50	53	15	7.80	704.36		72.91	0.279	27.09	15.79	644.8	19406.84	479.79	10058.28	1271.70
1168	A	2	H	1	55	58	15	7.85	708.77		71.11	0.274	28.89	17.08	375.1	22733.89	642.99	11847.70	1390.38
1168	A	2	H	1	60	63	15	7.90	713.18		75.94	0.237	24.06	16.61	259.3	16939.57	816.01	8577.34	1220.28
1168	A	2	H	1	65	68	15	7.95	717.59		73.74	0.210	26.26	15.05	150.6	16419.40	853.29	8589.97	1087.88
1168	A	2	H	1	70	73	15	8.00	722.00	62.66	84.43	0.185	15.57	13.39	169.7	11376.15	503.97	5993.10	683.06
1168	A	2	H	1	75	78	15	8.05	726.63	60.42	84.15	0.219	15.85	14.32	198.8	15803.36	675.20	8683.67	940.87
1168	A	2	H	1	80	83	15	8.10	731.25	57.56	75.10	0.251	24.90	17.11	236.6	18649.56	677.37	9724.10	1228.48
1168	A	2	H	1	85	88	15	8.15	735.88	61.27				12.20	205.2				
1168	A	2	H	1	90	93	15	8.20	740.50	59.57	83.96	0.162	16.04	11.80	64.5	10960.79	744.26	5633.17	747.03

Site	Hole	Core	Type	Section	Top [cm]	Bottom [cm]	Volume [cc]	Sample depth [mbsf]	Age [ka]	Lightness (L*)	Carbonate [%]	TOC [%]	Siliciclastics [%]	Coarse fraction [% > 63µm]	Chlorin [ng/g]	Aluminium [µg/g]	total Barium [µg/g]	Iron [µg/g]	Titanium [µg/g]
1168	A	2	H	1	95	98	15	8.25	745.13	68.56	86.39	0.289	13.61	13.42	134.4	9452.06	440.75	5088.86	564.34
1168	A	2	H	1	100	103	15	8.30	749.75	48.47	77.71	0.254	22.29	35.65	272.4	16542.93	604.48	8928.17	1090.91
1168	A	2	H	1	105	108	15	8.35	754.38	61.54	83.90	0.243	16.10	18.12	415.4	17395.99	507.50	9838.14	1087.60
1168	A	2	H	1	110	113	15	8.40	759.00	62.94	71.58	0.269	28.42	17.05	420.3	24242.54	521.02	12373.25	1478.33
1168	A	2	H	1	115	118	15	8.45	763.63	59.52	73.71	0.329	26.29	18.38	431.6	21414.90	564.76	11761.33	1346.80
1168	A	2	H	1	120	123	15	8.50	768.25	61.05	71.91	0.292	28.09	15.26	359.2	30138.44	604.59	13842.70	1891.96
1168	A	2	H	1	125	128	15	8.55	772.88	63.66	84.30	0.241	15.70	15.46	97.9	11685.83	700.23	5783.82	783.93
1168	A	2	H	1	130	133	15	8.60	777.50	69.63	87.00	0.269	13.00	10.76	161.3	10427.19	675.41	5199.50	665.39
1168	A	2	H	1	135	138	15	8.65	782.13	66.47	87.82	0.137	12.18	18.11	58.4	9791.51	658.61	4813.19	615.52
1168	A	2	H	1	140	143	15	8.70	786.75	65.54	85.00	0.143	15.00	36.07	35.7	10004.04	411.62	6569.84	663.87
1168	A	2	H	2	0	3	15	8.80	795.90	52.93	77.81	0.350	22.19	17.02	211.4	16367.20	537.60	8839.35	1136.74
1168	A	2	H	2	5	8	15	8.85	800.47	60.98	77.91	0.199	22.09	17.98	205.2	17582.25	473.92	9177.27	1195.48
1168	A	2	H	2	10	13	15	8.90	804.94	59.78	71.92	0.206	28.08	16.27	295.1	22418.21	472.18	10687.22	1573.31
1168	A	2	H	2	15	18	15	8.95	809.41	58.36	57.90	0.378	42.10	12.91	976.7	33413.69	555.86	15137.00	2303.12
1168	A	2	H	2	20	23	15	9.00	813.88	55.31	57.08	0.434	42.92	13.30	854.2	36065.54	642.11	14852.29	2353.48
1168	A	2	H	2	25	28	15	9.05	818.35	56.40	61.69	0.357	38.31	13.67	512.2	31476.03	735.83	13141.73	2160.52
1168	A	2	H	2	30	33	15	9.10	822.82	62.92	79.36	0.182	20.64	21.84	137.3	12258.39	648.24	10414.31	838.11
1168	A	2	H	2	35	38	15	9.15	827.29	64.69	82.56	0.171	17.44	17.67	140.4	13007.00	685.98	7053.17	875.60
1168	A	2	H	2	40	43	15	9.20	831.77	66.24	75.76	0.210	24.24	14.80	308.5	19161.24	752.68	9603.30	1288.44
1168	A	2	H	2	45	48	15	9.25	836.24	66.31	87.77	0.171	12.23	21.06	103.3	11453.78	602.81	5842.25	760.88
1168	A	2	H	2	50	53	15	9.30	840.71	63.49				27.14					
1168	A	2	H	2	55	58	15	9.35	845.18	64.31	83.32	0.203	16.68	19.36	349.2	12250.33	635.43	6107.68	859.29
1168	A	2	H	2	60	63	15	9.40	849.65	65.25	80.88	0.216	19.12	16.42	84.7	12284.67	535.77	6380.26	910.41
1168	A	2	H	2	65	68	15	9.45	854.12	63.62	79.36	0.217	20.64	15.93	120.9	14944.96	525.92	8059.38	1163.32
1168	A	2	H	2	70	73	15	9.50	858.59	59.31	75.20	0.277	24.80	18.33	348.8	19432.82	643.34	9878.79	1458.96
1168	A	2	H	2	75	78	15	9.55	863.06	61.62	78.50	0.256	21.50	18.23	319.2	17319.26	682.44	8817.23	1218.06
1168	A	2	H	2	80	83	15	9.60	867.53	60.05	82.17	0.294	17.83	17.65	259.3	12189.01	668.55	6797.74	846.34
1168	A	2	H	2	85	88	15	9.65	872.00	66.79	81.01	0.169	18.99	13.13	127.7	11151.14	510.70	6029.20	764.33
1168	A	2	H	2	90	93	15	9.70	876.80	62.05	80.84	0.189	19.16	10.88	127.3	13227.72	675.20	6807.91	912.95
1168	A	2	H	2	95	98	15	9.75	881.60	67.03	82.87	0.154	17.13	14.76	68.3	11620.85	676.28	6981.40	787.26
1168	A	2	H	2	100	103	15	9.80	886.40	63.40	83.26	0.125	16.74	20.40	86.9	11204.35	490.90	6247.44	827.78
1168	A	2	H	2	105	108	15	9.85	891.20	65.92	83.95	0.155	16.05	20.50	101.9	11171.73	600.85	5707.14	797.48
1168	A	2	H	2	110	113	15	9.90	896.00	61.39				13.62					
1168	A	2	H	2	115	118	15	9.95	900.80	62.77	77.51	0.209	22.49	12.84	95.7	15489.69	624.37	10019.76	1174.78
1168	A	2	H	2	120	123	15	10.00	905.60	61.76	78.15	0.202	21.85	10.78	106.5	15115.23	631.00	7959.12	1124.68
1168	A	2	H	2	125	128	15	10.05	910.40	61.20	76.31	0.220	23.69	13.50	153.1	16425.01	698.31	8885.01	1204.31
1168	A	2	H	2	130	133	15	10.10	915.20	61.34	77.88	0.166	22.12	10.82	142.0	16238.46	695.76	8735.51	1238.55
1168	A	2	H	2	135	138	15	10.15	920.00	60.35	74.35	0.325	25.65	12.46	311.0	20302.68	831.89	10225.40	1495.85
1168	A	2	H	2	140	143	15	10.20	924.80	56.28	72.09	0.363	27.91	20.61	267.1	20430.98	760.65	12345.66	1524.48
1168	A	2	H	2	145	148	15	10.25	929.60	56.98	74.24	0.332	25.76	34.09	464.7	18869.02	621.73	10192.65	1425.36

Site 1170A - Concentrations of the analysed proxies

Site	Hole	Core	Type	Section	Top [cm]	Bottom [cm]	Volume [cc]	Sample depth [mbsf]	Age [ka]	Lightness (L*)	Carbonate [%]	TOC [%]	Siliciclastics [%]	Coarse fraction [% > 63µm]	Chlorin [ng/g]	Aluminium [µg/g]	total Barium [µg/g]	Iron [µg/g]	Titanium [µg/g]
1170	A	1	H	1	0	1	15	0.00	0.21	63.88	92.49		7.51	27.44	73.7	3129.08	751.62	1635.22	157.53
1170	A	1	H	1	5	6	15	0.05	2.58	71.87	92.08		7.92	25.21		3427.15	792.23	1797.72	179.42
1170	A	1	H	1	10	11	15	0.10	4.96	72.18	91.75		8.25	25.12		3301.51	756.21	1721.46	174.38
1170	A	1	H	1	15	16	15	0.15	7.33	71.63	91.21		8.79	29.63		3922.61	781.10	2127.11	199.38
1170	A	1	H	1	20	21	15	0.20	9.70	70.36	90.48		9.52	29.77		4625.17	805.67	2593.29	258.14
1170	A	1	H	1	25	26	15	0.25	13.78	67.69	89.15		10.85	31.55	11.0	5975.59	837.53	3565.73	349.82
1170	A	1	H	1	30	31	15	0.30	17.85	65.29	88.71		11.29	36.83	10.9	5905.86	828.46	3598.56	357.54
1170	A	1	H	1	35	36	15	0.35	19.11	70.65	86.93		13.07	38.95	14.6	8200.32	915.38	4974.61	493.76
1170	A	1	H	1	40	41	15	0.40	20.37	67.52	84.85		15.15	34.65	12.5	9610.26	1086.13	6515.39	578.48
1170	A	1	H	1	45	46	15	0.45	21.64	68.24	81.68		18.32		12.9	10547.64	1159.19	6678.55	759.74
1170	A	1	H	1	50	51	15	0.50	22.90	69.52	83.70		16.30	43.36	34.0	8345.40	974.73	4353.83	745.40
1170	A	1	H	1	55	56	15	0.55	24.16	72.18	86.44		13.56	44.79	22.9	8366.48	983.91	4792.51	524.68
1170	A	1	H	1	60	61	15	0.60	25.42	72.69	86.56		13.44	39.93		8395.57	922.33	4377.95	492.57
1170	A	1	H	1	65	66	15	0.65	29.55	71.18	88.14		11.86	35.93		7371.36	813.46	4288.05	452.45
1170	A	1	H	1	70	71	15	0.70	33.68	73.41	87.62		12.38	36.47		6739.64	708.84	5856.24	393.79
1170	A	1	H	1	75	76	15	0.75	37.82	74.60	94.52		5.48	39.13		6775.91	759.20	5216.25	411.83
1170	A	1	H	1	80	81	15	0.80	41.95	75.81	88.94		11.06	38.95	33.6	6597.41	677.20	3594.33	390.49
1170	A	1	H	1	85	86	15	0.85	46.08	73.84	86.63		13.37	38.33		5989.14	623.43	4602.22	373.95
1170	A	1	H	1	90	91	15	0.90	50.21	71.48	88.33		11.67	37.33		6928.42	675.41	3634.70	419.79
1170	A	1	H	1	95	96	15	0.95	53.96	72.37	88.56		11.44	39.38		6693.44	634.53	3464.21	412.61
1170	A	1	H	1	100	101	15	1.00	57.72	66.35	88.17		11.83	33.15		7879.83	618.72	3888.10	458.72
1170	A	1	H	1	105	106	15	1.05	61.47	68.53	86.56		13.44	30.96	132.8	8913.35	741.30	5073.33	528.98
1170	A	1	H	1	110	111	15	1.10	65.22	70.55	84.71		15.29	26.96		9782.77	763.03	6276.12	571.62
1170	A	1	H	1	115	116	15	1.15	67.56	73.51	88.35		11.65	22.04		7749.43	667.16	4131.64	453.52
1170	A	1	H	1	120	121	15	1.20	69.90	76.13	89.72		10.28	27.57		6424.04	604.16	3698.68	374.85
1170	A	1	H	1	125	126	15	1.25	72.24	76.16	89.96		10.04	32.47		5466.97	584.12	3233.62	308.10
1170	A	1	H	1	130	131	15	1.30	74.57	70.79	91.30		8.70	32.84	16.7	4622.23	548.21	2910.79	262.38
1170	A	1	H	1	135	136	15	1.35	76.91	72.47	92.28		7.72	33.03		3903.88	575.50	2470.67	226.13
1170	A	1	H	1	140	141	15	1.40	79.25	76.10	92.53		7.47	33.39		3768.83	573.28	1937.71	205.64
1170	A	1	H	1	145	146	15	1.45	84.57	73.15	93.05		6.95	33.62		3424.97	572.55	1843.61	187.13
1170	A	1	H	CC	0	1	15	1.46	85.63		92.96		7.04	33.44	23.9				
1170	A	1	H	CC	5	6	15	1.51	90.95	77.66	92.80		7.20	37.80		3812.94	569.44	1829.52	215.16
1170	A	1	H	CC	10	11	15	1.56	93.49	75.73	93.58		6.42	36.23		3416.02	623.65	1585.73	187.05
1170	A	1	H	CC	15	16	15	1.61	96.04	71.22	93.47		6.53	36.46	18.6	3566.09	569.60	1786.57	194.13
1170	A	2	H	1	0	1	15	1.70	100.62	62.47	89.04		10.96	24.30	12.8				
1170	A	2	H	1	5	6	15	1.75	103.16	71.93	93.82		6.18	25.51		4079.25	835.84	2106.55	210.59
1170	A	2	H	1	10	11	15	1.80	105.70	69.60	91.59		8.41	29.28		4375.31	897.41	2174.24	248.32
1170	A	2	H	1	15	16	15	1.85	108.25	72.77	92.14		7.86	33.16		3867.18	654.08	2069.88	219.88
1170	A	2	H	1	20	21	15	1.90	110.79	76.84	93.45		6.55	30.16		3774.05	695.60	1714.42	206.78

Site	Hole	Core	Type	Section	Top [cm]	Bottom [cm]	Volume [cc]	Sample depth [mbsf]	Age [ka]	Lightness (L*)	Carbonate [%]	TOC [%]	Siliciclastics [%]	Coarse fraction [% > 63µm]	Chlorin [ng/g]	Aluminium [µg/g]	total Barium [µg/g]	Iron [µg/g]	Titanium [µg/g]
1170	A	2	H	1	25	26	15	1.95	122.56	72.08	92.82		7.18	30.36	20.7	3332.77	685.18	1576.99	174.69
1170	A	2	H	1	30	31	15	2.00	125.70	74.06	89.79		10.21	32.01	7.2	5893.87	718.25	3008.40	330.17
1170	A	2	H	1	35	36	15	2.05	128.83	74.22	90.03		9.97	28.54	7.0	5919.08	648.93	2867.60	346.94
1170	A	2	H	1	40	41	15	2.10	131.97	72.94	89.95		10.05	27.75		6072.47	700.70	2948.74	361.92
1170	A	2	H	1	45	46	15	2.15	135.10	70.64	87.96		12.04	25.11		7991.26	918.83	4556.58	483.28
1170	A	2	H	1	50	51	15	2.20	136.00	69.89	89.60		10.40	31.41		6870.59	852.26	3780.86	418.87
1170	A	2	H	1	55	56	15	2.25	136.90	64.79	87.52		12.48	24.01	37.9	9408.16	915.67	4501.51	531.90
1170	A	2	H	1	60	61	15	2.30	137.79	68.56	86.78		13.22	25.55		8380.47	751.22	4204.62	492.42
1170	A	2	H	1	65	66	15	2.35	138.69	70.20	87.16		12.84	25.97		8986.64	837.87	4833.07	530.22
1170	A	2	H	1	70	71	15	2.40	139.59	71.96	88.04		11.96	26.70		9055.40	844.16	4301.53	526.90
1170	A	2	H	1	75	76	15	2.45	140.49	69.65	88.20		11.80	28.94		8562.35	780.13	4320.67	494.95
1170	A	2	H	1	80	81	15	2.50	141.38	69.15	87.74		12.26	37.58	89.5	7040.26	701.80	5845.50	407.65
1170	A	2	H	1	85	86	15	2.55	142.28	64.82	87.56		12.44	27.76		7826.07	715.18	5452.67	448.01
1170	A	2	H	1	90	91	15	2.60	145.71	68.77	88.15		11.85	30.90		8264.06	765.27	4112.52	489.65
1170	A	2	H	1	95	96	15	2.65	149.15	68.99	87.18		12.82	23.29		8392.37	793.09	4580.91	477.63
1170	A	2	H	1	100	101	15	2.70	152.58	69.49	88.12		11.88	33.83		8371.03	787.40	4253.72	418.52
1170	A	2	H	1	105	106	15	2.75	154.45	68.48	86.48		13.52	28.34	201.3	9077.88	846.77	6751.74	521.14
1170	A	2	H	1	110	111	15	2.80	156.33	68.98	85.48		14.52	34.19		9651.99	996.17	5287.92	616.92
1170	A	2	H	1	115	116	15	2.85	158.20	65.85	85.35		14.65	30.49		10182.94	910.82	4621.76	589.68
1170	A	2	H	1	120	121	15	2.90	160.07	67.31	85.08		14.92	37.27		9990.55	984.66	4787.11	634.13
1170	A	2	H	1	125	126	15	2.95	161.94	67.25	84.80		15.20	34.83		10900.18	1000.49	5011.71	683.63
1170	A	2	H	1	130	131	15	3.00	163.82	67.90	82.65		17.35	33.99	21.8	12782.55	978.48	5929.98	773.49
1170	A	2	H	1	135	136	15	3.05	165.69	68.66	84.98		15.02	34.21	15.1	9435.57	954.37	5488.88	597.18
1170	A	2	H	1	140	141	15	3.10	167.56	69.74	85.67		14.33	36.26		9477.39	904.09	4752.91	557.45
1170	A	2	H	2	0	1	15	3.20	171.31	61.90	85.52		14.48	35.86	19.9	9571.94	907.34	4746.00	593.29
1170	A	2	H	2	5	6	15	3.25	173.18	67.67	84.93		15.07	36.17		9699.21	926.20	4836.80	609.25
1170	A	2	H	2	10	11	15	3.30	175.05	59.96	84.03		15.97	36.44		11268.78	1106.77	5431.90	683.35
1170	A	2	H	2	15	16	15	3.35	177.80	66.81	83.90		16.10	28.67	54.0	10407.52	982.61	6755.20	685.77
1170	A	2	H	2	20	21	15	3.40	180.55	68.31	84.50		15.50	27.79	15.3	10307.75	1104.36	5583.65	644.10
1170	A	2	H	2	25	26	15	3.45	183.30	67.92	84.58		15.42	29.63	85.2	10728.96	1133.53	5288.83	691.20
1170	A	2	H	2	30	31	15	3.50	185.74	69.64	83.09		16.91	32.76	24.0	10904.11	1135.00	5969.15	670.21
1170	A	2	H	2	35	36	15	3.55	188.19	68.18	85.99		14.01	34.20		8578.97	1059.87	4443.14	520.37
1170	A	2	H	2	40	41	15	3.60	190.63	70.22	87.25		12.75	33.08		7632.73	976.13	4199.08	433.41
1170	A	2	H	2	45	46	15	3.65	193.07	70.28	89.22		10.78	37.33		6107.26	966.18	2691.77	337.56
1170	A	2	H	2	50	51	15	3.70	195.88	70.68	90.44		9.56	37.87		5051.78	903.90	2709.70	279.93
1170	A	2	H	2	55	56	15	3.75	198.69	72.59	90.61		9.39	34.78	10.1	5015.45	928.50	2220.62	273.56
1170	A	2	H	2	60	61	15	3.80	201.50	72.99	90.29		9.71	33.93	5.6	4646.45	888.03	2327.73	257.88
1170	A	2	H	2	65	66	15	3.85	204.31	73.91	90.08		9.92	30.11		4649.27	775.22	2381.68	258.62
1170	A	2	H	2	70	71	15	3.90	207.11	71.38	91.71		8.30	32.78	7.8	4385.15	661.73	2262.49	250.29
1170	A	2	H	2	75	76	15	3.95	209.92	75.64	91.16		8.84	32.55	5.8	4449.67	865.17	2056.02	241.89

Site	Hole	Core	Type	Section	Top [cm]	Bottom [cm]	Volume [cc]	Sample depth [mbsf]	Age [ka]	Lightness (L*)	Carbonate [%]	TOC [%]	Siliciclastics [%]	Coarse fraction [% > 63µm]	Chlorin [ng/g]	Aluminium [µg/g]	total Barium [µg/g]	Iron [µg/g]	Titanium [µg/g]
1170	A	2	H	2	80	81	15	4.00	212.73	67.19	90.43		9.57	35.20	4.5	4404.23	891.78	1916.87	239.32
1170	A	2	H	2	85	86	15	4.05	215.54	73.80	90.32		9.68	31.98	4.1	4254.71	861.45	2129.04	228.82
1170	A	2	H	2	90	91	15	4.10	216.58	73.71	90.14		9.86	31.03	4.0	4580.95	887.05	2677.55	239.10
1170	A	2	H	2	95	96	15	4.15	217.62	69.06	89.33		10.67	30.76	2.0	4677.05	913.53	2564.13	250.78
1170	A	2	H	2	100	101	15	4.20	218.66	73.71	88.52		11.48	29.88	4.5	5486.56	914.99	2336.01	305.38
1170	A	2	H	2	105	106	15	4.25	219.70	73.32	88.66		11.34	30.52	3.1	6504.75	808.97	4145.66	376.99
1170	A	2	H	2	110	111	15	4.30	220.73	71.53	87.65		12.35	32.28	9.0	6956.97	767.55	3446.67	432.40
1170	A	2	H	2	115	116	15	4.35	221.77	71.70	86.70		13.30	33.33	6.6	7461.11	790.28	3543.16	449.09
1170	A	2	H	2	120	121	15	4.40	222.81	61.59	84.98		15.02	35.64	13.3	8235.07	848.31	4459.33	502.86
1170	A	2	H	2	125	126	15	4.45	223.85	61.45	85.00		15.00	31.94	9.9	8280.87	895.66	6022.23	506.61
1170	A	2	H	2	130	131	15	4.50	224.89	64.35	83.93		16.07	37.75	13.8	9820.74	1070.01	4384.48	594.99
1170	A	2	H	2	135	136	15	4.55	226.28	62.07	85.52		14.48	36.44	13.0	9197.22	1108.02	4073.51	549.45
1170	A	2	H	2	140	141	15	4.60	227.67	60.36	87.59		12.41	42.22		7045.30	951.90	3436.20	405.58
1170	A	2	H	2	145	146	15	4.65	229.06	65.38	86.53		13.47	31.90		7286.45	937.81	4817.93	427.25
1170	A	2	H	3	0	1	15	4.70	230.45		88.64		11.36	32.06	8.4	6105.79	942.90	2727.71	356.67
1170	A	2	H	3	5	6	15	4.75	231.85	67.38	89.16		10.84	33.50		6067.09	932.20	3619.94	339.68
1170	A	2	H	3	10	11	15	4.80	233.24	70.15	89.48		10.52	31.25		5346.41	960.12	3133.18	293.60
1170	A	2	H	3	15	16	15	4.85	234.63	68.58	90.40		9.60	30.68		4500.29	886.89	2683.43	253.25
1170	A	2	H	3	20	21	15	4.90	236.02	71.10	90.89		9.11	27.93		4646.21	893.40	1871.74	246.84
1170	A	2	H	3	25	26	15	4.95	237.41	73.82	92.44		7.56	28.52		4073.41	844.39	1793.05	217.89
1170	A	2	H	3	30	31	15	5.00	238.80	67.59	90.79		9.21	30.39	5.8	4224.83	812.56	1978.76	224.26
1170	A	2	H	3	35	36	15	5.05	240.19	74.30	92.18		7.83	24.29		4088.65	818.71	1715.99	215.61
1170	A	2	H	3	40	41	15	5.10	241.67	74.53	90.62		9.38	19.67		5477.91	879.62	2835.57	291.73
1170	A	2	H	3	45	46	15	5.15	243.15	75.37	90.63		9.37	21.75		5842.35	700.33	2608.64	339.32
1170	A	2	H	3	50	51	15	5.20	244.64	75.51	92.71		7.29	18.71		6200.03	612.34	2523.82	314.89
1170	A	2	H	3	55	56	15	5.25	246.12	76.45	90.95		9.05	19.56	5.7	5475.03	665.83	2525.99	310.36
1170	A	2	H	3	60	61	15	5.30	247.60	73.56	89.50		10.50	8.76		5682.43	761.99	3069.02	330.13
1170	A	2	H	3	65	66	15	5.35	248.84	73.40	88.04		11.96	11.01		6538.80	874.23	3807.14	375.34
1170	A	2	H	3	70	71	15	5.40	250.09	72.05	87.86		12.14	19.57		7037.02	954.47	3673.49	402.71
1170	A	2	H	3	75	76	15	5.45	251.33	72.67	89.72		10.28	7.41		5303.93	649.17	2653.04	327.12
1170	A	2	H	3	80	81	15	5.50	252.57	73.44	91.45		8.55	18.13	15.0	4612.09	498.02	2352.95	250.07
1170	A	2	H	3	85	86	15	5.55	253.81	73.12	92.73		7.27	19.56		4468.92	538.25	2166.98	241.90
1170	A	2	H	3	90	91	15	5.60	255.06	71.99	92.53		7.47	13.50		4052.94	476.99	1937.59	219.37
1170	A	2	H	3	95	96	15	5.65	256.30	76.14	92.64		7.36	16.15		3961.07	517.51	2074.62	217.32
1170	A	2	H	3	100	101	15	5.70	257.54	73.55	92.18		7.82	19.89		4381.06	498.44	2404.36	238.54
1170	A	2	H	3	105	106	15	5.75	258.78	75.77	91.89		8.11	25.26	66.9	4487.82	563.06	1910.05	247.46
1170	A	2	H	3	110	111	15	5.80	260.03	77.27	93.35		6.65	25.23		4082.36	465.55	2496.64	224.34
1170	A	2	H	3	115	116	15	5.85	261.27	75.39	93.40		6.60	16.14		3246.78	437.40	1596.41	179.37
1170	A	2	H	3	120	121	15	5.90	262.51	78.08	92.85		7.15	18.01		3207.16	459.54	2079.12	174.27
1170	A	2	H	3	125	126	15	5.95	263.75	74.72	93.65		6.35	17.81		3323.77	443.47	1766.51	178.92

Site	Hole	Core	Type	Section	Top [cm]	Bottom [cm]	Volume [cc]	Sample depth [mbsf]	Age [ka]	Lightness (L*)	Carbonate [%]	TOC [%]	Siliciclastics [%]	Coarse fraction [% > 63µm]	Chlorin [ng/g]	Aluminium [µg/g]	total Barium [µg/g]	Iron [µg/g]	Titanium [µg/g]
1170	A	2	H	3	130	131	15	6.00	265.00	76.35	93.39		6.61	19.81	70.4	3292.81	450.70	1814.17	175.75
1170	A	2	H	3	135	136	15	6.05	266.24	75.30	93.18		6.82	18.38		3259.34	457.69	1795.49	178.09
1170	A	2	H	3	140	141	15	6.10	267.48	75.70	93.83		6.17	17.00		3044.00	403.35	1430.57	165.00
1170	A	2	H	4	0	2	15	6.20	271.82	70.19	92.97		7.03	20.04	94.6	3684.30	515.16	2321.67	202.58
1170	A	2	H	4	5	7	15	6.25	273.99	72.67	94.20		5.80	18.91		2701.59	494.01	1386.33	146.09
1170	A	2	H	4	10	12	15	6.30	276.16	76.22	92.68		7.32	15.31		4249.51	492.63	2159.99	226.37
1170	A	2	H	4	15	17	15	6.35	278.32	76.07	93.25		6.75	16.91		3035.53	450.22	1792.28	158.03
1170	A	2	H	4	20	22	15	6.40	280.49	77.49	93.97		6.03	20.18		2392.74	467.83	1088.49	125.82
1170	A	2	H	4	25	27	15	6.45	282.66	75.33	94.01		5.99	21.00		2431.70	484.47	1483.13	128.98
1170	A	2	H	4	30	32	15	6.50	284.83	77.27	91.50		8.50	21.90	120.3	4066.15	486.39	2233.70	222.83
1170	A	2	H	4	35	37	15	6.55	287.00	78.85	93.85		6.15	19.41		2466.93	452.10	1012.61	123.18
1170	A	2	H	4	40	42	15	6.60	288.21	78.25	93.12		6.88	18.69		2839.41	416.35	1709.70	143.07
1170	A	2	H	4	45	47	15	6.65	289.42	76.09	94.10		5.90	14.68		2005.01	445.03	1442.87	101.95
1170	A	2	H	4	50	52	15	6.70	290.63	78.73	94.10		5.90	12.48		1964.44	438.66	1036.90	101.75
1170	A	2	H	4	55	57	15	6.75	291.84	77.63	93.60		6.40	14.53	61.8	2054.06	437.06	1300.69	105.89
1170	A	2	H	4	60	62	15	6.80	293.05	78.43	92.02		7.98	14.77		3256.64	536.04	1598.56	178.51
1170	A	2	H	4	65	67	15	6.85	294.26	79.01	92.88		7.12	11.38		2577.35	413.02	951.03	128.03
1170	A	2	H	4	70	72	15	6.90	295.47	75.78	93.06		6.94	12.02		2631.41	460.67	1147.56	138.22
1170	A	2	H	4	75	77	15	6.95	296.68	77.85	93.86		6.14	13.95		2219.12	423.75	1010.78	115.07
1170	A	2	H	4	80	82	15	7.00	297.90	77.61	93.44		6.56	11.70	58.4	2091.92	421.69	823.51	108.12
1170	A	2	H	4	85	87	15	7.05	299.11	78.00	92.62		7.38	14.85		2325.91	387.32	1021.14	127.70
1170	A	2	H	4	90	92	15	7.10	300.32	79.99	94.57		5.43	14.05		1847.69	428.87	1371.75	101.53
1170	A	2	H	4	95	97	15	7.15	301.53	78.51	94.47		5.53	15.67		1551.13	388.67	1136.23	81.37
1170	A	2	H	4	100	102	15	7.20	302.74	75.10	93.73		6.27	10.69		1921.43	425.33	902.30	103.83
1170	A	2	H	4	105	107	15	7.25	303.95	72.17	94.06		5.94	13.36	13.1	1592.60	404.93	715.86	83.47
1170	A	2	H	4	110	112	15	7.30	305.16	77.47	93.43		6.57	13.65		1267.74	353.50	665.64	62.32
1170	A	2	H	4	115	117	15	7.35	306.37	79.91	93.74		6.26	10.89		1861.79	432.57	1011.89	102.74
1170	A	2	H	4	120	122	15	7.40	307.58	77.89	94.63		5.37	12.93	7.7	1315.31	373.51	990.93	67.12
1170	A	2	H	4	125	127	15	7.45	308.79	76.50	94.60		5.40	11.06		1304.38	419.29	778.30	75.52
1170	A	2	H	4	130	132	15	7.50	310.00	81.36	94.35		5.65	11.11	13.4	1490.45	402.50	716.66	78.73
1170	A	2	H	4	135	137	15	7.55	313.50	78.08	95.30		4.70	12.08		1436.36	367.24	779.85	72.64
1170	A	2	H	4	140	142	15	7.60	317.00	80.39	95.03		4.97	12.55		1541.74	397.00	661.75	79.89
1170	A	2	H	4	145	147	15	7.65	320.50	78.46	93.80		6.20	12.85		1657.25	430.98	1343.15	85.10
1170	A	2	H	5	0	2	15	7.70	324.00		93.68		6.32	12.07	9.3	2148.37	497.33	1011.97	107.15
1170	A	2	H	5	5	7	15	7.75	327.50	78.33	93.96		6.04	11.42		2408.90	506.99	1185.65	120.35
1170	A	2	H	5	10	12	15	7.80	331.00	77.93	94.30		5.70	10.51		2486.01	515.96	1443.83	123.34
1170	A	2	H	5	15	17	15	7.85	331.50	79.78	94.62		5.38	9.55		2173.04	440.05	933.12	110.06
1170	A	2	H	5	20	22	15	7.90	332.00	80.88	94.00		6.00	8.98		2515.71	502.21	962.73	125.16
1170	A	2	H	5	25	27	15	7.95	332.50	77.39	93.86		6.14	10.35		2358.92	503.15	1032.63	118.82
1170	A	2	H	5	30	32	15	8.00	333.00	80.77	93.15		6.85	13.80	5.1	2556.07	575.00	969.01	129.54

Site	Hole	Core	Type	Section	Top [cm]	Bottom [cm]	Volume [cc]	Sample depth [mbsf]	Age [ka]	Lightness (L*)	Carbonate [%]	TOC [%]	Siliciclastics [%]	Coarse fraction [% > 63µm]	Chlorin [ng/g]	Aluminium [µg/g]	total Barium [µg/g]	Iron [µg/g]	Titanium [µg/g]
1170	A	2	H	5	35	37	15	8.05	333.50	79.67	93.80		6.20	12.58		2219.22	538.78	1021.32	117.61
1170	A	2	H	5	40	42	15	8.10	334.00	82.75	93.60		6.40	12.58		2461.86	506.62	1272.71	130.25
1170	A	2	H	5	45	47	15	8.15	334.50	81.87	94.02		5.98	12.52		2206.07	472.78	1012.15	117.61
1170	A	2	H	5	50	52	15	8.20	335.00	81.48	93.63		6.37	11.86		2596.30	499.19	2084.34	139.42
1170	A	2	H	5	55	57	15	8.25	335.50	79.80	93.03		6.97	11.33	8.4	2872.32	515.52	2518.39	154.11
1170	A	2	H	5	60	62	15	8.30	336.00	77.71	92.82		7.18	11.71		3173.78	547.66	1868.88	174.83
1170	A	2	H	5	65	67	15	8.35	336.50	72.61	92.32		7.68	11.77		3515.90	498.71	2971.18	205.18
1170	A	2	H	5	70	72	15	8.40	337.00	74.86	92.54		7.46	13.54		3977.70	554.55	2132.66	220.10
1170	A	2	H	5	75	77	15	8.45	337.50	72.36	91.54		8.46	15.41		4156.45	521.77	1910.93	236.11
1170	A	2	H	5	80	82	15	8.50	338.00	70.87	87.74		12.26	17.07	160.8	4279.91	466.23	3023.70	237.10
1170	A	2	H	5	85	87	15	8.55	338.50	69.03	87.96		12.04	14.97		5398.80	463.25	5521.35	294.23
1170	A	2	H	5	90	92	15	8.60	339.00	68.76	87.30		12.70	16.04		6887.64	544.23	5170.26	363.68
1170	A	2	H	5	95	97	15	8.65	339.50	69.85	89.27		10.73	14.50		7009.51	559.06	2880.10	363.59
1170	A	2	H	5	100	102	15	8.70	340.00	68.24	86.57		13.43	14.72		8464.90	577.76	3846.42	438.34
1170	A	2	H	5	105	107	15	8.75	340.50	67.55	87.39		12.61	15.59	284.2	8693.57	640.87	4387.17	444.81
1170	A	2	H	5	110	112	15	8.80	341.00	69.54	83.89		16.11	14.17		10758.61	793.57	5167.91	568.74
1170	A	2	H	5	115	117	15	8.85	342.68	70.01	83.52		16.48	13.10		11668.84	856.52	5398.44	602.92
1170	A	2	H	5	120	122	15	8.90	344.37	65.73	83.31		16.69	12.62		12549.01	785.39	6292.27	660.84
1170	A	2	H	5	125	127	15	8.95	346.05	63.98	82.49		17.51	13.15		13456.41	791.28	8099.09	715.34
1170	A	2	H	5	130	132	15	9.00	347.74	67.87	82.71		17.29	12.95	324.9	12317.20	756.73	5206.33	654.75
1170	A	2	H	5	135	137	15	9.05	349.42	68.36	86.19		13.81	12.63		8078.92	624.83	3629.77	439.23
1170	A	2	H	5	140	142	15	9.10	351.11	72.68	89.94		10.06	16.40		4966.69	571.43	2540.41	276.82
1170	A	2	H	6	0	1	15	9.20	354.47	61.90	88.14		11.86	19.11	61.1	6241.42	619.05	4754.53	356.54
1170	A	2	H	6	5	6	15	9.25	356.16	68.48	88.98		11.02	18.29		7024.64	620.71	3348.08	357.40
1170	A	2	H	6	10	12	15	9.30	357.84	72.65	87.96		12.04	18.24		6984.73	648.47	3467.52	389.66
1170	A	2	H	6	15	16	15	9.35	359.53	67.39	87.16		12.84	17.58		7425.12	705.08	3995.23	425.82
1170	A	2	H	6	20	21	15	9.40	361.21	69.67	90.02		9.98	20.37		4571.04	600.26	2898.49	255.26
1170	A	2	H	6	25	26	15	9.45	362.90	65.40	87.98		12.02	17.58		6887.51	740.13	3107.34	384.03
1170	A	2	H	6	30	32	15	9.50	364.58	72.02	87.89		12.11	21.63	83.3	6421.07	678.17	3072.56	361.68
1170	A	2	H	6	35	36	15	9.55	366.26	74.94	87.33		12.67	22.71		7511.91	740.89	3723.80	404.11
1170	A	2	H	6	40	42	15	9.60	367.95	70.22	87.68		12.32	23.76		7323.36	692.62	3336.94	401.31
1170	A	2	H	6	45	46	15	9.65	369.63	73.08	89.18		10.82			6518.71	789.84	2500.38	355.70
1170	A	2	H	6	50	51	15	9.70	371.32	72.81	89.33		10.67	15.80		5948.31	680.28	3038.78	328.76
1170	A	2	H	6	55	56	15	9.75	373.00	74.43	90.69		9.31	16.32	34.5	4763.52	674.45	2026.47	260.04
1170	A	2	H	6	60	62	15	9.80	374.68	73.44	92.89		7.11	15.20		3673.70	607.41	1731.12	195.47
1170	A	2	H	6	65	66	15	9.85	376.37	71.38	92.30		7.70	21.99		2639.86	469.73	1789.70	145.13
1170	A	2	H	6	70	72	15	9.90	378.05	76.12	92.27		7.73	10.12		3148.60	461.22	1223.43	168.66
1170	A	2	H	6	75	77	15	9.95	379.74	80.55	93.28		6.72	10.06		2630.56	401.84	1101.02	133.56
1170	A	2	H	6	80	82	15	10.00	381.42	80.94	94.88		5.12	11.44	9.8	1697.76	402.95	713.48	87.90
1170	A	2	H	6	85	87	15	10.05	383.11	81.89	94.15		5.85	11.91		1753.60	362.78	715.75	90.80

Site	Hole	Core	Type	Section	Top [cm]	Bottom [cm]	Volume [cc]	Sample depth [mbsf]	Age [ka]	Lightness (L*)	Carbonate [%]	TOC [%]	Siliciclastics [%]	Coarse fraction [% > 63µm]	Chlorin [ng/g]	Aluminium [µg/g]	total Barium [µg/g]	Iron [µg/g]	Titanium [µg/g]
1170	A	2	H	6	90	92	15	10.10	384.79	82.64	94.93		5.07	10.88		2107.42	398.83	814.78	106.08
1170	A	2	H	6	95	97	15	10.15	386.47	79.08	94.47		5.53	9.37		2565.37	417.87	1195.68	136.74
1170	A	2	H	6	100	102	15	10.20	388.16	79.73	93.28		6.72	10.72		2339.77	390.10	1291.70	119.79
1170	A	2	H	6	105	107	15	10.25	389.84	81.31	93.88		6.12	11.20	8.6	2088.61	396.80	929.40	102.93
1170	A	2	H	6	110	112	15	10.30	391.53	79.81	93.22		6.78	10.22		2202.85	383.63	940.46	105.91
1170	A	2	H	6	115	117	15	10.35	393.21	79.00	93.58		6.42	11.69		2440.96	404.30	2190.51	118.30
1170	A	2	H	6	120	122	15	10.40	394.90	81.67	94.07		5.93	14.60		1850.48	403.69	888.10	88.49
1170	A	2	H	6	125	127	15	10.45	396.58	75.47	93.49		6.51	12.62		1718.54	445.32	1400.63	86.36
1170	A	2	H	6	130	132	15	10.50	398.26	80.49	93.43		6.57	12.41	52.1	2115.88	427.39	1246.11	109.86
1170	A	2	H	6	135	137	15	10.55	399.95	81.55	94.38		5.62	11.19		1871.38	450.97	859.59	88.49
1170	A	2	H	6	140	142	15	10.60	401.63	82.18	94.20		5.80	12.14		1967.29	495.80	859.45	101.08
1170	A	2	H	6	145	147	15	10.65	403.32	80.36	93.80		6.20	11.83		1990.03	524.97	1674.09	99.68
1170	A	2	H	7	0	2	15	10.70	405.00		93.88		6.12	13.33	69.1	1924.64	546.58	1062.02	100.27
1170	A	2	H	7	5	7	15	10.75	406.21	77.90	94.63		5.37	14.44		1900.93	518.96	1079.31	96.06
1170	A	2	H	7	10	12	15	10.80	407.42	79.98	94.46		5.54	16.12	5.4	2182.35	520.36	969.68	118.56
1170	A	2	H	7	15	17	15	10.85	408.63	78.44	93.47		6.53	18.24	6.6	2200.34	481.02	1301.02	120.68
1170	A	2	H	7	20	22	15	10.90	409.83	79.04	93.10		6.90	20.65	3.3	2504.20	520.97	1172.76	134.51
1170	A	2	H	7	25	27	15	10.95	411.04	78.22	92.66		7.34	21.64	15.7	2584.15	506.22	1145.68	137.31
1170	A	2	H	7	30	32	15	11.00	412.25	75.36	92.58		7.42	23.29	8.6	2471.04	478.60	1084.94	131.54
1170	A	2	H	7	35	37	15	11.05	413.46	78.36	92.42		7.58	22.56	5.4	2914.60	518.15	1367.00	152.63
1170	A	2	H	7	40	42	15	11.10	414.67	76.94	92.86		7.14	24.08	59.1	2779.56	509.46	1110.99	143.44
1170	A	2	H	7	45	47	15	11.15	415.88	79.82	92.30		7.70	22.83	7.4	2952.62	576.80	1750.94	162.42
1170	A	2	H	7	50	52	15	11.20	417.08	73.44	92.52		7.48	20.60	39.3	2878.02	521.80	2491.70	154.96
1170	A	2	H	7	55	57	15	11.25	418.29	77.98	92.79		7.21	21.64	9.9	2238.58	406.67	995.81	113.00
1170	A	2	H	7	60	62	15	11.30	419.50	78.67	93.71		6.29	18.52	7.7	2597.85	478.84	1512.60	138.38
1170	A	2	H	7	65	67	15	11.35	420.71	74.74	93.88		6.12	20.15		1980.11	454.46	867.88	111.80
1170	A	2	H	7	70	72	15	11.40	421.92	78.96	93.98		6.02	20.12	6.1	1872.27	465.73	1265.66	108.20
1170	A	2	H	7	75	77	15	11.45	423.13	80.80	94.62		5.38	15.54	7.5	1936.85	473.60	1153.94	96.31
1170	A	2	H	7	80	82	15	11.50	424.33	80.45	94.78		5.22	17.77	12.5	1935.45	519.13	1018.93	99.19
1170	A	2	H	CC	0	2	15	11.56	425.78		95.48		4.52	13.36	6.1	1675.66	395.57	1105.86	95.11
1170	A	2	H	CC	5	7	15	11.61	426.75	82.88	95.82		4.18	15.28	4.9	2033.96	399.30	1030.84	114.37
1170	A	3	H	1	45	47	15	11.65	427.96	77.03	94.27		5.73	24.36		2742.04	531.47	1301.44	144.26
1170	A	3	H	1	50	52	15	11.70	429.17	78.28	94.25		5.75	23.50	4.3	2883.66	572.49	1144.72	155.33
1170	A	3	H	1	55	57	15	11.75	430.38	77.50	94.24		5.76	20.94	4.2	2972.04	552.37	1381.01	162.76
1170	A	3	H	1	60	62	15	11.80	431.58	76.54	94.30		5.70	20.37	8.5	2647.70	467.72	2168.30	143.57
1170	A	3	H	1	65	67	15	11.85	432.79	78.18	95.63		4.37	20.19	10.2	2063.51	450.47	1460.63	109.00
1170	A	3	H	1	70	72	15	11.90	434.00	79.86	95.61		4.39	17.30	8.1	1935.75	472.80	950.48	109.85
1170	A	3	H	1	75	77	15	11.95	435.18	81.20	95.49		4.51	15.28	5.7	1717.76	427.67	807.84	95.47
1170	A	3	H	1	80	82	15	12.00	436.36	79.68	96.53		3.47	13.85	7.2	1587.83	435.19	808.29	92.17
1170	A	3	H	1	85	87	15	12.05	437.55	80.67	95.19		4.81	14.20	9.0	1856.99	367.15	1931.42	101.64

Site	Hole	Core	Type	Section	Top [cm]	Bottom [cm]	Volume [cc]	Sample depth [mbsf]	Age [ka]	Lightness (L*)	Carbonate [%]	TOC [%]	Siliciclastics [%]	Coarse fraction [% > 63µm]	Chlorin [ng/g]	Aluminium [µg/g]	total Barium [µg/g]	Iron [µg/g]	Titanium [µg/g]
1170	A	3	H	1	90	92	15	12.10	438.73	74.84	95.11		4.89	15.06	8.2	2084.85	381.74	1226.59	120.16
1170	A	3	H	1	95	97	15	12.15	439.91	77.08	95.21		4.79	15.03	12.4	2245.07	389.09	1033.69	129.57
1170	A	3	H	1	100	102	15	12.20	441.09	75.56	94.19		5.81	15.57	14.8				
1170	A	3	H	1	105	107	15	12.25	442.27	78.55	95.37		4.63	16.32	1.2	2340.27	402.28	1190.98	129.71
1170	A	3	H	1	110	112	15	12.30	443.46	77.92	94.10		5.90	16.89	13.0	2573.87	429.08	1313.49	140.04
1170	A	3	H	1	115	117	15	12.35	444.64	77.11	94.95		5.05	16.47	14.4	2431.04	415.09	1150.17	137.28
1170	A	3	H	1	120	122	15	12.40	445.82	78.77	94.82		5.18	16.45	17.8	2524.76	427.40	1326.15	141.74
1170	A	3	H	1	125	127	15	12.45	447.00	78.09	94.55		5.45	18.29	30.7	2629.25	435.71	1502.41	149.44
1170	A	3	H	1	130	132	15	12.50	448.18	79.16	94.42		5.58	19.53	30.1	2641.14	445.89	1280.22	144.75
1170	A	3	H	1	135	137	15	12.55	449.36	79.42	94.88		5.12	16.23	26.8	2523.07	422.52	1262.22	136.85
1170	A	3	H	1	140	142	15	12.60	450.55	77.81	94.56		5.44	18.63	42.2	2571.79	419.80	1265.51	143.22

Site 1171A - Concentrations of the analysed proxies

Site	Hole	Core	Type	Section	Top [cm]	Bottom [cm]	Volume [cc]	Sample depth [mbsf]	Age [ka]	Lightness (L*)	Carbonate [%]	TOC [%]	Siliciclastics [%]	Coarse fraction [% > 63µm]	Chlorin [ng/g]	Aluminium [µg/g]	total Barium [µg/g]	Iron [µg/g]	Titanium [µg/g]
1171	A	1	H	1	0	1	15	0.00	0.32	60.10	95.01		4.99	38.44	39.9	1618.52	584.00	890.71	86.18
1171	A	1	H	1	5	6	15	0.05	2.31	73.98	94.90		5.10	37.27	27.5	1244.10	452.58	732.06	65.22
1171	A	1	H	1	10	11	15	0.10	4.27	73.59	95.97		4.03	41.40		1747.67	573.98	935.59	85.51
1171	A	1	H	1	15	17	15	0.15	6.24	74.16	94.81		5.19	40.92	52.1	2024.49	651.95	1114.65	103.49
1171	A	1	H	1	21	23	15	0.21	8.61	71.79	94.76		5.24	46.62	18.7	2101.76	660.03	1268.83	115.73
1171	A	1	H	1	25	26	15	0.25	10.13	80.49	95.12		4.88	46.58	16.4	2118.58	630.66	1332.28	125.63
1171	A	1	H	1	30	32	15	0.30	11.83	77.10	94.83		5.17	57.35	41.1	2107.55	601.52	2118.41	129.76
1171	A	1	H	1	35	37	15	0.35	13.52	72.69	94.17		5.83	63.94	32.3	2386.28	464.88	1920.17	162.27
1171	A	1	H	1	40	42	15	0.40	15.20	69.21	94.07		5.93	67.25	29.5	2690.97	481.19	1778.13	176.68
1171	A	1	H	1	45	46	15	0.45	16.33	71.34	94.94		5.06	57.11	27.3	2352.25	403.99	1484.62	146.91
1171	A	1	H	1	50	51	15	0.50	18.05	74.82				59.25					
1171	A	1	H	1	55	56	15	0.55	19.79	75.49	94.93		5.07	58.37	23.7	2354.31	428.24	1423.29	144.95
1171	A	1	H	1	60	61	15	0.60	21.52	77.75	94.67		5.33	58.40	28.7	2611.45	469.96	1604.09	160.18
1171	A	1	H	1	65	66	15	0.65	26.03	76.95	94.65		5.35	57.34	14.2	3005.40	456.19	1788.13	184.86
1171	A	1	H	1	69	71	15	0.69	29.64	78.25	94.62		5.38	41.80	34.9	2964.61	441.88	1828.94	188.58
1171	A	1	H	1	75	76	15	0.75	36.32	80.77									
1171	A	1	H	1	80	83	15	0.80	40.64	81.63				40.70					
1171	A	1	H	1	85	87	15	0.85	44.66	81.97	94.75		5.25	44.15	29.1	1830.56	428.87	859.95	98.34
1171	A	1	H	1	90	92	15	0.90	48.67	81.27	94.75		5.25	37.47	14.9	2006.32	544.43	986.98	108.46
1171	A	1	H	1	95	98	15	0.95	52.69	81.39	94.95		5.05	36.95	23.5	1689.50	457.49	1066.20	92.55
1171	A	1	H	1	100	102	15	1.00	57.24	80.63	95.50		4.50	39.65	19.1	1623.17	492.25	864.59	89.03
1171	A	1	H	1	105	106	15	1.05	61.90	81.54	95.07		4.93	38.94	2.8	1786.82	567.57	972.50	98.12
1171	A	1	H	1	110	112	15	1.10	67.18	80.79	94.80		5.20	42.15		1963.63	461.18	1019.63	109.41
1171	A	1	H	1	115	116	15	1.15	72.84	81.71	94.77		5.23	45.06	8.9	1932.25	433.52	1071.23	110.88
1171	A	1	H	1	120	121	15	1.20	78.02	80.31	94.48		5.52	42.45	14.4	1875.40	470.07	1456.74	105.75
1171	A	1	H	1	125	126	15	1.25	81.79	81.93	94.98		5.02	43.42	33.7	1863.23	487.34	1054.35	103.90
1171	A	1	H	1	130	132	15	1.30	85.54	81.81	94.66		5.34	43.24	6.7	1698.81	511.63	1074.91	91.32
1171	A	1	H	1	135	136	15	1.35	89.38	82.79	94.77		5.23	36.87	21.6				
1171	A	1	H	1	140	141	15	1.40	93.37	81.67	94.66		5.34	36.44	8.2	1960.81	600.02	982.11	99.17
1171	A	1	H	2	0	1	15	1.50	101.11	70.17	94.62		5.38	40.09	54.2				
1171	A	1	H	2	5	6	15	1.55	103.68	78.69	94.79		5.21	41.56	97.5	1788.17	514.23	1130.05	98.81
1171	A	1	H	2	10	11	15	1.60	105.36	78.99	94.45		5.55	40.94	9.9	1856.10	547.62	1464.97	100.88
1171	A	1	H	2	15	16	15	1.65	114.38	80.94	94.07		5.93	40.86	16.1	1667.80	536.90	1254.70	93.44
1171	A	1	H	2	20	22	15	1.70	126.41	81.09	94.65		5.35	40.88	41.7	2019.39	585.09	866.69	98.21
1171	A	1	H	2	25	26	15	1.75	129.33	79.79	95.54		4.46	45.06	201.1	1650.29	424.44	791.69	92.07
1171	A	1	H	2	30	32	15	1.80	132.25	81.37	95.75		4.25	37.91	64.8	1964.40	591.44	1021.51	104.65
1171	A	1	H	2	35	37	15	1.85	135.09	81.30	96.46		3.54	39.15	310.9				
1171	A	1	H	2	40	41	15	1.90	137.86	77.76	96.70		3.30	44.47	434.4	1839.25	464.99	1185.21	87.91
1171	A	1	H	2	45	46	15	1.95	140.58	75.31	95.99		4.01	45.37	371.5	2060.07	534.30	1050.67	110.12

Site	Hole	Core	Type	Section	Top [cm]	Bottom [cm]	Volume [cc]	Sample depth [mbsf]	Age [ka]	Lightness (L*)	Carbonate [%]	TOC [%]	Siliciclastics [%]	Coarse fraction [% > 63µm]	Chlorin [ng/g]	Aluminium [µg/g]	total Barium [µg/g]	Iron [µg/g]	Titanium [µg/g]
1171	A	1	H	2	50	51	15	2.00	143.27	75.28	95.97		4.03	43.58	19.2	2089.76	571.27	1044.86	131.07
1171	A	1	H	2	55	56	15	2.05	146.62	77.38	95.23		4.77	46.22	53.0	3610.57	640.89	1855.18	221.77
1171	A	1	H	2	60	61	15	2.10	152.62	77.27	94.38		5.62	49.51	28.2	3378.06	604.33	1703.73	207.60
1171	A	1	H	2	65	66	15	2.15	159.39	76.32	95.42		4.58	56.47		3309.22	571.14	2084.92	210.64
1171	A	1	H	2	70	71	15	2.20	164.71	73.87	95.10		4.90	50.41	32.4	3716.99	625.18	1836.18	234.30
1171	A	1	H	2	75	76	15	2.25	167.71	71.62	94.98		5.02	56.82		3988.48	755.15	2006.06	267.27
1171	A	1	H	2	80	81	15	2.30	169.65	72.05	95.37		4.63	59.83	25.0	3940.35	641.59	1993.49	258.06
1171	A	1	H	2	85	87	15	2.35	170.55	73.79	96.15		3.85	57.11	18.8	3046.33	618.38	1598.55	192.26
1171	A	1	H	2	90	91	15	2.40	171.45	74.34	95.72		4.28	56.18		3617.84	783.34	1884.96	241.42
1171	A	1	H	2	95	97	15	2.45	175.83	72.29	94.66		5.34	53.07	11.2	4398.96	933.84	2558.27	291.86
1171	A	1	H	2	100	102	15	2.50	180.20	74.94	93.56		6.44	50.26		3230.60	805.35	1645.49	201.34
1171	A	1	H	2	105	107	15	2.55	183.23	73.94	94.56		5.44	51.52	21.1	2371.87	682.66	1108.46	132.52
1171	A	1	H	2	110	112	15	2.60	186.51	77.52	94.85		5.15	49.71	5.7	2193.73	653.76	960.07	116.57
1171	A	1	H	2	115	116	15	2.65	189.75	77.82	94.69		5.31	47.79		1986.30	666.93	878.31	108.05
1171	A	1	H	2	120	121	15	2.70	192.62	77.60	93.72		6.28	46.91	2.3	1933.37	681.25	1008.77	105.61
1171	A	1	H	2	125	126	15	2.75	195.50	76.04	94.40		5.60	45.39		1897.92	655.62	1313.31	105.50
1171	A	1	H	2	130	132	15	2.80	205.95	78.89	94.42		5.58	48.85	25.9	2106.06	657.13	1026.94	118.35
1171	A	1	H	2	135	136	15	2.85	215.65	78.79	94.44		5.56	47.33	11.1	2549.06	697.12	1140.35	139.45
1171	A	1	H	2	140	141	15	2.90	225.42	72.76	93.81		6.19	49.87		2949.51	725.28	1480.21	184.42
1171	A	1	H	2	145	146	15	2.95	231.61	73.84	92.54		7.46	53.33	3.4	2888.33	737.31	1595.86	175.98
1171	A	1	H	3	0	1	15	3.00	236.38		93.85		6.15	40.11		2590.29	618.84	1361.34	150.83
1171	A	1	H	3	5	6	15	3.05	239.03	77.34	94.00		6.00	38.85	22.9	2461.92	615.03	1163.10	132.26
1171	A	1	H	3	10	11	15	3.10	241.65	78.02	94.16		5.84	40.06	20.8	2017.01	625.37	940.89	107.95
1171	A	1	H	3	15	16	15	3.15	245.07	79.35	93.35		6.65	42.01		2200.29	610.13	1396.49	116.00
1171	A	1	H	3	20	22	15	3.20	251.59	79.82	93.64		6.36	45.66	7.0	2228.56	515.23	1259.06	130.64
1171	A	1	H	3	25	26	15	3.25	256.65	80.25	95.13		4.87	50.37		2115.61	481.59	1208.52	126.10
1171	A	1	H	3	30	32	15	3.30	260.07	76.99	95.28		4.72	54.51	16.6	1947.72	476.13	1317.58	123.94
1171	A	1	H	3	35	37	15	3.35	263.30	75.31	94.30		5.70	53.24	7.6	2213.00	500.12	1567.16	144.76
1171	A	1	H	3	40	41	15	3.40	266.05	75.47	94.03		5.97	52.53		2317.05	480.92	1155.25	136.82
1171	A	1	H	3	45	46	15	3.45	268.69	74.63	94.85		5.15	53.97	5.1	2113.59	434.99	1289.20	128.13
1171	A	1	H	3	50	51	15	3.50	271.33	74.97				52.12					
1171	A	1	H	3	55	56	15	3.55	276.41	74.24	91.89		8.11	48.60		3368.68	600.81	1484.49	231.95
1171	A	1	H	3	60	61	15	3.60	280.35	74.69	93.35		6.65	46.76	24.0	3294.40	581.14	1501.55	207.01
1171	A	1	H	3	65	66	15	3.65	284.29	77.37	95.23		4.77	47.57	3.1	2125.10	483.54	1064.05	133.26
1171	A	1	H	3	70	72	15	3.70	288.24	80.72	95.69		4.31	40.06		1919.17	532.02	882.99	91.14
1171	A	1	H	3	75	76	15	3.75	291.10	80.00	95.60		4.40	44.77	3.9	1627.48	514.07	840.53	91.28
1171	A	1	H	3	80	82	15	3.80	293.51	78.27	95.21		4.79	48.92		1771.51	444.24	1283.79	103.08
1171	A	1	H	3	85	87	15	3.85	296.10	78.00	95.63		4.37	49.86	15.0	1932.47	416.97	1111.82	113.80
1171	A	1	H	3	90	92	15	3.90	298.68	77.43	94.79		5.21	49.59	4.9	2185.08	504.79	1133.38	127.66
1171	A	1	H	3	95	97	15	3.95	301.28	79.36	95.22		4.78	43.90		2468.15	514.73	959.42	112.02

Site	Hole	Core	Type	Section	Top [cm]	Bottom [cm]	Volume [cc]	Sample depth [mbsf]	Age [ka]	Lightness (L*)	Carbonate [%]	TOC [%]	Siliciclastics [%]	Coarse fraction [% > 63µm]	Chlorin [ng/g]	Aluminium [µg/g]	total Barium [µg/g]	Iron [µg/g]	Titanium [µg/g]
1171	A	1	H	3	100	102	15	4.00	303.86	80.12	95.67		4.33	45.81	13.9	1854.15	501.28	888.08	105.97
1171	A	1	H	3	105	106	15	4.05	305.33	78.56	95.32		4.68	38.14		1831.00	494.45	1108.95	99.86
1171	A	1	H	3	110	112	15	4.10	306.80	79.48	95.11		4.89	40.49	20.1	1840.08	516.78	1184.82	96.85
1171	A	1	H	3	115	116	15	4.15	308.28	79.93	95.62		4.38	40.01	8.1	1602.97	487.63	794.49	86.40
1171	A	1	H	3	120	121	15	4.20	309.74	80.28	95.64		4.36	36.09		1744.16	494.78	1018.36	86.81
1171	A	1	H	3	125	126	15	4.25	310.72	80.61	95.73		4.27	35.87	2.3	1811.44	553.54	877.90	97.95
1171	A	1	H	3	130	132	15	4.30	311.35	80.50	95.28		4.72	39.90		1748.41	552.09	929.67	95.00
1171	A	1	H	3	135	136	15	4.35	311.99	81.43	95.51		4.49	38.39	13.6	1746.28	585.41	948.48	93.54
1171	A	1	H	3	140	141	15	4.40	312.61	79.27	95.13		4.87	36.50	1.9	1792.34	602.14	928.79	98.02
1171	A	1	H	4	0	1	15	4.50	313.88	51.15	95.29		4.71	39.02	21.3	1939.50	538.74	1018.36	107.04
1171	A	1	H	4	5	6	15	4.55	314.51	65.76	95.01		4.99	41.52	301.7	1890.50	513.43	1010.10	102.76
1171	A	1	H	4	10	11	15	4.60	316.04	80.60	95.10		4.90	44.70	118.2	1885.68	517.16	969.96	112.36
1171	A	1	H	4	15	16	15	4.65	317.65	79.27	95.34		4.66	40.50	17.6	2612.63	405.57	1380.77	158.12
1171	A	1	H	4	20	21	15	4.70	319.17	79.31	95.65		4.35	31.75	57.7	2071.79	431.93	1178.42	120.33
1171	A	1	H	4	25	26	15	4.75	320.56	80.30	95.40		4.60	33.37	33.2	2267.24	391.73	1313.00	130.19
1171	A	1	H	4	30	32	15	4.80	321.38	77.04	95.34		4.66	27.94	338.4	2534.25	405.35	1335.15	146.27
1171	A	1	H	4	35	37	15	4.85	322.19	76.70	94.31		5.69	28.80	207.5	2803.75	390.55	1364.02	164.11
1171	A	1	H	4	40	42	15	4.90	323.00	74.14	94.23		5.77	27.56	128.0	2866.07	402.50	1647.19	159.30
1171	A	1	H	4	45	47	15	4.95	323.84	75.74	94.72		5.28	24.29	497.1	2616.44	404.81	1238.32	150.01
1171	A	1	H	4	50	52	15	5.00	324.68	78.50	94.79		5.21	24.85	66.1	2125.29	365.62	1000.97	125.22
1171	A	1	H	4	55	57	15	5.05	325.53	77.89	95.24		4.76	23.76	125.7				
1171	A	1	H	4	60	62	15	5.10	326.38	75.21	95.09		4.91	26.12	48.4	1864.29	321.51	948.33	109.50
1171	A	1	H	4	65	67	15	5.15	327.21	76.14	95.08		4.92	26.93	225.4	1844.26	350.92	1055.50	114.47
1171	A	1	H	4	70	72	15	5.20	328.30	79.82	95.90		4.10	25.43	241.0	2163.58	370.05	1028.17	126.20
1171	A	1	H	4	75	77	15	5.25	330.05	76.20	96.01		3.99	25.16	96.2				
1171	A	1	H	4	80	82	15	5.30	331.79	80.60	96.07		3.93	26.54	44.5	1532.84	369.11	724.19	87.82
1171	A	1	H	4	85	87	15	5.35	334.17	81.18	95.41		4.59	26.37	105.1	1676.03	395.15	668.61	89.80
1171	A	1	H	4	90	92	15	5.40	336.67	77.76	96.08		3.92	27.36	96.9	1420.55	367.77	934.99	88.06
1171	A	1	H	4	95	97	15	5.45	339.57	80.34	95.42		4.58	23.22	425.4	2224.77	327.81	1277.81	130.92
1171	A	1	H	4	100	102	15	5.50	344.00	78.26	95.28		4.72	24.35	340.1	1924.51	385.09	1086.60	111.79
1171	A	1	H	4	105	107	15	5.55	348.43	76.23	96.40		3.60	21.50	478.4	1702.16	358.35	792.75	96.72
1171	A	1	H	4	110	112	15	5.60	357.47	80.92	95.97		4.03	22.83	904.9	2381.09	384.54	1076.91	134.39
1171	A	1	H	4	115	117	15	5.65	361.34	82.24	96.19		3.81	20.10	832.8	1525.00	411.44	799.14	89.58
1171	A	1	H	4	120	122	15	5.70	364.87	81.96	96.48		3.52	18.55	631.7	1612.19	368.99	849.71	89.29
1171	A	1	H	4	125	127	15	5.75	367.97	79.33	96.65		3.35	20.00	11.6	1136.58	361.87	499.38	58.08
1171	A	1	H	4	130	132	15	5.80	372.49	76.95	96.38		3.62	18.84	16.0	1217.15	393.76	552.71	61.14
1171	A	1	H	4	135	137	15	5.85	379.19	77.21	96.81		3.19	24.20	98.5	1226.12	339.72	500.68	64.70
1171	A	1	H	4	140	142	15	5.90	384.44	82.60	97.15		2.85	16.58	53.5	742.97	302.13	446.40	49.75
1171	A	1	H	4	145	147	15	5.95	387.10	87.10	97.31		2.69	14.01	15.3	759.71	263.65	380.46	47.90
1171	A	1	H	5	0	1	15	6.00	388.22		96.92		3.08	13.59		786.68	300.55	325.22	45.01

Site	Hole	Core	Type	Section	Top [cm]	Bottom [cm]	Volume [cc]	Sample depth [mbsf]	Age [ka]	Lightness (L*)	Carbonate [%]	TOC [%]	Siliciclastics [%]	Coarse fraction [% > 63µm]	Chlorin [ng/g]	Aluminium [µg/g]	total Barium [µg/g]	Iron [µg/g]	Titanium [µg/g]
1171	A	1	H	5	5	7	15	6.05	389.40	86.16	96.79		3.21	13.07	3.3	841.24	293.32	345.78	48.40
1171	A	1	H	5	10	12	15	6.10	390.59	86.12	96.98		3.02	17.63		1013.66	297.66	477.51	54.17
1171	A	1	H	5	15	17	15	6.15	392.24	86.70	96.33		3.67	16.76	17.2	976.12	303.71	1434.93	54.73
1171	A	1	H	5	20	22	15	6.20	395.66	72.69	96.78		3.22	18.28	10.4	959.33	290.09	719.89	54.44
1171	A	1	H	5	25	27	15	6.25	396.69	82.22	95.48		4.52	13.53		1030.73	320.06	1153.98	53.91
1171	A	1	H	5	30	32	15	6.30	397.70	83.98	95.60		4.40	17.06	34.0	1068.42	383.10	573.68	53.14
1171	A	1	H	5	35	37	15	6.35	398.73	81.71	96.83		3.17	15.26		1030.60	395.00	500.76	56.40
1171	A	1	H	5	40	42	15	6.40	399.76	80.78	96.72		3.28	16.96	144.3	1035.70	382.35	515.65	54.92
1171	A	1	H	5	45	47	15	6.45	400.78	83.75	96.60		3.40	15.00	5.6	1131.04	447.23	534.11	56.11
1171	A	1	H	5	50	52	15	6.50	403.51	83.64	96.33		3.67	15.97	3.8	1104.80	382.62	521.83	59.09
1171	A	1	H	5	55	57	15	6.55	406.59	75.74	96.01		3.99	13.10		1031.04	374.75	945.67	57.61
1171	A	1	H	5	60	62	15	6.60	409.28	80.39	96.48		3.52	17.70	8.2	1174.79	391.67	762.66	58.94
1171	A	1	H	5	65	67	15	6.65	414.14	83.86	96.14		3.86	16.94	11.7	1141.38	410.06	478.02	62.07
1171	A	1	H	5	70	72	15	6.70	417.51	76.97	96.53		3.47	19.16	3.4	1356.32	414.34	700.05	75.77
1171	A	1	H	5	75	77	15	6.75	418.35	82.11	96.22		3.78	17.95					
1171	A	1	H	5	80	82	15	6.80	419.20	84.56	96.09		3.91	18.32		1582.08	464.75	752.60	90.77
1171	A	1	H	5	85	87	15	6.85	420.14	83.41	95.85		4.15	18.56	50.1	1696.44	458.18	836.05	92.55
1171	A	1	H	5	90	92	15	6.90	421.15	81.83	95.52		4.48	24.98	13.5	1755.67	450.72	919.78	107.15
1171	A	1	H	CC	0	2	15	6.94	421.95	72.85	95.30		4.70	30.09		1967.77	434.38	1122.59	115.08
1171	A	1	H	CC	5	7	15	6.99	422.96	77.17	96.15		3.85	34.99	6.5	1876.23	315.49	1218.17	113.97
1171	A	2	H	1	0	2	15	7.10	425.17		95.85		4.15	23.49		1481.60	365.17	786.60	82.03
1171	A	2	H	1	5	7	15	7.15	426.17	79.04	96.42		3.58	19.11	37.7	1004.74	326.54	573.50	84.84
1171	A	2	H	1	10	12	15	7.20	427.13	66.56	93.95		6.05	20.32	67.7	1502.54	382.08	726.68	108.96
1171	A	2	H	1	15	17	15	7.25	428.10	79.27	93.32		6.68	22.20		1224.43	369.62	677.98	67.46
1171	A	2	H	1	20	22	15	7.30	430.54	68.15	93.70		6.30	22.44	95.6	1415.06	372.85	770.34	111.58
1171	A	2	H	1	25	27	15	7.35	441.12	75.50	93.84		6.16	20.03		1348.86	374.58	743.85	78.11
1171	A	2	H	1	30	32	15	7.40	443.53	56.65	93.78		6.22	17.26	56.6	1168.51	366.46	560.45	63.06
1171	A	2	H	1	35	37	15	7.45	455.46	74.58	94.14		5.86	17.63	8.2	1101.07	402.39	425.29	56.31
1171	A	2	H	1	40	42	15	7.50	464.30	83.86	94.20		5.80	21.31		996.58	413.69	449.55	54.73
1171	A	2	H	1	45	47	15	7.55	471.52	84.50	94.65		5.35	20.64	11.0	1033.46	425.66	501.30	53.40
1171	A	2	H	1	50	52	15	7.60	477.40	84.24	93.60		6.40	23.06	20.4	1142.88	451.79	906.93	63.90
1171	A	2	H	1	55	57	15	7.65	482.74	81.27	93.22		6.78	25.09	40.6	1251.52	447.38	985.14	67.26
1171	A	2	H	1	60	62	15	7.70	488.08	71.40	93.95		6.05	29.13	84.5	1283.53	425.00	546.69	68.76
1171	A	2	H	1	65	67	15	7.75	490.23	80.41	93.08		6.92	31.56	383.4	1820.85	475.75	1006.77	103.06
1171	A	2	H	1	70	72	15	7.80	492.39	78.64	93.10		6.90	33.55	117.0	1419.34	438.37	785.21	73.18
1171	A	2	H	1	75	77	15	7.85	494.53	79.99	93.27		6.73	31.20	28.5	1710.85	519.78	1073.41	89.93
1171	A	2	H	1	80	82	15	7.90	496.69	80.53	95.00		5.00	32.96	18.9				
1171	A	2	H	1	85	87	15	7.95	498.84	80.54	95.23		4.77	31.35	8.7	1919.28	517.26	708.78	88.24
1171	A	2	H	1	90	92	15	8.00	500.98	81.37	95.80		4.20	31.83	170.5	1256.17	433.13	492.46	66.59
1171	A	2	H	1	95	97	15	8.05	503.54	82.05	95.92		4.08	30.82	21.8	1481.87	435.70	727.02	85.37

Site	Hole	Core	Type	Section	Top [cm]	Bottom [cm]	Volume [cc]	Sample depth [mbsf]	Age [ka]	Lightness (L*)	Carbonate [%]	TOC [%]	Siliciclastics [%]	Coarse fraction [% > 63µm]	Chlorin [ng/g]	Aluminium [µg/g]	total Barium [µg/g]	Iron [µg/g]	Titanium [µg/g]
1171	A	2	H	1	100	102	15	8.10	507.68	82.43	95.81		4.19	31.28		1333.21	384.94	635.98	73.66
1171	A	2	H	1	105	107	15	8.15	511.82	82.02	96.22		3.78	27.78	15.6	1257.43	430.77	656.75	75.87
1171	A	2	H	1	110	112	15	8.20	515.40	82.51	96.51		3.49	20.51	7.2	1220.91	407.04	575.52	70.29
1171	A	2	H	1	115	117	15	8.25	518.86	84.87	96.22		3.78	20.65		1046.35	394.04	644.44	71.72
1171	A	2	H	1	120	122	15	8.30	522.26	82.71	96.86		3.14	24.12		1545.33	410.83	524.32	81.08
1171	A	2	H	1	125	127	15	8.35	525.33	82.06	96.08		3.92	25.82		1533.37	419.35	672.74	87.66
1171	A	2	H	1	130	132	15	8.40	528.40	81.83	95.29		4.71	27.81	14.5	1850.90	467.10	1396.73	104.18
1171	A	2	H	1	135	137	15	8.45	531.46	82.21	95.40		4.60	34.88	6.2	2043.88	504.84	768.61	105.21
1171	A	2	H	1	140	142	15	8.50	534.53	79.37	94.15		5.85	34.33		1875.43	548.53	1028.32	110.92
1171	A	2	H	2	0	1	15	8.60	538.37	63.17	93.68		6.32	36.78		1998.99	552.17	1088.44	119.52
1171	A	2	H	2	5	6	15	8.65	539.54	78.11	93.10		6.90	39.36		2191.39	564.47	1064.72	129.19
1171	A	2	H	2	10	11	15	8.70	542.13	70.69	93.09		6.91	45.93	55.0	2553.11	674.82	1644.84	158.28
1171	A	2	H	2	15	17	15	8.75	545.07	68.85	91.69		8.31	44.05	20.1	2454.99	758.68	1291.89	147.63
1171	A	2	H	2	20	21	15	8.80	548.02	70.18	91.47		8.53	44.34	178.7	3195.62	534.02	1957.53	213.14
1171	A	2	H	2	25	26	15	8.85	552.11	68.55	91.47		8.53	35.28	165.3	3976.56	685.76	2163.71	245.58
1171	A	2	H	2	30	32	15	8.90	556.24	70.22	89.02		10.98	44.16	152.1	2966.05	615.64	2103.52	180.59
1171	A	2	H	2	35	37	15	8.95	560.68	75.48	91.61		8.39	45.25	31.1	2229.99	637.66	1280.00	136.04
1171	A	2	H	2	40	42	15	9.00	566.28	77.70	91.94		8.06	45.14	23.6	2064.43	656.13	1663.91	129.22
1171	A	2	H	2	45	46	15	9.05	572.34	75.39	94.47		5.53	47.76	15.9	1973.95	663.10	866.86	109.69
1171	A	2	H	2	50	51	15	9.10	578.38	76.01	93.49		6.51	49.09	13.8	1855.17	745.24	984.46	109.45
1171	A	2	H	2	55	56	15	9.15	584.42	76.80	93.32		6.68	52.26	19.2	2148.92	689.20	1320.93	122.28
1171	A	2	H	2	60	61	15	9.20	591.51	73.21	93.11		6.89	50.29	9.4	2366.27	618.71	1299.78	140.30
1171	A	2	H	2	65	66	15	9.25	593.83	75.71	92.68		7.32	50.06		2503.36	661.96	1371.93	158.77
1171	A	2	H	2	70	71	15	9.30	596.26	74.05	92.87		7.13	50.47		2857.28	733.38	1207.34	145.48
1171	A	2	H	2	75	76	15	9.35	598.90	70.84	92.48		7.52	48.91		2228.14	696.55	1154.45	140.04
1171	A	2	H	2	80	82	15	9.40	601.53	71.11	92.69		7.31	51.31	20.3	2257.06	620.19	1168.61	136.72
1171	A	2	H	2	85	87	15	9.45	603.43	70.18	91.16		8.84	52.68	18.7	2304.81	658.18	1200.22	139.04
1171	A	2	H	2	90	91	15	9.50	604.85	70.37	93.65		6.35	37.92					
1171	A	2	H	2	95	97	15	9.55	606.27	66.95	92.27		7.73	49.99		2492.73	673.39	1160.63	147.72
1171	A	2	H	2	100	101	15	9.60	608.73	73.47	93.10		6.90	50.09		2131.82	644.80	1107.43	124.97
1171	A	2	H	2	105	107	15	9.65	611.47	75.71	93.41		6.59	54.42		1965.03	671.79	1014.82	119.69
1171	A	2	H	2	110	112	15	9.70	614.02	75.18	93.16		6.84	53.64	23.6	2075.46	618.93	1110.58	119.53
1171	A	2	H	2	115	116	15	9.75	616.31	73.88	93.12		6.88	50.40	10.1	2083.59	636.90	1094.30	123.78
1171	A	2	H	2	120	121	15	9.80	618.60	75.24	92.81		7.19	53.27		2509.76	655.54	1244.96	136.36
1171	A	2	H	2	125	126	15	9.85	620.90	76.58	92.72		7.28	51.93		2392.24	588.10	1332.49	145.44
1171	A	2	H	2	130	131	15	9.90	623.25	74.99	93.40		6.60	56.24		2067.59	456.27	1333.80	126.43
1171	A	2	H	2	135	136	15	9.95	625.61	73.93	91.44		8.56	42.79	12.9	3415.37	736.14	1992.77	225.78
1171	A	2	H	2	140	141	15	10.00	627.96	73.23	90.62		9.38	48.04	8.6	3474.50	713.34	1899.21	230.20
1171	A	2	H	2	145	146	15	10.05	630.90	70.80	90.95		9.05	51.62		3271.51	624.78	1756.78	202.40

Site 1172A - Concentrations of the analysed proxies

Site	Hole	Core	Type	Section	Top [cm]	Bottom [cm]	Volume [cc]	Sample depth [mbsf]	Age [ka]	Lightness (L*)	Carbonate [%]	TOC [%]	Siliciclastics [%]	Coarse fraction [% > 63µm]	Chlorin [ng/g]	Aluminium [µg/g]	total Barium [µg/g]	Iron [µg/g]	Titanium [µg/g]
1172	A	1	H	1	3	4	15	0.03	2.11	49.42	84.14	0.234	15.86	32.33	70.6	8411.37	616.67	4976.23	520.88
1172	A	1	H	1	8	9	15	0.08	5.90	67.66	83.08	0.249	16.92	23.82	267.2	9443.03	671.47	5730.14	579.90
1172	A	1	H	1	13	14	15	0.13	9.70	61.33	80.18	0.271	19.82	30.02	204.0	10261.28	665.81	6156.31	623.82
1172	A	1	H	1	18	19	15	0.18	13.50	60.44	81.43	0.304	18.57	29.37	383.8	10563.47	683.12	6799.50	640.64
1172	A	1	H	1	23	24	15	0.23	17.29	59.69	79.98	0.306	20.02	40.19	251.1	12156.15	602.90	8428.84	803.71
1172	A	1	H	1	28	29	15	0.28	21.08	56.28	78.18	0.262	21.82	47.72	267.0				
1172	A	1	H	1	33	35	15	0.33	24.88	55.52	76.60	0.351	23.40	39.60	669.9	13351.03	621.47	7677.47	907.80
1172	A	1	H	1	38	39	15	0.38	29.97	53.93	73.69	0.436	26.31	40.42	958.8	15893.76	671.68	8421.78	1055.12
1172	A	1	H	1	43	44	15	0.43	35.94	56.27	80.27	0.314	19.73	47.84	1110.0	9969.62	604.04	5754.02	662.70
1172	A	1	H	1	48	49	15	0.48	41.90	59.92	80.56	0.359	19.44	35.19	303.8	10817.02	552.03	6604.32	714.88
1172	A	1	H	1	53	54	15	0.53	47.87	58.53	80.58	0.331	19.42	31.84	516.9	11898.57	583.18	6081.99	772.08
1172	A	1	H	1	58	60	15	0.58	53.82	60.36	79.33	0.416	20.67	32.20	584.9	11197.45	540.52	6353.45	733.38
1172	A	1	H	1	63	64	15	0.63	59.80	59.16	81.48	0.305	18.52	38.03	558.5	10739.88	577.45	6412.17	704.63
1172	A	1	H	1	68	70	15	0.68	65.76	58.52	78.99	0.342	21.01	47.61	976.5	12603.62	491.80	6608.89	828.48
1172	A	1	H	1	73	74	15	0.73	70.35	56.47	72.62	0.413	27.38	32.64	980.4	17182.92	559.15	8574.78	1149.29
1172	A	1	H	1	78	79	15	0.78	74.02	61.30	75.58	0.405	24.42	25.61	418.3	14779.28	560.80	7312.47	987.20
1172	A	1	H	1	83	84	15	0.83	77.70	61.84	80.54	0.343	19.46	29.83	1111.9				
1172	A	1	H	1	88	89	15	0.88	81.38	65.18	80.52	0.363	19.48	23.73	995.3	9930.99	562.45	5027.19	622.71
1172	A	1	H	1	93	94	15	0.93	84.88	60.51	80.11	0.444	19.89	27.65	1302.3	10464.69	456.87	5049.87	702.85
1172	A	1	H	1	98	99	15	0.98	88.38	61.97	84.44	0.352	15.56	25.15	1016.4	8168.70	524.40	4041.99	540.85
1172	A	1	H	1	103	104	15	1.03	91.89	61.62	82.53	0.253	17.47	33.25	400.3	10407.23	488.35	6417.49	663.72
1172	A	1	H	1	108	109	15	1.08	95.38	62.26	82.18	0.295	17.82	28.72	373.4	9347.11	589.87	5230.29	630.87
1172	A	1	H	1	113	115	15	1.13	98.89	62.14	83.23	0.244	16.77	27.53	333.5	8739.15	615.63	4951.26	534.90
1172	A	1	H	1	118	119	15	1.18	102.39	62.39	84.42	0.298	15.58	30.43	345.4	8006.97	607.25	4013.05	498.85
1172	A	1	H	1	123	124	15	1.23	105.90	62.37	85.13	0.287	14.87	30.86	421.4	8626.99	604.71	5329.93	541.78
1172	A	1	H	1	128	129	15	1.28	109.39	64.91	85.16	0.239	14.84	29.27	262.4	8377.67	623.69	5434.58	504.82
1172	A	1	H	1	133	134	15	1.33	113.19	65.12	85.48	0.206	14.52	28.58	395.8	7894.75	609.30	4198.64	484.39
1172	A	1	H	1	138	139	15	1.38	117.41	65.37	86.48	0.213	13.52	31.12	611.1	8535.93	637.20	4165.25	520.66
1172	A	1	H	1	143	144	15	1.43	121.81	65.51	85.61	0.202	14.39	27.80	603.4	9413.79	644.39	5735.60	562.50
1172	A	1	H	2	3	4	15	1.53	130.59	52.63	83.99	0.182	16.01	32.91	97.2	12353.35	565.80	7526.53	768.66
1172	A	1	H	2	8	9	15	1.58	134.54	60.63	82.85	0.252	17.15	35.04	309.8	9440.88	408.08	6317.34	590.59
1172	A	1	H	2	13	14	15	1.63	137.84	61.45	78.96	0.354	21.04	22.95	1054.6	12902.10	634.55	6320.93	832.02
1172	A	1	H	2	18	19	15	1.68	141.14	60.96	74.56	0.319	25.44	26.13	419.2	16762.56	590.45	8696.83	1091.48
1172	A	1	H	2	23	24	15	1.73	144.21	61.53	77.83	0.277	22.17	35.81	438.3	14357.05	543.25	7127.20	915.56
1172	A	1	H	2	28	29	15	1.78	147.12	60.23	78.56	0.347	21.44	36.15	978.6	13540.97	541.89	7243.42	875.91
1172	A	1	H	2	33	35	15	1.83	150.03	60.55	82.49	0.209	17.51		454.9	10305.83	489.06	5988.87	684.64
1172	A	1	H	2	38	39	15	1.88	152.94	60.33	80.64	0.374	19.36	35.71	1083.5	12391.85	592.62	7208.19	791.92

Site	Hole	Core	Type	Section	Top [cm]	Bottom [cm]	Volume [cc]	Sample depth [mbsf]	Age [ka]	Lightness (L*)	Carbonate [%]	TOC [%]	Siliciclastics [%]	Coarse fraction [% > 63µm]	Chlorin [ng/g]	Aluminium [µg/g]	total Barium [µg/g]	Iron [µg/g]	Titanium [µg/g]
1172	A	1	H	2	43	44	15	1.93	155.86	61.47	81.46	0.203	18.54	39.40	1015.4	11394.68	505.94	6065.96	729.46
1172	A	1	H	2	48	49	15	1.98	158.76	63.20	75.80	0.240	24.20	26.13	179.8	16072.97	591.04	8700.99	1025.29
1172	A	1	H	2	53	54	15	2.03	162.21	60.81	74.32	0.255	25.68	29.62	603.4	17367.12	673.61	9087.16	1113.96
1172	A	1	H	2	58	60	15	2.08	166.01	58.07	73.64	0.274	26.36	34.35	316.2	17177.31	602.77	10197.43	1163.46
1172	A	1	H	2	63	64	15	2.13	169.72	55.64	74.94	0.342	25.06	34.38	1619.2	17721.24	584.91	8220.57	1166.50
1172	A	1	H	2	68	69	15	2.18	172.98	57.00	76.46	0.278	23.54	32.07	383.7	14154.68	527.17	8515.84	964.67
1172	A	1	H	2	73	74	15	2.23	176.25	57.69	78.41	0.299	21.59	35.97	522.3	12655.45	543.27	7036.47	867.62
1172	A	1	H	2	78	79	15	2.28	179.52	57.15	77.08	0.265	22.92	35.14	432.3	14815.60	578.43	8047.71	1060.38
1172	A	1	H	2	83	84	15	2.33	182.79	59.78	74.18	0.222	25.82	28.59	193.5	17808.15	698.89	9869.16	1197.48
1172	A	1	H	2	88	89	15	2.38	186.06	63.42	83.19	0.162	16.81	30.42	96.4	10622.93	752.19	6742.03	676.36
1172	A	1	H	2	93	94	15	2.43	189.60	56.75	83.10	0.195	16.90	29.40	23.2	9689.78	735.45	5906.79	633.62
1172	A	1	H	2	98	99	15	2.48	194.27	58.53	80.11	0.216	19.89	37.06	69.2	12057.88	664.27	6785.76	841.00
1172	A	1	H	2	103	104	15	2.53	198.95	59.65	77.96	0.221	22.04	38.39	163.6	12871.49	665.63	7899.30	879.37
1172	A	1	H	2	108	109	15	2.58	203.61	64.05	80.30	0.235	19.70	34.84	45.0	11526.15	719.88	7020.09	765.15
1172	A	1	H	2	113	115	15	2.63	208.29	64.46	81.13	0.211	18.87	31.06	65.6	10200.71	701.19	7035.09	628.85
1172	A	1	H	2	118	119	15	2.68	212.96	62.21	79.78	0.199	20.22	35.01	15.3	12075.36	665.08	6704.60	776.74
1172	A	1	H	2	123	124	15	2.73	217.63	62.46	76.86	0.218	23.14	23.41	29.7	14749.96	616.54	9721.76	1012.67
1172	A	1	H	2	128	129	15	2.78	222.19	57.76	80.45	0.211	19.55	38.06	174.3	11532.92	587.16	6373.39	781.20
1172	A	1	H	2	133	134	15	2.83	226.66	58.74	71.77	0.204	28.23		87.6	21117.38	658.53	11706.95	1342.16
1172	A	1	H	2	138	139	15	2.88	231.26	61.32	73.93	0.212	26.07	22.27	193.0	15735.95	569.20	8011.99	1042.98
1172	A	1	H	2	143	144	15	2.93	236.06	62.77	80.19	0.200	19.81	19.97	509.2	13554.99	610.04	6588.54	847.73
1172	A	1	H	2	148	149	15	2.98	240.87		82.74	0.277	17.26	14.10	318.8	10854.77	596.49	5650.52	700.80
1172	A	1	H	3	3	4	15	3.03	245.67	62.48	85.96	0.273	14.04	16.68	238.3	7654.60	505.92	4590.36	478.41
1172	A	1	H	3	8	9	15	3.08	250.47	65.37	88.20	0.213	11.80	16.89	224.9	5999.55	454.86	3809.18	389.82
1172	A	1	H	3	13	14	15	3.13	255.28	66.58	87.11	0.253	12.89	23.06	351.2	6553.75	440.16	4247.47	417.52
1172	A	1	H	3	18	19	15	3.18	260.08	64.30	84.28	0.279	15.72	25.73	557.4	8272.36	421.77	4878.75	534.75
1172	A	1	H	3	23	24	15	3.23	264.88	63.13	83.12	0.244	16.88	22.23	478.1	10158.78	508.40	5144.11	647.81
1172	A	1	H	3	28	30	15	3.28	270.70	64.60	83.78	0.245	16.22	21.02	336.3	9815.20	607.83	5166.60	622.14
1172	A	1	H	3	33	34	15	3.33	277.21	65.49	84.46	0.227	15.54	20.16	389.2	9821.35	510.21	4991.70	604.11
1172	A	1	H	3	38	39	15	3.38	283.72	66.28	86.45	0.280	13.55	14.23	733.8	8667.27	529.35	4758.19	531.48
1172	A	1	H	3	43	44	15	3.43	290.24	64.32	85.75	0.282	14.25	18.42	465.8	7647.66	467.33	4036.05	466.46
1172	A	1	H	3	48	49	15	3.48	296.75	66.86	87.43	0.226	12.57	17.53	409.7	6925.88	477.43	3585.82	420.40
1172	A	1	H	3	53	54	15	3.53	303.26	66.27	87.74	0.240	12.26	16.00	556.9	7340.03	468.40	4036.52	447.60
1172	A	1	H	3	58	60	15	3.58	309.77	65.22	87.87	0.211	12.13	17.63	330.5	7157.70	453.91	3972.48	445.28
1172	A	1	H	3	63	64	15	3.63	316.29	64.54	87.31	0.211	12.69	16.74	435.9	8498.99	495.10	4566.84	509.91
1172	A	1	H	3	68	69	15	3.68	322.80	67.34	86.84	0.209	13.16	15.41	328.5	7721.14	516.86	4085.35	485.17
1172	A	1	H	3	73	74	15	3.73	326.10	65.09	86.54	0.176	13.46	20.58	81.9	8208.03	618.07	4384.75	487.24
1172	A	1	H	3	78	79	15	3.78	329.20	68.48	83.35	0.169	16.65	18.50	124.0	10533.33	672.79	6534.01	632.30
1172	A	1	H	3	83	84	15	3.83	333.53	67.98	83.43	0.126	16.57	30.10	41.9	9754.44	416.90	6798.41	604.68

Site	Hole	Core	Type	Section	Top [cm]	Bottom [cm]	Volume [cc]	Sample depth [mbsf]	Age [ka]	Lightness (L*)	Carbonate [%]	TOC [%]	Siliciclastics [%]	Coarse fraction [% > 63µm]	Chlorin [ng/g]	Aluminium [µg/g]	total Barium [µg/g]	Iron [µg/g]	Titanium [µg/g]
1172	A	1	H	3	88	89	15	3.88	336.73	59.66	83.69	0.164	16.31		167.7	9781.79	399.86	6565.64	622.24
1172	A	1	H	3	93	94	15	3.93	339.95	58.67	78.17	0.308	21.83	28.98	688.2	13980.98	526.12	7400.88	927.64
1172	A	1	H	3	98	99	15	3.98	341.62	61.07	82.14	0.255	17.86	33.30	794.9	11858.18	485.24	6300.21	771.39
1172	A	1	H	3	103	104	15	4.03	342.90	60.69	81.71	0.270	18.29	27.31	1198.3	12197.89	509.41	6024.46	778.51
1172	A	1	H	3	108	109	15	4.08	344.18	60.97	82.06	0.279	17.94	27.06	949.7	10075.64	412.79	5300.56	676.74
1172	A	1	H	3	113	115	15	4.13	345.46	60.74	77.15	0.294	22.85	23.72	1354.2	15556.64	450.87	7790.38	947.28
1172	A	1	H	3	118	119	15	4.18	346.74	61.28	76.98	0.290	23.02	21.08	1165.8	16294.94	487.56	7893.07	980.50
1172	A	1	H	3	123	124	15	4.23	348.02	63.29	74.63	0.224	25.37	18.47	409.6	17745.96	463.89	9749.95	1072.16
1172	A	1	H	3	128	129	15	4.28	349.30	60.33	77.33	0.238	22.67	25.29	857.5	15779.01	470.62	7331.57	971.27
1172	A	1	H	3	133	134	15	4.33	350.58	63.20				26.32					
1172	A	1	H	3	138	139	15	4.38	351.86	62.14	79.21	0.279	20.79	18.63	1114.2	13548.78	482.04	7274.93	848.42
1172	A	1	H	3	143	144	15	4.43	353.14	63.26	82.44	0.255	17.56	22.53	1014.9	10960.10	406.51	5385.71	716.59
1172	A	1	H	4	3	5	15	4.53	355.70	40.65	82.11	0.269	17.89	20.37	684.5	11531.55	454.86	6442.13	725.97
1172	A	1	H	4	8	10	15	4.58	356.97	64.10	85.60	0.222	14.40	15.21	534.1	9922.16	423.71	6272.12	617.56
1172	A	1	H	4	13	15	15	4.63	358.26	66.31	83.23	0.312	16.77	17.45	976.6	10455.66	420.41	5442.49	649.46
1172	A	1	H	4	18	20	15	4.68	359.58	66.55	84.28	0.321	15.72	15.49	754.8	8888.02	393.02	4592.60	549.08
1172	A	1	H	4	23	25	15	4.73	360.92	63.79	83.66	0.298	16.34	13.80		10388.61	444.61	5359.14	641.23
1172	A	1	H	4	28	30	15	4.78	362.26	64.69	82.00	0.274	18.00	14.95	743.9	11726.60	451.16	5900.59	716.64
1172	A	1	H	4	33	35	15	4.83	363.60	64.74	82.72	0.294	17.28	15.75	870.5	11138.27	453.58	5962.29	676.06
1172	A	1	H	4	38	40	15	4.88	364.94	66.25	83.38	0.241	16.62	15.38	851.7	10807.77	465.52	5694.65	644.66
1172	A	1	H	4	43	45	15	4.93	366.28	67.24	86.62	0.210	13.38	14.26	956.7	8069.81	458.21	4006.15	478.48
1172	A	1	H	4	48	50	15	4.98	367.62	66.55	87.83	0.154	12.17	13.94	1132.8	7649.88	483.44	3975.85	447.95
1172	A	1	H	4	53	55	15	5.03	368.96	66.03	88.78	0.152	11.22	12.12	879.0	7139.68	481.65	3827.32	409.75
1172	A	1	H	4	58	60	15	5.08	370.30	66.39	89.15	0.176	10.85	12.28	781.3	6619.08	459.00	3341.72	384.34
1172	A	1	H	4	63	65	15	5.13	371.63	66.78	85.80	0.223	14.20	8.21	1182.2	7901.46	527.04	4840.39	467.49
1172	A	1	H	4	68	70	15	5.18	372.98	68.00	87.36	0.254	12.64	11.77	470.7	6012.77	414.02	3085.14	348.81
1172	A	1	H	4	73	75	15	5.23	374.31	69.77	88.00	0.214	12.00	7.99	307.5	6015.43	433.21	3388.22	347.06
1172	A	1	H	4	78	80	15	5.28	375.65	68.34	86.80	0.222	13.20	8.25	325.9	7676.72	475.65	4164.63	450.21
1172	A	1	H	4	83	85	15	5.33	376.99	67.87	86.15	0.203	13.85	7.09	421.3	7878.06	502.60	4679.07	461.92
1172	A	1	H	4	88	90	15	5.38	378.33	70.34	86.40	0.268	13.60	8.34	1102.1	7943.53	475.63	3390.81	454.68
1172	A	1	H	4	93	95	15	5.43	380.14	71.85	88.45	0.179	11.55	7.49	421.9	6023.97	460.06	4131.47	352.80
1172	A	1	H	4	98	100	15	5.48	383.84	70.11	88.03	0.212	11.97	7.24	661.7	6284.08	470.48	2742.51	366.89
1172	A	1	H	4	103	105	15	5.53	387.55	71.43	88.03	0.310	11.97	7.27	131.8	5737.16	438.64	3081.06	334.39
1172	A	1	H	4	108	110	15	5.58	391.25	72.49	88.65	0.140	11.35	8.40	502.4	5247.43	419.26	2479.01	295.90
1172	A	1	H	4	113	115	15	5.63	394.96	72.58	89.29	0.090	10.71	10.04	134.3	5720.68	429.57	3304.90	314.53
1172	A	1	H	4	118	120	15	5.68	398.66	72.91	87.33	0.231	12.67	9.43	71.4	6191.97	469.30	3616.22	351.49
1172	A	1	H	5	3	5	15	5.73	401.95	73.95	86.44	0.132	13.56	10.05	47.2	8055.67	465.22	4195.15	461.71
1172	A	1	H	5	8	10	15	5.78	403.56	71.62	87.02	0.114	12.98	9.34	80.6	7913.67	447.32	3560.33	452.41
1172	A	1	H	5	13	15	15	5.83	405.17	69.41	85.80	0.186	14.20	9.33	119.0	8203.42	438.41	4731.76	459.56

Site	Hole	Core	Type	Section	Top [cm]	Bottom [cm]	Volume [cc]	Sample depth [mbsf]	Age [ka]	Lightness (L*)	Carbonate [%]	TOC [%]	Siliciclastics [%]	Coarse fraction [% > 63µm]	Chlorin [ng/g]	Aluminium [µg/g]	total Barium [µg/g]	Iron [µg/g]	Titanium [µg/g]
1172	A	1	H	5	18	20	15	5.88	406.78	68.75	84.94	0.208	15.06	8.32	240.1	8381.40	426.77	4451.35	483.22
1172	A	1	H	5	23	25	15	5.93	408.39	66.11	85.12	0.188	14.88	9.60	136.3	8715.39	449.15	4804.66	499.90
1172	A	1	H	5	28	30	15	5.98	409.99	68.48	86.18	0.149	13.82	8.02	268.1	8802.69	474.23	4293.88	495.55
1172	A	1	H	5	33	35	15	6.03	411.88	69.55	86.03	0.178	13.97	11.49	202.3	8122.50	489.74	4712.57	477.23
1172	A	1	H	5	38	40	15	6.08	414.83	69.08	86.73	0.167	13.27	12.27	453.8	8187.95	472.50	4260.02	477.26
1172	A	1	H	5	42	44	15	6.12	417.19	67.77	85.25	0.167	14.75	10.79	332.7	8394.46	496.37	5122.60	502.72
1172	A	1	H	CC	3	5	15	6.17	417.56		84.23	0.176	15.77	10.49	357.1	9401.20	515.52	5991.30	559.19
1172	A	1	H	CC	8	10	15	6.22	417.93		83.50	0.219	16.50	10.83	444.1	9777.99	518.26	5429.87	590.35
1172	A	2	H	1	3	5	15	6.33	418.74	57.07	87.68	0.129	12.32	9.54	249.9	6947.27	445.46	3718.84	391.56
1172	A	2	H	1	8	10	15	6.38	420.78	68.63	83.86	0.157	16.14	10.50	359.6	9668.69	477.74	5377.97	567.65
1172	A	2	H	1	13	15	15	6.43	423.31	68.31	85.97	0.117	14.03	12.96	270.2	8895.13	463.34	4862.72	521.64
1172	A	2	H	1	18	20	15	6.48	425.86	70.84	86.29	0.172	13.71	9.84		7745.85	437.00	4013.31	442.12
1172	A	2	H	1	23	25	15	6.53	427.06	66.70	84.55	0.155	15.45	8.80		9843.94	453.53	5128.87	573.91
1172	A	2	H	1	28	30	15	6.58	428.26	67.00	85.28	0.152	14.72	10.05	160.9	9052.15	480.92	5047.09	513.75
1172	A	2	H	1	33	35	15	6.63	429.47	66.86	74.19	0.177	25.81	12.77	395.2	18514.68	496.73	9628.13	1065.89
1172	A	2	H	1	38	40	15	6.68	430.67	66.04	77.76	0.165	22.24	16.45		15704.57	471.75	7800.79	941.28
1172	A	2	H	1	43	45	15	6.73	431.87	63.85	78.66	0.207	21.34	13.25	493.9	14108.43	469.53	7256.78	845.26
1172	A	2	H	1	48	50	15	6.78	433.07	64.83	82.91	0.166	13.75	11.55	376.1				
1172	A	2	H	1	53	55	15	6.83	434.23	67.72	79.49	0.182	20.51	12.98	658.5	12763.03	434.38	7737.69	802.26
1172	A	2	H	1	58	60	15	6.88	435.34	66.17	83.67	0.236	16.33	11.80	463.7	10396.91	460.65	5417.72	616.59
1172	A	2	H	1	63	65	15	6.93	436.46	66.46	83.85	0.169	16.15	13.20	488.1	10672.58	468.72	5632.86	639.02
1172	A	2	H	1	68	70	15	6.98	437.57	64.79	81.33	0.167	18.67	15.10	600.3	11978.49	451.39	6502.88	736.02
1172	A	2	H	1	73	75	15	7.03	438.69	64.51	81.56	0.215	18.44	15.25	707.2				
1172	A	2	H	1	78	80	15	7.08	439.80	67.44	83.74	0.162	16.26	17.36	270.8	10147.81	480.61	5505.09	637.40
1172	A	2	H	1	83	85	15	7.13	440.92	66.21	83.16	0.185	16.84	16.48	809.3	10448.84	468.33	5941.57	670.79
1172	A	2	H	1	88	90	15	7.18	442.03	63.04	82.21	0.126	17.79	18.41	1016.0	12477.07	451.47	5965.58	756.23
1172	A	2	H	1	93	95	15	7.23	443.15	63.33	78.48	0.163	21.52	32.00	1245.1	13944.30	405.09	8255.99	845.11
1172	A	2	H	1	98	100	15	7.28	444.26	63.05	77.63	0.171	22.37	17.33	668.3	15832.73	453.12	7701.59	950.31
1172	A	2	H	1	103	105	15	7.33	446.17	64.77	81.76	0.205	18.24	14.29	832.4	12384.21	508.53	5942.95	764.89
1172	A	2	H	1	108	110	15	7.38	448.63	69.28	86.55	0.178	13.45	10.45	379.0	7511.07	442.56	4332.78	458.24
1172	A	2	H	1	113	115	15	7.43	451.98	69.50	87.37	0.167	12.63	7.31	741.3	7820.52	414.25	3679.88	472.77
1172	A	2	H	1	118	120	15	7.48	458.66	69.31	86.69	0.167	13.31	14.00	522.0	8081.01	350.35	4483.35	480.69
1172	A	2	H	1	123	125	15	7.53	465.34	69.85	89.26	0.124	10.74	7.66	198.2	6160.03	355.70	3011.22	369.54
1172	A	2	H	1	128	130	15	7.58	471.84	71.21	89.66	0.105	10.34	7.96	304.0	5909.39	369.80	3153.29	351.69
1172	A	2	H	1	133	135	15	7.63	478.07	70.13	89.77	0.107	10.23	7.63	625.8	6245.49	342.38	2762.41	368.25
1172	A	2	H	1	138	140	15	7.68	484.31	69.21	89.90	0.106	10.10	7.89	579.8	6457.09	360.47	3913.19	377.80
1172	A	2	H	1	143	145	15	7.73	489.51	61.18	88.62	0.150	11.38	7.14	462.8	6805.65	365.18	4325.47	394.58
1172	A	2	H	2	3	4	15	7.83	492.06	66.27	89.33	0.152	10.67	6.06	745.9	6627.52	387.08	3368.48	384.32
1172	A	2	H	2	8	9	15	7.88	493.34	69.39	86.76	0.177	13.24	9.03	435.2	7542.82	370.35	4833.46	446.42

Site	Hole	Core	Type	Section	Top [cm]	Bottom [cm]	Volume [cc]	Sample depth [mbsf]	Age [ka]	Lightness (L*)	Carbonate [%]	TOC [%]	Siliciclastics [%]	Coarse fraction [% > 63µm]	Chlorin [ng/g]	Aluminium [µg/g]	total Barium [µg/g]	Iron [µg/g]	Titanium [µg/g]
1172	A	2	H	2	13	14	15	7.93	494.62	68.56	88.82	0.165	11.18	9.79	608.4	6918.64	426.83	4161.86	421.59
1172	A	2	H	2	18	19	15	7.98	495.89	69.29	89.00	0.175	11.00	7.94	795.8	6595.85	365.07	3170.53	392.79
1172	A	2	H	2	23	24	15	8.03	497.17	68.56	90.96	0.158	9.04	9.30	249.7	5145.19	401.33	2617.72	293.60
1172	A	2	H	2	28	29	15	8.08	498.45	69.55	88.93	0.189	11.07	8.19	423.4	6130.16	409.87	3515.20	314.65
1172	A	2	H	2	33	35	15	8.13	499.73	70.68	90.18	0.162	9.82	10.23	246.9	5585.02	440.31	2928.45	318.37
1172	A	2	H	2	38	39	15	8.18	501.00	71.19	89.22	0.243	10.78	9.91	281.2	5848.51	453.71	3755.90	324.44
1172	A	2	H	2	43	44	15	8.23	502.29	69.47	90.03	0.172	9.97	10.28	319.1	5485.85	435.16	3224.67	314.81
1172	A	2	H	2	48	49	15	8.28	503.56	69.75	90.06	0.189	9.94	11.10	390.1	5631.27	441.36	2952.00	330.05
1172	A	2	H	2	53	54	15	8.33	504.84	68.04	90.18	0.129	9.82	7.69	122.5	6296.90	493.05	3187.08	373.55
1172	A	2	H	2	58	59	15	8.38	506.11	67.46	89.58	0.157	10.42	10.67	213.5	6228.31	469.15	3080.98	367.43
1172	A	2	H	2	63	64	15	8.43	507.40	70.49	88.78	0.117	11.22	9.93	227.4	7132.27	480.84	4296.35	425.86
1172	A	2	H	2	68	69	15	8.48	508.67	70.86	87.77	0.162	12.23	12.33	138.0	6895.56	472.22	3995.65	411.75
1172	A	2	H	2	73	75	15	8.53	509.95	70.23	88.09	0.185	11.91	14.35	289.7	6822.64	467.11	4354.37	413.43
1172	A	2	H	2	78	79	15	8.58	511.23	70.88	88.08	0.126	11.92	12.26	178.6	7412.89	508.68	4687.22	444.31
1172	A	2	H	2	83	84	15	8.63	512.51	67.34	85.72	0.267	14.28	13.84	313.0	7154.14	503.26	3622.02	432.19
1172	A	2	H	2	88	89	15	8.68	513.78	67.93	85.30	0.299	14.70	10.62	356.8	7792.20	504.66	3789.71	453.24
1172	A	2	H	2	93	94	15	8.73	515.06	67.86	86.92	0.260	13.08	11.94	375.2	7146.32	518.78	3932.98	427.87
1172	A	2	H	2	98	99	15	8.78	516.32	67.65	87.70	0.169	12.30	12.34	468.9	7021.67	493.04	4043.09	419.46
1172	A	2	H	2	103	104	15	8.83	517.56	67.27	87.17	0.236	12.83	13.39	327.2	7243.17	476.89	3769.46	446.51
1172	A	2	H	2	108	109	15	8.88	518.79	68.60	88.22	0.244	11.78	11.10	453.4	6138.70	430.07	4395.99	369.83
1172	A	2	H	2	113	115	15	8.93	520.02	69.39	88.54	0.237	11.46	10.09	568.4	6487.07	405.32	3407.92	385.31
1172	A	2	H	2	118	119	15	8.98	521.25	69.92	88.50	0.291	11.50	11.44	516.3	5861.86	409.37	3310.96	343.84
1172	A	2	H	2	123	124	15	9.03	522.50	73.41	90.29	0.107	9.71	8.34	124.8	5650.64	438.38	3000.14	351.04
1172	A	2	H	2	128	129	15	9.08	524.38	71.92	90.19	0.106	9.81	8.95	273.6	5656.77	438.14	3197.21	348.08
1172	A	2	H	2	133	134	15	9.13	526.42	70.85	90.49	0.150	9.51	9.99	452.0	5513.97	431.77	3191.26	331.57
1172	A	2	H	2	138	139	15	9.18	528.45	70.59	89.98	0.190	10.02	10.49	592.5	5511.92	395.62	3045.53	330.49
1172	A	2	H	2	143	144	15	9.23	530.50	71.30	88.60	0.215	11.40	9.57	486.5	5305.23	384.73	2640.43	328.07
1172	A	2	H	2	148	149	15	9.28	532.55	67.08	89.25	0.225	10.75	10.28	336.3	5695.67	381.23	3168.35	353.48
1172	A	2	H	3	3	4	15	9.33	534.60	43.94	88.03	0.277	11.97	11.87	269.9	6539.13	405.46	3519.80	407.96
1172	A	2	H	3	8	9	15	9.38	536.03	70.68	87.51	0.246	12.49	12.48	248.1	6755.15	433.95	3992.94	418.60
1172	A	2	H	3	13	14	15	9.43	536.58	71.19	87.13	0.246	12.87	15.45					
1172	A	2	H	3	18	19	15	9.48	537.11	68.77	86.79	0.287	13.21	17.77	305.3	7458.84	468.36	4030.48	449.48
1172	A	2	H	3	23	24	15	9.53	537.66	68.09	86.09	0.285	13.91	18.85	395.5	7239.59	441.46	3415.65	449.83
1172	A	2	H	3	28	29	15	9.58	538.19	68.54	84.43	0.242	15.57	21.20	346.0				
1172	A	2	H	3	33	34	15	9.63	538.74	65.06	85.88	0.165	14.12	19.03	378.0	7725.47	492.73	4754.12	483.79
1172	A	2	H	3	38	40	15	9.68	539.28	65.05	84.68	0.206	15.32	24.39	393.8	5617.32	415.33	3590.08	310.48
1172	A	2	H	3	43	44	15	9.73	539.83	65.27	84.44	0.175	15.56	23.96	431.9	8642.99	525.17	5294.36	533.32
1172	A	2	H	3	48	49	15	9.78	540.37	63.96	84.46	0.229	15.54	29.46	418.0	8379.78	526.57	4760.70	518.85
1172	A	2	H	3	53	54	15	9.83	540.91	63.58	81.70	0.206	18.30	33.84	359.9	10348.24	535.08	6162.89	657.71

Site	Hole	Core	Type	Section	Top [cm]	Bottom [cm]	Volume [cc]	Sample depth [mbsf]	Age [ka]	Lightness (L*)	Carbonate [%]	TOC [%]	Siliciclastics [%]	Coarse fraction [% > 63µm]	Chlorin [ng/g]	Aluminium [µg/g]	total Barium [µg/g]	Iron [µg/g]	Titanium [µg/g]
1172	A	2	H	3	58	59	15	9.88	541.45	60.52	80.36	0.250	19.64	26.74	334.0	11825.64	562.55	7010.48	755.97
1172	A	2	H	3	63	64	15	9.93	542.00	62.84	79.03	0.312	20.97		997.9	13222.32	624.90	6643.36	825.22
1172	A	2	H	3	68	69	15	9.98	542.54	62.44	78.98	0.270	21.02	22.88	602.6	12825.21	620.54	6645.12	800.57
1172	A	2	H	3	73	74	15	10.03	544.70	62.85	79.58	0.254	20.42	26.49	871.5	12684.83	651.89	6445.30	804.12
1172	A	2	H	3	78	79	15	10.08	547.24	60.27	75.97	0.293	24.03	16.85	668.8	16187.34	765.80	8242.57	1019.12
1172	A	2	H	3	83	84	15	10.13	549.18	62.47	73.52	0.364	26.48	17.07	1440.5	17434.86	776.76	9042.56	1119.32
1172	A	2	H	3	88	89	15	10.18	551.11	59.75	73.24	0.31	26.76	17.89	1491.3	9767.92	680.93	7839.30	1105.32
1172	A	2	H	3	93	94	15	10.23	553.31	58.92	72.80	0.32	27.20	14.93	890.4	18555.03	742.20	9284.43	1174.47
1172	A	2	H	3	98	99	15	10.28	556.35	60.48	73.64	0.26	26.36	15.53	862.3	17341.51	714.21	9544.13	1108.70
1172	A	2	H	3	103	104	15	10.33	559.58	60.61	73.86	0.31	26.14	15.75	791.6	16846.40	683.14	8768.77	1082.54
1172	A	2	H	3	108	109	15	10.38	562.80	61.90	77.07	0.26	22.93	16.46	547.8	13871.36	654.52	7048.91	922.39
1172	A	2	H	3	113	115	15	10.43	566.52	62.78	78.24	0.27	21.76	21.01	719.8	13390.32	695.94	7390.79	876.67
1172	A	2	H	3	118	119	15	10.48	573.41	62.57	81.72	0.20	18.28	17.88	312.2	11087.40	625.32	5844.37	726.33
1172	A	2	H	3	123	124	15	10.53	581.00	62.70	81.46	0.20	18.54	17.08	237.8	11586.15	693.30	5681.11	756.71
1172	A	2	H	3	128	129	15	10.58	588.61	66.22	83.52	0.18	16.48	29.44	147.8				
1172	A	2	H	3	133	134	15	10.63	596.02	67.28	82.65	0.23	17.35	25.82	229.5	10523.55	694.30	5225.07	675.66
1172	A	2	H	3	138	139	15	10.68	602.39	65.66	82.09	0.09	17.91	30.96	45.3	10148.94	663.84	5728.61	643.18
1172	A	2	H	3	143	144	15	10.73	605.73	63.27	80.07	0.10	19.93	29.11	87.2	11477.12	591.99	7227.49	784.34

Site 1168A - Accumulation rates of analysed proxies

Site	Sample depth [mbsf]	Age [kyr]	SR [cm/kyr]	Bulk AR [g/cm²kyr]	AR Carbonate [g/cm²kyr]	AR TOC [g/cm²kyr]	AR Siliciclastics [g/cm²kyr]	AR coarse fraction [>63 µm, g/cm²kyr]	AR Chlorine [10⁻⁶g/cm²kyr]	AR Aluminium [10⁻³g/cm²kyr]	AR Iron [10⁻³g/cm²kyr]	AR Titanium [10⁻³g/cm²kyr]	AR excess Barium [10⁻³g/cm²kyr]
1168	0.05	7.81	2.490	2.052	1.659	0.006	0.393	0.602	0.82	26.056	16.669	1.688	1.179
1168	0.10	9.82	2.490	2.281	1.800	0.007	0.481	0.591	0.21	30.556	20.101	1.987	1.209
1168	0.15	11.83	2.490	1.809	1.364	0.005	0.446	0.435	0.54	29.605	23.564	2.041	0.806
1168	0.20	13.83	2.490	2.083	1.510	0.008	0.573	0.437	0.58	39.976	29.563	2.751	0.940
1168	0.25	15.84	2.490	2.223	1.548	0.010	0.675	0.403	1.63	29.199	17.391	2.054	0.461
1168	0.30	17.85	3.539	3.184	2.274	0.015	0.910	0.871	3.25	63.513	37.090	4.288	0.824
1168	0.35	18.67	6.112	5.080	3.478	0.027	1.602	1.516	6.34	116.457	62.275	6.711	2.133
1168	0.40	19.49	6.112	5.668	3.841	0.029	1.827	1.648	5.42	132.866	66.078	7.506	1.925
1168	0.45	20.30	6.112	5.441	3.720	0.028	1.721	1.587	7.28	134.722	63.407	7.989	2.475
1168	0.50	21.12	6.112	5.038	3.583	0.024	1.455	1.529	5.21	107.703	52.684	6.584	2.042
1168	0.55	21.94	2.298	1.922	1.356	0.010	0.566	0.637	2.29	44.797	20.924	2.760	0.457
1168	0.60	25.47	1.415	1.254	0.934	0.007	0.319	0.416	1.62	22.801	10.306	1.490	0.111
1168	0.75	36.08	1.415	1.442	1.256	0.003	0.186	0.186	0.16	12.778	8.616	0.759	0.515
1168	0.80	39.61	1.415	1.547	1.347	0.004	0.200	0.202	0.23	13.229	8.087	0.814	0.574
1168	0.85	43.14	1.415	1.615	1.402	0.004	0.213	0.121	0.80	14.799	8.708	0.956	0.588
1168	0.90	46.68	1.415	1.534	1.282	0.003	0.252	0.096	0.84	18.110	10.484	1.242	0.507
1168	0.95	50.21	1.225	1.318	1.074	0.004	0.244	0.169	1.89	25.403	14.276	1.768	0.389
1168	1.00	54.84	1.081	1.075	0.828	0.004	0.246	0.249	1.44	19.281	9.285	1.176	0.273
1168	1.05	59.46	1.081	1.038	0.765	0.004	0.273	0.196	0.86	21.706	11.211	1.337	0.234
1168	1.10	64.09	0.787	0.798	0.652	0.001	0.146	0.136	0.46	11.229	6.229	0.665	0.251
1168	1.15	72.16	0.619	0.653	0.549	0.001	0.104	0.120	0.38	7.676	4.066	0.451	0.149
1168	1.20	80.24	0.619	0.689	0.585	0.002	0.104	0.085	0.34	6.790	3.609	0.402	0.162
1168	1.25	88.31	0.619	0.646	0.568	0.001	0.078	0.051	0.15	4.678	2.436	0.268	0.279
1168	1.30	96.38	0.751	0.835	0.715	0.002	0.120	0.054	0.23	7.433	4.801	0.487	0.326
1168	1.35	101.62	0.955	1.011	0.819	0.002	0.193	0.110	0.52	13.000	7.218	0.819	0.262
1168	1.40	106.85	0.955	1.080	0.789	0.005	0.290	0.204	1.38	21.391	12.392	1.336	0.205
1168	1.50	117.32	0.955	0.947	0.677	0.005	0.271	0.150	1.36	21.229	11.267	1.164	0.262
1168	1.55	122.56	1.062	1.058	0.770	0.003	0.288	0.234	0.57	22.100	12.801	1.330	0.306
1168	1.60	126.74	1.196	1.165	0.854	0.003	0.311	0.232	0.90	24.064	13.240	1.438	0.324
1168	1.65	130.92	1.196	1.139	0.839	0.003	0.299	0.201	0.86	22.442	11.962	1.222	0.176
1168	1.70	135.10	0.414	0.452	0.356	0.001	0.096	0.047	0.24	6.574	3.442	0.422	0.092
1168	1.75	155.08	0.250	0.266	0.207	0.001	0.060	0.034	0.21	4.164	2.707	0.284	0.072
1168	1.80	175.05	0.345	0.363	0.277	0.001	0.086	0.046	0.38	5.763	3.169	0.378	0.066
1168	1.85	184.06	0.555	0.610	0.485	0.002	0.125	0.054	0.35	8.398	4.366	0.488	0.169
1168	1.90	193.07	0.606	0.688	0.508	0.002	0.179	0.128	0.59	13.928	7.369	0.832	0.163
1168	1.95	200.56	0.668	0.739	0.599	0.002	0.140	0.078	0.35	9.616	5.652	0.600	0.161
1168	2.00	208.05	0.668	0.725	0.519	0.002	0.206	0.109	0.55	15.834	7.714	0.848	0.177
1168	2.05	215.54	0.505	0.487	0.362	0.002	0.125	0.088	0.38	9.892	5.318	0.602	0.106
1168	2.10	227.87	0.406	0.408	0.300	0.001	0.108	0.075	0.35	8.634	4.535	0.514	0.103

Site	Sample depth [mbsf]	Age [kyr]	SR [cm/kyr]	Bulk AR [g/cm²kyr]	AR Carbonate [g/cm²kyr]	AR TOC [g/cm²kyr]	AR Siliciclastics [g/cm²kyr]	AR coarse fraction [>63 µm, g/cm²kyr]	AR Chlorine [10⁻³g/cm²kyr]	AR Aluminium [10⁻³g/cm²kyr]	AR Iron [10⁻³g/cm²kyr]	AR Titanium [10⁻³g/cm²kyr]	AR excess Barium [10⁻³g/cm²kyr]
1168	2.15	240.19	0.535	0.522	0.384	0.001	0.138	0.103	0.43	10.725	5.565	0.646	0.108
1168	2.20	246.56	0.785	0.813	0.618	0.003	0.195	0.056	0.58	15.107	8.100	0.910	0.173
1168	2.25	252.93	0.785	0.802	0.520	0.003	0.282	0.242	0.20	23.452	9.775	1.291	0.196
1168	2.30	259.30	0.785	0.796	0.565	0.003	0.231	0.132	0.63	18.610	9.132	1.136	0.152
1168	2.35	265.67	0.827	0.817	0.488	0.003	0.329	0.117	0.78	27.673	13.290	1.650	0.046
1168	2.40	271.39	0.875	0.849	0.517	0.004	0.333	0.123	0.81	26.752	14.698	1.624	0.044
1168	2.45	277.11	0.875	0.829	0.558	0.003	0.271	0.130	0.71	23.017	12.228	1.409	0.174
1168	2.50	282.82	0.875	0.885	0.732	0.002	0.154	0.127	0.43	11.479	6.002	0.672	0.245
1168	2.55	288.54	0.999	1.094	0.938	0.003	0.156	0.116	0.36	10.224	5.271	0.587	0.360
1168	2.60	292.83	1.165	1.261	1.123	0.001	0.138	0.099	0.42	9.526	5.095	0.542	0.541
1168	2.65	297.12	1.165	1.333	1.124	0.003	0.209	0.083	0.52	14.548	7.929	0.988	0.429
1168	2.70	301.42	1.165	1.218	1.009	0.002	0.208	0.160	0.52	14.857	8.003	0.879	0.258
1168	2.75	305.71	1.165	1.269	1.090	0.001	0.179	0.140	0.07	11.666	7.643	0.768	0.527
1168	2.80	310.00	1.178	1.299	1.055	0.003	0.244	0.149	0.92	17.562	9.377	1.053	0.296
1168	2.85	314.20	1.190	1.284	0.996	0.004	0.288	0.203	1.05	19.227	7.806	1.251	0.425
1168	2.90	318.40	1.190	1.235	1.014	0.003	0.221	0.199	0.62	14.965	7.926	0.900	0.333
1168	2.95	322.60	1.190	1.346	1.157	0.004	0.189	0.105	0.67	11.998	6.139	0.748	0.438
1168	3.00	326.80	1.190	1.374	1.235	0.002	0.139	0.095	0.26	9.021	4.657	0.501	0.546
1168	3.05	331.00	1.493	1.673	1.464	0.003	0.209	0.139	0.46	13.687	6.955	0.785	0.614
1168	3.10	333.50	2.000	2.247	1.933	0.005	0.314	0.172	0.76	21.245	11.349	1.252	0.931
1168	3.15	336.00	2.000	2.236	1.899	0.008	0.338	0.167	0.40	19.042	12.138	1.205	0.822
1168	3.20	338.50	2.000	2.225	1.731	0.010	0.494	0.150	1.33	34.751	18.824	2.409	0.732
1168	3.25	341.00	1.754	1.865	1.464	0.008	0.401	0.238	2.02	26.353	14.111	1.719	0.453
1168	3.30	344.20	1.563	1.704	1.315	0.006	0.389	0.169	0.96	27.603	13.684	1.565	0.292
1168	3.35	347.40	1.562	1.691	1.094	0.006	0.598	0.283	1.73	46.808	22.676	2.484	0.430
1168	3.40	350.60	1.562	1.719	1.124	0.005	0.595	0.306	0.64	48.886	23.724	2.606	0.688
1168	3.45	353.80	1.563	1.709	1.454	0.004	0.255	0.385	0.38	19.044	10.544	1.093	0.281
1168	3.50	357.00	1.563	1.831	1.588	0.003	0.243	0.543	0.35	16.511	9.304	1.013	0.481
1168	3.55	360.20	1.563	2.099	1.775	0.008	0.324	0.373	0.38	19.521	10.642	1.197	0.496
1168	3.60	363.40	1.562	1.945	1.671	0.004	0.274	0.507	0.49	15.212	8.865	0.898	0.422
1168	3.65	366.60	1.562	1.940	1.588	0.005	0.353	0.544	0.45	26.035	14.357	1.602	0.456
1168	3.70	369.80	1.563	1.700	1.445	0.004	0.255	0.472	0.22	16.877	9.137	1.029	0.387
1168	3.75	373.00	1.563	1.996	1.681	0.005	0.315	0.529	0.51	21.866	13.592	1.321	0.611
1168	3.80	376.20	1.563	1.981	1.539	0.005	0.443	0.520	0.79	23.577	17.340	1.407	0.295
1168	3.85	379.40	1.562	2.009	1.758	0.004	0.251	0.493	0.52	16.232	10.109	0.949	0.170
1168	3.90	382.60	1.562	1.964	1.657	0.006	0.307	0.928	0.68	21.792	12.995	1.297	0.317
1168	3.95	385.80	1.563	1.977	1.680	0.005	0.297	0.713	0.59	19.508	11.795	1.121	0.424
1168	4.00	389.00	1.563	2.071	1.804	0.005	0.267	1.068	0.36	14.158	11.967	0.832	0.250
1168	4.05	392.20	1.563	2.054	1.667	0.005	0.387	1.009	0.46	18.320	16.940	1.080	0.222
1168	4.10	395.40	1.563	1.889	1.618	0.005	0.271	0.601	0.66	18.682	14.385	1.082	0.304

Site	Sample depth [mbsf]	Age [kyr]	SR [cm/kyr]	Bulk AR [g/cm²kyr]	AR Carbonate [g/cm²kyr]	AR TOC [g/cm²kyr]	AR Siliciclastics [g/cm²kyr]	AR coarse fraction [>63 µm, g/cm²kyr]	AR Chlorine [10^{-6}g/cm²kyr]	AR Aluminium [10^{-3}g/cm²kyr]	AR Iron [10^{-3}g/cm²kyr]	AR Titanium [10^{-3}g/cm²kyr]	AR excess Barium [10^{-3}g/cm²kyr]
1168	4.15	398.60	1.563	1.932	1.557	0.005	0.375	0.455	0.44	25.894	15.439	1.538	0.496
1168	4.20	401.80	1.563	1.801	1.516	0.006	0.285	0.547	0.46	17.076	9.946	0.980	0.333
1168	4.25	405.00	1.841	1.920	1.598	0.008	0.322	0.487	0.52	20.018	12.916	1.173	0.384
1168	4.30	407.23	2.241	2.475	1.884	0.008	0.591	0.505	0.87	43.295	20.723	1.813	0.678
1168	4.35	409.46	2.242	2.464	2.074	0.006	0.389	0.506	0.42	29.732	16.087	1.675	1.142
1168	4.40	411.69	2.241	2.602	2.139	0.007	0.463	0.531	0.85	32.674	18.844	1.858	0.869
1168	4.50	416.15	2.241	2.494	1.989	0.009	0.505	0.494	0.65	38.365	20.480	2.236	1.372
1168	4.55	418.39	2.242	2.464	1.953	0.007	0.511	0.503	0.62	37.746	19.842	2.192	1.111
1168	4.60	420.62	2.242	2.510	1.972	0.007	0.537	0.459	0.26	40.185	19.461	2.361	1.274
1168	4.65	422.85	2.241	2.540	2.026	0.007	0.514	0.553	0.63	38.853	19.293	2.290	1.168
1168	4.70	425.08	2.241	2.411	1.696	0.006	0.715	0.344	0.18	47.433	26.222	3.037	1.041
1168	4.75	427.31	2.242	2.374	1.669	0.007	0.706	0.443	0.81	57.698	32.599	3.567	0.894
1168	4.80	429.54	2.242	2.319	1.464	0.007	0.854	0.486	0.84	71.104	34.210	4.342	0.610
1168	4.85	431.77	2.241	2.324	1.449	0.009	0.875	0.618	1.94	73.880	34.412	4.492	0.833
1168	4.90	434.00	1.577	1.709	1.012	0.008	0.697	0.510	1.23	56.784	29.743	3.463	0.637
1168	4.95	438.11	1.216	1.231	0.791	0.005	0.440	0.393	1.07	35.732	17.977	2.224	0.518
1168	5.00	442.22	1.216	1.280	0.863	0.004	0.417	0.456	0.78	30.034	21.627	1.941	0.540
1168	5.05	446.33	1.216	1.337	0.901	0.005	0.435	0.370	0.51	33.583	16.652	2.147	0.504
1168	5.10	450.44	1.216	1.346	1.121	0.003	0.225	0.243	0.13	13.959	8.034	0.823	0.615
1168	5.15	454.56	1.216	1.423	1.143	0.004	0.280	0.128	0.45	17.539	13.068	1.061	0.359
1168	5.20	458.67	1.216	1.412	1.207	0.004	0.205	0.228	0.46	12.127	6.044	0.709	0.609
1168	5.25	462.78	1.216	1.442	1.197	0.003	0.245	0.278	0.34	10.359	7.862	0.602	0.440
1168	5.30	466.89	1.216	1.377	1.148	0.004	0.228	0.200	0.84	14.909	11.035	0.878	0.463
1168	5.35	471.00	1.328	1.531	1.275	0.004	0.256	0.253	0.63	18.663	9.925	1.118	0.413
1168	5.40	474.42	1.463	1.610	1.364	0.005	0.247	0.240	0.46	17.686	9.626	1.023	0.406
1168	5.45	477.83	1.463	1.699	1.448	0.005	0.251	0.215	0.53	18.181	10.332	1.056	0.776
1168	5.50	481.25	1.463	1.779	1.484	0.003	0.295	0.284	0.15	21.044	11.099	1.425	1.025
1168	5.55	484.67	1.463	1.717	1.442	0.004	0.275	0.276	0.60	21.253	12.089	1.296	0.651
1168	5.60	488.08	1.463	1.634	1.298	0.005	0.336	0.230	0.75	26.809	14.357	1.607	0.540
1168	5.65	491.50	1.463	1.656	1.352	0.004	0.304	0.248	0.38	24.142	12.078	1.497	0.487
1168	5.70	494.92	1.463	1.701	1.400	0.004	0.301	0.268	0.28	24.373	13.030	1.507	0.494
1168	5.75	498.33	1.463	1.695	1.410	0.004	0.285	0.237	0.32	23.022	12.011	1.421	0.595
1168	5.80	501.75	1.463	1.705	1.365	0.005	0.340	0.259	0.31	23.635	12.991	1.421	0.607
1168	5.85	505.17	1.463	1.661	1.369	0.003	0.292	0.252	0.41	23.066	11.741	1.398	0.675
1168	5.90	508.58	1.463	1.671	1.228	0.008	0.442	0.339	0.00	27.052	15.272	1.459	0.541
1168	5.95	512.00	1.068	1.188	0.921	0.005	0.267	0.210	0.77	18.121	10.303	1.065	0.381
1168	6.00	517.95	0.841	1.059	0.860	0.003	0.199	0.251	0.58	14.568	7.630	0.857	0.356
1168	6.05	523.90	0.841	1.028	0.818	0.003	0.210	0.188	0.32	13.124	7.229	0.746	0.336
1168	6.10	529.84	0.841	0.952	0.762	0.002	0.190	0.178	0.47	14.042	7.619	0.841	0.306
1168	6.15	535.79	0.841	0.932	0.746	0.002	0.186	0.168	0.30	14.968	7.218	0.955	0.260

Site	Sample depth [mbsf]	Age [kyr]	SR [cm/kyr]	Bulk AR [g/cm²kyr]	AR Carbonate [g/cm²kyr]	AR TOC [g/cm²kyr]	AR Siliciclastics [g/cm²kyr]	AR coarse fraction [>63 µm, g/cm²kyr]	AR Chlorine [10⁻³g/cm²kyr]	AR Aluminium [10⁻³g/cm²kyr]	AR Iron [10⁻³g/cm²kyr]	AR Titanium [10⁻³g/cm²kyr]	AR excess Barium [10⁻³g/cm²kyr]
1168	6.20	541.74	0.841	0.942	0.763	0.003	0.179	0.134	0.23	14.025	7.541	0.864	0.315
1168	6.25	547.68	0.841	0.932	0.751	0.002	0.181	0.137	0.22	11.095	6.784	0.666	0.406
1168	6.30	553.63	0.841	0.991	0.841	0.002	0.150	0.179	0.20	10.809	5.742	0.628	0.363
1168	6.35	559.58	0.841	1.023	0.892	0.002	0.131	0.149	0.20	9.247	4.880	0.544	0.400
1168	6.40	565.53	0.841	1.005	0.875	0.002	0.130	0.142	0.17	9.181	5.163	0.523	0.445
1168	6.45	571.47	0.841	0.969	0.831	0.002	0.138	0.155	0.24	9.861	4.998	0.571	0.424
1168	6.50	577.42	0.841	0.963	0.820	0.002	0.144	0.134	0.12	9.834	5.401	0.579	0.393
1168	6.55	583.37	0.841	0.946	0.818	0.002	0.128	0.130	0.32	10.963	5.542	0.640	0.331
1168	6.60	589.32	0.841	1.005	0.841	0.002	0.164	0.139	0.33	11.313	6.139	0.659	0.317
1168	6.65	595.26	0.841	0.992	0.851	0.002	0.141	0.112	0.30	10.366	5.088	0.591	0.355
1168	6.70	601.21	0.841	0.991	0.829	0.002	0.162	0.102	0.31	11.388	5.810	0.643	0.440
1168	6.75	607.16	0.841	1.043	0.851	0.003	0.192	0.166	0.21	14.461	7.799	0.825	0.413
1168	6.80	613.11	0.841	1.059	0.843	0.003	0.216	0.163	0.38	15.381	7.937	0.976	0.305
1168	6.85	619.05	0.841	1.075	0.852	0.003	0.224	0.132	0.26	16.141	7.932	1.150	0.458
1168	6.90	625.00	0.966	1.096	0.879	0.003	0.217	0.195	0.41	14.502	8.308	1.053	0.493
1168	6.95	629.41	1.134	1.248	1.009	0.003	0.239	0.195	0.35	15.257	8.217	1.051	0.659
1168	7.02	635.58	1.134	1.323	1.096	0.003	0.226	0.235	0.21	13.248	7.602	0.922	0.650
1168	7.07	639.99	1.134	1.268	1.069	0.003	0.199	0.297	0.17	11.506	9.279	0.779	0.541
1168	7.12	644.40	1.134	1.268	1.087	0.002	0.181	0.283	0.15	12.380	6.583	0.828	0.616
1168	7.17	648.81	1.134	1.268				0.214					
1168	7.22	653.22	1.134	1.268	0.929	0.004	0.339	0.216	0.37	24.138	12.152	1.649	0.670
1168	7.30	660.27	1.134	1.214	0.864	0.002	0.349	0.211	0.18	28.060	14.719	1.709	0.648
1168	7.35	664.68	1.134	1.178	0.831	0.003	0.347	0.162	0.36				
1168	7.40	669.09	1.134	1.136	0.764	0.004	0.372	0.157	0.99	29.113	15.253	1.764	0.428
1168	7.45	673.50	1.134	1.214	0.900	0.004	0.314	0.228	0.60	24.985	13.743	1.558	0.473
1168	7.50	677.91	1.134	1.080	0.756	0.003	0.323	0.189	0.46	24.213	12.814	1.494	0.456
1168	7.55	682.32	1.134	1.128	0.813	0.003	0.315	0.194	0.23	25.270	13.179	1.550	0.533
1168	7.60	686.73	1.134	1.126	0.827	0.003	0.300	0.218	0.39	23.439	12.622	1.441	0.475
1168	7.65	691.14	1.134	1.013	0.721	0.003	0.291	0.190	0.44	16.817	8.464	1.019	0.328
1168	7.70	695.55	1.134	1.079	0.867	0.002	0.212	0.191	0.20	13.687	7.004	0.832	0.433
1168	7.75	699.96	1.134	1.187	0.843	0.004	0.344	0.230	0.68	26.963	14.799	1.645	0.444
1168	7.80	704.36	1.134	0.988	0.720	0.003	0.268	0.156	0.64	19.167	9.934	1.256	0.316
1168	7.85	708.77	1.134	1.187	0.844	0.003	0.343	0.203	0.45	26.987	14.064	1.650	0.555
1168	7.90	713.18	1.134	1.176	0.893	0.003	0.283	0.195	0.30	19.924	10.088	1.435	0.779
1168	7.95	717.59	1.134	1.220	0.900	0.003	0.320	0.184	0.18	20.028	10.478	1.327	0.874
1168	8.00	722.00	1.107	1.139	0.962	0.002	0.177	0.153	0.19	12.957	6.826	0.778	0.476
1168	8.05	726.63	1.081	1.218	1.025	0.003	0.193	0.174	0.24	19.245	10.575	1.146	0.678
1168	8.10	731.25	1.081	1.051	0.790	0.003	0.262	0.180	0.25	19.609	10.224	1.292	0.549
1168	8.15	735.88	1.081	1.097				0.134	0.23				
1168	8.20	740.50	1.081	1.216	1.021	0.002	0.195	0.144	0.08	13.332	6.852	0.909	0.791

Site	Sample depth [mbsf]	Age [kyr]	SR [cm/kyr]	Bulk AR [g/cm²kyr]	AR Carbonate [g/cm²kyr]	AR TOC [g/cm²kyr]	AR Siliciclastics [g/cm²kyr]	AR coarse fraction [>63 µm, g/cm²kyr]	AR Chlorine [10⁻³g/cm²kyr]	AR Aluminium [10⁻³g/cm²kyr]	AR Iron [10⁻³g/cm²kyr]	AR Titanium [10⁻³g/cm²kyr]	AR excess Barium [10⁻³g/cm²kyr]
1168	8.25	745.13	1.081	1.245	1.075	0.004	0.169	0.167	0.17	11.763	6.333	0.702	0.460
1168	8.30	749.75	1.081	1.038	0.807	0.003	0.231	0.370	0.28	17.173	9.268	1.132	0.485
1168	8.35	754.38	1.081	1.065	0.893	0.003	0.171	0.193	0.44	18.523	10.476	1.158	0.394
1168	8.40	759.00	1.081	1.026	0.735	0.003	0.292	0.175	0.43	24.877	12.697	1.517	0.344
1168	8.45	763.63	1.081	0.985	0.726	0.003	0.259	0.181	0.42	21.085	11.580	1.326	0.389
1168	8.50	768.25	1.081	1.035	0.744	0.003	0.291	0.158	0.37	31.196	14.328	1.958	0.379
1168	8.55	772.88	1.081	1.163	0.980	0.003	0.183	0.180	0.11	13.589	6.726	0.912	0.699
1168	8.60	777.50	1.081	1.219	1.061	0.003	0.159	0.131	0.20	12.714	6.340	0.811	0.721
1168	8.65	782.13	1.081	1.139	1.000	0.002	0.139	0.206	0.07	11.153	5.483	0.701	0.662
1168	8.70	786.75	1.089	1.293	1.099	0.002	0.194	0.466	0.05	12.933	8.493	0.858	0.424
1168	8.80	795.90	1.093	1.206	0.938	0.004	0.268	0.205	0.25	19.738	10.660	1.371	0.476
1168	8.85	800.47	1.106	1.119	0.872	0.002	0.247	0.201	0.23	19.682	10.273	1.338	0.362
1168	8.90	804.94	1.118	1.226	0.882	0.003	0.344	0.200	0.36	27.486	13.103	1.929	0.336
1168	8.95	809.41	1.118	1.177	0.681	0.004	0.495	0.152	1.15	39.324	17.815	2.711	0.313
1168	9.00	813.88	1.118	1.254	0.716	0.005	0.538	0.167	1.07	45.217	18.621	2.951	0.433
1168	9.05	818.35	1.118	1.186	0.732	0.004	0.454	0.162	0.61	37.330	15.586	2.562	0.550
1168	9.10	822.82	1.118	1.215	0.964	0.002	0.251	0.265	0.17	14.898	12.657	1.019	0.659
1168	9.15	827.29	1.118	1.205	0.994	0.002	0.210	0.213	0.17	15.668	8.496	1.055	0.693
1168	9.20	831.77	1.118	1.232	0.933	0.003	0.299	0.182	0.38	23.611	11.833	1.588	0.727
1168	9.25	836.24	1.118	1.261	1.107	0.002	0.154	0.266	0.13	14.448	7.370	0.960	0.639
1168	9.30	840.71	1.118	1.291				0.350					
1168	9.35	845.18	1.118	1.249	1.041	0.003	0.208	0.242	0.44	15.302	7.629	1.073	0.658
1168	9.40	849.65	1.118	1.235	0.999	0.003	0.236	0.203	0.10	15.173	7.881	1.124	0.520
1168	9.45	854.12	1.118	1.332	1.057	0.003	0.275	0.212	0.16	19.908	10.736	1.550	0.505
1168	9.50	858.59	1.118	1.221	0.919	0.003	0.303	0.224	0.43	23.736	12.067	1.782	0.561
1168	9.55	863.06	1.118	1.195	0.938	0.003	0.257	0.218	0.38	20.702	10.540	1.456	0.632
1168	9.60	867.53	1.118	1.275	1.048	0.004	0.227	0.225	0.33	15.544	8.669	1.079	0.717
1168	9.65	872.00	1.079	1.271	1.030	0.002	0.241	0.167	0.16	14.177	7.665	0.972	0.527
1168	9.70	876.80	1.042	1.189	0.961	0.002	0.228	0.129	0.15	15.730	8.096	1.086	0.666
1168	9.75	881.60	1.042	1.196	0.991	0.002	0.205	0.177	0.08	13.902	8.352	0.942	0.690
1168	9.80	886.40	1.042	1.193	0.994	0.001	0.200	0.243	0.10	13.372	7.456	0.988	0.461
1168	9.85	891.20	1.042	1.181	0.991	0.002	0.190	0.242	0.12	13.189	6.738	0.941	0.591
1168	9.90	896.00	1.042	1.203				0.164					
1168	9.95	900.80	1.042	1.196	0.927	0.003	0.269	0.154	0.11	18.530	11.987	1.405	0.570
1168	10.00	905.60	1.042	1.254	0.980	0.003	0.274	0.135	0.13	18.948	9.977	1.410	0.613
1168	10.05	910.40	1.042	1.238	0.945	0.003	0.293	0.167	0.19	20.331	10.998	1.491	0.677
1168	10.10	915.20	1.042	1.146	0.893	0.002	0.254	0.124	0.16	18.613	10.013	1.420	0.619
1168	10.15	920.00	1.042	1.150	0.855	0.004	0.295	0.143	0.36	23.358	11.764	1.721	0.740
1168	10.20	924.80	1.042	1.092	0.787	0.004	0.305	0.225	0.29	22.307	13.479	1.664	0.621
1168	10.25	929.60	1.042	1.135	0.843	0.004	0.292	0.387	0.53	21.418	11.570	1.618	0.502

Site 1170A - Accumulation rates of analysed proxies

Site	Sample depth [mbsf]	Age [kyr]	SR [cm/kyr]	Bulk AR [g/cm²kyr]	AR Carbonate [g/cm²kyr]	AR TOC [g/cm²kyr]	AR Siliciclastics [g/cm²kyr]	AR coarse fraction [>63 µm, g/cm²kyr]	AR Chlorine [10⁻⁶g/cm²kyr]	AR Aluminium [10⁻³g/cm²kyr]	AR Iron [10⁻³g/cm²kyr]	AR Titanium [10⁻³g/cm²kyr]	AR excess Barium [10⁻³g/cm²kyr]
1170	0.00	0.21	2.107	1.896	1.754		0.142	0.520	0.14	5.934	3.101	0.299	1.388
1170	0.05	2.58	2.107	1.797	1.655		0.142	0.453		6.160	3.231	0.322	1.383
1170	0.10	4.96	2.108	1.941	1.781		0.160	0.488		6.409	3.342	0.339	1.425
1170	0.15	7.33	2.107	2.013	1.836		0.177	0.596		7.895	4.281	0.401	1.521
1170	0.20	9.70	1.551	1.507	1.364		0.144	0.449		6.972	3.909	0.389	1.165
1170	0.25	13.78	1.227	1.152	1.027		0.125	0.364	0.01	6.886	4.109	0.403	0.914
1170	0.30	17.85	1.874	1.839	1.632		0.208	0.677	0.02	10.863	6.619	0.658	1.441
1170	0.35	19.11	3.964	3.848	3.345		0.503	1.499	0.06	31.552	19.141	1.900	3.283
1170	0.40	20.37	3.964	3.742	3.175		0.567	1.296	0.05	35.959	24.379	2.165	3.791
1170	0.45	21.64	3.962	3.692	3.016		0.677		0.05	38.943	24.658	2.805	3.926
1170	0.50	22.90	3.964	3.655	3.059		0.596	1.585	0.12	30.502	15.913	2.724	3.219
1170	0.55	24.16	3.964	3.448	2.980		0.468	1.544	0.08	28.846	16.524	1.809	3.164
1170	0.60	25.42	1.854	1.770	1.533		0.238	0.707		14.864	7.751	0.872	1.523
1170	0.65	29.55	1.210	1.162	1.024		0.138	0.417		8.563	4.981	0.526	0.879
1170	0.70	33.68	1.210	1.166	1.022		0.144	0.425		7.859	6.828	0.459	0.769
1170	0.75	37.82	1.210	1.204	1.138		0.066	0.471		8.159	6.281	0.496	0.852
1170	0.80	41.95	1.210	1.078	0.959		0.119	0.420	0.04	7.110	3.874	0.421	0.677
1170	0.85	46.08	1.210	1.148	0.995		0.154	0.440		6.878	5.285	0.429	0.662
1170	0.90	50.21	1.268	1.140	1.007		0.133	0.426		7.901	4.145	0.479	0.710
1170	0.95	53.96	1.332	1.230	1.090		0.141	0.484		8.235	4.262	0.508	0.717
1170	1.00	57.72	1.332	1.266	1.116		0.150	0.420		9.974	4.922	0.581	0.710
1170	1.05	61.47	1.332	1.242	1.075		0.167	0.384	0.16	11.068	6.299	0.657	0.838
1170	1.10	65.22	1.642	1.556	1.318		0.238	0.419		15.223	9.766	0.890	1.075
1170	1.15	67.56	2.138	2.055	1.816		0.239	0.453		15.924	8.490	0.932	1.253
1170	1.20	69.90	2.138	2.008	1.802		0.206	0.554		12.900	7.427	0.753	1.118
1170	1.25	72.24	2.139	2.055	1.849		0.206	0.667		11.236	6.646	0.633	1.121
1170	1.30	74.57	2.138	1.982	1.810		0.172	0.651	0.03	9.163	5.770	0.520	1.021
1170	1.35	76.91	2.138	1.998	1.843		0.154	0.660		7.799	4.936	0.452	1.093
1170	1.40	79.25	1.306	1.212	1.122		0.091	0.405		4.569	2.349	0.249	0.664
1170	1.45	84.57	0.940	0.875	0.814		0.061	0.294		2.997	1.613	0.164	0.480
1170	1.46	85.63	0.940	0.869	0.808		0.061	0.291	0.02				
1170	1.51	90.95	1.272	1.176	1.091		0.085	0.445		4.484	2.152	0.253	0.638
1170	1.56	93.49	1.966	1.818	1.701		0.117	0.658		6.209	2.882	0.340	1.091
1170	1.61	96.04	1.966	1.817	1.699		0.119	0.663	0.03	6.481	3.247	0.353	0.991
1170	1.70	100.62	1.966	1.801	1.603		0.197	0.438	0.02				
1170	1.75	103.16	1.966	1.829	1.716		0.113	0.467		7.463	3.854	0.385	1.481
1170	1.80	105.70	1.966	1.966	1.800		0.165	0.576		8.600	4.274	0.488	1.703
1170	1.85	108.25	1.966	1.825	1.681		0.143	0.605		7.056	3.777	0.401	1.143
1170	1.90	110.79	0.699	0.691	0.646		0.045	0.208		2.608	1.185	0.143	0.463

Site	Sample depth [mbsf]	Age [kyr]	SR [cm/kyr]	Bulk AR [g/cm²kyr]	AR Carbonate [g/cm²kyr]	AR TOC [g/cm²kyr]	AR Siliciclastics [g/cm²kyr]	AR coarse fraction [>63 µm, g/cm²kyr]	AR Chlorine [10^{-6}g/cm²kyr]	AR Aluminium [10^{-3}g/cm²kyr]	AR Iron [10^{-3}g/cm²kyr]	AR Titanium [10^{-3}g/cm²kyr]	AR excess Barium [10^{-3}g/cm²kyr]
1170	1.95	122.56	0.671	0.648	0.601		0.047	0.197	0.01	2.160	1.022	0.113	0.430
1170	2.00	125.70	1.595	1.570	1.409		0.160	0.502	0.01	9.251	4.722	0.518	1.062
1170	2.05	128.83	1.595	1.548	1.394		0.154	0.442	0.01	9.164	4.440	0.537	0.937
1170	2.10	131.97	1.595	1.641	1.476		0.165	0.456		9.967	4.840	0.594	1.075
1170	2.15	135.10	2.480	2.525	2.221		0.304	0.634		20.180	11.506	1.220	2.166
1170	2.20	136.00	5.571	5.347	4.791		0.556	1.680		36.739	20.217	2.240	4.275
1170	2.25	136.90	5.571	5.388	4.715		0.673	1.294	0.20	50.690	24.254	2.866	4.572
1170	2.30	137.79	5.571	5.625	4.881		0.743	1.437		47.139	23.650	2.770	3.877
1170	2.35	138.69	5.571	5.246	4.572		0.673	1.362		47.141	25.353	2.781	4.045
1170	2.40	139.59	5.571	5.340	4.702		0.639	1.426		48.360	22.972	2.814	4.154
1170	2.45	140.49	5.571	5.354	4.723		0.632	1.549		45.843	23.133	2.650	3.843
1170	2.50	141.38	5.571	5.347	4.692		0.655	2.009	0.48	37.646	31.257	2.180	3.478
1170	2.55	142.28	2.309	2.185	1.913		0.272	0.607		17.102	11.916	0.979	1.440
1170	2.60	145.71	1.456	1.373	1.210		0.163	0.424		11.346	5.646	0.672	0.966
1170	2.65	149.15	1.456	1.389	1.211		0.178	0.323		11.656	6.362	0.663	1.018
1170	2.70	152.58	1.885	1.830	1.613		0.217	0.619		15.318	7.784	0.766	1.344
1170	2.75	154.45	2.670	2.446	2.115		0.331	0.693	0.49	22.206	16.516	1.275	1.911
1170	2.80	156.33	2.670	2.481	2.121		0.360	0.848		23.948	13.120	1.531	2.279
1170	2.85	158.20	2.670	2.446	2.088		0.358	0.746		24.906	11.304	1.442	2.046
1170	2.90	160.07	2.670	2.362	2.009		0.352	0.880		23.595	11.306	1.498	2.137
1170	2.95	161.94	2.671	2.502	2.122		0.380	0.871		27.268	12.538	1.710	2.287
1170	3.00	163.82	2.670	2.488	2.057		0.432	0.846	0.05	31.807	14.756	1.925	2.192
1170	3.05	165.69	2.670	2.417	2.054		0.363	0.827	0.04	22.805	13.266	1.443	2.125
1170	3.10	167.56	2.670	2.440	2.090		0.350	0.885		23.124	11.596	1.360	2.034
1170	3.20	171.31	2.670	2.420	2.069		0.350	0.868	0.05	23.164	11.485	1.436	2.015
1170	3.25	173.18	2.670	2.459	2.088		0.371	0.889		23.852	11.894	1.498	2.089
1170	3.30	175.05	2.164	1.953	1.641		0.312	0.712		22.009	10.609	1.335	1.993
1170	3.35	177.80	1.818	1.756	1.474		0.283	0.504	0.09	18.278	11.863	1.204	1.574
1170	3.40	180.55	1.818	1.679	1.419		0.260	0.467	0.03	17.305	9.374	1.081	1.718
1170	3.45	183.30	1.926	1.687	1.427		0.260	0.500	0.14	18.101	8.923	1.166	1.765
1170	3.50	185.74	2.047	1.840	1.529		0.311	0.603	0.04	20.069	10.986	1.233	1.933
1170	3.55	188.19	2.047	1.805	1.553		0.253	0.617		15.489	8.022	0.939	1.795
1170	3.60	190.63	2.047	1.788	1.560		0.228	0.591		13.649	7.509	0.775	1.648
1170	3.65	193.07	1.904	1.629	1.453		0.176	0.608		9.947	4.384	0.550	1.504
1170	3.70	195.88	1.780	1.665	1.506		0.159	0.631		8.412	4.512	0.466	1.446
1170	3.75	198.69	1.780	1.722	1.560		0.162	0.599	0.02	8.636	3.823	0.471	1.539
1170	3.80	201.50	1.780	1.702	1.537		0.165	0.578	0.01	7.910	3.963	0.439	1.456
1170	3.85	204.31	1.780	1.620	1.459		0.161	0.488		7.531	3.858	0.419	1.203
1170	3.90	207.11	1.780	1.728	1.585		0.143	0.566	0.01	7.577	3.910	0.432	1.089
1170	3.95	209.92	1.780	1.722	1.570		0.152	0.560	0.01	7.661	3.540	0.416	1.437

Site	Sample depth [mbsf]	Age [kyr]	SR [cm/kyr]	Bulk AR [g/cm²kyr]	AR Carbonate [g/cm²kyr]	AR TOC [g/cm²kyr]	AR Siliciclastics [g/cm²kyr]	AR coarse fraction [>63 µm, g/cm²kyr]	AR Chlorine [10^{-6}g/cm²kyr]	AR Aluminium [10^{-3}g/cm²kyr]	AR Iron [10^{-3}g/cm²kyr]	AR Titanium [10^{-3}g/cm²kyr]	AR excess Barium [10^{-3}g/cm²kyr]
1170	4.00	212.73	1.780	1.653	1.494		0.158	0.582	0.01	7.278	3.168	0.395	1.424
1170	4.05	215.54	2.599	2.431	2.196		0.235	0.777	0.01	10.344	5.176	0.556	2.024
1170	4.10	216.58	4.812	4.713	4.248		0.465	1.463	0.02	21.588	12.618	1.127	4.038
1170	4.15	217.62	4.812	4.444	3.969		0.474	1.367	0.01	20.783	11.394	1.114	3.919
1170	4.20	218.66	4.812	4.508	3.990		0.518	1.347	0.02	24.733	10.530	1.377	3.951
1170	4.25	219.70	4.815	4.364	3.869		0.495	1.332	0.01	28.385	18.091	1.645	3.323
1170	4.30	220.73	4.815	4.264	3.738		0.526	1.376	0.04	29.667	14.698	1.844	3.041
1170	4.35	221.77	4.812	4.332	3.756		0.576	1.444	0.03	32.325	15.350	1.946	3.179
1170	4.40	222.81	4.812	4.215	3.582		0.633	1.502	0.06	34.715	18.798	2.120	3.309
1170	4.45	223.85	4.812	4.262	3.623		0.639	1.361	0.04	35.295	25.668	2.159	3.545
1170	4.50	224.89	4.115	3.645	3.059		0.586	1.376	0.05	35.795	15.981	2.169	3.627
1170	4.55	226.28	3.595	3.302	2.823		0.478	1.203	0.04	30.366	13.449	1.814	3.430
1170	4.60	227.67	3.595	3.175	2.781		0.394	1.341		22.368	10.910	1.288	2.860
1170	4.65	229.06	3.595	3.184	2.755		0.429	1.016		23.198	15.339	1.360	2.814
1170	4.70	230.45	3.595	3.088	2.737		0.351	0.990	0.03	18.852	8.422	1.101	2.773
1170	4.75	231.85	3.596	3.067	2.734		0.332	1.027		18.607	11.102	1.042	2.728
1170	4.80	233.24	3.596	3.609	3.229		0.380	1.128		19.294	11.307	1.060	3.331
1170	4.85	234.63	3.595	3.533	3.194		0.339	1.084		15.900	9.481	0.895	3.021
1170	4.90	236.02	3.595	3.393	3.084		0.309	0.948		15.766	6.352	0.838	2.926
1170	4.95	237.41	3.595	3.415	3.157		0.258	0.974		13.912	6.124	0.744	2.790
1170	5.00	238.80	3.595	3.459	3.140		0.318	1.051	0.02	14.613	6.844	0.776	2.713
1170	5.05	240.19	3.481	3.502	3.228		0.274	0.850		14.317	6.009	0.755	2.772
1170	5.10	241.67	3.374	3.390	3.072		0.318	0.667		18.570	9.613	0.989	2.857
1170	5.15	243.15	3.374	3.247	2.942		0.304	0.706		18.967	8.469	1.102	2.135
1170	5.20	244.64	3.374	3.411	3.162		0.249	0.638		21.145	8.608	1.074	1.953
1170	5.25	246.12	3.374	3.222	2.930		0.292	0.630	0.02	17.640	8.138	1.000	2.019
1170	5.30	247.60	3.670	3.706	3.317		0.389	0.324		21.058	11.373	1.223	2.670
1170	5.35	248.84	4.024	3.809	3.353		0.455	0.419		24.904	14.500	1.430	3.150
1170	5.40	250.09	4.024	3.960	3.480		0.481	0.775		27.869	14.548	1.595	3.579
1170	5.45	251.33	4.024	3.745	3.360		0.385	0.277		19.864	9.936	1.225	2.277
1170	5.50	252.57	4.025	3.814	3.488		0.326	0.692	0.06	17.592	8.975	0.954	1.779
1170	5.55	253.81	4.024	3.633	3.369		0.264	0.710		16.234	7.872	0.879	1.845
1170	5.60	255.06	4.023	3.788	3.505		0.283	0.511		15.351	7.339	0.831	1.702
1170	5.65	256.30	4.024	3.804	3.524		0.280	0.614		15.067	7.891	0.827	1.864
1170	5.70	257.54	4.024	3.858	3.556		0.302	0.767		16.900	9.275	0.920	1.807
1170	5.75	258.78	4.024	3.608	3.315		0.293	0.912	0.24	16.193	6.892	0.893	1.919
1170	5.80	260.03	4.026	3.786	3.534		0.252	0.955		15.455	9.452	0.849	1.655
1170	5.85	261.27	4.024	3.799	3.548		0.251	0.613		12.334	6.065	0.681	1.576
1170	5.90	262.51	4.023	3.778	3.508		0.270	0.680		12.116	7.855	0.658	1.653
1170	5.95	263.75	4.024	3.936	3.686		0.250	0.701		13.082	6.953	0.704	1.657

Site	Sample depth [mbsf]	Age [kyr]	SR [cm/kyr]	Bulk AR [g/cm²kyr]	AR Carbonate [g/cm²kyr]	AR TOC [g/cm²kyr]	AR Siliciclastics [g/cm²kyr]	AR coarse fraction [>63 µm, g/cm²kyr]	AR Chlorine [10⁻⁶g/cm²kyr]	AR Aluminium [10⁻³g/cm²kyr]	AR Iron [10⁻³g/cm²kyr]	AR Titanium [10⁻³g/cm²kyr]	AR excess Barium [10⁻³g/cm²kyr]
1170	6.00	265.00	4.024	3.770	3.520		0.249	0.747	0.27	12.413	6.839	0.662	1.615
1170	6.05	266.24	4.024	3.569	3.325		0.244	0.656		11.633	6.408	0.636	1.553
1170	6.10	267.48	2.688	2.436	2.286		0.150	0.414		7.417	3.485	0.402	0.932
1170	6.20	271.82	2.305	2.193	2.039		0.154	0.440	0.21	8.080	5.091	0.444	1.074
1170	6.25	273.99	2.305	1.538	1.448		0.089	0.291		4.154	2.132	0.225	0.731
1170	6.30	276.16	2.306	2.174	2.015		0.159	0.333		9.238	4.696	0.492	1.009
1170	6.35	278.32	2.305	2.207	2.058		0.149	0.373		6.700	3.956	0.349	0.950
1170	6.40	280.49	2.305	2.129	2.000		0.128	0.430		5.093	2.317	0.268	0.962
1170	6.45	282.66	2.305	2.092	1.967		0.125	0.439		5.087	3.103	0.270	0.980
1170	6.50	284.83	2.305	2.243	2.053		0.191	0.491	0.27	9.122	5.011	0.500	1.028
1170	6.55	287.00	2.959	2.822	2.648		0.174	0.548		6.961	2.857	0.348	1.232
1170	6.60	288.21	4.131	3.854	3.589		0.265	0.720		10.944	6.589	0.551	1.535
1170	6.65	289.42	4.131	3.814	3.589		0.225	0.560		7.647	5.503	0.389	1.648
1170	6.70	290.63	4.131	3.965	3.731		0.234	0.495		7.788	4.111	0.403	1.688
1170	6.75	291.84	4.131	3.824	3.579		0.245	0.556	0.24	7.855	4.974	0.405	1.620
1170	6.80	293.05	4.131	4.095	3.768		0.327	0.605		13.336	6.546	0.731	2.103
1170	6.85	294.26	4.131	4.145	3.850		0.295	0.472		10.684	3.942	0.531	1.645
1170	6.90	295.47	4.131	3.934	3.662		0.273	0.473		10.353	4.515	0.544	1.744
1170	6.95	296.68	4.131	3.990	3.745		0.245	0.556		8.854	4.033	0.459	1.633
1170	7.00	297.90	4.131	4.020	3.756		0.264	0.470	0.23	8.409	3.310	0.435	1.640
1170	7.05	299.11	4.131	3.874	3.588		0.286	0.575		9.011	3.956	0.495	1.438
1170	7.10	300.32	4.130	3.969	3.753		0.215	0.558		7.333	5.444	0.403	1.651
1170	7.15	301.53	4.131	3.869	3.655		0.214	0.606		6.002	4.396	0.315	1.464
1170	7.20	302.74	4.131	3.895	3.651		0.244	0.416		7.484	3.515	0.404	1.606
1170	7.25	303.95	4.131	4.000	3.762		0.237	0.534	0.05	6.370	2.863	0.334	1.578
1170	7.30	305.16	4.131	3.799	3.549		0.249	0.518		4.816	2.529	0.237	1.313
1170	7.35	306.37	4.131	3.829	3.589		0.240	0.417		7.129	3.875	0.393	1.607
1170	7.40	307.58	4.131	3.809	3.604		0.205	0.493	0.03	5.010	3.774	0.256	1.390
1170	7.45	308.79	4.131	3.734	3.532		0.202	0.413		4.870	2.906	0.282	1.530
1170	7.50	310.00	2.123	1.996	1.883		0.113	0.222	0.03	2.975	1.431	0.157	0.784
1170	7.55	313.50	1.429	1.267	1.207		0.060	0.153		1.820	0.988	0.092	0.454
1170	7.60	317.00	1.429	1.373	1.305		0.068	0.172		2.117	0.909	0.110	0.531
1170	7.65	320.50	1.429	1.371	1.286		0.085	0.176		2.272	1.842	0.117	0.576
1170	7.70	324.00	1.429	1.408	1.319		0.089	0.170	0.01	3.024	1.424	0.151	0.681
1170	7.75	327.50	1.429	1.401	1.316		0.085	0.160		3.374	1.661	0.169	0.689
1170	7.80	331.00	2.500	2.424	2.286		0.138	0.255		6.026	3.500	0.299	1.213
1170	7.85	331.50	10.000	9.635	9.117		0.518	0.920		20.937	8.990	1.060	4.106
1170	7.90	332.00	10.000	9.756	9.171		0.585	0.876		24.544	9.393	1.221	4.746
1170	7.95	332.50	10.000	9.623	9.032		0.591	0.996		22.699	9.937	1.143	4.698
1170	8.00	333.00	10.000	10.170	9.473		0.697	1.403	0.05	25.994	9.854	1.317	5.682

Site	Sample depth [mbsf]	Age [kyr]	SR [cm/kyr]	Bulk AR [g/cm²kyr]	AR Carbonate [g/cm²kyr]	AR TOC [g/cm²kyr]	AR Siliciclastics [g/cm²kyr]	AR coarse fraction [>63 µm, g/cm²kyr]	AR Chlorine [10⁻⁶g/cm²kyr]	AR Aluminium [10⁻³g/cm²kyr]	AR Iron [10⁻³g/cm²kyr]	AR Titanium [10⁻³g/cm²kyr]	AR excess Barium [10⁻³g/cm²kyr]
1170	8.05	333.50	10.000	9.975	9.356		0.619	1.255		22.137	10.188	1.173	5.227
1170	8.10	334.00	10.000	10.461	9.792		0.669	1.316		25.754	13.314	1.363	5.128
1170	8.15	334.50	10.000	10.376	9.756		0.620	1.299		22.891	10.502	1.220	4.752
1170	8.20	335.00	10.000	9.999	9.363		0.637	1.186		25.961	20.842	1.394	4.816
1170	8.25	335.50	10.000	10.145	9.438		0.707	1.150	0.09	29.140	25.550	1.563	5.033
1170	8.30	336.00	10.000	9.926	9.214		0.713	1.162		31.504	18.551	1.735	5.218
1170	8.35	336.50	10.000	9.914	9.153		0.762	1.167		34.858	29.457	2.034	4.688
1170	8.40	337.00	10.000	10.145	9.388		0.757	1.373		40.355	21.636	2.233	5.345
1170	8.45	337.50	10.000	9.562	8.753		0.809	1.473		39.743	18.272	2.258	4.705
1170	8.50	338.00	10.000	10.133	8.891		1.242	1.729	1.63	43.369	30.640	2.403	4.422
1170	8.55	338.50	10.000	9.550	8.400		1.149	1.430		51.557	52.727	2.810	4.070
1170	8.60	339.00	10.000	9.708	8.474		1.233	1.558		66.863	50.191	3.530	4.838
1170	8.65	339.50	10.000	9.756	8.710		1.047	1.415		68.387	28.099	3.547	5.007
1170	8.70	340.00	10.000	9.586	8.298		1.288	1.411		81.146	36.872	4.202	5.009
1170	8.75	340.50	10.000	10.036	8.771		1.265	1.565	2.85	87.248	44.029	4.464	5.869
1170	8.80	341.00	4.579	4.478	3.757		0.722	0.635		48.180	23.144	2.547	3.233
1170	8.85	342.68	2.969	2.951	2.465		0.486	0.387		34.434	15.930	1.779	2.303
1170	8.90	344.37	2.968	2.791	2.325		0.466	0.352		35.028	17.564	1.845	1.960
1170	8.95	346.05	2.968	2.910	2.401		0.510	0.383		39.163	23.571	2.082	2.041
1170	9.00	347.74	2.969	2.886	2.387		0.499	0.374	0.94	35.547	15.025	1.890	1.946
1170	9.05	349.42	2.969	2.875	2.478		0.397	0.363		23.228	10.436	1.263	1.637
1170	9.10	351.11	2.969	2.831	2.546		0.285	0.464		14.062	7.193	0.784	1.519
1170	9.20	354.47	2.969	3.102	2.734		0.368	0.593	0.19	19.360	14.748	1.106	1.781
1170	9.25	356.16	2.969	2.944	2.619		0.324	0.538		20.678	9.856	1.052	1.695
1170	9.30	357.84	2.969	2.965	2.608		0.357	0.541		20.712	10.282	1.155	1.777
1170	9.35	359.53	2.968	2.892	2.521		0.371	0.509		21.476	11.555	1.232	1.884
1170	9.40	361.21	2.968	2.759	2.484		0.275	0.562		12.611	7.996	0.704	1.567
1170	9.45	362.90	2.969	2.861	2.517		0.344	0.503		19.703	8.889	1.099	1.979
1170	9.50	364.58	2.969	2.843	2.498		0.344	0.615	0.24	18.253	8.734	1.028	1.798
1170	9.55	366.26	2.969	2.727	2.382		0.345	0.619		20.486	10.155	1.102	1.882
1170	9.60	367.95	2.968	2.914	2.555		0.359	0.692		21.340	9.724	1.169	1.871
1170	9.65	369.63	2.968	2.957	2.637		0.320			19.277	7.394	1.052	2.203
1170	9.70	371.32	2.969	3.041	2.717		0.324	0.481		18.090	9.241	1.000	1.943
1170	9.75	373.00	2.969	3.066	2.781		0.286	0.500	0.11	14.607	6.214	0.797	1.968
1170	9.80	374.68	2.969	3.062	2.845		0.218	0.466		11.250	5.301	0.599	1.785
1170	9.85	376.37	2.968	3.055	2.819		0.235	0.672		8.064	5.467	0.443	1.379
1170	9.90	378.05	2.969	3.088	2.849		0.239	0.313		9.722	3.777	0.521	1.358
1170	9.95	379.74	2.969	3.019	2.817		0.203	0.304		7.943	3.325	0.403	1.163
1170	10.00	381.42	2.969	3.045	2.889		0.156	0.348	0.03	5.169	2.172	0.268	1.193
1170	10.05	383.11	2.969	2.890	2.721		0.169	0.344		5.067	2.068	0.262	1.015

Site	Sample depth [mbsf]	Age [kyr]	SR [cm/kyr]	Bulk AR [g/cm²kyr]	AR Carbonate [g/cm²kyr]	AR TOC [g/cm²kyr]	AR Siliciclastics [g/cm²kyr]	AR coarse fraction [>63 µm, g/cm²kyr]	AR Chlorine [10⁻³g/cm²kyr]	AR Aluminium [10⁻³g/cm²kyr]	AR Iron [10⁻³g/cm²kyr]	AR Titanium [10⁻³g/cm²kyr]	AR excess Barium [10⁻³g/cm²kyr]
1170	10.10	384.79	2.968	2.939	2.790		0.149	0.320		6.194	2.395	0.312	1.133
1170	10.15	386.47	2.968	2.910	2.749		0.161	0.273		7.466	3.480	0.398	1.166
1170	10.20	388.16	2.969	3.012	2.810		0.203	0.323		7.048	3.891	0.361	1.130
1170	10.25	389.84	2.969	3.117	2.926		0.191	0.349	0.03	6.510	2.897	0.321	1.196
1170	10.30	391.53	2.968	3.134	2.921		0.213	0.320		6.904	2.947	0.332	1.160
1170	10.35	393.21	2.968	2.968	2.778		0.191	0.347		7.245	6.502	0.351	1.156
1170	10.40	394.90	2.969	3.124	2.939		0.185	0.456		5.781	2.775	0.276	1.226
1170	10.45	396.58	2.969	3.099	2.897		0.202	0.391		5.326	4.340	0.268	1.346
1170	10.50	398.26	2.969	3.052	2.851		0.201	0.379	0.16	6.458	3.803	0.335	1.262
1170	10.55	399.95	2.968	3.080	2.907		0.173	0.345		5.764	2.647	0.273	1.355
1170	10.60	401.63	2.968	3.033	2.857		0.176	0.368		5.967	2.607	0.307	1.465
1170	10.65	403.32	2.969	3.099	2.907		0.192	0.367		6.167	5.188	0.309	1.588
1170	10.70	405.00	3.458	3.546	3.329		0.217	0.473	0.25	6.825	3.766	0.356	1.893
1170	10.75	406.21	4.137	4.182	3.958		0.225	0.604		7.950	4.514	0.402	2.120
1170	10.80	407.42	4.137	4.263	4.027		0.236	0.687	0.02	9.303	4.134	0.505	2.155
1170	10.85	408.63	4.139	4.410	4.122		0.288	0.805	0.03	9.705	5.738	0.532	2.054
1170	10.90	409.83	4.137	4.213	3.922		0.291	0.870	0.01	10.549	4.940	0.567	2.123
1170	10.95	411.04	4.137	4.283	3.969		0.314	0.927	0.07	11.068	4.907	0.588	2.094
1170	11.00	412.25	4.139	4.270	3.953		0.317	0.994	0.04	10.550	4.632	0.562	1.973
1170	11.05	413.46	4.137	4.283	3.958		0.325	0.966	0.02	12.483	5.855	0.654	2.137
1170	11.10	414.67	4.137	4.494	4.173		0.321	1.082	0.27	12.492	4.993	0.645	2.208
1170	11.15	415.88	4.139	4.421	4.080		0.341	1.009	0.03	13.052	7.740	0.718	2.459
1170	11.20	417.08	4.137	4.243	3.925		0.317	0.874	0.17	12.211	10.572	0.657	2.131
1170	11.25	418.29	4.137	4.132	3.834		0.298	0.894	0.04	9.250	4.115	0.467	1.622
1170	11.30	419.50	4.139	4.234	3.968		0.266	0.784	0.03	11.000	6.405	0.586	1.954
1170	11.35	420.71	4.137	4.298	4.035		0.263	0.866		8.511	3.730	0.481	1.893
1170	11.40	421.92	4.137	4.474	4.204		0.270	0.900	0.03	8.377	5.663	0.484	2.023
1170	11.45	423.13	4.139	4.209	3.983		0.226	0.654	0.03	8.153	4.857	0.405	1.942
1170	11.50	424.33	4.138	4.375	4.146		0.228	0.777	0.05	8.467	4.457	0.434	2.216
1170	11.56	425.78	4.551	5.242	5.005		0.237	0.700	0.03	8.784	5.797	0.499	2.011
1170	11.61	426.75	4.138	4.168	3.994		0.174	0.637	0.02	8.477	4.296	0.477	1.604
1170	11.65	427.96	3.724	3.796	3.578		0.218	0.925		10.408	4.940	0.548	1.948
1170	11.70	429.17	4.137	4.152	3.913		0.239	0.976	0.02	11.974	4.753	0.645	2.296
1170	11.75	430.38	4.139	4.416	4.161		0.254	0.924	0.02	13.123	6.098	0.719	2.348
1170	11.80	431.58	4.137	4.268	4.024		0.243	0.869	0.04	11.300	9.254	0.613	1.919
1170	11.85	432.79	4.137	4.283	4.096		0.187	0.865	0.04	8.838	6.256	0.467	1.871
1170	11.90	434.00	4.184	4.245	4.058		0.186	0.734	0.03	8.217	4.035	0.466	1.948
1170	11.95	435.18	4.230	4.631	4.422		0.209	0.707	0.03	7.955	3.741	0.442	1.925
1170	12.00	436.36	4.232	4.299	4.150		0.149	0.595	0.03	6.825	3.474	0.396	1.821
1170	12.05	437.55	4.232	4.288	4.082		0.206	0.609	0.04	7.963	8.282	0.436	1.520

Site	Sample depth [mbsf]	Age [kyr]	SR [cm/kyr]	Bulk AR [g/cm²kyr]	AR Carbonate [g/cm²kyr]	AR TOC [g/cm²kyr]	AR Siliciclastics [g/cm²kyr]	AR coarse fraction [>63 µm, g/cm²kyr]	AR Chlorine [10^{-6}g/cm²kyr]	AR Aluminium [10^{-3}g/cm²kyr]	AR Iron [10^{-3}g/cm²kyr]	AR Titanium [10^{-3}g/cm²kyr]	AR excess Barium [10^{-3}g/cm²kyr]
1170	12.10	438.73	4.230	4.415	4.199		0.216	0.665	0.04	9.205	5.415	0.531	1.619
1170	12.15	439.91	4.230	4.415	4.203		0.212	0.663	0.05	9.912	4.564	0.572	1.646
1170	12.20	441.09	4.230	4.523	4.260		0.263	0.704	0.07				
1170	12.25	442.27	4.230	4.441	4.235		0.206	0.725	0.01	10.392	5.289	0.576	1.714
1170	12.30	443.46	4.232	4.417	4.156		0.260	0.746	0.06	11.368	5.801	0.619	1.817
1170	12.35	444.64	4.232	4.350	4.130		0.219	0.716	0.06	10.575	5.003	0.597	1.730
1170	12.40	445.82	4.230	4.307	4.084		0.223	0.708	0.08	10.874	5.712	0.610	1.764
1170	12.45	447.00	4.230	4.410	4.169		0.241	0.807	0.14	11.595	6.625	0.659	1.838
1170	12.50	448.18	4.230	4.348	4.105		0.243	0.849	0.13	11.484	5.567	0.629	1.859
1170	12.55	449.36	4.232	4.612	4.376		0.236	0.749	0.12	11.637	5.822	0.631	1.869
1170	12.60	450.55	4.232	4.288	4.055		0.233	0.799	0.18	11.029	5.427	0.614	1.723

Site 1171A - Accumulation rates of analysed proxies

Site	Sample depth [mbsf]	Age [kyr]	SR [cm/kyr]	Bulk AR [g/cm²kyr]	AR Carbonate [g/cm²kyr]	AR TOC [g/cm²kyr]	AR Siliciclastics [g/cm²kyr]	AR coarse fraction [>63 µm, g/cm²kyr]	AR Chlorine [10⁻³g/cm²kyr]	AR Aluminium [10⁻³g/cm²kyr]	AR Iron [10⁻³g/cm²kyr]	AR Titanium [10⁻³g/cm²kyr]	AR excess Barium [10⁻³g/cm²kyr]
1171	0.00	0.32	2.532	2.307	2.192		0.115	0.887	0.09	3.734	2.055	0.199	1.322
1171	0.05	2.31	2.532	2.192	2.080		0.112	0.817	0.06	2.727	1.605	0.143	0.974
1171	0.10	4.27	2.545	2.311	2.218		0.093	0.957		4.039	2.162	0.198	1.302
1171	0.15	6.24	2.535	2.243	2.126		0.116	0.918	0.12	4.540	2.500	0.232	1.433
1171	0.21	8.61	2.574	2.308	2.187		0.121	1.076	0.04	4.850	2.928	0.267	1.490
1171	0.25	10.13	2.795	2.514	2.391		0.123	1.171	0.04	5.326	3.350	0.316	1.546
1171	0.30	11.83	2.950	2.679	2.541		0.138	1.536	0.11	5.647	5.676	0.348	1.568
1171	0.35	13.52	2.967	2.569	2.419		0.150	1.643	0.08	6.131	4.933	0.417	1.142
1171	0.40	15.20	3.559	3.170	2.982		0.188	2.132	0.09	8.530	5.636	0.560	1.455
1171	0.45	16.33	3.509	3.346	3.177		0.169	1.911	0.09	7.871	4.968	0.492	1.290
1171	0.50	18.05	2.890	2.524				1.495					
1171	0.55	19.79	2.882	2.525	2.397		0.128	1.474	0.06	5.944	3.593	0.366	1.035
1171	0.60	21.52	1.603	1.451	1.374		0.077	0.847	0.04	3.789	2.327	0.232	0.653
1171	0.65	26.03	1.108	1.029	0.974		0.055	0.590	0.01	3.094	1.841	0.190	0.446
1171	0.69	29.64	0.971	0.899	0.851		0.048	0.376	0.03	2.666	1.645	0.170	0.376
1171	0.75	36.32	1.000	0.951				0.000					
1171	0.80	40.64	1.200	1.120				0.456					
1171	0.85	44.66	1.245	1.175	1.113		0.062	0.519	0.03	2.151	1.010	0.116	0.489
1171	0.90	48.67	1.245	1.199	1.136		0.063	0.449	0.02	2.405	1.183	0.130	0.636
1171	0.95	52.69	1.167	1.103	1.047		0.056	0.407	0.03	1.863	1.176	0.102	0.492
1171	1.00	57.24	1.085	1.049	1.002		0.047	0.416	0.02	1.703	0.907	0.093	0.505
1171	1.05	61.90	1.006	0.965	0.918		0.048	0.376	0.00	1.725	0.939	0.095	0.536
1171	1.10	67.18	0.914	0.831	0.787		0.043	0.350		1.631	0.847	0.091	0.372
1171	1.15	72.84	0.923	0.816	0.774		0.043	0.368	0.01	1.577	0.874	0.091	0.342
1171	1.20	78.02	1.117	1.041	0.984		0.057	0.442	0.02	1.952	1.517	0.110	0.475
1171	1.25	81.79	1.330	1.184	1.125		0.059	0.514	0.04	2.207	1.249	0.123	0.562
1171	1.30	85.54	1.317	1.182	1.119		0.063	0.511	0.01	2.009	1.271	0.108	0.591
1171	1.35	89.38	1.277	1.181	1.119		0.062	0.435	0.03				
1171	1.40	93.37	1.279	1.216	1.151		0.065	0.443	0.01	2.384	1.194	0.121	0.714
1171	1.50	101.11	1.455	1.468	1.389		0.079	0.589	0.08				
1171	1.55	103.68	2.354	2.259	2.141		0.118	0.939	0.22	4.039	2.553	0.223	1.133
1171	1.60	105.36	0.935	0.889	0.840		0.049	0.364	0.01	1.650	1.302	0.090	0.476
1171	1.65	114.38	0.475	0.444	0.418		0.026	0.181	0.01	0.741	0.557	0.041	0.233
1171	1.70	126.41	0.669	0.595	0.563		0.032	0.243	0.02	1.201	0.515	0.058	0.341
1171	1.75	129.33	1.712	1.578	1.508		0.070	0.711	0.32	2.604	1.249	0.145	0.651
1171	1.80	132.25	1.738	1.693	1.621		0.072	0.642	0.11	3.325	1.729	0.177	0.979
1171	1.85	135.09	1.783	1.564	1.509		0.055	0.612	0.49				
1171	1.90	137.86	1.820	1.602	1.549		0.053	0.713	0.70	2.947	1.899	0.141	0.727
1171	1.95	140.58	1.848	1.720	1.651		0.069	0.780	0.64	3.542	1.807	0.189	0.895

Site	Sample depth [mbsf]	Age [kyr]	SR [cm/kyr]	Bulk AR [g/cm²kyr]	AR Carbonate [g/cm²kyr]	AR TOC [g/cm²kyr]	AR Siliciclastics [g/cm²kyr]	AR coarse fraction [>63 µm, g/cm²kyr]	AR Chlorine [10⁻³g/cm²kyr]	AR Aluminium [10⁻³g/cm²kyr]	AR Iron [10⁻³g/cm²kyr]	AR Titanium [10⁻³g/cm²kyr]	AR excess Barium [10⁻³g/cm²kyr]
1171	2.00	143.27	1.656	1.521	1.459		0.061	0.663	0.03	3.178	1.589	0.199	0.844
1171	2.05	146.62	1.070	0.898	0.855		0.043	0.415	0.05	3.242	1.666	0.199	0.550
1171	2.10	152.62	0.783	0.648	0.612		0.036	0.321	0.02	2.191	1.105	0.135	0.375
1171	2.15	159.39	0.827	0.717	0.684		0.033	0.405		2.374	1.496	0.151	0.391
1171	2.20	164.71	1.201	0.942	0.895		0.046	0.475	0.03	3.500	1.729	0.221	0.561
1171	2.25	167.71	2.024	1.560	1.482		0.078	0.886		6.222	3.129	0.417	1.125
1171	2.30	169.65	3.527	2.827	2.696		0.131	1.691	0.07	11.138	5.635	0.729	1.722
1171	2.35	170.55	5.556	4.281	4.117		0.165	2.445	0.08	13.042	6.844	0.823	2.544
1171	2.40	171.45	1.894	1.562	1.495		0.067	0.878		5.652	2.945	0.377	1.176
1171	2.45	175.83	1.143	0.913	0.864		0.049	0.484	0.01	4.014	2.334	0.266	0.819
1171	2.50	180.20	1.351	1.146	1.072		0.074	0.576		3.703	1.886	0.231	0.894
1171	2.55	183.23	1.585	1.258	1.190		0.068	0.648	0.03	2.985	1.395	0.167	0.838
1171	2.60	186.51	1.533	1.450	1.376		0.075	0.721	0.01	3.182	1.392	0.169	0.927
1171	2.65	189.75	1.637	1.405	1.330		0.075	0.671		2.791	1.234	0.152	0.918
1171	2.70	192.62	1.741	1.538	1.441		0.097	0.721	0.00	2.973	1.551	0.162	1.027
1171	2.75	195.50	0.750	0.676	0.638		0.038	0.307		1.283	0.888	0.071	0.434
1171	2.80	205.95	0.496	0.437	0.412		0.024	0.213	0.01	0.920	0.449	0.052	0.281
1171	2.85	215.65	0.514	0.414	0.391		0.023	0.196	0.00	1.055	0.472	0.058	0.281
1171	2.90	225.42	0.627	0.509	0.477		0.031	0.254		1.500	0.753	0.094	0.357
1171	2.95	231.61	0.913	0.737	0.682		0.055	0.393	0.00	2.128	1.176	0.130	0.527
1171	3.00	236.38	1.348	1.266	1.188		0.078	0.508		3.278	1.723	0.191	0.759
1171	3.05	239.03	1.896	1.811	1.702		0.109	0.703	0.04	4.458	2.106	0.239	1.083
1171	3.10	241.65	1.656	1.550	1.459		0.090	0.621	0.03	3.126	1.458	0.167	0.948
1171	3.15	245.07	1.006	1.011	0.944		0.067	0.425		2.225	1.412	0.117	0.602
1171	3.20	251.59	0.864	0.832	0.779		0.053	0.380	0.01	1.855	1.048	0.109	0.415
1171	3.25	256.65	1.179	1.106	1.052		0.054	0.557		2.339	1.336	0.139	0.515
1171	3.30	260.07	1.504	1.364	1.299		0.064	0.743	0.02	2.656	1.797	0.169	0.628
1171	3.35	263.30	1.672	1.433	1.351		0.082	0.763	0.01	3.172	2.246	0.207	0.691
1171	3.40	266.05	1.855	1.598	1.503		0.095	0.839		3.703	1.846	0.219	0.741
1171	3.45	268.69	1.894	1.670	1.584		0.086	0.901	0.01	3.530	2.153	0.214	0.700
1171	3.50	271.33	1.295	1.178				0.614					
1171	3.55	276.41	1.109	0.918	0.843		0.074	0.446		3.091	1.362	0.213	0.525
1171	3.60	280.35	1.269	1.071	1.000		0.071	0.501	0.03	3.528	1.608	0.222	0.594
1171	3.65	284.29	1.267	1.175	1.119		0.056	0.559	0.00	2.498	1.251	0.157	0.549
1171	3.70	288.24	1.470	1.421	1.360		0.061	0.569		2.727	1.255	0.129	0.740
1171	3.75	291.10	1.898	1.851	1.770		0.081	0.829	0.01	3.013	1.556	0.169	0.930
1171	3.80	293.51	1.998	1.894	1.803		0.091	0.926		3.355	2.431	0.195	0.817
1171	3.85	296.10	1.934	1.731	1.656		0.076	0.863	0.03	3.346	1.925	0.197	0.697
1171	3.90	298.68	1.932	1.747	1.656		0.091	0.866	0.01	3.817	1.980	0.223	0.854
1171	3.95	301.28	1.931	1.855	1.766		0.089	0.814		4.579	1.780	0.208	0.929

Site	Sample depth [mbsf]	Age [kyr]	SR [cm/kyr]	Bulk AR [g/cm²kyr]	AR Carbonate [g/cm²kyr]	AR TOC [g/cm²kyr]	AR Siliciclastics [g/cm²kyr]	AR coarse fraction [>63 µm, g/cm²kyr]	AR Chlorine [10⁻³g/cm²kyr]	AR Aluminium [10⁻³g/cm²kyr]	AR Iron [10⁻³g/cm²kyr]	AR Titanium [10⁻³g/cm²kyr]	AR excess Barium [10⁻³g/cm²kyr]
1171	4.00	303.86	2.466	2.337	2.236		0.101	1.071	0.03	4.334	2.076	0.248	1.140
1171	4.05	305.33	3.401	3.413	3.253		0.160	1.302		6.250	3.785	0.341	1.645
1171	4.10	306.80	3.396	3.243	3.085		0.159	1.313	0.07	5.968	3.843	0.314	1.636
1171	4.15	308.28	3.401	3.184	3.045		0.140	1.274	0.03	5.104	2.530	0.275	1.518
1171	4.20	309.74	4.098	3.969	3.796		0.173	1.432		6.922	4.041	0.345	1.920
1171	4.25	310.72	6.211	5.878	5.627		0.251	2.108	0.01	10.648	5.160	0.576	3.181
1171	4.30	311.35	7.874	7.878	7.507		0.372	3.143		13.775	7.324	0.748	4.255
1171	4.35	311.99	7.937	7.592	7.252		0.341	2.915	0.10	13.258	7.201	0.710	4.355
1171	4.40	312.61	7.930	8.236	7.835		0.401	3.006	0.02	14.761	7.649	0.807	4.857
1171	4.50	313.88	7.895	7.864	7.494		0.371	3.069	0.17	15.253	8.009	0.842	4.131
1171	4.55	314.51	4.622	3.515	3.340		0.175	1.459	1.06	6.645	3.550	0.361	1.759
1171	4.60	316.04	3.190	3.084	2.933		0.151	1.379	0.36	5.816	2.991	0.347	1.551
1171	4.65	317.65	3.195	3.211	3.061		0.150	1.300	0.06	8.388	4.433	0.508	1.238
1171	4.70	319.17	3.436	3.453	3.303		0.150	1.096	0.20	7.155	4.070	0.416	1.439
1171	4.75	320.56	4.525	4.415	4.212		0.203	1.473	0.15	10.009	5.797	0.575	1.657
1171	4.80	321.38	6.135	5.716	5.450		0.266	1.597	1.93	14.486	7.632	0.836	2.212
1171	4.85	322.19	6.173	5.760	5.433		0.328	1.659	1.20	16.151	7.857	0.945	2.131
1171	4.90	323.00	6.042	5.594	5.272		0.323	1.542	0.72	16.034	9.215	0.891	2.139
1171	4.95	323.84	5.952	5.790	5.484		0.306	1.407	2.88	15.149	7.170	0.869	2.234
1171	5.00	324.68	5.917	5.617	5.324		0.293	1.396	0.37	11.938	5.623	0.703	1.965
1171	5.05	325.53	5.882	5.257	5.007		0.250	1.249	0.66				
1171	5.10	326.38	5.952	5.755	5.472		0.283	1.503	0.28	10.729	5.458	0.630	1.771
1171	5.15	327.21	5.208	5.066	4.817		0.249	1.364	1.14	9.344	5.347	0.580	1.705
1171	5.20	328.30	3.521	3.446	3.304		0.141	0.876	0.83	7.455	3.543	0.435	1.220
1171	5.25	330.05	2.865	2.594	2.491		0.104	0.653	0.25				
1171	5.30	331.79	2.430	2.367	2.274		0.093	0.628	0.11	3.629	1.714	0.208	0.848
1171	5.35	334.17	2.049	2.140	2.042		0.098	0.564	0.23	3.587	1.431	0.192	0.822
1171	5.40	336.67	1.852	1.845	1.772		0.072	0.505	0.18	2.621	1.725	0.162	0.658
1171	5.45	339.57	1.364	1.421	1.356		0.065	0.330	0.60	3.161	1.816	0.186	0.442
1171	5.50	344.00	1.128	1.157	1.102		0.055	0.282	0.39	2.226	1.257	0.129	0.429
1171	5.55	348.43	0.742	0.726	0.700		0.026	0.156	0.35	1.237	0.576	0.070	0.251
1171	5.60	357.47	0.775	0.747	0.717		0.030	0.171	0.68	1.779	0.804	0.100	0.275
1171	5.65	361.34	1.351	1.372	1.320		0.052	0.276	1.14	2.092	1.096	0.123	0.549
1171	5.70	364.87	1.508	1.527	1.473		0.054	0.283	0.96	2.461	1.297	0.136	0.546
1171	5.75	367.97	1.312	1.344	1.299		0.045	0.269	0.02	1.527	0.671	0.078	0.476
1171	5.80	372.49	0.891	0.861	0.830		0.031	0.162	0.01	1.048	0.476	0.053	0.333
1171	5.85	379.19	0.837	0.816	0.790		0.026	0.198	0.08	1.001	0.409	0.053	0.271
1171	5.90	384.44	1.264	1.293	1.256		0.037	0.214	0.07	0.960	0.577	0.064	0.382
1171	5.95	387.10	2.649	2.689	2.617		0.072	0.377	0.04	2.043	1.023	0.129	0.693
1171	6.00	388.22	4.357	4.609	4.466		0.142	0.626		3.625	1.499	0.207	1.359

Site	Sample depth [mbsf]	Age [kyr]	SR [cm/kyr]	Bulk AR [g/cm²kyr]	AR Carbonate [g/cm²kyr]	AR TOC [g/cm²kyr]	AR Siliciclastics [g/cm²kyr]	AR coarse fraction [>63 µm, g/cm²kyr]	AR Chlorine [10⁻³g/cm²kyr]	AR Aluminium [10⁻³g/cm²kyr]	AR Iron [10⁻³g/cm²kyr]	AR Titanium [10⁻³g/cm²kyr]	AR excess Barium [10⁻³g/cm²kyr]
1171	6.05	389.40	4.211	4.219	4.083		0.136	0.552	0.01	3.549	1.459	0.204	1.212
1171	6.10	390.59	3.515	3.548	3.441		0.107	0.626		3.596	1.694	0.192	1.032
1171	6.15	392.24	1.972	1.927	1.856		0.071	0.323	0.03	1.881	2.765	0.105	0.572
1171	6.20	395.66	2.247	2.179	2.109		0.070	0.398	0.02	2.091	1.569	0.119	0.617
1171	6.25	396.69	4.902	4.775	4.560		0.216	0.646		4.922	5.511	0.257	1.496
1171	6.30	397.70	4.914	4.730	4.522		0.208	0.807	0.16	5.053	2.713	0.251	1.780
1171	6.35	398.73	4.854	4.821	4.668		0.153	0.736		4.969	2.414	0.272	1.870
1171	6.40	399.76	4.878	4.774	4.617		0.157	0.809	0.69	4.944	2.461	0.262	1.792
1171	6.45	400.78	2.667	2.754	2.661		0.094	0.413	0.02	3.115	1.471	0.155	1.212
1171	6.50	403.51	1.721	1.818	1.751		0.067	0.290	0.01	2.008	0.949	0.107	0.682
1171	6.55	406.59	1.733	1.663	1.597		0.066	0.218		1.715	1.573	0.096	0.611
1171	6.60	409.28	1.325	1.319	1.273		0.046	0.234	0.01	1.550	1.006	0.078	0.507
1171	6.65	414.14	1.215	1.228	1.181		0.047	0.208	0.01	1.402	0.587	0.076	0.494
1171	6.70	417.51	2.372	2.547	2.459		0.088	0.488	0.01	3.455	1.783	0.193	1.031
1171	6.75	418.35	5.917	6.128	5.897		0.232	1.100					
1171	6.80	419.20	5.602	5.753	5.528		0.225	1.054		9.102	4.330	0.522	2.608
1171	6.85	420.14	5.128	5.484	5.256		0.228	1.018	0.27	9.303	4.585	0.508	2.449
1171	6.90	421.15	4.959	5.354	5.114		0.240	1.337	0.07	9.399	4.924	0.574	2.341
1171	6.94	421.95	4.986	4.653	4.434		0.219	1.400		9.156	5.223	0.535	1.954
1171	6.99	422.96	4.973	4.277	4.112		0.164	1.496	0.03	8.024	5.210	0.487	1.288
1171	7.10	425.17	4.984	3.863	3.703		0.160	0.908		5.724	3.039	0.317	1.371
1171	7.15	426.17	5.095	4.426	4.267		0.159	0.846	0.17	4.447	2.538	0.376	1.398
1171	7.20	427.13	5.181	4.243	3.987		0.257	0.862	0.29	6.376	3.084	0.462	1.563
1171	7.25	428.10	2.933	2.316	2.161		0.155	0.514		2.835	1.570	0.156	0.836
1171	7.30	430.54	0.768	0.728	0.682		0.046	0.163	0.07	1.030	0.561	0.081	0.261
1171	7.35	441.12	0.770	0.698	0.655		0.043	0.140		0.942	0.519	0.055	0.255
1171	7.40	443.53	0.697	0.643	0.603		0.040	0.111	0.04	0.751	0.360	0.041	0.230
1171	7.45	455.46	0.481	0.463	0.436		0.027	0.082	0.00	0.510	0.197	0.026	0.183
1171	7.50	464.30	0.623	0.642	0.605		0.037	0.137		0.640	0.289	0.035	0.261
1171	7.55	471.52	0.763	0.775	0.733		0.041	0.160	0.01	0.801	0.388	0.041	0.325
1171	7.60	477.40	0.891	0.941	0.881		0.060	0.217	0.02	1.075	0.853	0.060	0.418
1171	7.65	482.74	0.936	0.926	0.863		0.063	0.232	0.04	1.159	0.912	0.062	0.406
1171	7.70	488.08	1.335	1.297	1.218		0.078	0.378	0.11	1.664	0.709	0.089	0.540
1171	7.75	490.23	2.320	2.220	2.066		0.154	0.701	0.85	4.041	2.235	0.229	1.027
1171	7.80	492.39	2.326	2.249	2.093		0.155	0.754	0.26	3.191	1.766	0.165	0.965
1171	7.85	494.53	2.326	2.320	2.164		0.156	0.724	0.07	3.969	2.490	0.209	1.180
1171	7.90	496.69	2.323	2.362	2.244		0.118	0.778	0.04				
1171	7.95	498.84	2.331	2.329	2.218		0.111	0.730	0.02	4.470	1.651	0.206	1.179
1171	8.00	500.98	2.128	2.372	2.272		0.100	0.755	0.40	2.979	1.168	0.158	1.007
1171	8.05	503.54	1.493	1.506	1.445		0.062	0.464	0.03	2.232	1.095	0.129	0.640

Site	Sample depth [mbsf]	Age [kyr]	SR [cm/kyr]	Bulk AR [g/cm²kyr]	AR Carbonate [g/cm²kyr]	AR TOC [g/cm²kyr]	AR Siliciclastics [g/cm²kyr]	AR coarse fraction [>63 µm, g/cm²kyr]	AR Chlorine [10⁻³g/cm²kyr]	AR Aluminium [10⁻³g/cm²kyr]	AR Iron [10⁻³g/cm²kyr]	AR Titanium [10⁻³g/cm²kyr]	AR excess Barium [10⁻³g/cm²kyr]
1171	8.10	507.68	1.208	1.253	1.200		0.053	0.392		1.670	0.797	0.092	0.471
1171	8.15	511.82	1.295	1.395	1.342		0.053	0.387	0.02	1.754	0.916	0.106	0.587
1171	8.20	515.40	1.420	1.523	1.470		0.053	0.312	0.01	1.860	0.877	0.107	0.607
1171	8.25	518.86	1.458	1.589	1.529		0.060	0.328		1.662	1.024	0.114	0.612
1171	8.30	522.26	1.544	1.620	1.569		0.051	0.391		2.503	0.849	0.131	0.649
1171	8.35	525.33	1.629	1.770	1.701		0.069	0.457		2.714	1.191	0.155	0.723
1171	8.40	528.40	1.633	1.700	1.620		0.080	0.473	0.02	3.147	2.375	0.177	0.772
1171	8.45	531.46	1.631	1.704	1.626		0.078	0.594	0.01	3.483	1.310	0.179	0.838
1171	8.50	534.53	2.169	2.198	2.070		0.129	0.755		4.123	2.261	0.244	1.175
1171	8.60	538.37	2.997	3.073	2.879		0.194	1.130		6.143	3.345	0.367	1.651
1171	8.65	539.54	2.661	2.588	2.410		0.179	1.019		5.672	2.756	0.334	1.419
1171	8.70	542.13	1.807	1.681	1.565		0.116	0.772	0.09	4.291	2.764	0.266	1.101
1171	8.75	545.07	1.698	1.495	1.371		0.124	0.658	0.03	3.670	1.931	0.221	1.106
1171	8.80	548.02	1.420	1.299	1.188		0.111	0.576	0.23	4.150	2.542	0.277	0.659
1171	8.85	552.11	1.217	1.062	0.972		0.091	0.375	0.18	4.224	2.298	0.261	0.696
1171	8.90	556.24	1.167	0.867	0.772		0.095	0.383	0.13	2.571	1.823	0.157	0.514
1171	8.95	560.68	0.996	0.789	0.723		0.066	0.357	0.02	1.760	1.010	0.107	0.490
1171	9.00	566.28	0.858	0.691	0.636		0.056	0.312	0.02	1.427	1.150	0.089	0.442
1171	9.05	572.34	0.826	0.628	0.594		0.035	0.300	0.01	1.240	0.545	0.069	0.408
1171	9.10	578.38	0.827	0.684	0.639		0.045	0.336	0.01	1.268	0.673	0.075	0.500
1171	9.15	584.42	0.762	0.636	0.593		0.043	0.332	0.01	1.367	0.840	0.078	0.429
1171	9.20	591.51	1.063	0.822	0.765		0.057	0.413	0.01	1.945	1.069	0.115	0.494
1171	9.25	593.83	2.105	1.696	1.572		0.124	0.849		4.247	2.327	0.269	1.089
1171	9.30	596.26	1.972	1.546	1.436		0.110	0.780		4.417	1.867	0.225	1.105
1171	9.35	598.90	1.898	1.543	1.427		0.116	0.755		3.438	1.781	0.216	1.047
1171	9.40	601.53	2.208	1.666	1.544		0.122	0.855	0.03	3.759	1.946	0.228	1.004
1171	9.45	603.43	3.012	2.334	2.128		0.206	1.230	0.04	5.380	2.802	0.325	1.496
1171	9.50	604.85	3.527	2.997	2.807		0.190	1.137					
1171	9.55	606.27	2.577	2.039	1.881		0.158	1.019		5.083	2.367	0.301	1.335
1171	9.60	608.73	1.923	1.657	1.542		0.114	0.830		3.532	1.835	0.207	1.042
1171	9.65	611.47	1.890	1.460	1.363		0.096	0.794		2.868	1.481	0.175	0.958
1171	9.70	614.02	2.064	1.603	1.493		0.110	0.860	0.04	3.326	1.780	0.192	0.968
1171	9.75	616.31	2.183	1.731	1.611		0.119	0.872	0.02	3.606	1.894	0.214	1.075
1171	9.80	618.60	2.179	1.819	1.689		0.131	0.969		4.566	2.265	0.248	1.161
1171	9.85	620.90	2.151	1.720	1.595		0.125	0.893		4.115	2.292	0.250	0.980
1171	9.90	623.25	2.123	1.723	1.610		0.114	0.969		3.563	2.298	0.218	0.759
1171	9.95	625.61	2.123	1.994	1.823		0.171	0.853	0.03	6.809	3.973	0.450	1.411
1171	10.00	627.96	1.890	1.698	1.538		0.159	0.816	0.01	5.898	3.224	0.391	1.162
1171	10.05	630.90	1.890	1.578	1.435		0.143	0.815		5.163	2.773	0.319	0.946

Site 1172A - Accumulation rates of analysed proxies

Site	Sample depth [mbsf]	Age [kyr]	SR [cm/kyr]	Bulk AR [g/cm²kyr]	AR Carbonate [g/cm²kyr]	AR TOC [g/cm²kyr]	AR Siliciclastics [g/cm²kyr]	AR coarse fraction [>63 µm, g/cm²kyr]	AR Chlorine [10⁻⁶g/cm²kyr]	AR Aluminium [10⁻³g/cm²kyr]	AR Iron [10⁻³g/cm²kyr]	AR Titanium [10⁻³g/cm²kyr]	AR excess Barium [10⁻³g/cm²kyr]
1172	0.03	2.11	1.318	1.102	0.928	0.003	0.175	0.356	0.08	9.273	5.486	0.574	0.608
1172	0.08	5.90	1.318	1.185	0.984	0.003	0.201	0.282	0.32	11.188	6.789	0.687	0.709
1172	0.13	9.70	1.316	1.014	0.813	0.003	0.201	0.304	0.21	10.406	6.243	0.633	0.596
1172	0.18	13.50	1.317	1.127	0.918	0.003	0.209	0.331	0.43	11.904	7.663	0.722	0.679
1172	0.23	17.29	1.319	1.068	0.854	0.003	0.214	0.429	0.27	12.983	9.002	0.858	0.536
1172	0.28	21.08	1.318	1.112	0.869	0.003	0.243	0.531	0.30				
1172	0.33	24.88	1.125	0.961	0.736	0.003	0.225	0.381	0.64	12.832	7.379	0.872	0.487
1172	0.38	29.97	0.904	0.729	0.537	0.003	0.192	0.295	0.70	11.591	6.142	0.769	0.393
1172	0.43	35.94	0.838	0.715	0.574	0.002	0.141	0.342	0.79	7.128	4.114	0.474	0.372
1172	0.48	41.90	0.839	0.734	0.591	0.003	0.143	0.258	0.22	7.940	4.848	0.525	0.339
1172	0.53	47.87	0.839	0.700	0.564	0.002	0.136	0.223	0.36	8.335	4.260	0.541	0.340
1172	0.58	53.82	0.838	0.722	0.573	0.003	0.149	0.233	0.42	8.090	4.590	0.530	0.324
1172	0.63	59.80	0.838	0.726	0.591	0.002	0.134	0.276	0.41	7.793	4.653	0.511	0.355
1172	0.68	65.76	0.948	0.861	0.680	0.003	0.181	0.410	0.84	10.850	5.689	0.713	0.334
1172	0.73	70.35	1.211	0.987	0.717	0.004	0.270	0.322	0.97	16.966	8.466	1.135	0.409
1172	0.78	74.02	1.360	1.113	0.841	0.005	0.272	0.285	0.47	16.448	8.138	1.099	0.486
1172	0.83	77.70	1.359	1.059	0.853	0.004	0.206	0.316	1.18				
1172	0.88	81.38	1.394	1.168	0.940	0.004	0.227	0.277	1.16	11.599	5.871	0.727	0.565
1172	0.93	84.88	1.429	1.233	0.988	0.005	0.245	0.341	1.61	12.907	6.228	0.867	0.454
1172	0.98	88.38	1.427	1.242	1.049	0.004	0.193	0.312	1.26	10.148	5.021	0.672	0.567
1172	1.03	91.89	1.429	1.255	1.035	0.003	0.219	0.417	0.50	13.058	8.052	0.833	0.508
1172	1.08	95.38	1.428	1.316	1.081	0.004	0.235	0.378	0.49	12.298	6.882	0.830	0.672
1172	1.13	98.89	1.427	1.219	1.014	0.003	0.204	0.335	0.41	10.652	6.035	0.652	0.668
1172	1.18	102.39	1.428	1.102	0.931	0.003	0.172	0.335	0.38	8.827	4.424	0.550	0.600
1172	1.23	105.90	1.429	1.302	1.108	0.004	0.194	0.402	0.55	11.230	6.938	0.705	0.698
1172	1.28	109.39	1.371	1.173	0.999	0.003	0.174	0.343	0.31	9.829	6.376	0.592	0.657
1172	1.33	113.19	1.247	1.091	0.933	0.002	0.159	0.312	0.43	8.617	4.583	0.529	0.598
1172	1.38	117.41	1.160	0.988	0.854	0.002	0.134	0.307	0.60	8.433	4.115	0.514	0.565
1172	1.43	121.81	1.138	0.998	0.854	0.002	0.144	0.277	0.60	9.393	5.723	0.561	0.572
1172	1.53	130.59	1.178	0.889	0.746	0.002	0.142	0.292	0.09	10.978	6.689	0.683	0.417
1172	1.58	134.54	1.380	1.197	0.992	0.003	0.205	0.419	0.37	11.304	7.564	0.707	0.400
1172	1.63	137.84	1.515	1.313	1.037	0.005	0.276	0.301	1.38	16.936	8.297	1.092	0.695
1172	1.68	141.14	1.571	1.401	1.045	0.004	0.356	0.366	0.59	23.485	12.185	1.529	0.635
1172	1.73	144.21	1.672	1.476	1.149	0.004	0.327	0.529	0.65	21.195	10.522	1.352	0.632
1172	1.78	147.12	1.718	1.427	1.121	0.005	0.306	0.516	1.40	19.323	10.336	1.250	0.616
1172	1.83	150.03	1.718	1.412	1.164	0.003	0.247	0.000	0.64	14.548	8.454	0.966	0.569
1172	1.88	152.94	1.715	1.589	1.281	0.006	0.308	0.567	1.72	19.685	11.451	1.258	0.783
1172	1.93	155.86	1.718	1.371	1.116	0.003	0.254	0.540	1.39	15.616	8.313	1.000	0.567
1172	1.98	158.76	1.574	1.436	1.089	0.003	0.348	0.375	0.26	23.084	12.496	1.472	0.663

Site	Sample depth [mbsf]	Age [kyr]	SR [cm/kyr]	Bulk AR [g/cm²kyr]	AR Carbonate [g/cm²kyr]	AR TOC [g/cm²kyr]	AR Siliciclastics [g/cm²kyr]	AR coarse fraction [>63 µm, g/cm²kyr]	AR Chlorine [10⁻³g/cm²kyr]	AR Aluminium [10⁻³g/cm²kyr]	AR Iron [10⁻³g/cm²kyr]	AR Titanium [10⁻³g/cm²kyr]	AR excess Barium [10⁻³g/cm²kyr]
1172	2.03	162.21	1.379	1.113	0.827	0.003	0.286	0.330	0.67	19.322	10.110	1.239	0.593
1172	2.08	166.01	1.332	1.152	0.849	0.003	0.304	0.396	0.36	19.795	11.751	1.341	0.526
1172	2.13	169.72	1.435	1.177	0.882	0.004	0.295	0.404	1.90	20.850	9.672	1.372	0.515
1172	2.18	172.98	1.531	1.123	0.859	0.003	0.264	0.360	0.43	15.897	9.564	1.083	0.456
1172	2.23	176.25	1.529	1.265	0.992	0.004	0.273	0.455	0.66	16.013	8.903	1.098	0.549
1172	2.28	179.52	1.529	1.405	1.083	0.004	0.322	0.494	0.61	20.811	11.304	1.490	0.625
1172	2.33	182.79	1.529	1.421	1.054	0.003	0.367	0.406	0.27	25.300	14.021	1.701	0.779
1172	2.38	186.06	1.467	1.276	1.061	0.002	0.214	0.388	0.12	13.551	8.600	0.863	0.851
1172	2.43	189.60	1.218	1.077	0.895	0.002	0.182	0.317	0.02	10.437	6.362	0.682	0.706
1172	2.48	194.27	1.070	0.937	0.750	0.002	0.186	0.347	0.06	11.294	6.356	0.788	0.523
1172	2.53	198.95	1.071	0.907	0.707	0.002	0.200	0.348	0.15	11.672	7.163	0.797	0.503
1172	2.58	203.61	1.071	0.920	0.738	0.002	0.181	0.320	0.04	10.599	6.456	0.704	0.573
1172	2.63	208.29	1.070	0.999	0.810	0.002	0.188	0.310	0.07	10.185	7.025	0.628	0.621
1172	2.68	212.96	1.071	0.907	0.723	0.002	0.183	0.317	0.01	10.950	6.080	0.704	0.514
1172	2.73	217.63	1.083	1.016	0.781	0.002	0.235	0.238	0.03	14.991	9.881	1.029	0.497
1172	2.78	222.19	1.107	1.002	0.806	0.002	0.196	0.381	0.17	11.555	6.385	0.783	0.490
1172	2.83	226.66	1.103	0.888	0.637	0.002	0.251	0.000	0.08	18.745	10.392	1.191	0.434
1172	2.88	231.26	1.064	0.936	0.692	0.002	0.244	0.208	0.18	14.728	7.499	0.976	0.410
1172	2.93	236.06	1.041	0.869	0.697	0.002	0.172	0.174	0.44	11.778	5.725	0.737	0.437
1172	2.98	240.87	1.041	0.916	0.758	0.003	0.158	0.129	0.29	9.938	5.173	0.642	0.465
1172	3.03	245.67	1.042	0.962	0.827	0.003	0.135	0.160	0.23	7.361	4.414	0.460	0.429
1172	3.08	250.47	1.041	1.016	0.896	0.002	0.120	0.171	0.23	6.093	3.868	0.396	0.412
1172	3.13	255.28	1.041	0.947	0.825	0.002	0.122	0.218	0.33	6.204	4.021	0.395	0.367
1172	3.18	260.08	1.042	0.948	0.799	0.003	0.149	0.244	0.53	7.839	4.623	0.507	0.336
1172	3.23	264.88	0.942	0.838	0.697	0.002	0.141	0.186	0.40	8.516	4.312	0.543	0.358
1172	3.28	270.70	0.811	0.735	0.616	0.002	0.119	0.155	0.25	7.215	3.798	0.457	0.389
1172	3.33	277.21	0.768	0.718	0.607	0.002	0.112	0.145	0.28	7.054	3.585	0.434	0.312
1172	3.38	283.72	0.768	0.736	0.637	0.002	0.100	0.105	0.54	6.382	3.503	0.391	0.340
1172	3.43	290.24	0.767	0.699	0.600	0.002	0.100	0.129	0.33	5.348	2.822	0.326	0.286
1172	3.48	296.75	0.768	0.677	0.592	0.002	0.085	0.119	0.28	4.686	2.426	0.284	0.287
1172	3.53	303.26	0.768	0.679	0.596	0.002	0.083	0.109	0.38	4.985	2.742	0.304	0.280
1172	3.58	309.77	0.768	0.700	0.615	0.001	0.085	0.123	0.23	5.007	2.779	0.312	0.278
1172	3.63	316.29	0.767	0.720	0.629	0.002	0.091	0.121	0.31	6.119	3.288	0.367	0.310
1172	3.68	322.80	1.019	0.931	0.809	0.002	0.123	0.144	0.31	7.192	3.805	0.452	0.424
1172	3.73	326.10	1.563	1.424	1.232	0.002	0.192	0.293	0.12	11.686	6.243	0.694	0.793
1172	3.78	329.20	1.347	1.205	1.004	0.002	0.201	0.223	0.15	12.693	7.874	0.762	0.715
1172	3.83	333.53	1.328	1.178	0.983	0.001	0.195	0.355	0.05	11.494	8.011	0.713	0.401
1172	3.88	336.73	1.556	1.372	1.148	0.002	0.224	0.000	0.23	13.418	9.006	0.854	0.441
1172	3.93	339.95	2.045	1.818	1.421	0.006	0.397	0.527	1.25	25.411	13.451	1.686	0.744
1172	3.98	341.62	3.396	3.135	2.575	0.008	0.560	1.044	2.49	37.171	19.749	2.418	1.216

Site	Sample depth [mbsf]	Age [kyr]	SR [cm/kyr]	Bulk AR [g/cm²kyr]	AR Carbonate [g/cm²kyr]	AR TOC [g/cm²kyr]	AR Siliciclastics [g/cm²kyr]	AR coarse fraction [>63 µm, g/cm²kyr]	AR Chlorine [10⁻³g/cm²kyr]	AR Aluminium [10⁻³g/cm²kyr]	AR Iron [10⁻³g/cm²kyr]	AR Titanium [10⁻³g/cm²kyr]	AR excess Barium [10⁻³g/cm²kyr]
1172	4.03	342.90	3.906	3.478	2.841	0.009	0.636	0.950	4.17	42.420	20.951	2.707	1.430
1172	4.08	344.18	3.906	3.326	2.729	0.009	0.597	0.900	3.16	33.510	17.629	2.251	1.089
1172	4.13	345.46	3.906	3.431	2.647	0.010	0.784	0.814	4.65	53.374	26.728	3.250	1.137
1172	4.18	346.74	3.906	3.256	2.506	0.009	0.750	0.686	3.80	53.054	25.699	3.192	1.185
1172	4.23	348.02	3.906	3.238	2.417	0.007	0.821	0.598	1.33	57.467	31.574	3.472	1.065
1172	4.28	349.30	3.899	3.407	2.634	0.008	0.772	0.862	2.92	53.756	24.977	3.309	1.186
1172	4.33	350.58	3.906	3.279				0.863					
1172	4.38	351.86	3.906	3.390	2.685	0.009	0.705	0.632	3.78	45.931	24.663	2.876	1.272
1172	4.43	353.14	3.902	3.223	2.657	0.008	0.566	0.726	3.27	35.328	17.360	2.310	1.019
1172	4.53	355.70	3.916	3.370	2.767	0.009	0.603	0.686	2.31	38.858	21.708	2.446	1.225
1172	4.58	356.97	3.912	3.506	3.001	0.008	0.505	0.533	1.87	34.792	21.993	2.165	1.213
1172	4.63	358.26	3.831	3.096	2.577	0.010	0.519	0.540	3.02	32.372	16.851	2.011	1.048
1172	4.68	359.58	3.759	2.948	2.485	0.009	0.463	0.457	2.23	26.202	13.539	1.619	0.955
1172	4.73	360.92	3.731	3.233	2.704	0.010	0.528	0.446	0.00	33.583	17.325	2.073	1.176
1172	4.78	362.26	3.731	2.904	2.381	0.008	0.523	0.434	2.16	34.051	17.134	2.081	1.048
1172	4.83	363.60	3.731	3.082	2.549	0.009	0.533	0.485	2.68	34.330	18.377	2.084	1.135
1172	4.88	364.94	3.731	3.249	2.709	0.008	0.540	0.500	2.77	35.119	18.504	2.095	1.249
1172	4.93	366.28	3.731	3.322	2.877	0.007	0.444	0.474	3.18	26.807	13.308	1.589	1.322
1172	4.98	367.62	3.738	3.283	2.884	0.005	0.400	0.458	3.72	25.118	13.054	1.471	1.402
1172	5.03	368.96	3.731	3.054	2.712	0.005	0.343	0.370	2.68	21.807	11.690	1.252	1.313
1172	5.08	370.30	3.738	3.272	2.917	0.006	0.355	0.402	2.56	21.659	10.935	1.258	1.344
1172	5.13	371.63	3.731	3.132	2.687	0.007	0.445	0.257	3.70	24.750	15.162	1.464	1.466
1172	5.18	372.98	3.731	3.054	2.668	0.008	0.386	0.359	1.44	18.365	9.423	1.065	1.130
1172	5.23	374.31	3.745	3.284	2.890	0.007	0.394	0.263	1.01	19.755	11.127	1.140	1.279
1172	5.28	375.65	3.731	3.316	2.879	0.007	0.438	0.274	1.08	25.459	13.811	1.493	1.389
1172	5.33	376.99	3.731	3.183	2.742	0.006	0.441	0.226	1.34	25.072	14.891	1.470	1.414
1172	5.38	378.33	3.180	2.655	2.294	0.007	0.361	0.221	2.93	21.090	9.003	1.207	1.111
1172	5.43	380.14	1.815	1.567	1.386	0.003	0.181	0.117	0.66	9.439	6.474	0.553	0.651
1172	5.48	383.84	1.350	1.171	1.031	0.002	0.140	0.085	0.78	7.360	3.212	0.430	0.497
1172	5.53	387.55	1.350	1.226	1.079	0.004	0.147	0.089	0.16	7.032	3.776	0.410	0.486
1172	5.58	391.25	1.350	1.177	1.044	0.002	0.134	0.099	0.59	6.178	2.918	0.348	0.450
1172	5.63	394.96	1.350	1.207	1.078	0.001	0.129	0.121	0.16	6.908	3.991	0.380	0.471
1172	5.68	398.66	1.430	1.260	1.100	0.003	0.160	0.119	0.09	7.801	4.556	0.443	0.535
1172	5.73	401.95	2.041	1.872	1.618	0.002	0.254	0.188	0.09	15.078	7.852	0.864	0.762
1172	5.78	403.56	3.110	2.741	2.385	0.003	0.356	0.256	0.22	21.693	9.760	1.240	1.070
1172	5.83	405.17	3.106	2.872	2.464	0.005	0.408	0.268	0.34	23.557	13.588	1.320	1.093
1172	5.88	406.78	3.106	2.510	2.132	0.005	0.378	0.209	0.60	21.034	11.171	1.213	0.918
1172	5.93	408.39	3.115	2.708	2.305	0.005	0.403	0.260	0.37	23.604	13.012	1.354	1.046
1172	5.98	409.99	2.865	2.804	2.416	0.004	0.387	0.225	0.75	24.679	12.038	1.389	1.154
1172	6.03	411.88	2.066	1.904	1.638	0.003	0.266	0.219	0.39	15.467	8.974	0.909	0.818

Site	Sample depth [mbsf]	Age [kyr]	SR [cm/kyr]	Bulk AR [g/cm²kyr]	AR Carbonate [g/cm²kyr]	AR TOC [g/cm²kyr]	AR Siliciclastics [g/cm²kyr]	AR coarse fraction [>63 µm, g/cm²kyr]	AR Chlorine [10⁻³g/cm²kyr]	AR Aluminium [10⁻³g/cm²kyr]	AR Iron [10⁻³g/cm²kyr]	AR Titanium [10⁻³g/cm²kyr]	AR excess Barium [10⁻³g/cm²kyr]
1172	6.08	414.83	1.693	1.442	1.250	0.002	0.191	0.177	0.65	11.805	6.142	0.688	0.595
1172	6.12	417.19	3.299	2.962	2.525	0.005	0.437	0.319	0.99	24.861	15.171	1.489	1.282
1172	6.17	417.56	3.299	2.883	2.428	0.005	0.454	0.302	1.03	27.101	17.271	1.612	1.283
1172	6.22	417.93	5.607	4.900	4.091	0.011	0.809	0.531	2.18	47.907	26.604	2.892	2.175
1172	6.33	418.74	5.607	5.151	4.516	0.007	0.634	0.491	1.29	35.784	19.155	2.017	2.040
1172	6.38	420.78	2.189	2.047	1.716	0.003	0.330	0.215	0.74	19.790	11.008	1.162	0.831
1172	6.43	423.31	1.969	1.923	1.653	0.002	0.270	0.249	0.52	17.106	9.352	1.003	0.765
1172	6.48	425.86	2.663	2.271	1.960	0.004	0.311	0.223	0.00	17.594	9.116	1.004	0.866
1172	6.53	427.06	4.167	4.033	3.410	0.006	0.623	0.355	0.00	39.703	20.686	2.315	1.538
1172	6.58	428.26	4.149	3.799	3.240	0.006	0.559	0.382	0.61	34.393	19.176	1.952	1.581
1172	6.63	429.47	4.149	4.041	2.998	0.007	1.043	0.516	1.60	74.823	38.910	4.308	1.465
1172	6.68	430.67	4.167	3.541	2.754	0.006	0.787	0.583	0.00	55.616	27.626	3.333	1.251
1172	6.73	431.87	4.167	3.386	2.663	0.007	0.723	0.448	1.67	47.767	24.570	2.862	1.229
1172	6.78	433.07	4.237	3.684	3.054	0.006	0.507	0.425	1.39				
1172	6.83	434.23	4.405	3.685	2.929	0.007	0.756	0.478	2.43	47.031	28.513	2.956	1.228
1172	6.88	435.34	4.484	3.543	2.965	0.008	0.579	0.418	1.64	36.840	19.197	2.185	1.357
1172	6.93	436.46	4.484	3.624	3.039	0.006	0.585	0.478	1.77	38.675	20.412	2.316	1.407
1172	6.98	437.57	4.494	4.136	3.364	0.007	0.772	0.625	2.48	49.538	26.893	3.044	1.483
1172	7.03	438.69	4.484	3.838	3.130	0.008	0.708	0.585	2.71				
1172	7.08	439.80	4.484	3.912	3.276	0.006	0.636	0.679	1.06	39.697	21.535	2.493	1.566
1172	7.13	440.92	4.484	3.818	3.175	0.007	0.643	0.629	3.09	39.894	22.685	2.561	1.465
1172	7.18	442.03	4.484	3.704	3.045	0.005	0.659	0.682	3.76	46.217	22.097	2.801	1.319
1172	7.23	443.15	4.484	4.006	3.144	0.007	0.862	1.282	4.99	55.856	33.071	3.385	1.196
1172	7.28	444.26	3.306	2.597	2.016	0.004	0.581	0.450	1.74	41.122	20.003	2.468	0.866
1172	7.33	446.17	2.288	1.846	1.509	0.004	0.337	0.264	1.54	22.858	10.969	1.412	0.761
1172	7.38	448.63	1.721	1.579	1.366	0.003	0.212	0.165	0.60	11.857	6.840	0.723	0.607
1172	7.43	451.98	0.997	0.941	0.822	0.002	0.119	0.069	0.70	7.361	3.464	0.445	0.334
1172	7.48	458.66	0.749	0.677	0.587	0.001	0.090	0.095	0.35	5.468	3.034	0.325	0.196
1172	7.53	465.34	0.759	0.681	0.608	0.001	0.073	0.052	0.14	4.196	2.051	0.252	0.211
1172	7.58	471.84	0.786	0.710	0.637	0.001	0.073	0.057	0.22	4.195	2.239	0.250	0.231
1172	7.63	478.07	0.802	0.738	0.662	0.001	0.076	0.056	0.46	4.609	2.038	0.272	0.218
1172	7.68	484.31	0.874	0.787	0.708	0.001	0.080	0.062	0.46	5.084	3.081	0.297	0.246
1172	7.73	489.51	1.935	1.804	1.599	0.003	0.205	0.129	0.83	12.278	7.804	0.712	0.569
1172	7.83	492.06	3.912	3.577	3.195	0.005	0.381	0.217	2.67	23.704	12.048	1.375	1.211
1172	7.88	493.34	3.914	3.432	2.977	0.006	0.454	0.310	1.49	25.885	16.587	1.532	1.078
1172	7.93	494.62	3.922	3.462	3.075	0.006	0.387	0.339	2.11	23.952	14.408	1.460	1.294
1172	7.98	495.89	3.914	3.443	3.065	0.006	0.379	0.273	2.74	22.713	10.918	1.353	1.087
1172	8.03	497.17	3.906	3.262	2.967	0.005	0.295	0.303	0.81	16.782	8.538	0.958	1.188
1172	8.08	498.45	3.914	3.432	3.052	0.006	0.380	0.281	1.45	21.038	12.063	1.080	1.271
1172	8.13	499.73	3.922	3.644	3.286	0.006	0.358	0.373	0.90	20.350	10.670	1.160	1.458

Site	Sample depth [mbsf]	Age [kyr]	SR [cm/kyr]	Bulk AR [g/cm²kyr]	AR Carbonate [g/cm²kyr]	AR TOC [g/cm²kyr]	AR Siliciclastics [g/cm²kyr]	AR coarse fraction [>63 µm, g/cm²kyr]	AR Chlorine [10⁻³g/cm²kyr]	AR Aluminium [10⁻³g/cm²kyr]	AR Iron [10⁻³g/cm²kyr]	AR Titanium [10⁻³g/cm²kyr]	AR excess Barium [10⁻³g/cm²kyr]
1172	8.18	501.00	3.906	3.518	3.139	0.009	0.379	0.349	0.99	20.578	13.215	1.142	1.453
1172	8.23	502.29	3.906	3.425	3.084	0.006	0.341	0.352	1.09	18.790	11.045	1.078	1.355
1172	8.28	503.56	3.922	3.567	3.213	0.007	0.354	0.396	1.39	20.089	10.531	1.177	1.426
1172	8.33	504.84	3.922	3.116	2.810	0.004	0.306	0.240	0.38	19.623	9.932	1.164	1.390
1172	8.38	506.11	3.906	3.373	3.021	0.005	0.351	0.360	0.72	21.005	10.391	1.239	1.426
1172	8.43	507.40	3.906	3.419	3.035	0.004	0.384	0.339	0.78	24.387	14.690	1.456	1.461
1172	8.48	508.67	3.922	3.450	3.028	0.006	0.422	0.425	0.48	23.791	13.786	1.421	1.450
1172	8.53	509.95	3.906	3.122	2.750	0.006	0.372	0.448	0.90	21.297	13.593	1.291	1.296
1172	8.58	511.23	3.906	3.396	2.991	0.004	0.405	0.416	0.61	25.174	15.917	1.509	1.537
1172	8.63	512.51	3.922	3.257	2.792	0.009	0.465	0.451	1.02	23.300	11.796	1.408	1.462
1172	8.68	513.78	3.914	3.075	2.623	0.009	0.452	0.327	1.10	23.962	11.654	1.394	1.376
1172	8.73	515.06	3.937	3.293	2.862	0.009	0.431	0.393	1.24	23.535	12.952	1.409	1.531
1172	8.78	516.32	4.008	3.502	3.071	0.006	0.431	0.432	1.64	24.592	14.160	1.469	1.542
1172	8.83	517.56	4.049	3.568	3.110	0.008	0.458	0.478	1.17	25.844	13.450	1.593	1.501
1172	8.88	518.79	4.057	3.636	3.207	0.009	0.428	0.404	1.65	22.320	15.983	1.345	1.394
1172	8.93	520.02	4.065	3.643	3.226	0.009	0.417	0.367	2.07	23.634	12.416	1.404	1.300
1172	8.98	521.25	4.040	3.543	3.135	0.010	0.407	0.405	1.83	20.767	11.730	1.218	1.297
1172	9.03	522.50	3.195	2.906	2.624	0.003	0.282	0.242	0.36	16.423	8.720	1.020	1.146
1172	9.08	524.38	2.551	2.191	1.976	0.002	0.215	0.196	0.60	12.394	7.005	0.763	0.864
1172	9.13	526.42	2.457	2.290	2.072	0.003	0.218	0.229	1.04	12.628	7.309	0.759	0.893
1172	9.18	528.45	2.448	2.198	1.978	0.004	0.220	0.231	1.30	12.113	6.693	0.726	0.778
1172	9.23	530.50	2.439	2.135	1.892	0.005	0.243	0.204	1.04	11.326	5.637	0.700	0.733
1172	9.28	532.55	2.439	2.179	1.945	0.005	0.234	0.224	0.73	12.409	6.903	0.770	0.734
1172	9.33	534.60	2.874	2.794	2.460	0.008	0.334	0.332	0.75	18.273	9.836	1.140	0.989
1172	9.38	536.03	5.063	5.007	4.382	0.012	0.625	0.625	1.24	33.823	19.993	2.096	1.909
1172	9.43	536.58	9.259	8.589	7.484	0.021	1.105	1.327	0.00				
1172	9.48	537.11	9.217	8.797	7.636	0.025	1.162	1.563	2.69	65.619	35.458	3.954	3.622
1172	9.53	537.66	9.259	8.216	7.073	0.023	1.143	1.549	3.25	59.478	28.062	3.696	3.161
1172	9.58	538.19	9.302	7.489	6.323	0.018	1.166	1.588	2.59				
1172	9.63	538.74	9.174	7.564	6.496	0.012	1.068	1.439	2.86	58.439	35.962	3.660	3.266
1172	9.68	539.28	9.174	7.893	6.684	0.016	1.210	1.925	3.11	44.340	28.338	2.451	2.970
1172	9.73	539.83	9.174	7.482	6.318	0.013	1.164	1.792	3.23	64.669	39.614	3.990	3.427
1172	9.78	540.37	9.217	7.765	6.558	0.018	1.207	2.288	3.25	65.066	36.965	4.029	3.581
1172	9.83	540.91	9.259	7.731	6.317	0.016	1.415	2.616	2.78	80.006	47.648	5.085	3.496
1172	9.88	541.45	9.174	7.976	6.409	0.020	1.567	2.133	2.66	94.318	55.914	6.029	3.727
1172	9.93	542.00	9.174	7.674	6.065	0.024	1.609	0.000	7.66	101.470	50.982	6.333	3.998
1172	9.98	542.54	3.704	3.015	2.381	0.008	0.634	0.690	1.82	38.669	20.036	2.414	1.567
1172	10.03	544.70	2.128	1.920	1.528	0.005	0.392	0.509	1.67	24.350	12.373	1.544	1.057
1172	10.08	547.24	2.235	1.909	1.451	0.006	0.459	0.322	1.28	30.907	15.738	1.946	1.217
1172	10.13	549.18	2.584	2.169	1.595	0.008	0.574	0.370	3.12	37.819	19.615	2.428	1.379

Site	Sample depth [mbsf]	Age [kyr]	SR [cm/kyr]	Bulk AR [g/cm²kyr]	AR Carbonate [g/cm²kyr]	AR TOC [g/cm²kyr]	AR Siliciclastics [g/cm²kyr]	AR coarse fraction [>63 µm, g/cm²kyr]	AR Chlorine [10^{-6}g/cm²kyr]	AR Aluminium [10^{-3}g/cm²kyr]	AR Iron [10^{-3}g/cm²kyr]	AR Titanium [10^{-3}g/cm²kyr]	AR excess Barium [10^{-3}g/cm²kyr]
1172	10.18	551.11	2.421	2.004	1.468	0.006	0.536	0.358	2.99	19.572	15.707	2.215	1.085
1172	10.23	553.31	1.908	1.608	1.170	0.005	0.437	0.240	1.43	29.832	14.927	1.888	0.955
1172	10.28	556.35	1.595	1.339	0.986	0.004	0.353	0.208	1.15	23.218	12.778	1.484	0.769
1172	10.33	559.58	1.550	1.267	0.936	0.004	0.331	0.200	1.00	21.340	11.108	1.371	0.693
1172	10.38	562.80	1.440	1.267	0.976	0.003	0.291	0.209	0.69	17.573	8.930	1.169	0.682
1172	10.43	566.52	0.943	0.808	0.632	0.002	0.176	0.170	0.58	10.821	5.973	0.708	0.473
1172	10.48	573.41	0.691	0.564	0.461	0.001	0.103	0.101	0.18	6.256	3.298	0.410	0.301
1172	10.53	581.00	0.658	0.569	0.463	0.001	0.106	0.097	0.14	6.592	3.233	0.431	0.340
1172	10.58	588.61	0.666	0.581	0.485	0.001	0.096	0.171	0.09				
1172	10.63	596.02	0.726	0.614	0.507	0.001	0.106	0.158	0.14	6.457	3.206	0.415	0.374
1172	10.68	602.39	1.029	0.870	0.714	0.001	0.156	0.269	0.04	8.832	4.985	0.560	0.507
1172	10.73	605.73	1.029	0.850	0.681	0.001	0.169	0.247	0.07	9.755	6.143	0.667	0.419

Curriculum Vitae

Biographical Data

Name:	Brughmans, Natasja
Address:	Lüdemannstr 56 D-24114 Kiel, Germany
Email:	nb@planetarium.fh-kiel.de
Date of birth:	February 6th, 1975
Place of birth:	Mechelen, Belgium
Citizenship:	Belgian

Education

August 2002 – July 2003:	PhD at the Christian-Albrechts-University in Kiel (D)
October 1998 – July 2000:	Master of coastal geosciences and engineering at the Christian-Albrechts-University in Kiel (D)
October 1993 – July 1998:	Geology at the University of Ghent (B)
June 1993:	End of high-school education at the Scheppersinstituut in Mechelen (B)

Work Experience

August 2002 – July 2003: Scientist at GEOMAR, Kiel (D)

Student jobs:

November 1998 – July 2000:	Sedimentology, paleoceanography, sampling of cores at Geomar in Kiel (D)
15.08.1999 – 15.09.1999:	Digitizing and scanning at the University in Ghent (B)
01.08.1998 – 21.08.1998:	Research of the soil at the firm Esher in Ghent (B)

Participant of scientific cruises:

Mai – June 2000:	Meteor M47/2 Fortaleza-Libreville
Mai – June 2002:	Sonne SO164 Balboa-Balboa

Erklärung

Hiermit erkläre ich, dass die Abhandlung - abgesehen von der Beratung durch meine akademischen Lehrer - nach Inhalt und Form meine eigene Arbeit ist.
Diese Arbeit hat an keiner anderen Stelle im Rahmen eines Prüfungsverfahrens vorgelegen.

Kiel, den 28.05.2003

Natasja Brughmans